To the Graduate Council:

I am submitting herewith a thesis written by Philip F. Keebler entitled "A Large Volume Microwave Plasma Facility for Plasma Ion Implantation Studies". I have examined the final copy of this thesis for form and content and recommend that it be accepted in partial fulfillment of the requirements for the degree of Master of Science, with a major in Electrical Engineering.

J. Reece Roth, Major Professor

We have read this thesis
and recommend its acceptance:

Igor Alexeff

R. A. Buchanan

Accepted for the Council:

Vice Provost
and Dean of The Graduate School

STATEMENT OF PERMISSION TO USE

In presenting this thesis in partial fulfillment of the requirements for a Master's degree at The University of Tennessee, Knoxville, I agree that the Library shall make it available to borrowers under the rules of the Library. Brief quotes from this thesis are allowable without special permission, provided that accurate acknowledgement of the source is made.

Permission for extensive quotation from or reproduction of this thesis may be granted by my major professor, or in his absence, by the Head of Interlibrary Services when, in the opinion of either, the proposed use of the material is for scholarly purposes. Any copy or use of the material in this thesis for financial gain shall not be allowed without my written permission.

Signature Philip Frank Keelle

Date July 27, 1990

A LARGE VOLUME MICROWAVE PLASMA FACILITY FOR PLASMA ION IMPLANTATION STUDIES

A Thesis
Presented for the
Master of Science
Degree
The University of Tennessee, Knoxville

Philip Frank Keebler
August 1990

DEDICATION

This thesis is dedicated to my parents
James Philip Keebler
&
Nancy Armstrong Keebler

and to my sister
Gretchen Keebler Corum

and to my grandparents
Mr. and Mrs. James Hendrix Armstrong
&
Mr. and Mrs. William Frank Keebler

without whom the completion of my education
would have been impossible.

ACKNOWLEDGEMENTS

The author wishes to express his sincere appreciation to Dr. Robert R. Reeber of the Materials Division at the Army Research Office for giving Professor J. Reece Roth and his graduate students the opportunity to engineer a high-voltage switching circuit for the plasma ion implantation process by funding a short-term innovative research contract so that a research program in industrial plasma engineering could be started. The author also wishes to express his appreciation to Dr. Reeber for funding a follow-up three-year research program to investigate the implantation and corrosion inhibition of metals by the method of plasma ion implantation. Dr. Reeber is also thanked for supporting the First Workshop on Research and Technology Transfer of Ion Implantation Technology for Specialty Materials held during the month of October in Knoxville, Tennessee.

The author also thanks Professor William Snyder, Dean of the College of Engineering, for his willingness to provide the state-of-the-art equipment needed for this research project, including a new mass spectrometer and a new ion gauge.

Professor Joseph C. Danko, Director of the Center for Materials Processing, is thanked for the financial and moral support he has given this research program.

The author wishes to extend his appreciation to Professor Joseph M. Googe, Department Head of the Electrical and Computer

Engineering Department, for his support of this research. Professor Googe, of whom the author has had the opportunity to be a student, has contributed much to the author's education from its beginning in the circuits courses to the present, by the advice and motivation given to the author during the author's graduate education.

The author then wishes to express his sincere appreciation to Professor J. Reece Roth, of the Department of Electrical and Computer Engineering, for teaching the author everything he knows about plasmas and plasma science. The author also thanks Professor Roth for giving him the opportunity to utilize his talents at the University of Tennessee, Knoxville Plasma Science Laboratory. He also wishes to thank him for his professional leadership, financial support, helpful advice, and patience during this research program.

The author also would like to express his grateful appreciation to the remaining members of his committee, Professor Raymond A. Buchanan of the Material's Science and Engineering Department and Professor Igor Alexeff of the Electrical and Computer Engineering Department, both at the University of Tennessee, Knoxville. Professor Buchanan helped the author obtain a better understanding of corrosion characteristics and how corrosion tests are made. Professor Alexeff was very helpful in explaining other not-well-understood plasma ion implantation procedures and in understanding some of the phenomena of microwave generated plasmas.

Another faculty member, who helped the author in the development of the microwave discharge, is Associate Professor David Rosenburg of the Electrical and Computer Engineering Department. Professor Rosenburg was helpful in locating information pertaining to microwave engineering and in learning how to use critical features of the Hewlett-Packard 8510 Network Analyzer.

A very special appreciation is extended to Mr. John E. Crowley, who gave the author critical assistance with the design and construction of the high-voltage switching circuit. He also thanks Mr. Crowley for his friendship, encouragement, and motivation during the entire course of this project.

The remaining staff of the UTK Plasma Science Laboratory, Mr. Fred Dyer, Research Assistant and Mr. Mark S. Rader, Senior Graduate Research Assistant under Professor Alexeff were both of great assistance. They answered many of the author's questions while gaining knowledge about the operations of the laboratory and their support is very much appreciated.

Mr. Paul D. Spence and Mr. Min Wu, former students of the UTK Plasma Science Laboratory are thanked for their contributions to this work.

Dr. In-Seop Lee and Mr. Abhijit Gupta of the Material's Science and Engineering Department are also thanked for their contributions to this work. Dr. Lee analyzed many metal samples and Mr. Gupta assisted the author in diagnosing problems associated with the high-

voltage switching circuit and also helped in the fabrication of the new microwave plasma system.

This study of the microwave plasma, using the multimode microwave cavity, would not be possible without the guidance, leadership, advice, patience, and understanding of Mr. Douglas Fielden, foreman of Mechanical Systems Machine Shop in the Material's Science and Engineering Department and his crew.

Finally, the author wishes to express his most sincere appreciation to his family and friends for their mental and financial support and continued encouragement during the seven and one-half years spent at the University of Tennessee. Mr. Jerry J. Griffey, Mr. Richard L. Bean, and Mr. Herman Potts gave me much encouragement, motivation, and support. A special friend, Mrs. Elizabeth F. Hobbs, also encouraged me and helped me make decisions. Without these people, the author would not have been able to go this far in his life.

The short-term innovative research program was supported by the Army Research Office under contract number DAAL03-88-K-0161. The remaining work was also supported by the Army Research Office under grant number DAAL03-89-G-0125. This work was partially supported from the beginning by the University of Tennessee, Knoxville, Center for Materials Processing.

ABSTRACT

A multimode microwave cavity resonator to generate and contain in the steady state a large volume plasma was designed and fabricated. This microwave plasma facility is intended for plasma ion implantation studies using a high-voltage switching circuit which was also designed, fabricated, and tested. The cavity is energized by a 3 kW, 2.45 GHz microwave generator operating in the TE_{01} mode. The facility provides for enhancement of the confinement of plasma electrons by installing many oriented ceramic permanent magnets on the outer cavity surface. The facility was tested in terms of it base pressure (2×10^{-6} torr), background mass spectra, and microwave impedance matching. With this information, the plasma can be created and maintained for plasma ion implantation studies.

TABLE OF CONTENTS

CHAPTER PAGE

I. INTRODUCTION 1

A. The Materials Problem 1

B. The Corrosion Problem 1

C. Early Processes to Inhibit Corrosion 2

D. Historical Review of Ion Implantation 4

E. Ion Implantation Processes 6

1. Ion Beam Implantation 6

2. Plasma Ion Implantation 8

a. Low-Voltage Plasma Ion Implantation 8

b. High-Voltage Plasma Ion Implantation 9

c. Incorporating a Switching Circuit 11

d. A Call for a Faster Switching Circuit 13

II. A HIGH-VOLTAGE SWITCHING CIRCUIT FOR PLASMA ION IMPLANTATION 14

A. Switching Circuits 14

B. Ideal Switching Voltage Signals 17

C. Required Isolation of Switching Circuit 19

D. The Switching Element and Signal Flow Diagrams 24

E. Testing of the Vacuum Tube 30

F. High-Voltage Switching Circuit Power Source 32

G. Implantation Power Source 34

H. High-Voltage Switching Circuit Block Diagram and Waveforms 35

I. Electronic Circuits....39
1. Fiber Optic Transmitter Circuit....40
2. Fiber Optic Light Guide....44
3. Fiber Optic Receiver Circuit....45
4. Vacuum Tube Circuits....48
a. The Control Grid Circuit....50
b. The Screen Grid Circuit....59
c. The Filament Power Circuit....61
5. Power Circuits....67
a. The Control Grid Power Supply....67
b. The Screen Grid Power Supply....71
c. The Filament Power Supply....72
6. Total Power Consumption....73
7. Cooling Requirements....78
8. Power Distribution and Fusing of Electronic Circuits....80
9. Faraday Shielding....84
10. List and Identification of Components....88
III. PLASMA ION IMPLANTATION IN A UNIFORM PENNING DISCHARGE....93
A. The Penning Discharge Vacuum System....92
B. The Magnetic Field Profile....97
C. Powering the Penning Discharge....99
D. Testing the High-Voltage Switching Circuit in the Penning Discharge....101
E. The First Plasma Ion Implantation....141

F. Removing Samples from the Penning Discharge.....142

IV. A NON-MAGNETIZED PLASMA FOR PLASMA ION IMPLANTATION.....144

A. Advantages Over a Magnetized, DC Gaseous Discharge Plasma.....144

B. The Microwave Power Source.....147

C. The Multimode Microwave Cavity.....171

1. Choosing a Geometry.....171

2. Choosing a Metallic Material.....175

3. Choosing the Dimensions.....176

4. The Cavity Q's.....180

5. The Q with a Plasma.....186

6. Microwave Discharge Mechanism.....194

7. Vacuum System Design.....196

8. The Waveguide-Vacuum Interface.....217

9. Tuning and Matching.....218

10. Enhancing the Electron Number Density.....223

11. Cooling the Cavity Walls.....230

12. The High Vacuum Pumping Station.....231

13. The Mass Spectrometer and Various Mass Spectra...239

14. Starting the Plasma.....247

15. Conclusions.....248

BIBLIOGRAPHY.....250

APPENDICES.....255

A. MACROSCOPIC THEORY OF PLASMA ION IMPLANTATION.....256

B. CHARGING THE BATTERY IN THE HIGH-VOLTAGE SWITCHING CIRCUIT 283

C. THE PLASMA ION IMPLANTATION PROCESS USING THE PENNING DISCHARGE 287

D. OPERATING THE PENNING DISCHARGE PLASMA FOR PLASMA ION IMPLANTATION 296

E. OPERATING THE VACUUM SYSTEM IN THE PENNING DISCHARGE 300

F. CHANGING THE SAMPLE AFTER A PLASMA ION IMPLANTATION EXPERIMENT 306

G. A TRUE-BASIC™ PROGRAM FOR CALCULATING THE Q OF A MEDIUM-FREE RIGHT CIRCULAR CYLINDRICAL MULTIMODE MICROWAVE CAVITY RESONATOR 316

H. A TRUE-BASIC™ PROGRAM FOR CALCULATING THE Q OF A PLASMA BASED ON THE LORENTZ CONDUCTIVITY MODEL FOR ELECTRON COLLISIONS 319

I. COMMENTS ON THE PRODUCTION OF THIS THESIS 321

VITA 323

LIST OF TABLES

TABLE		PAGE
II.1	High Power Switching Tube Ratings and Characteristics	26
II.2	Power Consumption of High-Voltage Switching Circuit	76
II.3	Power Consumption for Diagnostics Used in Plasma Ion Implantation	77
II.4	List and Identification of Components for the High-Voltage Switching Circuit	89
IV.1	Unloaded Quality Factor (Q) of Several Low and High Order Modes in the Multimode Microwave Cavity	187
IV.2	Plasma Quality Factor	192

LIST OF FIGURES

FIGURE PAGE

I.1 Conventional ion beam implantation system showing ion source, extraction grid, accelerating grids, high-energy ion trajectories, and planar target 7

I.2 Initial arrangement for plasma ion implantation of a complex metallic object immersed in a plasma 10

I.3 Plasma ion implantation of a complex metallic object immersed in a plasma 12

II.1 An ideal switching voltage signal generated by the high-voltage switching circuit when receiving a signal from the fiber optic transmitter 18

II.2 Block diagram for high-voltage switching circuit showing the major components including the Del Electronics 50 kV, 1 A implantation power source with a low internal impedance 21

II.3 Side view of the power grid tube showing the dimensions 25

II.4 Circuit used to test the filament of the power grid tube 31

II.5 Switching signals from the fiber optic transmitter to the sample holder negative bias delivered by the vacuum tube 36

II.6 Front panel of Wavetek Model 191 signal generator showing the appropriate knobs controlling the frequency and bias on time of the high-voltage switching signal 38

II.7 Schematic of fiber optic transmitter circuit responsible for delivering an infrared light beam to the fiber optic light guide (cable) connected to the fiber optic receiver circuit of Figure II.8.....42

II.8 Schematic of fiber optic receiver circuit responsible for delivering an analog voltage signal to the voltage comparator in the TMOS grid switching circuit of Figure II.10.....46

II.9 Oscillogram showing fiber optic receiver signal on upper trace rising to a voltage of 700 mV and the transmitted signal input to the fiber optic transmitter rising to a voltage of 4 V on the lower trace.....49

II.10 Schematic of TMOS grid switching circuit responsible for delivering a negative 400 V signal between the cathode and the control grid of the vacuum tube of Figure II.2.....53

II.11 Transistor switching scheme when control signal is low, resulting in the control grid of the vacuum tube being off and the vacuum tube being on.....55

II.12 Transistor switching scheme when control signal is high, resulting in the control grid of the vacuum tube being biased negative (control grid connection is a positive ground connection) and the vacuum tube being off.....56

II.13 Screen grid power supply and components.....60

II.14 A schematic diagram of the circuit required to power the directly-heated cathode filament.....63

II.15 Control grid power supply and components.....68

II.16 Proposed feedback circuit for control grid power supply if it is desired not to use the high-power voltage regulator to set the DC to DC converter input voltage at a voltage which will cause the output to be 415 V.....70

II.17 Fusing diagram for the fuse blocks in the power distribution box. 81

II.18 Geometrical representation of a corona shield covering a printed circuit board....86

III.1 The Penning discharge with the copper anode cylinder electrode arrangement used in the first plasma ion implantation experiment....94

III.2 The magnetic field profile for the modified Penning discharge used in all plasma ion implantation experiments (Spence, 1990)....98

III.3 The first sample holder system used in plasma ion implantation experiments....102

III.4 The system used to test the high-voltage switching circuit and to conduct the first plasma ion implantation experiment....104

III.5 (Run CCC-1) Oscillogram showing the control signal (upper trace with 2 V per vertical division) and the sample holder voltage (lower trace with -2 kV per vertical division) using the Tektronix probe for a negative bias-on time of 20 μsec, a negative bias-off time of 1 msec, a negative bias of - 5 kV, and a sample holder current of 2.6 mA....105

III.6 (Run CCC-1) Oscillogram showing the sample holder voltage using the Jennings instrument (upper trace) and using the Tektronix probe (lower trace with -2 kV per vertical division) for the same HVSC and plasma conditions as in Figure III.5....106

III.7 (Run CCC-2) Oscillogram showing the control signal (upper trace with 2 V per vertical division) and the sample holder voltage (lower trace with -2 kV per vertical division) using the Tektronix probe for a negative bias-on time of 20 μsec, a negative bias-off time of 100 μsec, a negative bias of - 5 kV, and a sample holder current of 23 mA.....107

III.8 (Run CCC-2) Oscillogram showing several sample holder voltage pulses using the Jennings instrument (upper trace) and the Tektronix probe (lower trace with -2 kV per vertical division).....108

III.9 (Run CCC-3) Oscillogram showing several control signal pulses (upper trace with 2 V per vertical division) and sample holder voltage pulses (lower trace with -5 kV per vertical division) using the Tektronix probe for a negative bias-on time of 20 μsec, a negative bias-off time of 80 μsec, a negative bias of - 10 kV, and a sample holder current of 50 mA.....109

III.10 (Run CCC-3) Oscillogram showing several sample holder voltage pulses using the Jennings instrument (upper trace) and the Tektronix probe (lower trace with -5 kV per vertical division).....110

III.11 (Run CCC-4) Oscillogram showing the control signal (upper trace with 2 V per vertical division) and the sample holder voltage (lower trace with -5 kV per vertical division) using the Tektronix probe for a negative bias-on time of 20 μsec, a negative bias-off time of 400 μsec, a negative bias of -15 kV, and a sample holder current of 16 mA.....111

III.12 (Run CCC-4) Oscillogram showing several sample holder voltage pulses using the Jennings instrument (upper trace) and the Tektronix probe (lower trace with -5 kV per vertical division).....112

III.13 (Run CCC-5) Oscillogram showing the control signal (upper trace with 2 V per vertical division) and the sample holder voltage (lower trace with -5 kV per vertical division) using the Tektronix probe for a negative bias-on time of 20 μsec, a negative bias-off time of 400 μsec, a negative bias of -20 kV, and a sample holder current of 33 mA.....113

III.14 (Run CCC-5) Oscillogram showing a sample holder voltage pulse using the Jennings instrument (upper trace) and the Tektronix probe (lower trace with -5 kV per vertical division).....114

III.15 (Run CCC-6) Oscillogram showing a sample holder voltage pulse using the Jennings instrument (upper trace) and the Tektronix probe (lower trace with -5 kV per vertical division) for a negative bias-on time of 20 μsec, a negative bias-off time of 1 msec, a negative bias of -20 kV, and a sample holder current of 9 mA.....115

III.16 (Run CCC-6) Oscillogram showing several sample holder voltage pulses using the Jennings instrument (upper trace) and the Tektronix probe (lower trace with -5 kV per vertical division.....116

III.17 (Run CCC-7) Oscillogram showing the control signal (upper trace with 2 V per vertical division) and the sample holder voltage (lower trace with -5 kV per vertical division) using the Tektronix probe for a negative bias-on time of 5 μsec, a negative bias-off time of 1 msec, and a negative bias of -20 kV.....118

III.18 (Run CCC-7) Oscillogram showing the control signal (upper trace with 2 V per vertical division) and the sample holder voltage (lower trace with -5 kV per vertical division) using the Tektronix probe for a negative bias-on time of 15 μsec, a negative bias-off time of 1 msec, and a negative bias of -20 kV.....119

III.19 (Run CCC-7) Oscillogram showing the control signal (upper trace with 2 V per vertical division) and the sample holder voltage (lower trace with -5 kV per vertical division) using the Tektronix probe for a negative bias-on time of 30 μsec, a negative bias-off time of 1 msec, and a negative bias of -20 kV.....120

III.20 (Run CCC-7) Oscillogram showing the control signal (upper trace with 2 V per vertical division) and the sample holder voltage (lower trace with -5 kV per vertical division) using the Tektronix probe for a negative bias-on time of 40 μsec, a negative bias-off time of 1 msec, and a negative bias of -20 kV.....121

III.21 (Run CCC-7) Oscillogram showing the control signal (upper trace with 2 V per vertical division) and the sample holder voltage (lower trace with -5 kV per vertical division) using the Tektronix probe for a negative bias-on time of 50 μsec, a negative bias-off time of 1 msec, and a negative bias of -20 kV.....122

III.22 (Run CCC-7) Oscillogram showing the control signal (upper trace with 2 V per vertical division) and the sample holder voltage (lower trace with -5 kV per vertical division) using the Tektronix probe for a negative bias-on time of 100 μsec, a negative bias-off time of 1 msec, and a negative bias of -20 kV.....123

III.23 (Run CCC-8) Oscillogram showing a sample holder voltage pulse using the Jennings instrument (upper trace) and the Tektronix probe (lower trace with -1 kV per vertical division) for a negative bias-on time of 20 μsec, a negative bias-off time of 1 msec, and a negative bias of -1 kV.....131

III.24 (Run CCC-8) Oscillogram showing a sample holder voltage pulse using the Jennings instrument (upper trace) and the Tektronix probe (lower trace with -1 kV per vertical division) for a negative bias-on time of 20 μsec, a negative bias-off time of 1 msec, and a negative bias of -2.5 kV.....132

III.25 (Run CCC-8) Oscillogram showing a sample holder voltage pulse using the Jennings instrument (upper trace) and the Tektronix probe (lower trace with -2 kV per vertical division) for a negative bias-on time of 20 μsec, a negative bias-off time of 1 msec, and a negative bias of -5 kV.....133

III.26 (Run CCC-8) Oscillogram showing a sample holder voltage pulse using the Jennings instrument (upper trace) and the Tektronix probe (lower trace with -2 kV per vertical division) for a negative bias-on time of 20 μsec, a negative bias-off time of 1 msec, and a negative bias of -7.5 kV.....134

III.27 (Run CCC-8) Oscillogram showing a sample holder voltage pulse using the Jennings instrument (upper trace) and the Tektronix probe (lower trace with -5 kV per vertical division) for a negative bias-on time of 20 μsec, a negative bias-off time of 1 msec, and a negative bias of -10 kV.....135

III.28 (Run CCC-8) Oscillogram showing a sample holder voltage pulse using the Jennings instrument (upper trace) and the Tektronix probe (lower trace with -5 kV per vertical division) for a negative bias-on time of 20 μsec, a negative bias-off time of 1 msec, and a negative bias of -12.5 kV.....136

III.29 (Run CCC-8) Oscillogram showing a sample holder voltage pulse using the Jennings instrument (upper trace) and the Tektronix probe (lower trace with -5 kV per vertical division) for a negative bias-on time of 20 μsec, a negative bias-off time of 1 msec, and a negative bias of -15 kV....137

III.30 (Run CCC-8) Oscillogram showing a sample holder voltage pulse using the Jennings instrument (upper trace) and the Tektronix probe (lower trace with -5 kV per vertical division) for a negative bias-on time of 20 μsec, a negative bias-off time of 1 msec, and a negative bias of -17.5 kV....138

III.31 Oscillogram showing a sample holder voltage pulse using the Tektronix instrument (-5 kV per vertical division) for a negative bias-on time of 22 μsec, a negative bias-off timeof 3 msec, and a negative bias of - 45 kV with no plasma....140

III.32 Potentiostat curve graphing the current density on the abscissa and the applied potential between the sample and an electrode on the ordinate for the first plasma ion implantation experiment....143

IV.1 Side and front view of the Varian-Eimac Model PPS-2.5AS Power Pack....149

IV.2 Power feed connections for microwave generated plasma....150

IV.3 Apparatus for measuring the power spectrum for each of the two microwave sources....151

IV.4 Graph of transmission coefficient, S_{21}, generated with the Hewlett-Packard 8510 Network Analyzer for the two fixed attenuators and the two variable attenuators used in measuring the power spectrum of the microwave power sources....155

IV.5 Graph of the Varian magnetron power on the microwave source control panel versus the forward power as measured by the HP732A microwave power meter.....156

IV.6 Graph of the Varian magnetron power on the microwave source control panel versus the forward power as indicated by the power meter of the Varian power meter box.....158

IV.7 Power spectrum from HP 8555A spectrum analyzer for Varian Model PPS-2.5AS microwave power source. The largest peak is at 2.45032 GHz with a power of 159 W....160

IV.8 Power spectrum from HP 8555A spectrum analyzer for Varian Model PPS-2.5AS microwave power source. The largest peak is at 2.45032 GHz with a power of 251.2 W.....161

IV.9 Power spectrum from HP 8555A spectrum analyzer for Varian Model PPS-2.5AS microwave power source. The largest peak is at 2.4501 GHz with a power of 630.4 W.....162

IV.10 Power spectrum from HP 8555A spectrum analyzer for Varian Model PPS-2.5AS microwave power source. The largest peak is at 2.4498 GHz with a power of 794.3 W.....163

IV.11 Power spectrum from HP 8555A spectrum analyzer for Varian Model PPS-2.5 microwave power source. The largest peak is at 2.449 GHz with a power of 316.2 W.....166

IV.12 Power spectrum from HP 8555A spectrum analyzer for Varian Model PPS-2.5 microwave power source. The largest peak is at 2.4488 GHz with a power of 630.9 W...167

IV.13 Power spectrum from HP 8555A spectrum analyzer for Varian Model PPS-2.5 microwave power source. The largest peak is at 2.44875 GHz with a power of 1.58 kW.....168

IV.14 Power spectrum from HP 8555A spectrum analyzer for Varian Model PPS-2.5 microwave power source. The largest peak is at 2.44865 GHz with a power of 2.51 kW.....169

IV.15 Graph of the a geometry factor, 2a/d, versus the form factor for several TE and TM modes in a right circular cylinder (Heald, et al., 1978).....178

IV.16 Electric and magnetic field configurations of some TE_{nml} modes in a right circular cylindrical multimode microwave cavity (Gandhi, 1981).....184

IV.17 Graph of electron number density versus plasma quality factor for the plasma in the multimode microwave cavity with an electron collision frequency of 600 kHz and a microwave driving frequency of 2.45 GHz.....193

IV.18 Vacuum pumping flange port used in multimode microwave cavity showing the maximum pumping cross-section of 3.75".....199

IV.19 A color photograph of the vacuum pumping port installed on a milling machine for the finishing of the flange surface.....200

IV.20 Top flange plate used in the multimode microwave cavity including five standard 4" flange ports, sixteen bolt holes, and four threaded eye hooks for lifting.....203

IV.21 Bottom flange plate used in the multimode microwave cavity including four standard 4" flange ports, one vacuum pumping port, and sixteen bolt holes.....204

IV.22 Ring flanges for top and bottom flange plates used in the multimode microwave cavity showing a cross-section with the cavity side wall, O-ring groove, and bolt holes.....206

IV.23 A color photograph of Ray Bellamy vacuum welding a layer of Type 316 stainless steel to the chamfered grooves between the outer edge of the cylinder and the inner edge of one of the ring flanges..... 207

IV.24 Diagnostic port flange used in the multimode microwave cavity at a distance of 10" (25.4 cm) from the bottom flange plate..... 209

IV.25 Mass spectrometer flange port used in the multimode microwave cavity showing the O-ring groove and the non-standard bolt hole pattern..... 211

IV.26 Microwave waveguide flange port used in the multimode microwave cavity showing the overlap of the WR-284 waveguide on the short circular waveguide section.....213

IV.27 Diagnostic viewport flange used in the multimode microwave cavity..... 215

IV.28 The complete multimode microwave cavity showing all ports except the mass spectrometer port located on the rear of the tank..... 216

IV.29 The complete experimental apparatus for the microwave generated plasma showing the microwave power source, the multimode microwave cavity, the high vacuum pumping station, and all necessary microwave hardware to create and maintain the plasma with microwave power.....219

IV.30 A color photograph of the microwave generator (green) with the microwave hardware installed..... 221

IV.31 A color photograph of the complete microwave generated plasma apparatus for plasma ion implantation studies....222

IV.32 Checkerboard array of oriented ceramic permanent magnets that can be wrapped around a cylindrical containment vessel..... 225

IV.33 Cross-section of the multimode microwave cavity showing the 34 columns of permanent magnets equally spaced in the azimuthal direction.....227

IV.34 Geometrical configuration of permanent magnets on top and bottom flange plates.....228

IV.35 Valving system for high vacuum pumping station used in the microwave generated plasma ion implantation experiment.....234

IV.36 A mass spectrum taken with the microprocessor-based mass spectrometer set up in the analog mode for a mass range of 2 to 250 Daltons.....241

IV.37 A mass spectrum taken with the microprocessor-based mass spectrometer set up in the histogram mode (fast analysis) for a mass range of 2 to 45 Daltons.....243

IV.38 A mass spectrum taken with the microprocessor-based mass spectrometer set up in the analog mode for a mass range of 2 to 45 Daltons.....244

IV.39 A mass spectrum taken with the microprocessor-based mass spectrometer set up in the analog mode for a mass range of 2 to 250 Daltons at a base pressure of 0.77 μtorr with no liquid nitrogen in the cold trap.....245

IV.40 A mass spectrum taken with the microprocessor-based mass spectrometer set up in the analog mode for a mass range of 2 to 250 Daltons at a base pressure of 0.03 μtorr with liquid nitrogen in the cold trap.....246

A.1 An accelerator used as a device for accelerating ions to high energies for ion implantation.....258

A.2 Graph of ion kinetic temperature versus ion number density showing three regions for the ratio of plasma ion implantation to ion beam implantation fluxes.....265

A.3 Graph of electron kinetic temperature versus ion number density (quasi neutral plasma assumed) showing ten regions for the Debye distance ranging from more than 5 cm to less than 0.1 mm.....267

A.4 The case where the Debye distance is much greater than the characteristic radius of the roughness of the surface.....269

A.5 The case where the Debye distance is approximately equal to the characteristic radius of the roughness of the surface.....270

A.6 The case where the Debye distance is much less than the characteristic radius of the roughness of the surface.....271

A.7 A graph of the total exposure time on the ordinate versus the average ion current to the sample on the abscissa for a fixed sample area of 112.5 square centimeters.....281

LIST OF SYMBOLS

β_{nm}	Propagation constant for an nm mode in a circular waveguide
δ_s	Skin depth in centimeters (cm)
ε'	Real part of dielectric constant of a plasma in Henrys per meter (H/m)
ε''	Imaginary part of dielectric constant of a plasma in Henrys per meter (H/m)
ε_o	Permittivity of free space, 8.8542 x 10^{-12} Farads/m
λ_D	Debye distance in meters (m), centimeters (cm), or millimeters (mm)
λ_o	Wavelength of a particular nml mode
Λ	Characteristic diffusion length of a right circular cylinder in centimeters (cm)
μ_0	Permeability of free space, $(1/4\pi)$ x 10^{-7} H/m
ν_c	Electron collision frequency in Hertz (Hz)
π	Pi, 3.1415926535898
ρ	Density of target material in kilograms per cubic meter (kg/m^3)
σ	Electrical conductivity in inverse ohm-meters ($\Omega^{-1}m^{-1}$)
σ	Complex conductivity associated with Lorentz model for electron collisions ($\Omega^{-1}m^{-1}$)
σ_r	Real part of complex conductivity in inverse ohm-meters ($\Omega^{-1}m^{-1}$)
σ_i	Imaginary part of complex conductiviey in inverse ohm-meters ($\Omega^{-1}m^{-1}$)
Φ	Azimuthal angle in degrees (°)
Φ_{ibi}	Flux of ions emitted from an ion source used in ion beam implantation in ions per square meter per second (ions/m^2-sec)
Φ_{pii}	Flux of ions incident upon a Langmuir probe in ion saturation used in plasma ion implantation in ions per square meter per second (ions/m^2-sec)
ω	Driving frequency of microwave energy in radians per second (rad/sec)

ω_{pe}	Electron plasma frequency in radians per second (rad/sec)
a	Radius of right circular cylinder in centimeters (cm)
A_o	Avogadro's number 6.023 x 10^{26} in atoms per kilogram-atom (atoms/kg-atom)
A_{sh}	Surface area of sample exposed to plasma in square centimeters (cm^2)
$A+$	Constant for positive electromagnetic wave
A^-	Constant for negative electromagnetic wave
d	Length of right circular cylinder in centimeters (cm)
d	Distance between accelerating grids in meters (m)
e	Electronic charge, 1.602 x 10^{-19} Coulombs
E	Energy stored in plasma as a result of electrons and ions in Joules (J)
E_{max}	Maximum electric field within the cavity resonator
E_o	Electric field between accelerating grids in kilovolts (kV)
E_r	Radial electric field distribution in the multimode microwave cavity
E_z	Axial electric field distribution in the multimode microwave cavity
E_ϕ	Azimuthal electric field distribution in the multimode microwave cavity
f	Driving frequency of microwave energy in Hertz (Hz)
f_{nml}	Resonant frequency for each resonant mode in Hertz (Hz)
F	Duty cycle pertaining to the switching signal in percent (%)
F_{ions}	Fluence of ions incident upon sample surface area in ions per square centimeter (ions/cm^2)
H_r	Radial magnetic field distribution in the multimode microwave cavity
H_z	Axial magnetic field distribution in the multimode microwave cavity
H_ϕ	Azimuthal magnetic field distribution in the multimode microwave cavity
I_{Anode}	Penning discharge anode current in milliamperes (mA)
$\bar{I}_{sh}$	Average ion current flowing into sample in milliamperes (mA)
j	Imaginary unit, square root of -1

J_{Ibl} Current density for space-charge limited current flow used in ion beam implantation

$J_n(p'_{nm} r / a)$ Value of the Bessel function of the nth kind at a radius **r** for a fixed inside radius of **a**

k Boltzmann's constant, 1.3807 x 10^{-23} Joules/K

$k_{c,nm}$ Eigenvalues for the propagation equation

k_0 Wave number for each resonant mode in meters (m^{-1})

l Depth of implantation in micrometers (μm)

l 3rd mode number in a circular waveguide of a non-zero length describing the number of maxima in the axial direction

L Length of plasma column in Penning discharge in meters (m)

m 2nd mode number in a circular waveguide describing the number of maxima in the aximuthal direction

m_e Electron mass, 9.109 x 10^{-31} kg

m_i Ion mass in kilograms (kg)

M_1 Atomic mass number of implanted ion in kilograms per kilogram-atom (kg/kg-atom)

M_2 Atomic mass number of target atoms in kilograms per kilogram-atom (kg/kg-atom)

n 1st mode number in a circular waveguide describing the number of maxima in the radial direction

n_e Electron number density in electrons per cubic centimeter (electrons/cm^3)

n_i Ion number density in ions per cubic centimeter (ions/cm^3)

N Number density of implanted ions in ions per cubic meter (ions/m^3)

N.E. Total number of negative pulses (exposures) for the sample must be exposed to achieve the desired effect

$N_{ions\ implanted}$ Total number of ions implanted during elapsed process time in ions (ions)

p'_{nm} Roots of the derivative of the Bessel function

P Power transferred to a gas per unit volume in Watts per cubic meter (W/m^3)

P_l Power loss in the walls of a right circular cylindrical cavity resonator in Watts (W)

P_{Input} Power input to the Penning discharge plasma in Watts (W)

Q	Total charge contained in plasma in Coulombs (C)
Q	Quality factor of a microwave cavity resonator (no dimensions)
Q'	Loaded quality factor including loss due to walls and plasma (no dimensions)
Q_d	Plasma quality factor (no dimensions)
r	Radial length used in Bessel functions to describe electromagnetic field distributions in centimeters (cm)
R	Characteristic radius of the surface roughness of a metal (units correlated with Debye distance)
R_m	Surface resistivity of an electrical conductor in ohm-meters (Ω-m)
t_c	Plasma particle containment time in microseconds (μsec) or microseconds (μsec)
t_e	Plasma energy containment time in microseconds (μsec) or microseconds (μsec)
t_{ept}	Elapsed time from the beginning of the plasma ion implantation process to the end in minutes (min)
t_{max}	Time for all plasma ions to be withdrawn through sample in seconds (sec) or minutes (min)
$t_{nb\ off}$	Time for which there is no negative bias applied to the sample during one period in microseconds (μsec)
$t_{nb\ on}$	Time for which the negative bias is applied to the sample during one period in microseconds (μsec)
t_o	Total plasma ion implantation exposure time in seconds (sec) or minutes (min)
T	Period of the switching signal in microseconds (μsec)
T_e	Electron kinetic temperature in degrees Kelvin (K)
T_e'	Electron kinetic temperature in electron-volts (eV)
T_i	Ion kinetic temperature in degrees Kelvin (K)
T_i'	Ion kinetic temperature in electron-volts (eV)
TE_{nml}	Transverse-electric electromagnetic wave in a right circular cylinder
U_{max}	Maximum stored energy in a maximum electric field in Joules (J)

V	Volume of right circular cylindrical cavity resonator in cubic meters (m^3)
v_i	Arithmetic mean speed of ions in meters per second (m/sec)
V_b	Voltage applied to the cathode of the high-voltage switching circuit in kilovolts (kV)
V_i	Effective ion accelerating voltage used in plasma ion implantation in kilovolts (kV)
V_o	Accelerating voltage between two grids in kilovolts (kV)
V_p	Plasma potential in kilovolts (kV)
V_{plasma}	Volume of plasma in cubic meters (m^3)
W	Stored energy in a right circular cylindrical cavity resonator in Joules (J)
X	Mole fraction of implanted species in percent (%)
z	Length along the axis of the right circular cylinder used in the Bessel functions when describing the electromagnetic fields in centimeters (cm)
$Z_{h,nm}$	Wave impedance for each mode in Ohms (Ω)
Z_o	Characteristic impedance of free space, 377 Ω

CHAPTER 1

INTRODUCTION

A. The Materials Problem

Nearly all engineering applications, dating from the early 16th century to our present technologically-based, 20th century world, required the use of elemental metals or alloys to perform the required tasks reliably and efficiently. Many of these metallic materials are subject to conditions which may degrade their characteristic properties. Since, in most cases, the surroundings or conditions cannot be altered, the only other way to maintain performance is to change the characteristic properties of the material. Such characteristic properties include wear resistance, hardness, corrosion and fatigue resistance, electrical, magnetic, optical, and nuclear properties.

B. The Corrosion Problem

The characteristic property of interest in this research is corrosion resistance. This property is one of the most important in the field of materials science and engineering, since degradation of the structural properties of many metals often occurs as the metal surface is continuously attacked due to corrosion reactions. Many

current corrosion problems arise from the use of light-weight, strong materials of military interest in marine environments. These applications include large ships at sea, where different types of steel are used, and aircraft exposed to corrosive marine environments, where aluminum alloys are used. Other sectors where corrosion inhibition is important include the chemical industry, where reactive chemicals must be processed or transported in containers which do not react with their contents. Another application of great importance to the health of the population, is corrosion processes associated with bacterial growth on the inside walls of underground piping used to transport "clean and treated" water.

C. Early Processes to Inhibit Corrosion

Early methods of protecting the surfaces of metals against corrosion involved the application of specialized liquids or paints. Later, galvanization and electroplating processes were developed to further protect the surface of a metal in a corrosive environment, usually in pipes. The spray coatings were also used. The addition of a small amount of one type of metal to another, called alloying, has been used extensively to reduce corrosion. However, alloying can have disadvantages, such as increased cost and/or a decrease in the strength of the material. Thus, alloying is infeasible in many applications. Surface treatments, mentioned above, have their disadvantages too. In many cases, corrosion eventually develops

between the coating and the substrate. Also, another problem with surface coatings is that it can be difficult to allow for the variable thicknesses of a coating when fabricating precision-fitted parts for corrosive environments (Dearnaley, et al., 1973).

Since the ultimate objective of the research being conducted here is to enhance the corrosion resistance of metals, it is necessary to briefly explain some of the underlying metallurgical principles relating to the effects of ion implantation. The enhancement of the aqueous corrosion resistance of substrate materials by implantation of high energy ions can be carried out by creating novel alloys in a thin surface layer, and by enhancing the passivation characteristics of the material. A thin novel alloy layer is composed of the substrate material (majority volume) and the ion-implanted material (minority volume) and is difficult or impossible to obtain using diffusion techniques. The percentage of alloying is a function of implantation time and ion fluence. Enhancing passivation characteristics involves the creation of a layer buried within the surface which forms a passive surface on the material. Enhancement of corrosion resistance can also be achieved by creating an amorphous or glassy surface layer, leaving the resulting surface resistant to corrosion attack at the grain boundaries, where corrosion often occurs (Destefani, 1988).

D. Historical Review of Ion Implantation

A process to inhibit corrosion, which makes no use of surface coatings by either self-induced chemical reactions (painting or spraying) or electromotive force-driven reactions (electroplating), originated with an observation made in the 1930's that high energy particles can produce significant physical changes in the surface of certain solid materials. At that time, such modification of surfaces was simply viewed as undesirable.

Further stimulus arose from an interest in the 1940's in investigating the effects of high energy neutron bombardment on materials used in early nuclear reactors. Also, at about this time, developers of materials for the nuclear reactor industry became interested in the penetration depth of a high energy ion in a material.

Efforts to improve the performance of electronics by modifying the electrical properties of semiconductors led to the investigation of methods to dope these materials to further improve their performance. In the early 1950's, a silicon diode material was bombarded with helium (He) ions which led to improved performance as a rectifier. In the mid 1950's, germanium (Ge) was bombarded with an energetic beam of several types of ions. These were the first known attempts to alter a material's properties using energetic ions. In 1957, Shockley, a great contributor to the field of materials applied to electronics, obtained one of many patents on the "ion-implantation" technique (Dearnaley, et al., 1973).

After semiconductor researchers achieved satisfactory state-of-the-art results, further development of ion accelerators took place in laboratories where ion beam production and handling was well-developed, including the Oak Ridge National Laboratory. These laboratories began studying ion motion through crystals. About 1965, the first international meeting took place at Aarhus University in Denmark. Leaders in the field of ion beam production and interactions from Oak Ridge National Laboratory and elsewhere met to initiate studies of ion channeling and ion penetration. These and similar interests continued to attract scientists to this new field, called ion implantation. The underlying physics and technology of ion implantation became the primary interest of investigators at the Atomic Energy Research Institute in Harwell. Also included among their activities were the design of machines capable of carrying out this new process on an industrial scale for the semiconductor industry.

The first meeting of a regular series of conferences was held in 1970 on "Applications of Ion Beams to Semiconductor Technology", in Thousand Oaks, California. A series of meetings on atomic collision processes in solids was held starting in 1973 at Gatlinburg, Tennessee (Dearnaley, et al., 1973).

E. Ion Implantation Processes

The well-developed technology of ion beam sources has made it possible to focus research on ion implantation processes instead of ion production processes. This, along with the strong interest in changing material characteristics for semiconductor and other applications, is the reason that ion implantation techniques using ion beams have become so widespread. Ion beam implantation is a low-temperature process, and for this reason, only the surface properties of the metal are affected. A new process, plasma ion implantation, will be compared with ion beam implantation in the next chapter. This process is of interest to the ion implantation community because of its potential for implanting complex objects in a single exposure and in a shorter exposure time.

1. Ion Beam Implantation

Ion beam implantation has demonstrated that implanting high energy ions into metal surfaces has desirable effects on the characteristic properties of metals. Ion beam implantation results from the extraction of low energy ions from an ion source and their acceleration to high energy. The ion source is usually a plasma, made up of ions, electrons, and some neutral atoms. Figure I.1 is a schematic of a generalized ion beam implantation system. The ions are extracted from the plasma by a negatively-biased grid near the

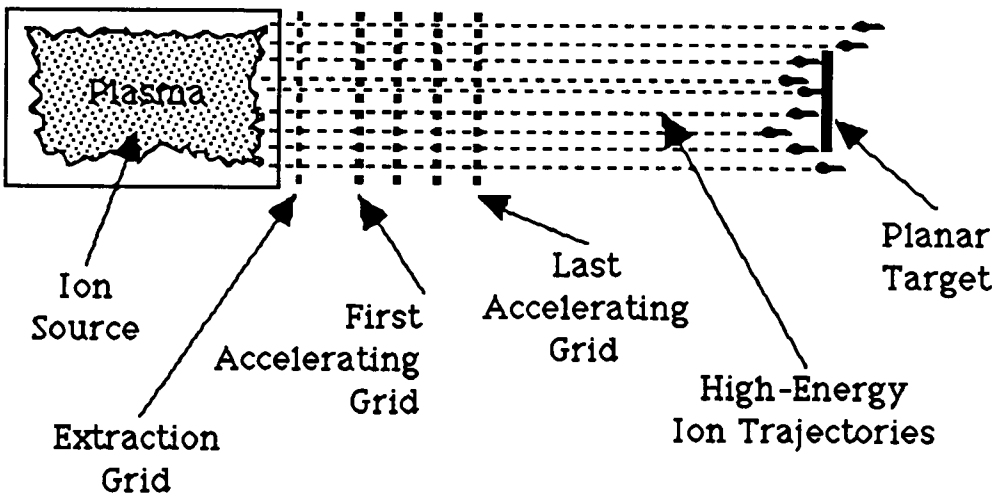


Figure I.1 Conventional ion beam implantation system showing ion source, extraction grid, accelerating grids, high-energy ion trajectories, and planar target.

plasma boundary. Once captured by electric fields associated with this grid, they are accelerated through one or more additional negatively-biased grids until they reach the desired energy. The ion beam is then unidirectional, with the ions traveling with parallel trajectories. A target, at the opposite end of ion source and aligned with the central axis, is normally bombarded on surfaces perpendicular to the ion trajectories. In order to implant an object of complex shape, the surface of the target must be manipulated to be normal to the ion beam. Target manipulation requires the installation and operation of complicated mechanical linkages, which, in most cases, are unique to the object undergoing implantation. This equipment significantly increases the cost of the implantation process.

2. Plasma Ion Implantation

a. Low-Voltage Plasma Ion Implantation

Low-voltage plasma ion implantation can be referred to as plasma surface modification. This technology is used in the fabrication of microelectronic circuits for the semiconductor industry. It is important to distinguish between low- and high-voltage plasma ion implantation, since both processes utilize a negative biasing voltage but are totally different in their application. In one form of low-voltage plasma ion implantation, a substrate is biased negative

to as much as -200 Volts to attract reactive ions to etch a trench in the substrate (Cowburn, 1983). In high-voltage plasma ion implantation, the negative bias can be as low as -2 kV, and can assume values above - 50 kV. In this technology, ions are attracted to a metal surface and are implanted into the surface. This research is focused on high-voltage plasma ion implantation.

b. High-Voltage Plasma Ion Implantation

High-voltage plasma ion implantation did not originate at the University of Tennessee's Plasma Science Laboratory, but with efforts of the group at the University of Wisconsin. After researchers at the University of Wisconsin had the idea of submerging an object in a plasma and biasing it to a highly negative voltage with respect to the plasma, it was found that the plasma was quenched when the implantation process was carried out (Conrad, 1989). The negative potential was applied to the sample by simply closing the switch in Figure I.2. The idea was to get the ions into the target surface by creating a strong electric field near the surface to attract the ions. The ions were attracted to the surface so well that all of the ions exited the plasma and it quenched. Under these conditions, no plasma ion implantation can take place.

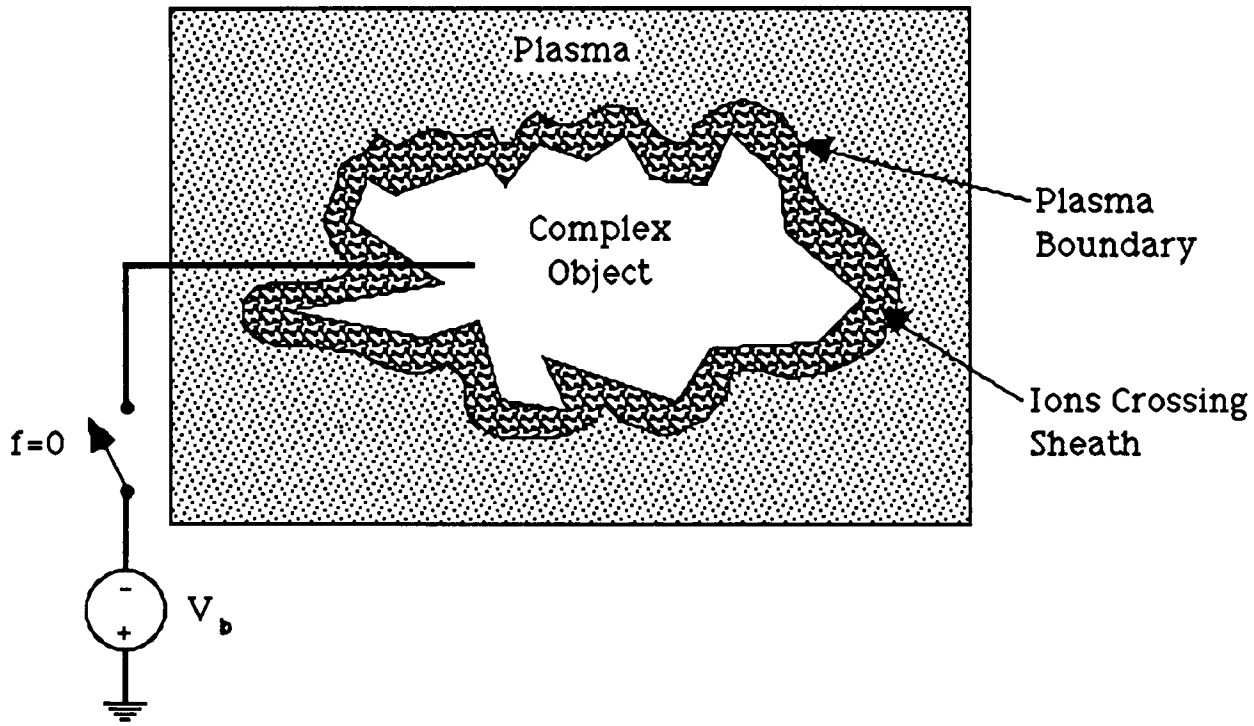


Figure I.2 Initial arrangement for plasma ion implantation of a complex metallic object immersed in a plasma. The plasma "hugs" the object and forms a sheath where ions are accelerated before bombarding the surface. The switch represents the connection of the power supply to the sample holder. When the switch is closed, all of the available ions in the plasma are drawn into the target and the plasma is quenched.

c. Incorporating a Switching Circuit

After initial attempts to implant a target in a plasma using a constant biasing voltage, it was determined that biasing the target for a short time, and then turning the bias off, was the correct procedure to use. The duration of the bias voltage was not important, as long as it removed only a small population of ions from the plasma. Figure I.3 is similar to the arrangement in Figure I.2 but with a device that opens and closes a switch at a low frequency, f. The time between the high-voltage pulses is long, but variable. During the time that the bias is turned off, the plasma replenishes ions lost due to implantation (Keebler, et al., 1989).

After realizing that some type of electrical switch was needed, a high-current pulse modulator, which had been developed for other research programs, was applied at the University of Wisconsin. This circuit employed a high-current (8 A), high-voltage vacuum tube with minimal electronic control circuity. No stablized power supply, which supplied the power across the cathode and anode of the tube was used. The same capacitor bank, used in the initial attempts at ion implantation, was used as the power source to the pulse modulator (Conrad, 1988).

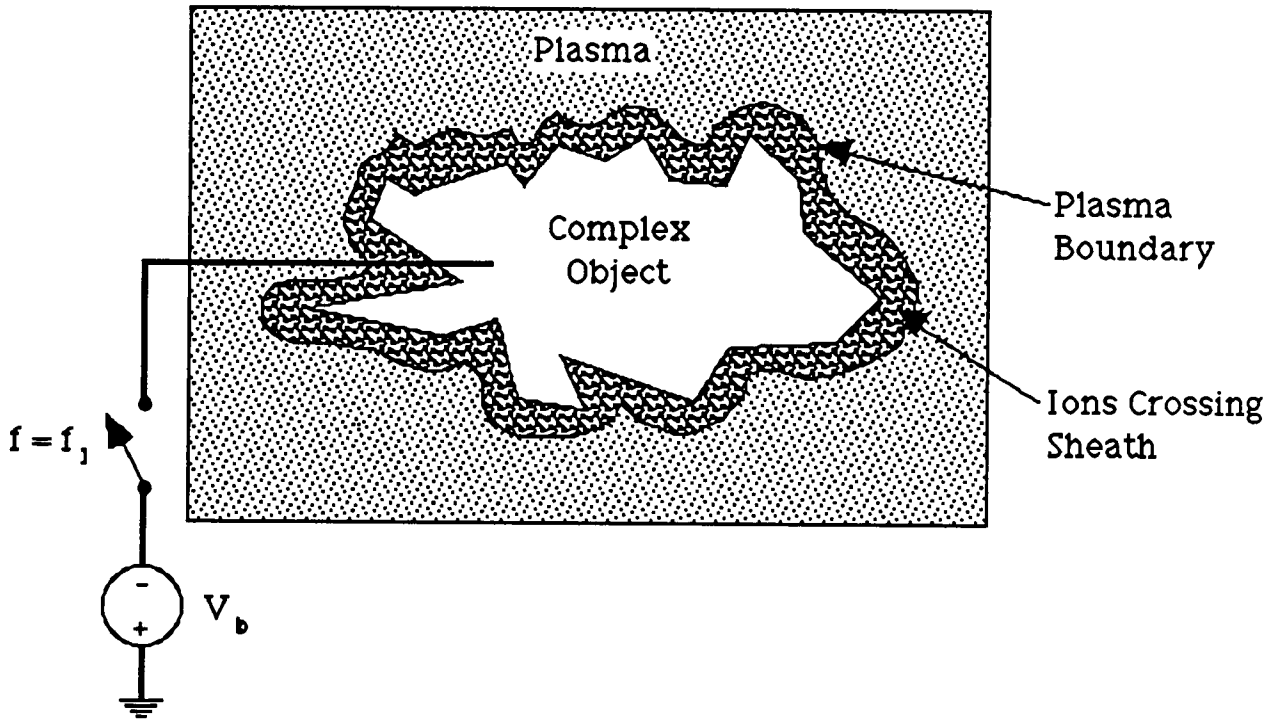


Figure I.3 Plasma ion implantation of a complex metallic object immersed in a plasma. The plasma "hugs" the object and forms a sheath across which ions are accelerated before bombarding the surface. The switch represents the pulse-modulator (switching circuit) which opens and closes at the frequency, f, and the positively-grounded power source represents the high-voltage power supply for the energy of the ions.

d. A Call for a Faster Switching Circuit

After becoming interested in the field of plasma ion implantation, J. R. Roth at the University of Tennessee, initiated a new research program. Roth called for the design of an electronic switching circuit suitable for plasma ion implantation. Roth engaged the services of John E. Crowley, an experienced designer of electronics and a former Graduate Research Assistant in the UTK Plasma Science Laboratory, to design such a circuit. At this point, Roth had already formulated a first approximation (Roth, 1986) to the theory of plasma ion implantation based on a Langmuir probe in ion saturation. Results of this first approximation predicted approximate switching times that must be incorporated into the design of this new switching circuit. A macroscopic theory of plasma ion implantation is presented in Appendix A and the design strategy and new high-speed switching circuit are presented in Chapter 2.

CHAPTER 2

A HIGH-VOLTAGE SWITCHING CIRCUIT FOR PLASMA ION IMPLANTATION

In Appendix A, where a rough, macroscopic approximation to the theory of plasma ion implantation is presented, it is shown that the high voltage pulse width, $t_{bias\ on}$, must be less than or equal to the plasma particle containment time, t_c, and the time required for all of the ions in the plasma to be removed through the sample holder, t_{max}. These times are given by Equation (A.24). Now that the single pulse exposure time has been established, a switching circuit capable of operating at high voltage over a range which can be adjusted to this maximum time, must be developed.

A. Switching Circuits

Before deciding upon the switching circuit to be used for plasma ion implantation, its design requirements must be considered. They are the following:

- Since the implantation species is a positively-charged ion, the implantation bias voltage must be negative.
- Since the single pulse exposure time depends upon the electrically conducting area of the sample holder exposed to the plasma, as well as several of the plasma parameters, the on-time and the duration between pulses of the power switching tube must be adjustable.

- Since it is desirable to minimize the total time required to expose a sample in the plasma, fast switching is required.

- Since the sample bias must be negative and of high voltage to obtain the desired implantation effects, the switching circuit can be electrically isolated from all other exterior potentials.

- If electrical isolation is utilized, the switching circuit can most simply employ an exterior fast pulse forming circuit.

- Since the switching circuit requires electrical power to operate the necessary electronic components to meet the above requirements, a power source must be included in the design.

- Since the depth of the implanted species is very dependent upon the magnitude of the negative high-voltage pulse, it is desired that the pulse be as uniform as possible during this time.

High-voltage electronic circuitry is needed to meet the above design requirements. Several design approaches are possible, and one design, other than the one presented here, will be discussed briefly for comparison and illustration. A solid-state, high-voltage switching circuit which can switch voltages greater than 1,000 Volts in switching times as small as a few microseconds has been tested (Bernius, et al., 1989). This circuit uses a transistor-transistor logic (TTL) control signal which triggers an optoisolator device serving as the high voltage isolation between the control circuit and the switching transistors. These transistors are MOSFETs, which have only 1,000-Volt blocking capability, the maximum available. Thus, a stacking of these devices is required to deal with high-voltages. This

is a disadvantage for voltages as high as 100,000 Volts, and becomes very costly to implement. For voltages no higher than 25,000 Volts, this switching mechanism could be economically employed. The design of Bernius (Bernius, et al., 1989) requires that a significant number of semiconductor components float at the negative high-voltage. The above design requirements could be met using this design, but the complexity of the circuit suggests that the switching circuit discussed below is superior for plasma ion implantation.

The switching circuit chosen for this application meets all of the above design requirements, with the additional advantage of using a small number of semiconductor components. The major component used in this circuit is an internal anode forced air cooled tetrode vacuum tube with a plate (anode) dissipation of 1,000 Watts maximum. The basic approach of this design is to use this power tube as the switching element to apply negative high voltage to the sample in the plasma. A detailed discussion of this power tube is given below. The high-voltage switching circuit utilizes a small number of semiconductor components, powered by off-the-shelf DC to DC power converters and/or simple voltage-regulated power circuits, to supply the filament heating and grids of the power tube. The control of the high-voltage switching circuit is established by a high-speed fiber-optic link which provides the necessary high voltage isolation.

B. Ideal Switching Voltage Signals

The nature of the ion implantation voltage switching signal was presented earlier. It must have adjustable on- and off-times (period), the desired amplitude, and a square negative high-voltage pulse during the on-time. In addition, it is also desirable to minimize the rise and fall time of the implantation voltage pulse. Pictured below in Figure II.1 is an ideal implantation voltage signal. The abscissa is the time axis. The high-voltage switching circuit must turn off the voltage to the sample to allow the plasma to recover from its lost ions. The sum of all the bias-on time intervals is the total exposure time during which ion implantation occurs. The ordinate is the negative high-voltage axis and can range from 0 to -50,000 Volts in this research. Notice the constancy of the voltage during the bias-on time interval. This is desirable to achieve constant-energy ions during implantation.

Another characteristic of an ideal switching voltage signal is to have the capability of adjusting the bias-on and bias-off times with the turn of a knob exterior to the high-voltage switching circuit. The duty cycle, given by Equation (A.27), should be adjusted to keep the total required exposure time for a fixed ion dose to a minimum, subject to other constraints, such as sample heating. Obviously the duty cycle cannot be 100%, or the high-voltage switching circuit would not be needed and the plasma would quench due to loss of its ion population. Duty cycles as low as 2% (bias-on time is 20 microseconds, bias-off time is 1 millisecond) can be carried out,

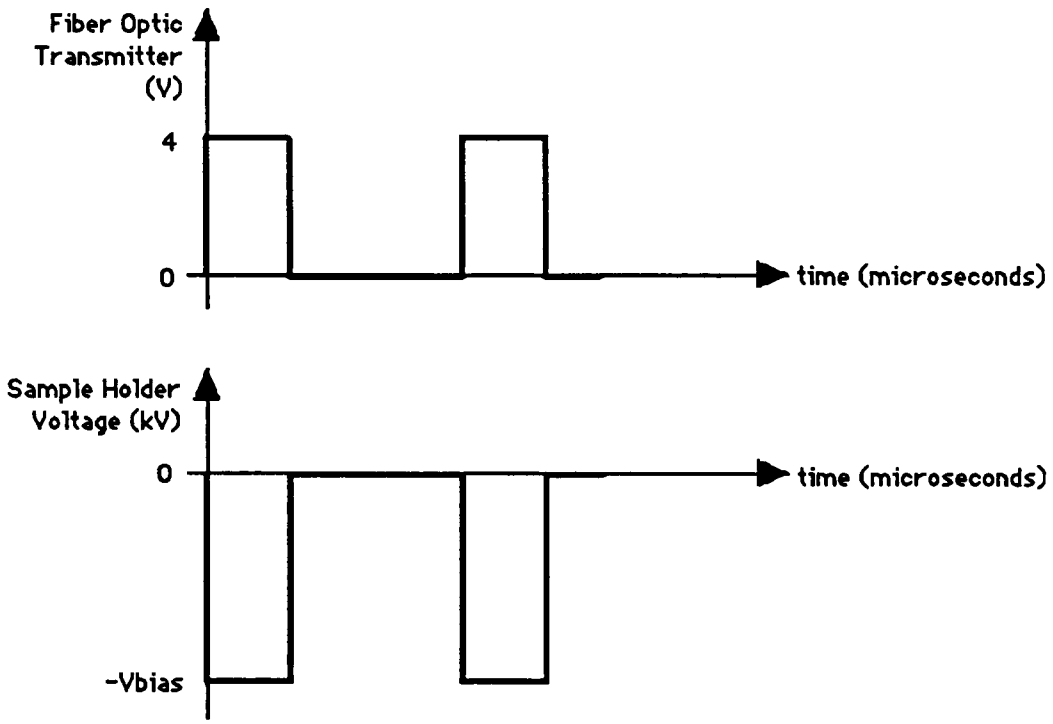


Figure II.1 An ideal switching voltage signal generated by the high-voltage switching circuit when receiving a signal from the fiber optic transmitter.

resulting in total exposure times around 20 minutes and beneficial ion implantation effects. If large objects are to be implanted, requiring large ion currents and large anode power dissipation in the vacuum tube, the average power can be decreased by lowering the duty cycle. This also increases the total exposure time. If small objects are to be implanted, such as screws, gears, or cutting edges of knives or blades, the duration of the implantation voltage can be decreased to a limit determined by the minimum of the plasma particle containment time and the time required for all ions to impinge upon the sample. If the bias-on time is the maximum allowed for implantation, then the bias-off time must be at least as long to allow the plasma to recover. Recovery is assured if the bias-off time is at least three times the bias-on time, resulting in a maximum duty cycle of 33.3%.

In summary, decreasing the duty cycle increases the total exposure time, lowers the power dissipated across the vacuum tube, lowers the average ion current flowing from the plasma, reduces the power required by the ion implantation power source, and lowers the power required to operate the high-voltage switching circuit. Thus, an adjustable period and bias-on time is a definite advantage.

C. Required Isolation of Switching Circuit

Because a high-voltage power supply is necessary to implant an ion species to the desired depth, it is also necessary to include

isolation to separate the high-voltage from the laboratory environment. The isolation barrier chosen is 3/4" (1.9 cm) thick Acrylite plexiglass, which can provide electrical isolation up to 375 kV for a 3/4" (1.9 cm) thickness (relative permittivity is 3.40). One of the electrical connections made through this isolation barrier, indicated in Figure II.2, is from the negative side of the implantation power supply to the cathode of the vacuum tube. This connection is made by an RG-8/U coaxial cable. The center conductor of the cable is connected to the cathode of the vacuum tube with a ceramic insulating standoff inside the high-voltage switching circuit. Isolation of the center conductor is provided by the cylindrical dielectric which is good below 50,000 Volts. The braiding of this coax is removed to expose the dielectric to a distance of about 12" (30.5 cm) away from the box, and is connected to ground. The other electrical connection made through this barrier is from the anode of the vacuum tube to the sample holder in the plasma. This connection is made with the center conductor and dielectric, with the braiding and outside plastic covering entirely removed along the entire length of the cable. This reduces the capacitance between the sample holder and ground. The length of this cable is about 4' (121.9 cm) and is kept to a minimum to reduce capacitive effects. There is no physical connection between the anode of the vacuum tube and any other component inside the high-voltage switching circuit. Another connection is made through this isolation barrier for the pulse control system. This connection is a fiber-optic light guide provided by Hewlett-Packard. Total electrical isolation is provided by this light

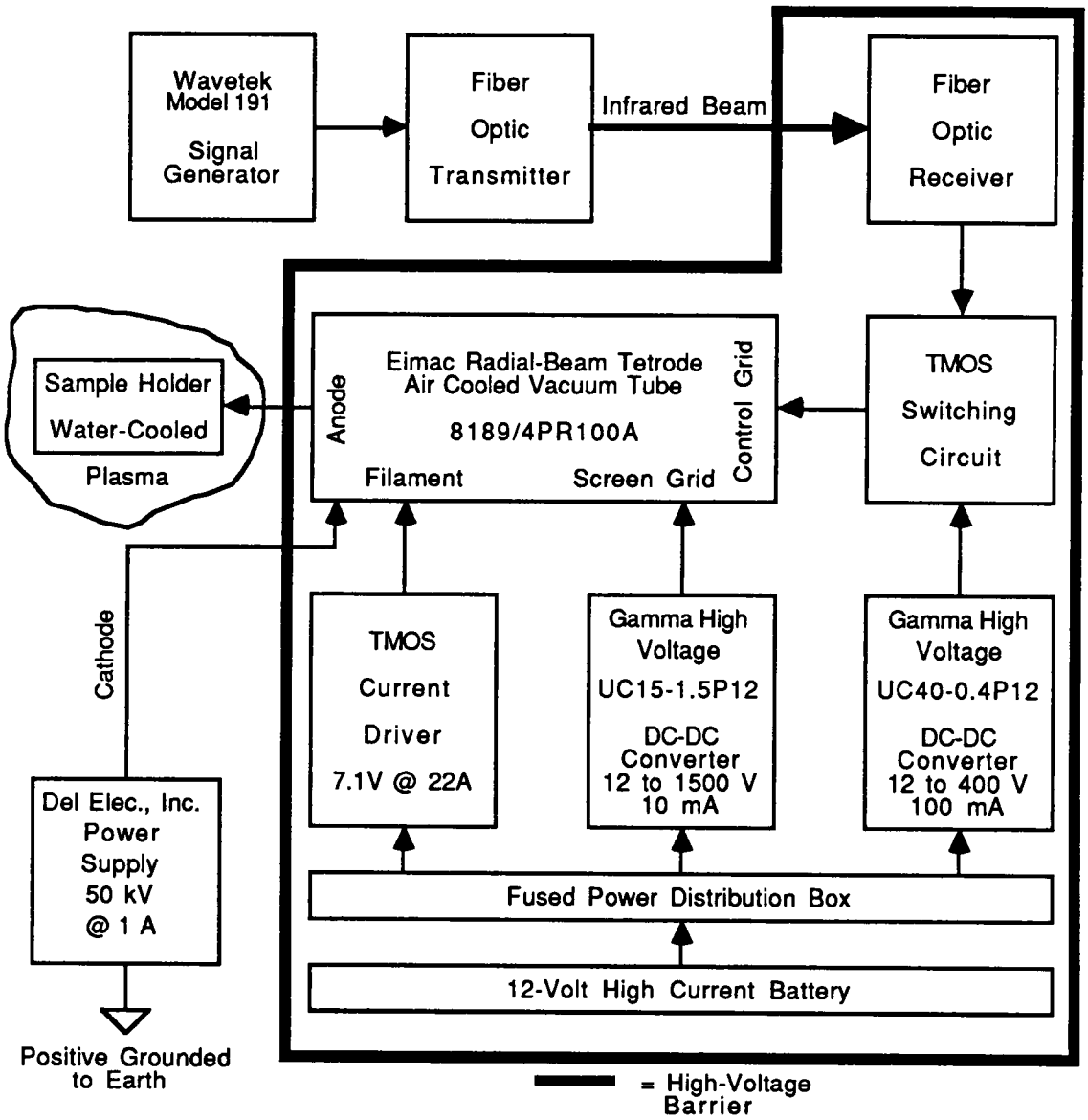


Figure II.2 Block diagram for high-voltage switching circuit showing the major components including the Del Electronics 50 kV, 1 A implantation power source with a low internal impedance.

guide cable. All three of these cables are inserted through the 3/4" (1.9 cm) plexiglass via a small hole.

Since air cooling is required inside the high-voltage switching circuit, which must be vented through a series of holes with cooling fans, high voltage protection must be included in these areas. Each cooling fan, located on the outside, has a screenwire mesh placed on the outside of the fan. This mesh is grounded, which is intended to protect users from danger if an arc occurs near any of the cooling fans. The remaining holes drilled into the plexiglass from the outside are filled with silicone caulking.

Since the high-voltage switching circuit must be accessible for modifications, adjustments, and repairs, the top of the plexiglass enclosure is removable. This top rests on the plexiglass enclosure. A small air gap exists between the top and the upper edge of the enclosure. To protect against arcing through this gap, five layers of 3" (7.6 cm) wide mylar film are fixed to this area. Each layer of mylar film can stand off about 20,000 Volts. The corners of the plexiglass enclosure, even though they are glued together with plexiglass cement, are also covered with five layers of mylar film.

Not only is the high-voltage switching circuit a potential danger to users, but the sample holder assembly (to be discussed later), which extends to the outside of the vacuum system, is at high-voltage. Two protective issues arise here: isolation of the sample holder from users, and isolation of the cooling water entering and leaving the sample holder. The shield constructed for this sample holder serves multiple functions. It is a 22" (55.9 cm) section of 10"

(25.4 cm) Schedule 40 PVC piping. This piping serves as a support for two 20' (6.1 m) lengths of rubber hose coiled inside, for each water connection. These lengths are coiled in an opposing fashion in parallel such that a potential gradient is formed along an effective resistance of about 7 megohms from the point of water entry/exit on the sample holder to the point where the rubber hose is connected to two grounded copper water lines. The rubber hoses pass through two tightly-fitted holes in the bottom of the PVC cylinder. The amount of the potential gradient is inversely proportional to the length of rubber hose, and the leakage current is proportional to the conductivity of the water. A length of 20' (6.1 m) for each line is sufficient to ensure that the resistance of the water is high enough to avoid large parasitic current losses. The PVC cylinder, along with a Veeco-fitted A-lite stand-off insulator which is rated above 50 kV, also protect users from the high voltage. The end of the PVC cylinder is capped with a 1/4" (0.64 cm) thick circular plexiglass plate. The anode of the vacuum tube in the high-voltage switching circuit is connected to the sample holder through a small hole in this PVC cylinder. A high-voltage probe, used to monitor the implantation voltage signal, is connected to the sample holder end through another small hole in the side of the PVC cylinder. This probe is rated at 20,000 Volts DC and 40,000 peak Volts AC and derates in voltage with frequency. It has been useful up to 50,000 Volts in this experiment.

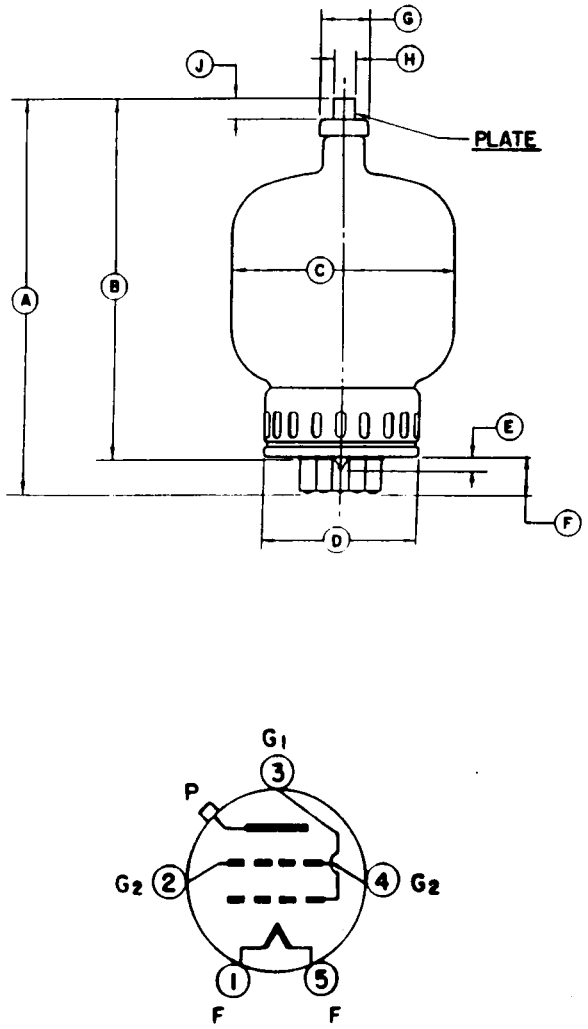
A final isolation barrier, which is used to shield against radio frequency interference (to be discussed later), also serves as a

secondary shield from the high-voltage. This is constructed of ordinary grounded screenwire which is about 18" (45.7 cm) from all high-voltage areas and covers all exposed areas where high-voltage or radio frequency fields may be present.

D. The Switching Element and Signal Flow Diagrams

As mentioned earlier in this thesis, the major component of the high-voltage switching circuit is the internal anode forced air cooled tetrode vacuum tube. This tube is an Eimac (Varian) Model 4PR1000A/8189 radial-beam pulse tetrode which can be used as a pulsed-modulator, pulsed-oscillator, or pulsed-amplifier. The tube dimensions and its pin out diagram are shown in Figure II.3. Such a vacuum device is quite expensive (about $1,000.00). This tube features reduced internal coupling between input and output, low internal inductance and capacitance, improved linearity, and high operating efficiency. It is designed for long operating life, is built to withstand electrical and physical abuse, and can operate under extreme environmental conditions. The tube requires a minimum of 150 Watts filament power. The power tube, as a pulsed modulator, has the ratings listed in Table II.1.

This power tube utilizes free electron flow through a vacuum and has an emitting cathode, and one collecting surface, the anode. The control and screen grids are used to control the flow of free electrons emitted from the directly-heated cathode. This high power



Dimensional Data (Dimensions in Inches)	
Reference	Nominal
A	9.250
B	8.375
C	5.250
D	3.625
E	0.313
F	0.875
G	1.250
H	0.566
J	0.484
K	60
L	30
M	30
N	1.500
P	0.374

Figure II.3 Side view of the power grid tube showing the dimensions. Also pictured is a pin out diagram showing the cathode connections (1 and 5), the control grid connection (3), the screen grid connections (2 and 4), and the anode connection (P) for plate.

Table II.1

High Power Switching Tube Ratings and Characteristics

Maximum Rating or Characteristic	Value
DC Plate Voltage*	30 kV
DC Screen Voltage	2.5 kV
DC Grid Voltage	-1.0 kV
Peak Plate Current	8.0 A
Plate Dissipation (Average)	1 kW
Screen Dissipation (Average)	75 W
Grid Dissipation (Average)	25 W
Filament Voltage	7.5 V
Filament Current	22.7 A
Grid-Plate Capacitance	0.35 pF
Input Capacitance	32.4 pF
Output Capacitance	9.4 pF

*50 kV may be achieved using short tube on times.

tube is rated at 1000 Watts anode dissipation. The directly-heated cathode is a thoriated tungsten filament (Varian, 1989) in which thorium oxide is added to the filament to increase electron emission. This filament is carburized to reduce the evaporation of thorium oxide from the filament. This filament is also tolerant to ion bombardment and thus allows the application of high voltages to the tube. Filament operating temperatures are about 1900 °K and provide emission of 70 to 100 milliamperes per Watt of filament heating power. The filament is a typical bar filament with spring loading to compensate for thermal expansion.

The control grid is made up of a series of equally-spaced grid bars and is mounted closest to the cathode. This grid controls the flow of electrons from the cathode to the anode. When the control grid is biased negative with respect to the cathode, electrons cannot flow from the cathode, because of the repelling electric field between the control grid and the cathode. When there is no potential between the cathode and control grid, the emission of electrons from the cathode occurs freely, limited by capacitance between the anode and control grid.

To reduce this capacitance, a second grid, called the screen grid, was added to the triode, resulting in a tetrode. The tetrode is being used in our application. The effects of biasing the screen grid positive with respect to the cathode are as follows. Interception of the electric field of the anode by the screen grid reduces the capacitance between the anode and the control grid to a very low value. Some capacitance does exist between the screen grid and the

anode. This can be placed in parallel with the load impedance (plasma) by shorting the screen grid to the cathode. Here, the screen grid to anode capacitance does not result in an increased effective capacitance. However, such a connection will reduce the anode current to zero since the screen grid is now shielding the anode from the control grid and the cathode. The result of this is that no electrons are attracted to the anode and no current will flow through the tube. To overcome this, the screen grid is positively biased with respect to the cathode.

With the control grid biased negative and the screen grid positive with respect to the cathode, the electrons do not see the electric field created by the screen grid, only that of the control grid, a repelling field. This results from precision alignment of the grid bars of the control and screen grids, making the tube sensitive to shock.

With the control grid at zero potential and the screen grid biased positively, the electrons see the potential at the screen grid and they are accelerated towards the anode. Those that strike the grid bars of the screen grid are captured, but those which pass through the gaps arrive at the anode and constitute a current through the tube. The electron flow due to electrons passing through these spacings is much greater than that lost on the screen grid bars.

In this application, the cathode is directly heated by a filament supply, the control grid is pulsed on and off by a TMOS switching circuit, and the screen grid is held at a constant potential by a DC to DC converter. The potential of the implantation voltage applied to

the cathode is increased as the ion implantation process gets under way, until a desired value is reached. The high-voltage switching circuit is then turned on, and the ion implantation power source is then energized. As long as the ion implantation voltage is below the screen voltage of about +2,000 Volts, electrons emitted from the cathode, which pass through the control grid when its at zero potential, are decelerated after passing through the screen grid. However, they reach the anode because of their kinetic energy, acquired as they travel from the cathode to the screen grid. This is why one sees an implantation voltage signal as the implantation power supply is first turned on. In this voltage range (0 to +2,000 Volts), electrons striking the anode do not create very many secondary electrons.

As the implantation voltage approaches the screen grid potential under the same switching conditions, electrons that pass through the screen reach the anode with negligible change in energy. Secondary electrons may be produced more readily and may reach the screen, if they have sufficient kinetic energy to overcome the effects of any space charge on the screen grid.

As the implantation voltage is increased above 2,000 Volts, *all* the electrons passing through the screen grid reach the anode. Secondary electrons will be produced, especially as the implantation voltage increases. However, they will be returned to the anode due to the repelling field of the screen grid, contributing nothing to the tube current (Hill, 1961).

E. Testing of the Vacuum Tube

Before the power tube could be used, the filament was slowly energized using the circuit of Figure II.4. The break-in and degassing of the power tube was conducted very slowly since the tube was in storage for a number of years. The circuit for the initial break-in of the tube consisted of a 120-Volt Variac connected in series with an analog amprobe, a digital amprobe, and a digital voltmeter placed across the directly-heated cathode (filament). Cooling, using the two fans mentioned earlier, was also provided. The voltage applied to the filament using the Variac was taken from 0.38 Volts at 3.1 Amperes and was held there for about 17 hours. It was next taken to 1.00 Volts at 6.1 Amperes and held there for about 30 minutes since most of the degassing and breaking-in took place during the initial startup. It was next taken to 2.5 Volts at 10.5 Amperes and held there for about 24 hours. It was then taken to 3.0 Volts at 11 Amperes and held there for about 2 hours. The Variac became current limited and the tube test was then terminated. At that time, a Lambda power supply rated at 5 Volts at 80 Amperes was connected in place of the 120-Volt Variac. The filament voltage was slowly taken up to the previous 3-Volt level and was then increased to 4.88 Volts at 16 Amperes and held there for about 10 hours. The Lambda power supply became voltage limited due to the resistance of the filament, about 0.3 Ohms. The test was again terminated and a step-up current transformer was connected in place of the Lambda power supply. This transformer was powered

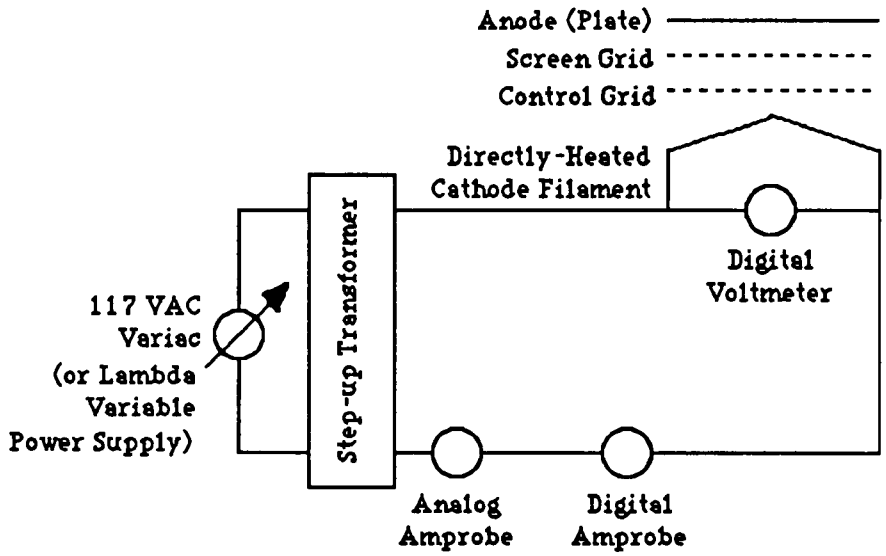


Figure II.4 Circuit used to test the filament of the power grid tube. The first test was conducted without the step-up transformer and with the variac. The second test was conducted using the Lambda power supply. The third test, the one with the most available current at a voltage near 7.5 V, was conducted using the step-up transformer and the Variac.

using the 120-Volt Variac so that the current could be taken up very slowly. The filament voltage was slowly increased to 7.5 Volts, its rated nominal operating value, at about 23 Amperes, its rated value. It was held at this level for about 8 hours. The tube filament power test was then complete and the power tube, as far as the filament was concerned, was in good condition. A second power tube was broken in, using essentially the same procedure, to serve as a back-up, should the first tube fail.

F. High-Voltage Switching Circuit Power Source

Since the power required to operate the high-voltage switching circuit must come from a source biased to negative high voltages, the source must be located within the high-voltage switching circuit enclosure, whether it be a rectified AC signal source or a DC source. Initially, an AC motor was going to be used to mechanically power a generator by means of an insulating shaft. The generator power was then to be rectified and delivered to the high-voltage switching circuit enclosure for circuit operation. This design appeared to involve too many complications and too much upkeep. After this, it was decided that a large 12-Volt truck battery would be used to provide the necessary operating power. The battery selected for this application was a commercial Exide 12-Volt battery which is capable of 860 cranking amperes and must be recharged after 330 minutes of operation. It can be charged easily using available high-current

DC power supplies after the high-voltage switching circuit is shut down.

The plexiglass enclosure is equipped with two 3/8" (0.95 cm) holes in its lid for battery recharging from a 0 to 40 Volt, 0 to 25 Ampere DC power supply. Two 15-foot No. 10 AWG stranded conductors, equipped with male banana plugs, are connected to the charging power supply output (pins 8 for positive, 11 for negative). The battery connecting posts were modified so that these banana plugs could be inserted through the plexiglass lid for recharging. The battery voltage at full charge is about 12.38 Volts. For recharging, the power supply should be set for about 12.75 Volts by adjusting the voltage control knob on the front of the supply. The charging current can then be set, using the current control knob, to about 3 Amperes. Charging should be conducted at least overnight or preferably for more than 24 hours. All of the cooling fans should be left on during the charging procedure to ensure that none of the gases (which include hydrogen) emitted from the battery during charging become trapped in the plexiglass enclosure. Such trapped gases could result in an explosion. A periodic check of the battery water level is recommended. Use only distilled water when refilling the battery and never fill unless needed. The battery should only be filled to the bottom of the plastic insert. For a detailed list of the steps to follow when charging the battery, refer to Appendix B.

G. Implantation Power Source

The high-voltage power supply necessary for plasma ion implantation must be capable of at least 50,000 Volts and up to 1 A. The high voltage power supplies available in the UTK Plasma Science Laboratory include a 50 kV, 50-milliampere Model CS-60H70 NJE (New Jersey Electric) DC power supply and a 50 kV, 1 A Model 40-1000-1 Del Electronics, Inc. power supply. The NJE power supply uses four oil-cooled, vacuum rectifier tubes along with a full-wave choke input filter bridge rectifier circuit to achieve the desired high voltage (NJE, 1959). The power supply is reversible in potential and was reset for positive grounding, since the implantation of positively-charged ions requires a negative high voltage. The power supply is also Variac controlled and has analog readouts for both applied voltage and current. The current scales range from 0 to 5 milliamperes, 0 to 25 milliamperes, and 0 to 50 milliamperes. The voltage scales range from 0 to 12.5 kilovolts, 0 to 25 kilovolts, and 0 to 50 kilovolts. The power supply was checked using a Hipotronics precision voltmeter that can measure up to 100,000 Volts. The analog voltmeter was found to read about 1.5 % below the actual voltage on the low end, and about 3 % below on the high end of the voltage scale. The Del power supply uses twelve triodes immersed in an oil bath along with a motor-controlled Variac to deliver the needed voltage. The current meter is 1 A full scale and the voltage meter is 50 kV full scale. The current and voltage meters have three range multiplier settings: 0.1, 0.5, and 1.0.

The NJE power supply was chosen for the implantation power source in initial experiments, and the Del for powering the Penning discharge. However, due to the low internal impedance of the Del power supply, it was reconnected as the implantation power source and the NJE now powers the Penning discharge. Operation of the Del power supply for the implantation power source when conducting an implantation is discussed in Appendix C. Operation of the NJE power supply for the Penning discharge power source when conducting an implantation is discussed in Appendix D.

H. High-Voltage Switching Circuit Block Diagram and Waveforms

Figure II.2 represents the system block diagram for the high-voltage switching circuit. The area enclosed in the heavy black line contains components which are isolated from the laboratory environment by the plexiglass enclosure. This includes eight subsystems which are required to switch high voltages. Two other subsystems outside this area are also necessary, but do not require isolation since there is no electrical connection between them and the high voltage switching circuit. The operation of the high-voltage switching circuit will be discussed using Figure II.2, along with Figure II.5, which illustrates the AC control signals at different points in the high-voltage switching circuit.

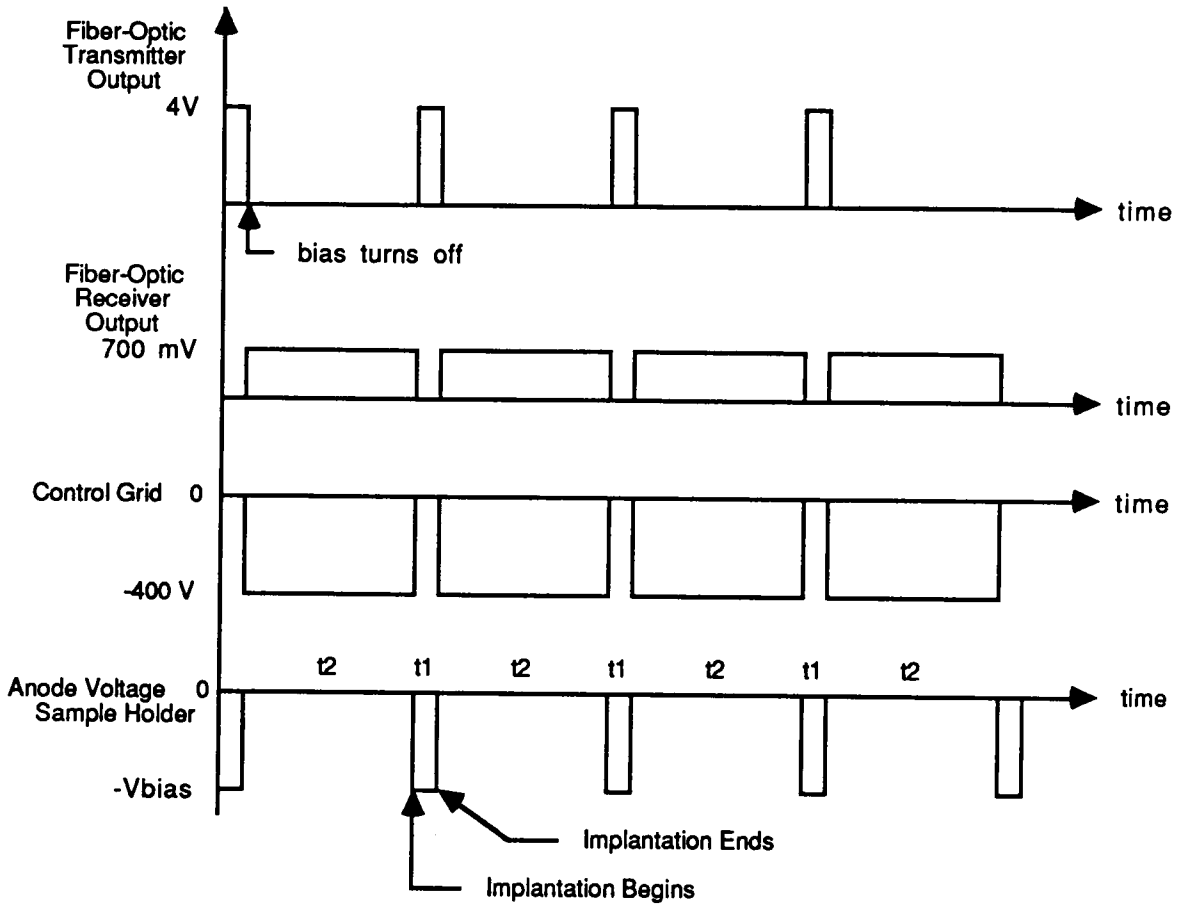


Figure II.5 Switching signals from the fiber optic transmitter to the sample holder negative bias delivered by the vacuum tube.

The high-voltage switching circuit is controlled using a signal generator. Chosen for this application is a Wavetek Model 191 signal generator which has an adjustable pulse delay feature. This is shown in Figure II.6. The output signal from this generator is input to a fiber optic transmitter which was designed and built for this project. In Figure II.5, the first signal is that applied to the input of the fiber optic transmitter. An infrared light beam is then directed through a fiber optic light guide, and into the fiber optic receiver, located in the plexiglass enclosure. This is the second signal in Figure II.5. The signal is then converted back into an electrical signal and delivered to the TMOS switching circuit. This circuit instructs the 400-Volt DC to DC converter when to deliver a 400-Volt DC signal to the control grid of the vacuum tube. This signal is the third signal in Figure II.5. Hence, the fiber optic receiver, the TMOS switching circuit, and the 400-Volt DC to DC converter are the three subsystems inside the plexiglass enclosure which are responsible for determining when high-voltage pulses are applied to the sample holder. The high-voltage pulses are represented by the last signal in Figure II.5.

The remaining subsystems in the enclosure are necessary for proper operation of the vacuum tube. The 1500-Volt DC to DC converter keeps the screen grid of the vacuum tube biased to a constant potential as long as the high-voltage switching circuit is energized. The TMOS current driver circuit is responsible for delivering the filament power to the directly-heated cathode necessary to produce electrons from the cathode of the tube. All of these subsystems are powered from the 12-Volt high-current

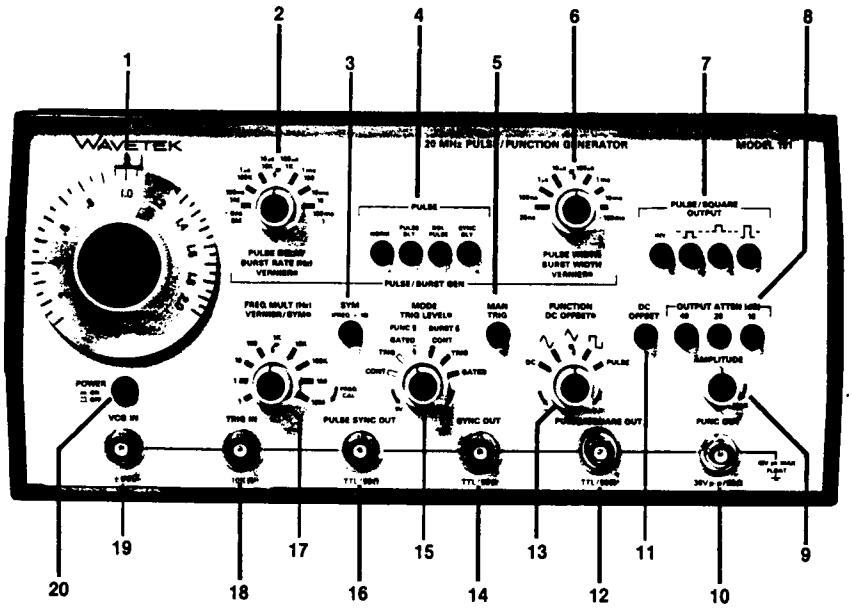


Figure II.6 Front panel of Wavetek Model 191 signal generator showing the appropriate knobs controlling the frequency and bias on time of the high-voltage switching signal. The minimum frequency is 0.01 Hz and the maximum is not the signal generator maximum but determined by characteristic plasma and implantation times.

battery and are fused through a power distribution box. Further discussion of these circuits and their fusing will follow.

I. Electronic Circuits

Now that the AC waveforms responsible for switching the high voltage have been discussed, the electronic circuits necessary to switch these high-voltage pulses can be described. Since this application uses the vacuum tube discussed above, these AC waveforms must be produced. Every subsystem, with the exception of the signal generator, was designed by John E. Crowley, a former Graduate Research Assistant at the UTK Plasma Science Laboratory, to fit the application. These subsystems included: the fiber optic transmitter, fiber optic receiver, control grid switching circuit and power supply, screen grid power supply, filament power supply, and power distribution system.

An important design consideration was that of using the vacuum tube for an unintended application such as this. Also of concern was the design of a circuit which could switch up to 500-Volts to turn the control grid off and on. Finally, attention was given to a circuit which could supply high current at low voltage for the vacuum tube filament. The development of each of these subsystems, along with their modifications, carried out by Philip F. Keebler, the current Graduate Research Assistant for this research program at the UTK Plasma Science Laboratory, is presented below.

The first subsystem considered was the control signal circuit. This set included the main control signal source, the Wavetek signal generator; the fiber optic transmitter; the fiber optic light guide; and the fiber optic receiver. Since this design must provide an adjustable duty cycle for the high-voltage switching circuit, a signal generator with an adjustable pulse delay feature was selected. Also, it was desired that the input control signal to the fiber optic transmitter be a TTL pulse. Most signal generators do not have adjustable signal frequencies for TTL pulses. The TTL pulse is a fixed 4-Volt amplitude square wave. Figure II.6 depicts the front panel of the Wavetek Model 191 signal generator.

1. Fiber Optic Transmitter Circuit

The major component of the fiber optic transmitter circuit is the Hewlett-Packard HFBR-1204 fiber optic transmitter. This device was selected because of its very short rise and fall time (10 % to 90 %) characteristics, both 11 nanoseconds. The device is a etched-well 820 nanometer GaAlAs emitter which requires a small current pulse to cause the diode to emit red laser light. More than -10 dBm of optical power can be coupled into 100 to 140 micrometer Hewlett-Packard HFBR-3000 fiber optic cable and connector assemblies. Due to this high power level, the fiber optic light guide can extend up to 3,281' (1000 m). Precision alignment of the diode to the mechanical fitting reduces the dynamic range requirement of the fiber optic

receiver. This allows the receiver power rail to be as low as 5 Volts. The fiber optic transmitter design used here delivers only small current pulses to the diode, resulting in low power consumption and extended life for the transmitter. This is important since such devices are expensive. Interference problems are avoided by the insulation of both diode ends from the casing and by the electrostatic shield provided with the HFBR-4202 mounting hardware kit.

Figure II.7 depicts the necessary electronics to provide a current pulse to the diode transmitter. The recommended forward voltage for the diode is between 1.44 and 1.94 Volts. Here, a standard 5-Volt AC to DC power converter was chosen, along with a value for R3 of 34.9 Ohms, 1 Watt and for R4 of 10 Ohms, 1/4 Watt. This power supply is a Computer Products Model 84-05-150 which uses standard 120-Volt AC, single-phase power. The power supply is fused using a Buss Model MDL 15, 15 Ampere fuse, F1B, which is removable and replacable from the rear panel of the fiber optic transmitter enclosure. The power to the converter is switched using a single-pole, single-throw miniswitch, S1, mounted on the front panel. A small green-colored, neon lamp, L1, is also included as an indicator to let the user know when the fiber optic transmitter is energized. When this lamp is on, a pulse of laser light is being generated by the fiber optic transmitter. Capacitor C1 of 0.1 microfarads is used as a bypass capacitor. Capacitor C2, a polarized tantalum capacitor of 100 microfarads is used as a "speed up" capacitor and provides a pre-bias current of 1 milliampere which ensures rise and fall times of 10 nanoseconds or less. The digital

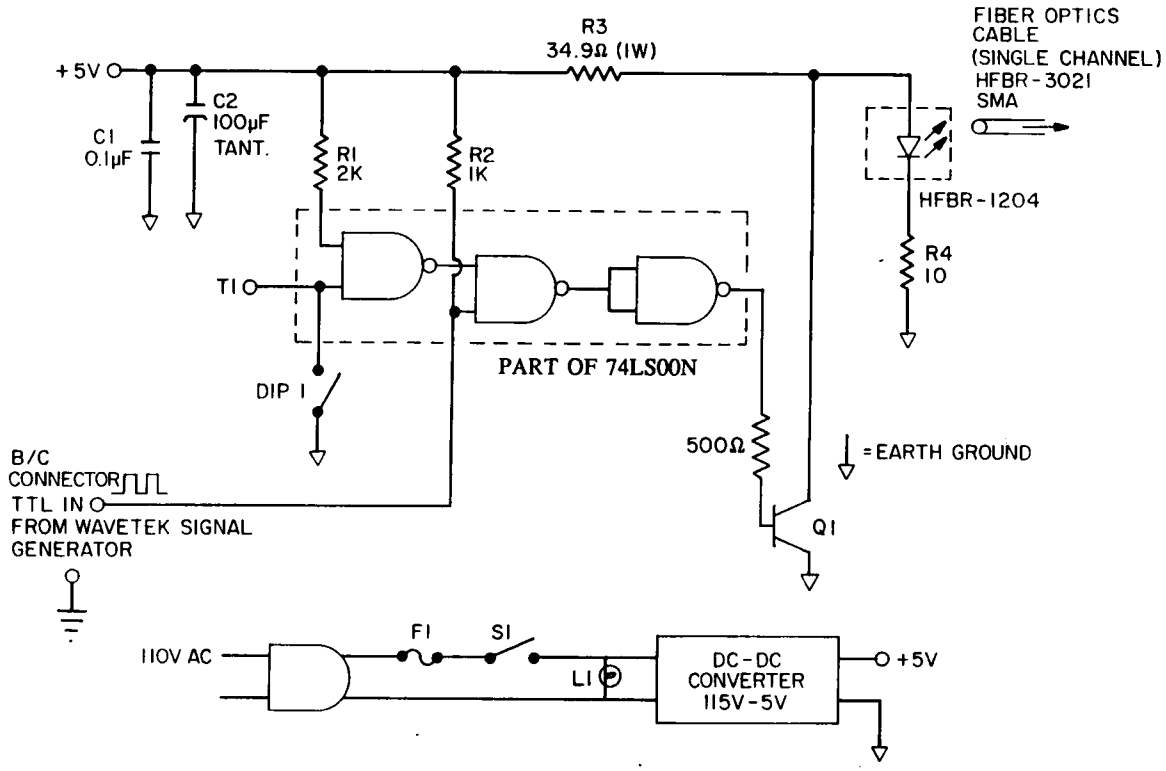


Figure II.7 Schematic of fiber optic transmitter circuit responsible for delivering an infrared light beam to the fiber optic light guide (cable) connected to the fiber optic receiver circuit of Figure II.8.

integrated circuit used for the TTL is one-half of a SN74LS00N NAND gate.

This TTL circuit is designed so that an internal or external signal source can be used. A simple variable pulse delay square pulse generator could be designed and substituted for the Wavetek signal generator. The dipswitch, DIP 1, provides this capability in the TTL circuit. If an external signal generator is used, as in this application, the dipswitch remains closed and the input to terminal T1 is not used. If an internal signal generator is used, the dipswitch remains open and the TTL input terminal is not used. In this design, the output of the Wavetek signal generator is input to the TTL with the dipswitch closed. The resistor R1 of 2 kilohms, 1/4 Watt is a pull-up resistor which "pulls-up" one of the inputs of the first NAND gate. Resistor R2 of 1 kilohm, 1/4 Watt provides a path for current to flow when the control signal is zero, a pull-down resistor when it is needed. The third NAND gate provides an inversion since the vacuum tube is to be on for a short time (control grid off) and is used in this way because of its availability in this circuit. Otherwise, a second digital circuit would be needed. Resistor R3 of 34.9 Ohms, 1 Watt drops most of the 5 Volts. The majority of the current from the 5-Volt power supply flows through R3; hence, a high power resistor is needed. This current continues to flow through Q1, a bipolar transistor. An RCA SK3854 is used here. The transistor is on only when the output of the last NAND gate is high (1). The 500-Ohm resistor, R5, reduces the turn-on voltage of the transistor, Q1, to extend its life. Resistor R4 of 10 Ohms, 1/4 Watt reduces the flow of

current through the diode emitter when it is on, since the forward resistance of the diode emitter is small.

The fiber optic transmitter is mounted on a separate circuit board equipped with a 3-pin connector plug for easy removal if repair or replacement is needed. Care must be taken when handling the transmitter device as it is very sensitive to static charges. A specially-designed protection device, which electrically grounds the human body eliminating static charge buildup, should be worn when handling this device. The remaining electronics are mounted on a prefabricated printed circuit board and housed in a plastic enclosure. The enclosure is vented at the top for cooling and the cooling passages are covered with copper screen wire to shield against radio frequency interference. The power cord is a two-pole polarized, grounded cord.

2. Fiber Optic Light Guide

The fiber optic light guide cable used is a 100/140 micrometer glass-filled cable. The connector style is SMA and the cable is a Hewlett-Packard HFBR-3021 single channel connected, 32.8' (10 m) long piece of light guide. SMA connectors are provided on each end and care must be taken not to damage the faces of the light guide alignment system. Both ends have been prepolished and must be covered with the plastic covers provided when not being used. Attachment to the fiber optic transmitter or receiver is made by

carefully inserting the brass pin into the hollow shaft and rotating the connector nut clockwise a few turns. It is important that the cable be protected at all times and it should not be pinched as damage to the light guide will result.

3. Fiber Optic Receiver Circuit

Once the laser light pulse has been injected into the fiber optic light guide and travels to the end, it must be reconverted into an electrical signal. The required circuit is completely contained in the Hewlett-Packard HFBR-2204 receiver. This device is a discrete PIN (Positive-Injection-Negative) photodiode connected to the input of a preamplifier integrated circuit. The integrated circuit converts the light pulse into an analog signal like the one input to the fiber optic transmitter but attenuated in amplitude. The device is a four-pin device, the pins of which are shown in Figure II.8. The power supply voltage necessary to energize the preamplifier is 7 Volts. The maximum analog output signal from this device can be no more than 1 Volt. The output impedance of the amplifier is typically 20 Ohms. The problem in using this device in the high-voltage switching circuit is not the capture of the analog signal, but the biasing of the preamplifier, since the high-voltage switching circuit is biased at negative high voltages. A simple biasing circuit, employing a 9-Volt battery, was selected. The design uses a negative 5 Volt fixed regulator which takes 9 Volts and converts it to 5-Volts. The

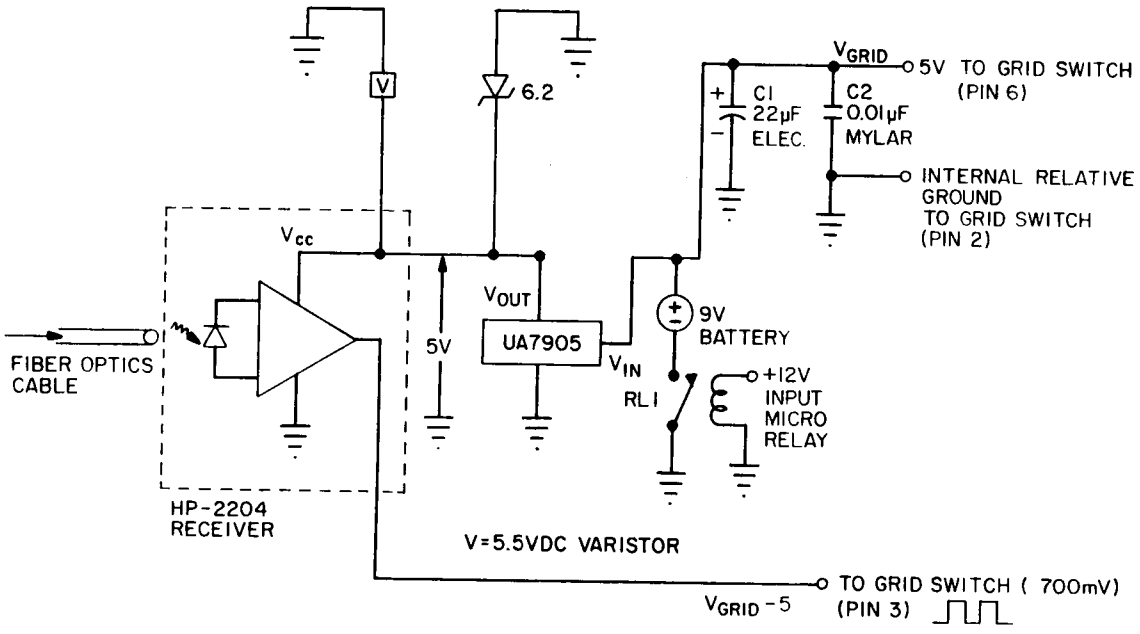


Figure II.8 Schematic of fiber optic receiver circuit responsible for delivering an analog voltage signal to the voltage comparator in the TMOS grid switching circuit of Figure II.10.

regulator is a UA7905 device, which is powered by a 9-Volt battery. The battery is not connected to the input of the regulator unless power is applied to the high-voltage switching circuit. In other words, when the high-voltage switching circuit is turned on, 12 Volts is applied to a 12-Volt Magnecraft Model 45F330 microrelay which is fused in the power distribution box using a 6/10 Ampere fuse. This closes a switch (relay reeds) connecting the 9-Volt battery to the input of the regulator.

This 5-Volt power supply actually has two purposes. It powers the preamplifier in the fiber optic transmitter (5 Volts above the reference) and also powers the comparator circuit in the control grid transistor switch (5 Volts below the reference). The supply voltage terminal on the fiber optic receiver is doubly protected. It is protected with a 6.2 Volt Zener diode which will short if the voltage to this terminal is above 6.2 Volts. This is used because it has a fast response time. A device which has a faster response time is a varistor. A 5.5-Volt metal-oxide varistor (MOV) is used here, since the maximum supply voltage is 7 Volts. These devices must be included in the design, since voltage spikes are possible and could permanently damage the fiber optic receiver. The receiver is about four times the cost of the transmitter and is more easily burned out in this application. Capacitor C1, a 22 microfarad electrolytic, 25 WVDC, capacitor provides decoupling between the negative 5 Volt regulator and the power rail of the comparator circuit in the control grid switching circuit. Capacitor C2 is a 0.01 microfarad Mylar capacitor. This capacitor has very low leakage current, and provides

a bypassing effect for the power supply terminal. The electronics are mounted on a horizontal printed circuit board and are contained in the high-voltage switching circuit. The output of the preamplifier is connected directly to a No. 20 AWG stranded wire leading to the input of the dual comparator integrated circuit of the control grid transistor switch. This output, as seen by the lower trace of Figure II.9, is about 700 millivolts, the expected value when using the proper fiber optic cables and connectors. The upper trace of Figure II.9 is the control signal from the Wavetek signal generator input to the fiber optic receiver. Careful inspection of the two signals on the time axis indicates about a 0.75-microsecond delay. This is well within the expected delay for this fiber optic link design.

4. Vacuum Tube Circuits

In order to sucessfully apply this 700 millivolt, high-speed control signal to turn the vacuum tube on and off, electronic circuits, using state-of-the-art semiconductor devices were designed. The most important circuit for operation of the vacuum tube is the electronic transistor switching circuit used to repeatedly apply a DC voltage to the control grid. The other two electronic circuits needed are to bias the screen grid at a constant DC potential, and to supply power to the directly-heated cathode filament of the vacuum tube.

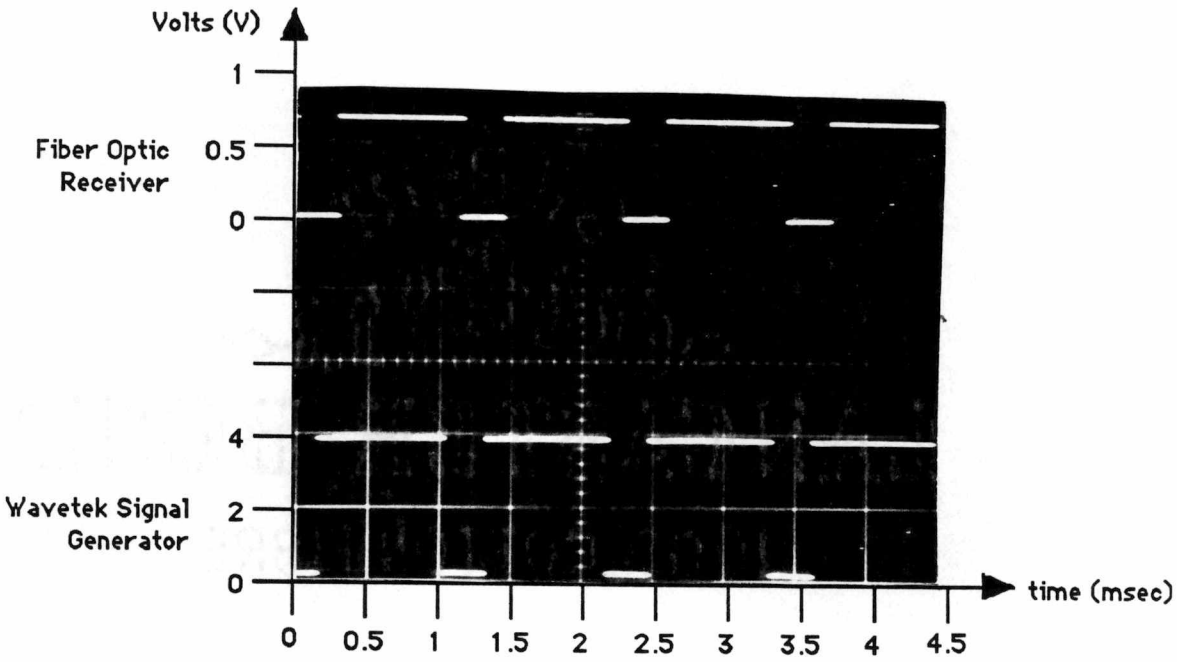


Figure II.9 Oscillogram showing fiber optic receiver signal on upper trace rising to a voltage of 700 mV and the transmitted signal input to the fiber optic transmitter rising to a voltage of 4 V on the lower trace. The frequency was about 111 Hz.

a. The Control Grid Circuit

The switching speed of the control grid circuit must be fast. In addition to this, the device selected to carry out the switching must be capable of holding off up to 1,000 Volts DC. This is the maximum DC control grid voltage that the vacuum tube can withstand before breakdown. Since relatively high control grid switching voltages are required, it only takes a few tens of milliamperes flowing through these devices to dissipate power levels of a few tens of Watts. For this reason, Motorola's enhancement mode silicon gate TMOS (T-channel metal oxide semiconductor) power field effect transistors were selected. The N-channel device is a Motorola MTP2N50 which has a standoff voltage of 500 Volts. The turn-on time and turn-off time of this device is 50 and 200 nanoseconds, respectively. This device has a power rating of 75 Watts at a temperature of 25 degrees Celsius. The P-channel device is a Motorola MTP2P50 which also has a standoff voltage of 500 Volts. The turn-on time and turn-off time of this device is 50 and 150 nanoseconds, respectively, and the power rating is the same as that of the N-channel.

There are two major disadvantages of using these devices. One is that they are extremely sensitive to static charge buildup, and in handling them care must be taken. The other is that, in the P-channel devices, the semiconductor junction technology only allows a maximum standoff voltage of 500 Volts. At this time, the 500-Volt models (MTP2P50) have been discontinued. The next available transistor in voltages lower than 500 Volts is one with a standoff

voltage of 450 Volts, a Model MTP2P45, which are readily available. This P-channel device is currently being used. However, due to the problems in availability of the N-channel devices, MTP2N90, a 900-Volt, 75 Watt device, and MTM2N100, a 1000-Volt, 150 Watt device, are currently being used. MTP devices are enclosed in a TO-220 package and MTM devices are enclosed in a TO-218 package, a larger package for higher power dissipations.

The minimum turn-on gate-to-source voltage for these devices is 2.0 Volts. Obviously, the output signal of 700 millivolts from the fiber optic receiver cannot be used to turn these devices on. The control grid circuit must perform two functions: it must connect the control grid to the output of a DC to DC converter to turn the vacuum tube off and it must connect the control grid to a zero potential or reference potential to keep any stray voltage from being placed on the control grid and turn the vacuum tube on. Hence, a dual-function transistor switch is needed. This also means that a dual-function semiconductor device with two outputs and one input is needed to switch on and off both of these transistor stages. One input is needed because there is only one signal, the fiber optic receiver output signal, being used to trigger this electronic switch. For this reason, a dual comparator, a Motorola Model LM 393, is selected. This comparator can be connected such that it only looks at one input, but has two outputs. The negative input of comparator 1 is connected to the positive input of comparator 2. The positive input of comparator 1 is connected to the negative input of comparator 2. This is the point at which the fiber optic receiver output signal is also connected.

The potential of the open-collector outputs reverses, based on the state (high or low) of the single input. This device is a silicon monolithic integrated circuit and can be energized using a single supply, eliminating the need for extra power supplies in an already negatively-biased high-voltage switching circuit. The range of this supply voltage is from 2 to 36 Volts, and the current requirement is low, 0.4 milliamperes. The output voltages are compatible with MOS devices such as those selected above. An LM 393N, an eight-pin dip package, was selected.

To avoid using an extra power supply for the power supply of this comparator, the single supply voltage is floated off of the positive rail of the DC to DC converter. This rail is referred to as V_{grid}. In order to do this, the output of the UA7905 negative 5-Volt voltage regulator is used. This allows the power supply rail of the voltage comparator to be V_{grid} -(5 Volts), thus energizing this device. The voltage for which the comparator changes state will be the power supply rail voltage unless a voltage divider resistor network is used. The voltage signal which is to be compared is the 700-millivolt output signal from the fiber optic receiver. Hence, the comparator must distinguish between a voltage of 0 and 700 millivolts.

The TMOS switching circuit for the control grid of the vacuum tube, including the dual comparator, five TMOS transistors, several biasing resistors, and a protective device on the output, is shown in Figure II.10 below. Notice the location of the resistors R1 and R2 which are used to set the comparator voltage according to

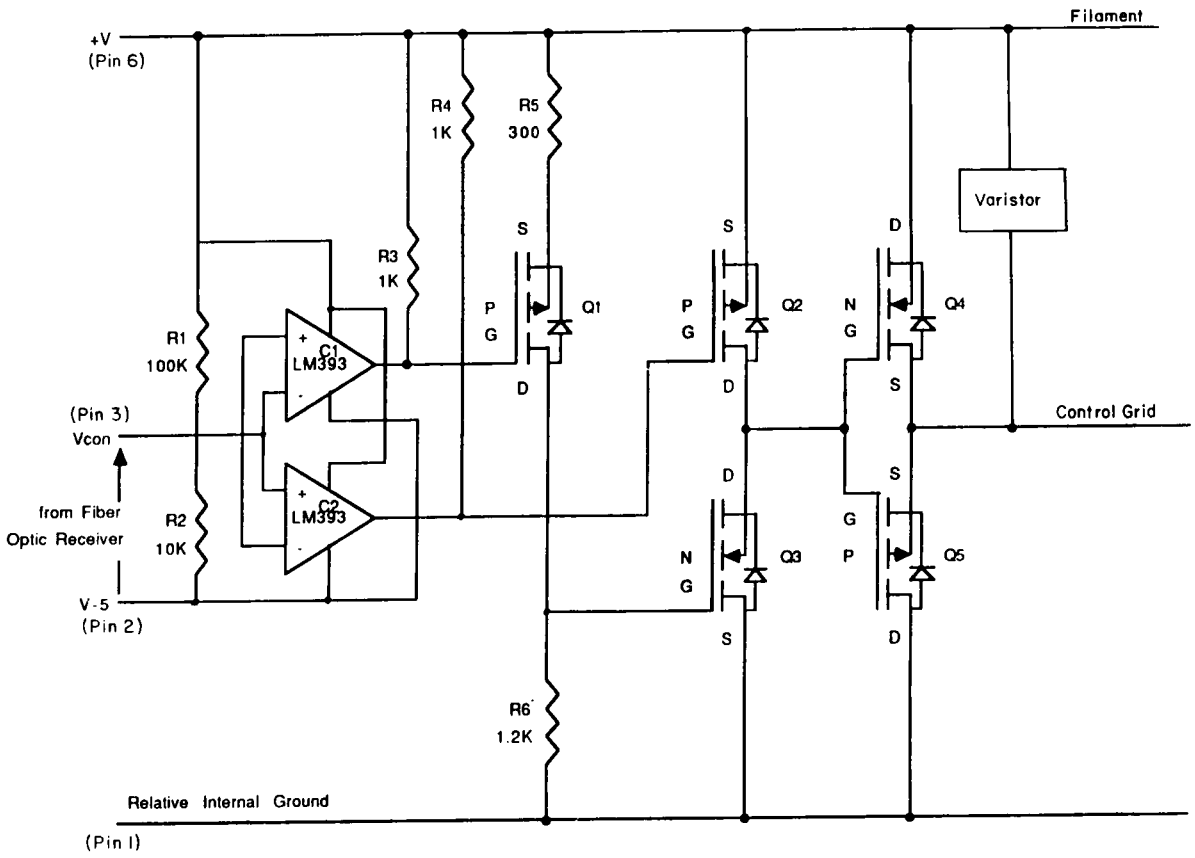


Figure II.10 Schematic of TMOS grid switching circuit responsible for delivering a negative 400 V signal between the cathode and the control grid of the vacuum tube of Figure II.2.

$$V_{com} = \left(\frac{R2}{R1+R2}\right) \times V_{out} \qquad \text{(III.1)}$$

where V_{com} is the comparison voltage, and V_{out} is the output voltage of the UA7905 negative 5-volt voltage regulator, which is 5 Volts. Choosing R1 to be 100 kilohms and R2 to be 10 kilohms, V_{com} is set at about 454 millivolts. Hence, when the fiber optic receiver output signal is below 454 millivolts, comparator 1 is low and its output is high; and comparator 2 is high, and its output is low. In contrast, when the fiber optic receiver output signal is above 454 millivolts, the comparator output conditions are reversed. Resistors R3 and R4 provide a current path for the open-collector circuits in the comparator.

The output of comparator 1 is connected to the gate of Q1, a P-channel device. The current drain through transistor Q1 is limited by resistors R5 of 300 Ohms, 1/2 Watt, and R6 of 1.2 kilohms, 1/2 Watt. Q1 is the first stage of one-half of the switching circuit. Transistor Q2 is the first stage of the other half of the switching circuit. It is also a P-channel device, and its gate is connected to the output of comparator 2. Transistors Q3, an N-channel device and Q5, a P-channel device are the second and third stages, respectively, of one-half of the switching circuit. Transistor Q4, an N-channel device is the second stage of the other half of the switching circuit. Figures II.11 and II.12 show the switching actions of the five TMOS transistors during one period of the fiber optic receiver output signal.

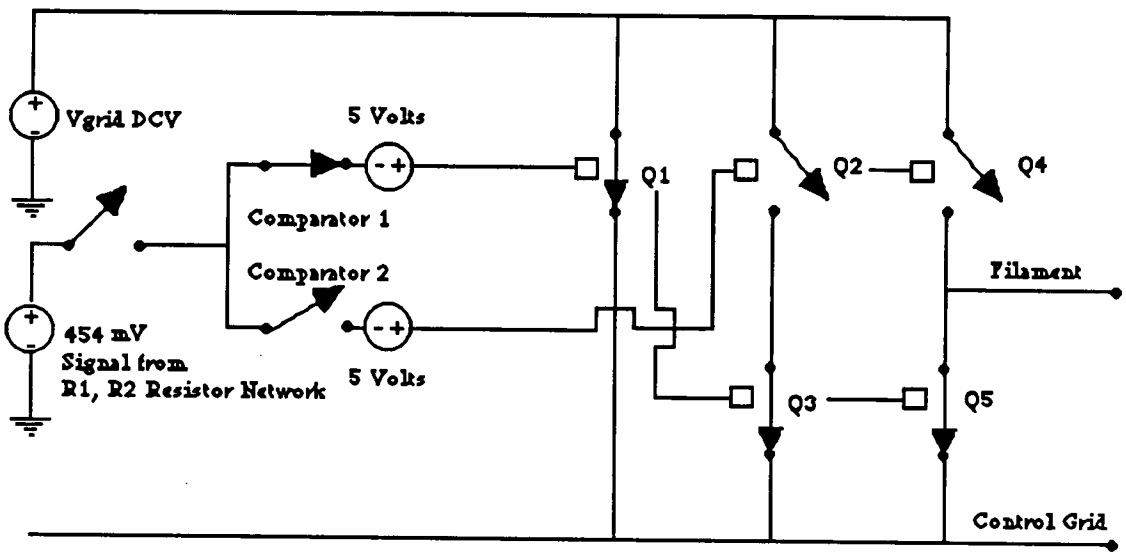


Figure II.11 Transistor switching scheme when control signal is low, resulting in the control grid of the vacuum tube being off and the vacuum tube being on.

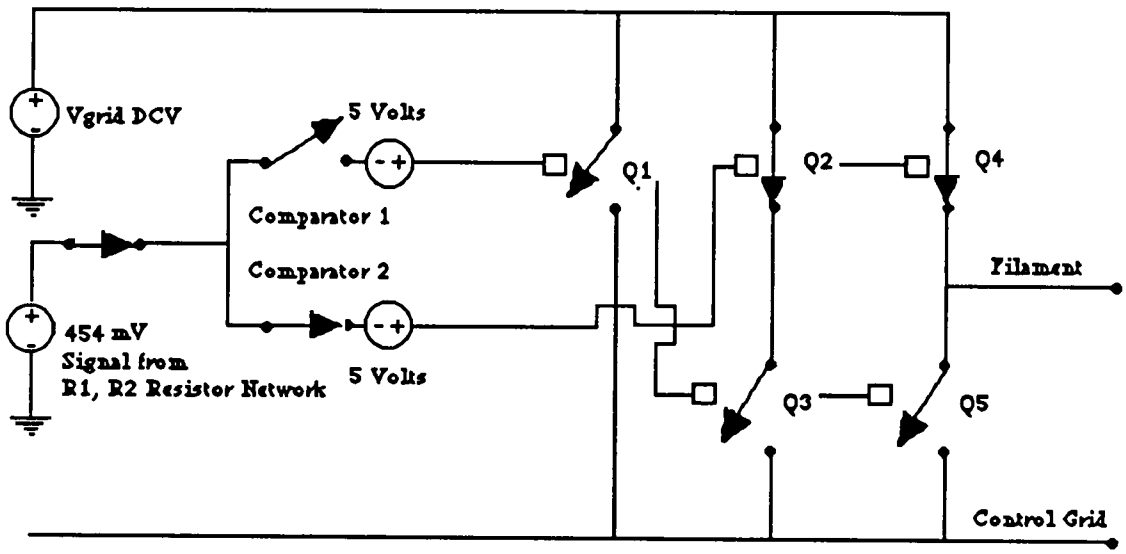


Figure II.12 Transistor switching scheme when control signal is high, resulting in the control grid of the vacuum tube being biased negative (control grid connection is a positive ground connection) and the vacuum tube being off.

Referring to Figure II.11 when the output of the fiber optic receiver is low (control signal is high) for a short time, the high state of the output of comparator 1 turns Q1 on (Q1 switch is closed) and the low state of the output of comparator 2 turns Q2 off (Q2 switch is open). The current flowing through Q1 develops a voltage drop across resistor R6, which also appears across the gate-to-source junction of Q3, turning it on (Q3 switch is closed). This drives Q4 off (Q4 switch is open) and Q5 on (Q5 switch is closed). Hence, there is no potential difference between the filament and control grid. This results in the vacuum tube being on. It is on for only a short time, conducting ion current from the plasma.

Referring to Figure II.12 when the output of the fiber optic receiver is high (control signal is low) for a longer time, the high state of the output of comparator 2 turns Q2 on (Q2 switch is closed) and the low state of the output of comparator 1 turns Q1 off (Q1 switch is open). Thus, Q2 is on for a longer time than Q1, requiring that Q2 be provided with a heat-sink. Since no current flows through Q1, Q3 is turned off (Q3 switch is open). This drives Q4 on (Q4 switch is closed) and Q5 off (Q5 switch is open). Thus, Q4 is on for a longer time than Q5, requiring that Q4 also be provided with a heat-sink. This action applies a negative potential difference between the filament and control grid, with the filament being at the higher potential. This results in the vacuum tube being turned off, stopping the flow of ion current through the tube from the plasma.

Due to voltage spikes and/or transients that can be developed from the plate (anode) of the tube to the control grid of the tube

caused by random plasma effects, a device to protect the outputs of transistors Q4 and Q5 was included in the design. The device selected is a metal oxide varistor. They are voltage dependent, non-linear devices which have an electrical behavior similar to back-to-back Zener diodes. They also have sharp, symmetrical breakdown characteristics which enable the device to provide excellent transient supression. When the device is exposed to a voltage greater than its characteristic threshold, its impedance changes from a near open circuit to a high conductive level. This clamps the transient voltage to a safe level. The destructive energy of the incoming transient pulse is absorbed by the varistor, protecting vulnerable circuit components. This device is a voltage controlled resistor, hence the name "varistor."

Specifically, this device is a General Electric Model V321DA40 industrial high energy package rated a 460-Joule absorbing energy. The continuous RMS clamping voltage is 320 Volts and the continuous DC clamping voltage is 420 Volts. This model was selected because of the limited standoff voltage of the P-channel TMOS transistors, 450 Volts. The clamping voltage must be between the power rail voltage of the TMOS switching circuit and the maximum standoff voltage of the TMOS transistors. The continuous DC clamping voltage was selected for reference here because the control grid signal is a square wave which assumes two values: zero potential and the power rail voltage. This signal is not a continuously changing signal like that of an AC signal with a definite frequency. The selection of this varistor places a limit on the control grid circuit

power supply. Hence, it must be less than 420 Volts. It must be mentioned that there are other transistors available which have internal energy absorbing mechanisms. These are also available from General Electric and have parasitic diodes included in the junctions which can absorb transients. The standoff voltages of these transistors do go above 500 Volts in both the P-channel and N-channel devices. Although these devices are very expensive, if voltages greater than 50,000 Volts are to be used, it is recommended that these devices be considered, since the switching voltage of the control grid in the vacuum tube must be increased if the cathode to anode switching voltage is also to be increased (General Electric, 1986).

b. The Screen Grid Circuit

The power output from a tetrode is very sensitive to screen grid voltage. For this reason, any application requiring high switching powers requires a well-regulated screen grid power supply. The maximum screen grid voltage that can be used is 2,500 Volts and the maximum power that can be dissipated across the screen is 75 Watts. Figure II.13 shows the screen grid power supply along with a "bleed off" resistor and a low-energy varistor combination. The case of the power supply is connected to the internal ground of the high-voltage switching circuit. However, since isolation is required, the negative terminal of the output is connected

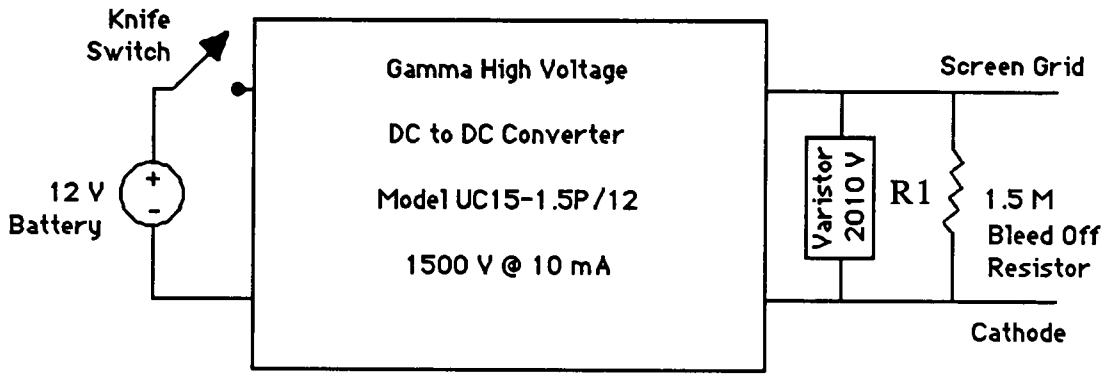


Figure II.13 Screen grid power supply and components. The output of the supply has a 2010-V varistor and a 1.5 megohm bleed off resistor connected across it. The varistor protects the output stages from transient voltage spikes that may be applied across the output during the operation of the high-voltage switching circuit. The bleed off resistor bleeds off 1 mA which insures that the supply never sees an open circuit.

to the tube cathode instead of the frame of the high-voltage power supply.

Referring to the circuitry around this power supply, a 15-megohm resistor, R1, is placed across the output to provide a "bleed-off" current of 1 milliampere. Four varistors are connected in series across the output terminals to provide protection of the output stage of the supply. The clamping voltage is set at 2,010 Volts DC by using two RCA SKMV480G varistors rated at a clamping voltage of 640 VDC and an absorbing energy of 105 Joules and two RCA SKMV373A varistors rated at a clamping voltage of 365 VDC and an absorbing energy of 1.7 Joules. The power supply and the electronics mentioned above are mounted on a vector board which is easily removed by disconnecting a 6-pin connector.

c. The Filament Power Circuit

The cathode of the vacuum tube is a thoriated tungsten filament through which an electrical current flows. The filament has a resistance of about 0.3 Ohms, and it provides a flow of low-energy thermionically-emitted electrons from its surface. The flow of these electrons makes it possible for the tube to act like a conductor while in the "on" state. In order for the tube to function according to specifications, the potential applied across the cathode must be the rated voltage of 7.5 Volts. The filament current may range from 20.0 to 22.7 Amperes.

The 12-Volt high current battery cannot be connected directly to the filament, since the filament will burn out. For this reason, a voltage-controlled high-current power transistor circuit is used to regulate the current through the filament based on the voltage applied across it. If a potential of 7.5 Volts is applied, then a current of around 22 Amperes will flow. This high current requires power transistors.

The circuit of Figure II.14 applies 7.5 Volts at about 22 Amperes to the filament. The 7.5-Volt potential is obtained by voltage regulation with an RCA SK9215 adjustable voltage regulator. The voltage across the input of this regulator is taken directly from the high-current battery inside the high-voltage switching circuit. Variable resistors R1 and R2 of Figure II.14 are used to set the filament potential. Variable resistor R1 is used as a fine adjustment and R2 as a coarse adjustment. R1 was chosen to be a 220-Ohm 15-turn trimpot potentiometer, and R2 a 1.11-kilohm 15-turn trimpot potentiometer. This selection insures a variable output voltage around the nominal 7.5-Volt level.

The essence of this circuit is the following. An operational amplifier with negative feedback is used to control a high-power transistor. The operational amplifier selected for this application is the RCA Model SK 3692. The 7.5-Volt potential is applied across its non-inverting input. The output is connected to the gate(s) of the transistor. The source of the transistor is fed back through a resistor, R3, to the inverting input of the operational amplifier. The choice of 10 kilohms for resistor R3 is a common one for feedback

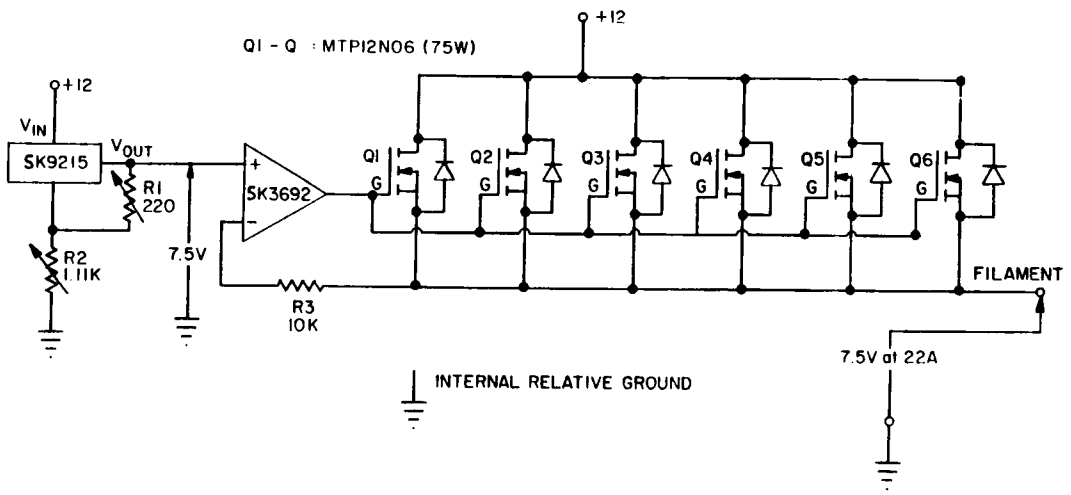


Figure II.14 A schematic diagram of the circuit required to power the directly-heated cathode filament. The input voltage is 12 V and is input to a variable voltage regulator adjustable by the two potentiometers. The 7.5 V is input to an operational amplifier which controls six high-power TMOS transistors, drawing current from the high-current battery.

resistances in operational amplifier feedback circuits. The drain of the transistor is connected to a high-current source, biased at a potential higher than 7.5 Volts. The source of the transistor is connected to the internal ground of the high voltage switching system, the negative terminal of the 12-Volt battery.

Once 7.5 Volts is applied to the input of the operational amplifier, the amplifier tries to stabilize itself by making the inverting input the same potential. During this process the output of the operational amplifier begins to rise linearly, turning the transistor on, until the operational amplifier is stabilized. The transistor is then on. The operational amplifier is powered by a No. 413 Eveready 30-Volt battery. The battery is automatically connected, using a Magnecraft Model W193RE1A3-12G minirelay powered by the 12-Volt high-current battery, to the power supply rails of the operational amplifier when the main power switch of the high-voltage switching circuit is engaged. The maximum supply voltage that the operational amplifier can withstand is 36 Volts DC. The use of a high supply voltage allows the operational amplifier output to stabilize at higher voltage levels, thus fully using the operational amplifier and allowing more current to flow through the power transistors. The sum of the turn-on voltage of the power transistor (about 3.0 Volts DC) and the regulated voltage applied to the operational amplifier (7.5 Volts DC) should never be more than the source voltage (12 Volts DC). Thus, one has a voltage-regulated current supply limited by the amount of current the power transistor can handle. If this value is not large enough, several power

transistors should be paralleled together to split the current load up among the transistors.

At a voltage of 7.5 Volts at current levels of around 22 Amperes, the power dissipated is 165 Watts. This power level is too high for a single device to handle. However, several devices can be paralleled together. Motorola N-channel enhancement mode silicon gate TMOS power field effect transistors were selected for this application. These are the same devices used in the transistor switching circuit for the control grid of the vacuum tube. The device selected is a Model MTP12N06 rated at a power level of 75 Watts. The maximum source-to-drain voltage of this device is 60 Volts DC, which is well under the 12-Volt source voltage from the high-current battery. This device is also a 12-Ampere device and has a maximum gate-to-source turn-on voltage of 20 Volts DC. Strictly, only two of these devices are needed; however, this would result in a small performance margin, so the initial design used four. This would divide the current among each device, resulting in about 5.5 Amperes in each. An overload could result from current above 12 Amperes flowing through one of these devices. This could occur if the gate-to-source threshold voltage of the two devices deviated by more than about 0.5 Volt. The threshold voltage of the device is the voltage at which the transistor first begins to conduct current. In an ideal design, one would want all of the transistors to turn on at the same voltage and allow the current flowing through each of the junctions to increase at the same rate. However, practical limitations seldom allow this, as in all other semiconductor devices. The gate-

to-source threshold voltage of these devices ranges from about 2.0 to 4.5 Volts DC and is normally around 3.0 Volts DC.

A problem occurred initially when the filament of the tube was energized with four power transistors connected in parallel. One or more of these transistors would burn out due to high transient currents that flowed through one of them. This happened for two reasons: (1) the resistance of the filament was slightly higher than 0.3 Ohms when first energizing the circuit (at low temperatures) and (2) the gate-to-source threshold voltages of four power transistors selected at random varied too much. It is obvious that the filament resistance cannot be changed; however, careful selection of power transistors with matched threshold voltages can help the second problem. To help reduce the load on each transistor, two additional transistors were paralleled with the original four, resulting in six transistors, each of which carried about 3.7 Amperes of the filament current.

To help reduce the heat load on these power transistors, each power transistor was heat-sinked using vertical cooling fins. Room temperature air, blowing at a speed of about 120 cubic feet per minute, is passed across these cooling fins. The cooling fan must be energized independently of the main power in the high-voltage switching circuit by depressing a push-button switch located on the upper panel of the high-voltage switching circuit behind the power distribution box. A plexiglass rod is provided for this. The fan must be allowed to run several minutes after the main power switch for the high-voltage switching circuit has been disengaged.

5. Power Circuits

a. The Control Grid Power Supply

From the above section on the control grid circuit, it was determined that the power supply voltage required by the selected electronic components was 400 Volts DC. The power supply selected is a Gamma High Voltage Research, Inc. Model UC40-0.4P12, 500 Volt, 100 milliampere DC to DC converter. The power supply is powered by 12 Volts from the battery, and can dissipate 50 Watts. The required input current is 4.17 Amperes for a 500-Volt, 100 milliampere output. However, 400 Volts is required in this application. Since the input and the output of this supply are linear, the input voltage can be lowered so that the output voltage remains at 400 Volts DC. If 400 Volts at 100 milliamperes (assuming a worst case) are required, the input current requirement is 3.33 Amperes.

To set the input voltage, a simple high-power variable voltage regulator is used. The circuit of Figure II.15 is used. The regulator is an RCA SK 9344 , 75 Watt device. The power is the product of the difference between 12 and about 8.6 Volts and 3.33 Amperes, or 11.3 Watts. It is mounted on a large, air-cooled, finned heatsink to remove the heat generated by the device. The output voltage of the regulator can be varied by adjusting R1, a 500 Ohm, 15 turn potentiometer. This adjustment may be made from outside the high-

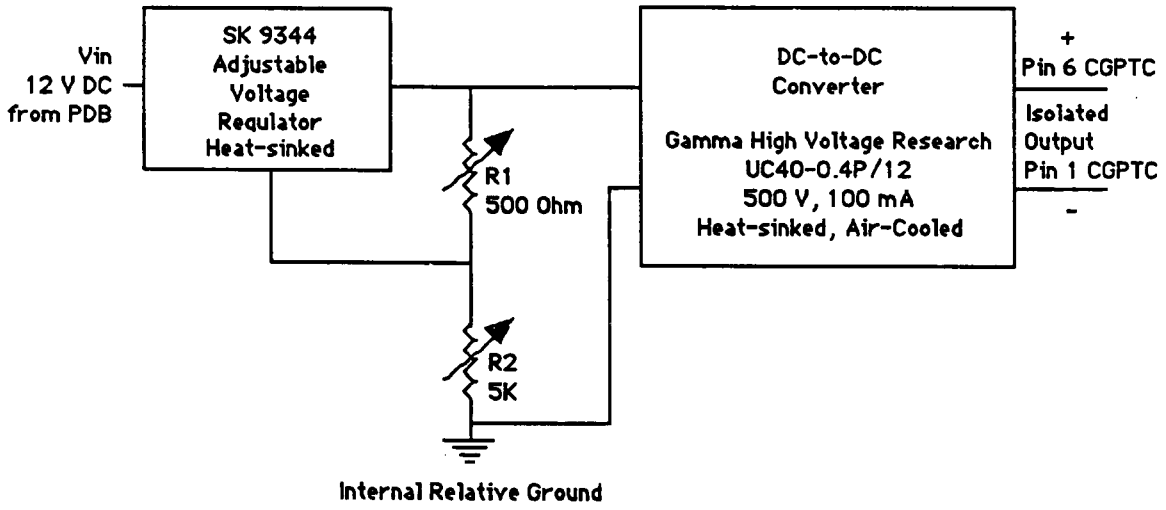


Figure II.15 Control grid power supply and components. The input voltage from the high-current battery is regulated to a value of about 8.9 V. At this value, the DC to DC converter outputs a 415 V DC signal into the TMOS control grid switching circuit of Figure II.10.

voltage switching circuit by inserting a small insulated screwdriver through a 1/8" hole provided in the sidewall of the high-voltage switching circuit. One must be careful in adjusting this voltage. With no load on the vacuum tube (no ion current into the sample), the no-load voltage from the control grid power supply will appear across one of the transistors in the control grid transistor switch. There is no danger provided the breakdown voltage of this transistor is not exceeded. The potentiometer R1 is set so the voltage on the output of the control grid power supply with no load is about 415 Volts DC. This is just under the cutoff of 420 Volts DC for the varistor on the output of the control grid transistor switch. When the control grid transistor switch is energized, this voltage drops to about 400 Volts DC. This setting for the control grid switching voltage is acceptable for switching voltages up to 45,000 Volts DC. If higher implantation voltages are required, the control grid switching voltage must be increased and not taken past the limit of 1,000 Volts DC, the maximum that the control grid inside the vacuum tube can handle. The input voltage for this power supply is taken from the 12-Volt battery.

For reference, a feedback control circuit can be added to the control grid power supply to increase the applied input voltage as the control grid power supply is loaded down by the operation of the control grid transistor switch or by additional load caused by switching higher implantation voltages. This circuit is pictured in Figure II.16. It is a straightforward feedback control circuit except for one requirement. The control grid power supply input must

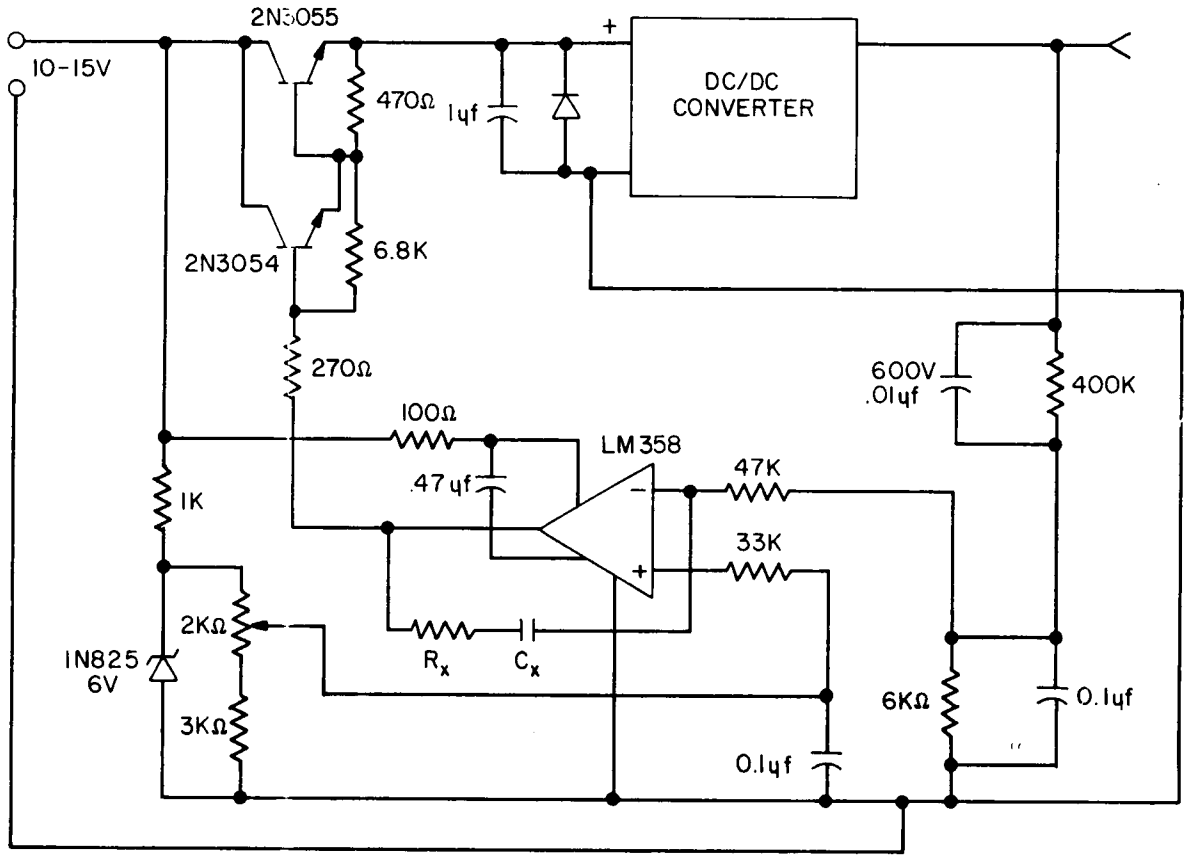


Figure II.16 Proposed feedback circuit for control grid power supply if it is desired not to use the high-power voltage regulator to set the DC to DC converter input voltage at a voltage which will cause the output to be 415 V.

remain isolated from its output. This could be accomplished in the circuit of Figure II.16 by the addition of an optical isolator, a common approach in isolating control circuits. This is a good project for one willing to further upgrade the high-voltage switching circuit while learning how the circuit operates.

b. The Screen Grid Power Supply

The power supply for the screen grid circuit is a DC to DC converter manufactured by Gamma High Voltage Research, Inc, model UC15-1.5P/12. This power supply utilizes high frequency sinusoidal power conversion techniques to produce the high voltage while maintaining low stored energy. The circuit is shown in Figure II.13. The input voltage is a 12-Volt DC signal, supplied by a No. 16 AWG stranded wire, and is applied only when the main switch of the high-voltage switching circuit is engaged. The output, which is isolated from the input, is rated at 1,500 Volts DC at 10 milliamperes maximum. Thus, the power of this device is 15 Watts and the input current requirement is 1.25 Amperes. The output of this device is proportional to the input with only 0.1 % ripple per Watt. The electronics within are fully encapsulated, which insures corona free, reliable operation. The output is also short circuit protected, should a very high energy arc occur within the tube which may cause the varistor to fail, shorting out the output terminals. The high-voltage

output wire is a flying lead capable of 15,000 Volts DC maximum. The operating temperature should not exceed 50 degrees Celsius.

c. The Filament Power Supply

The power needed to supply current to the filament cathode is controlled using the circuit of Figure II.14. This circuit requires three power inputs to operate. It requires power for the voltage regulator, for the operational amplifier, and, of course, for the filament. Since the current required for the filament is high (around 22 Amperes), No. 12 AWG solid copper conductors are used. The power is fed directly into the drains of the six TMOS transistors. These high currents are not passed through the voltage regulator on the filament power circuit of Figure II.14. However, the power required to operate the voltage regulator is taken from the same source. The power required to operate the operational amplifier is taken from a 30-Volt battery mounted on the same vector board on which the screen grid power supply is mounted. This was done for convenience. The battery raised the potential of the upper power rail 30 Volts above the lower power rail, which is at the internal relative ground (the negative of the high-current battery) of the high-voltage switching circuit system. This is necessary in order for the operational amplifier to turn on the TMOS transistors.

6. Total Power Consumption

The total power consumed by the plasma ion implantation process consists of four parts. In order of highest to lowest power, it consists of the power to create the discharge (electrical or microwave), the power deposited on the sample surface area exposed to plasma ions (power across the vacuum tube), the power to operate the high-voltage switching circuit (excluding the plate power of the vacuum tube), and the power to drive the diagnostic instruments such as the mass spectrometer and the oscilloscopes.

The power necessary to create the discharge, which is to be minimized, consists of the magnet coil power and the Penning anode power. This minimization is one of the subjects of this thesis. The first plasma ion implantation studies were carried out in a uniform Penning discharge. The layout of this vacuum discharge will be presented in Chapter 4. The majority of the power required to operate the Penning discharge is dissipated in the magnetic field coils. This power can be as high as 40,000 Watts when the maximum magnetic field intensity of 0.2 Tesla is used. The implantations carried out in the Penning discharge used magnet coil power on the order of 13,000 Watts, where the magnet coil current was 650 Amperes DC and the voltage was 20 Volts DC. The power required to initiate breakdown of the working gas is the anode power, which can be as high as 300 Watts for the Penning discharge anode/cathode arrangement used in this research. The implantations carried out used anode powers on the order of 100 Watts. Typical Penning

anode voltages range from 1,500 to 3,000 Volts DC and currents from as low as 10 milliamperes to as high has 50 milliamperes. Thus, the total power for the Penning discharge, including magnet power, is on the order of 20,000 Watts. The microwave discharge, which will be discussed in Chapter 5, uses a power of no more than 3,000 Watts. The power required to sustain the vacuum in the Penning discharge and in the microwave discharge is roughly the same and will not be presented for comparison here.

The average power required to implant a metal sample with ions of energies on the order of 50 keV immersed in a plasma discharge can be as high as 1,000 Watts. This power level is not the limit of the implantation power source, but is the limit of the vacuum tube used in our high-voltage switch. The power limit of the implantation power source is 40,000 Watts DC. The average power deposited on the sample, or across the vacuum tube, in our initial studies was on the order of 750 Watts. The instantaneous power can be higher than 1,000 Watts since the high-voltage switching circuit pulsing frequency can be easily decreased, allowing the vacuum tube to cool off between pulses. The vacuum tube can withstand power levels higher than 1,000 Watts for durations as long as 30 microseconds, the time that implantation is occuring.

It is important to know the total power consumed to operate the high-voltage switching circuit when determining the load placed on the 12-Volt high-current battery. There is no question that this battery can handle the load; however, the total power drawn from this battery will determine how long it can be operated before it

must be recharged. The power required to operate the high-voltage switching circuit includes several parts. In order of highest to lowest power, it consists of the power required to heat the filament, to operate the control signal generator, to drive the control grid transistor switch, to bias the screen grid, to operate the fiber optic transmitter, and to operate the fiber optic receiver. The control signal generator and the fiber optic transmitter are included in the total power consumption calculation, even though they are exterior to the high-voltage switching circuit enclosure, because they are necessary to operate the high-voltage switching circuit system. These powers are listed in Table II.2 below. This total power consumption for the high-voltage switching circuit, excluding the implantation power source, is about 328 Watts. Hence, the average direct current drawn from the 12-Volt high-current battery is about 27 Amperes.

The diagnostics used when implanting a sample include a mass spectrometer to examine the gas species present in the vacuum system, an oscilloscope to capture a waveform of the control signal, and another oscilloscope to capture a waveform of the sample holder voltage and current. These diagnostics will be discussed in Chapter 4. The power to operate these diagnostics is listed in Table II.3 below. The total power consumption of these diagnostics is about 2 kW.

The total power consumed by the high-voltage switching circuit during an implantation is a maximum of roughly 1,500 Watts, 67 % of which is used directly to implant the ions into a metal surface.

Table II.2

Power Consumption of High-Voltage Switching Circuit

Device	Voltage	Current	Power
Filament	7.5 V DC	22.7 A	170.25 W
Control Signal Generator	120 V AC	750 mA	90 W
Control Grid Power Supply	400 V DC	100 mA	40 W
Screen Grid Power Supply	1500 V DC	10 mA	15 W
Fiber Optic Transmtr.	120 V AC	100 mA	12 W
Fiber Optic Receiver	5 V DC	3.4 mA	17 mW

Table II.3

Power Consumption for Diagnostics Used in Plasma Ion Implantation

Diagnostic	Voltage	Current	Power
Mass Spectrometer	115 V AC	2 A	230 W
Vacuum Measuring Instruments	115 V AC	2.25 A	259 W
Control Signal Monitoring Oscilloscope	115 V AC	6.25 A	719 W
Sample Holder Monitoring Oscilloscope	115 V AC	7 A	805 W

This power level is approximately fixed. In the Penning discharge system, where large currents are required to create the confining magnetic field, the total power for an implantation is roughly 22,000 Watts including the high-voltage switching circuit power, 91 % of which is magnet coil power. This high power level can be reduced by using a non-magnetized plasma ion implantation system where the total power level for an implantation is less than 5,000 Watts, a more than 75 % reduction in power.

7. Cooling Requirements

Due to the thermal radiation emitted from the directly-heated cathode and to the power dissipated across the cathode-anode electrode pair, adequate cooling of the tube is necessary to ensure a long lifetime of the tube envelope and seals. The rate of deterioration of the tube and seals increases with operating temperature. Inadequate cooling is certain to invite a loss of tube vacuum or permanent damage to the anode. At the maximum power rating of the anode, the forced air cooling requirement is 36 cubic feet per minute. Cooling performance is maximized by the use of an Eimac SK-510 air-system six-pin socket which incorporates low loss insulating materials, plated terminals for corrosion protection, non-ferrous spring alloy, silver plated contact surfaces for positive contact and long life, and open construction providing adequate air flow for proper cooling of the envelope and tube pins.

To direct the air flow around the envelope, an Eimac SK-506 air chimney is used. In this application, five equally-spaced, 3/4" (1.9 cm) holes were drilled on the outside wall of the air chimney. Outside air from the laboratory is drawn into the high-voltage switching circuit enclosure by the use of a 4" (10.2 cm), 120-cubic feet per minute fan. Some of this air is drawn down into these five holes and up through the socket opening. The air then flows through the bottom of the tube base, past the terminal pins, and through several slots in the exterior wall of the tube base. The air then passes around the tube envelope, past the finned, heat-dissipating anode connector. This connector is an Eimac HR-8 plate connector. It provides sufficient heat transfer from the plate inside the tube and the glass seal to the outside air. This connector is machined from dural rod, and is provided with set screws which are used to connect it to the anode terminal on top of the tube and to connect the coaxial wire, leading to the sample holder, to this connector (Varian, 1989). After the air is passed around the tube envelope, it exits the high-voltage switching circuit enclosure through the top lid into another 4" (10.2 cm), 120-cubic feet per minute cooling fan.

Two additional cooling fans are used in the high-voltage switching circuit. One is mounted on the outside of the plexiglass enclosure, and forces air into the enclosure and across the glass chimney to help cool the outside wall of the chimney. This fan is operated from a 12-Volt DC power supply located outside the plexiglass enclosure. A second fan, powered by standard 120 V current, is also mounted on the outside of the enclosure. This drags

hot air away from the electronics inside the enclosure. All three cooling fans located outside the enclosure have standard aluminum screen wire mounted on their exterior faces. This wire is attached to laboratory ground to provide a ground plane at the fan exit which helps to prevent any arcs from escaping the enclosure when the high voltage is on.

8. Power Distribution and Fusing of Electronic Circuits

The power for each electronic circuit must be made available by busswork and each electronic circuit must be protected by a fuse. The leads from the 12-Volt battery are standard battery cables. Red is used for the positive and black for the negative, or internal relative ground. The black cable is the common point inside the high-voltage switching circuit.

A power distribution box made of bakelite was constructed which includes two copper buss bars, one for the positive connection and the other for the negative connection. Each buss bar is capable of supporting 10 conductors. For fusing, this box also contains 5 dual fuse blocks capable of carrying 10 Amperes with a maximum 250-Volt potential drop across each fuse holder. This is a total of 10 fused branches available for protecting various circuits and power supplies.

Figure II.17 is the fusing diagram for the power distribution box inside the high-voltage switching circuit. Fuses 1, 2, and 3 are

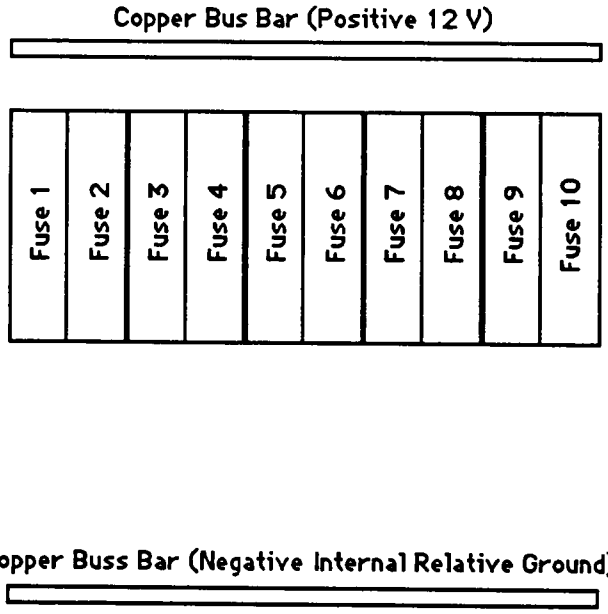


Figure II.17 Fusing diagram for the fuse blocks in the power distribution box. Fuses 1, 2, and 3 are wired in parallel and are for the TMOS filament heater board. Fuses 4 and 5 are blank. Fuse 6 is for the fiber optic transmitter. Fuse 7 powers the microrelay delivering power to the operational amplifier in the TMOS filament heater board. Fuse 8 is blank. Fuse 9 powers the 1,500-V DC to DC converter for the screen grid. Fuse 10 powers the 400-V DC to DC converter for the TMOS control grid switching circuit which turns the vacuum tube on and off.

used to protect the directly-heated cathode (filament). These are connected in parallel. Since the selected fuses are rated at high enough current values, fuse slot 1 was not used. At least two fuses are required because each fuse block can only conduct 10 Amperes of current. Fuse 2 is a Model 3AG, 10 A, 32 V Slo-Blow Littlefuse and fuse 3 is a Model MDL 20, 20 A, 32 V Slo-Blow Buss fuse. Slo-Blow fuses do not open up at their rated current. Instead, they open up only if the excess current persists. These fuses are installed before the directly-heated cathode power transistor circuit and are used to protect the filament. When the filament is initially energized, the filament resistance is low. This causes a high current to flow for a short time until the filament resistance rises with increasing temperature. Thus, more than 22.7 Amperes may flow when the filament is first turned on.

If the filament cathode power transistor circuit becomes shorted in the extreme on condition, the filament could draw a very large current. If very large currents flow through these fuses, they will blow in a shorter time than if only a marginally higher current flows through them. In addition to this protection, the filament is also protected after the directly-heated cathode power transistor circuit by fuse F1C. This fuse is a Model 3AB, 25 A, 32 V Littlefuse and is supported by a single-fuse fuse holder mounted on the plywood base close to the filament connection with the tube. If the filament becomes shorted and causes a very large current to flow for a short time, this fuse will blow and damage to the power transistor circuit should be prevented. Obviously, if the filament becomes

shorted, the vacuum tube can no longer be used and must be replaced.

Fuse 6 is used to protect the negative, 5 V, fixed voltage regulator in the fiber-optic receiver circuit. It is a Model AGC, 6/10 A, 250 V Buss fuse.

Fuse 7 is used to protect the Magnecraft minirelay used to apply 5 Volts DC to the fiber optic receiver amplifier and to the comparator used in the control grid transistor switch. This fuse is a Model AGC, 6/10 A, 250 V Buss fuse.

Fuse 9 is used to protect the screen grid power supply. This fuse is also installed on the positive input lead because if the resistor, varistor, or screen grid inside the vacuum tube becomes shorted, high currents will be stopped before they damage the power supply. Also, there is no reason to install a fuse on the output of this power supply since there are no significant electronics other than a resistor and varistor on the output. This fuse is a Model MDL, 2 A, 32 V Buss fuse. This fuse is also rated 25 % above the rated input current for the control grid power supply. This is acceptable, as stated by the manufacturer.

Fuse 10 is used to protect the control grid power supply. This fuse is installed on the positive input lead because if the control grid power transistor circuit becomes shorted, high currents will be prevented. There is no reason to install a fuse on the output of this supply or on the output of the control grid power transistor circuit. This fuse is a Model AGC, 5 A, 32 V Buss fuse. This fuse is rated 25 %

above the rated input current for the control grid power supply. This is acceptable, as stated by the manufacturer.

There is no fuse to protect the small cooling fans mounted on the control grid power supply and the screen grid power supply. Fuses 1, 4, 5, and 8 are spare slots which can be used for additional power or electronic circuits.

9. Faraday Shielding

Above about 25,000 Volts, small electrical discharges, called corona discharges, can appear on sharp-pointed objects such as screw heads and screw threads, corners of metal boxes, electrical connectors, etc. These corona discharges, which occur more often in humid air than in dry air, can result in significant power drains when the potential is high. For this application, the current levels are on the order of a few tens of milliamperes and corona may cause a significant reduction in the current available to the vacuum tube. Hence, at voltages around 50,000 Volts, some power drain due to corona discharges can be expected.

To prevent corona discharges from occuring or to reduce their effects, an equipotential surface can be placed over the area of expected corona discharge. This is done by constructing a shield made of an electrically-conducting thin metal, and mounting it over the area of interest. This area might be an electronic circuit board or a power supply enclosed in a metal case or any part of a circuit

where sharp edges may be present. Figure II.18 is a simple example of such a shield. A very high electric field will be established in the region between the electronics and the inner surface of the metal shield. This electric field will terminate at the shield and not extend into the enclosure. The shield should be grounded to the common point in the circuit, preventing charge from building up on the shield surfaces. If several electronic circuits are to be shielded, then all of the shields should be grounded to the same point in the system.

In the high-voltage switching circuit, the fiber optic receiver circuit board, the control grid power transistor circuit board, the control grid power supply, the screen grid power supply, and the filament cathode power transistor circuit are shielded with 0.020" thick aluminum sheeting. Each shield was constructed to fit around its respective circuit or power supply, since space is limited within the enclosure. All of these shields are connected to the internal ground of the high-voltage switching circuit and can be easily removed if repair or adjustment to the high-voltage switching circuit becomes necessary.

In addition to this, a Faraday cage, constructed of standard aluminum screen wire on a wooden frame, was erected around the high-voltage switching circuit, the sample holder area, and one-half of the Penning discharge plasma region. This shielding eliminates radio frequency interference resulting from the switching of the high-voltage during implantation. This was determined by surveying the area both inside and outside the shield, using a Narda Health Physics survey instrument with an electric field sensing head

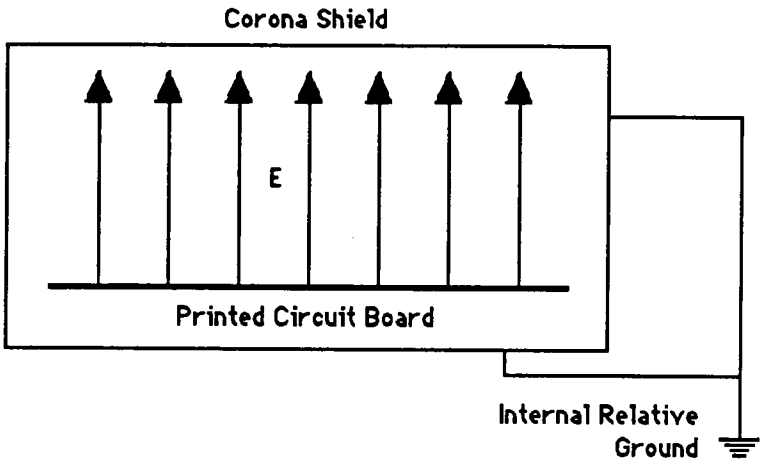


Figure II.18 Geometrical representation of a corona shield covering a printed circuit board. The shield can completely surround the printed circuit board in three dimensions. It can also surround it in two dimensions, if air must flow across the face of the printed circuit board to cool the components.

ranging in frequency from 0.3 to 300 megaHertz. No radio frequency interference was detected outside the Faraday shield when the high-voltage switching circuit was taken up to about 50,000 Volts. The shielding is necessary to keep the radio frequency interference from jamming the diagnostic electronics, where it interferes with the control signal, and from jamming nearby AM and FM radios. If the radio frequency interference is allowed to interfere with the control signal generator, it could cause the high-voltage switching circuit to deliver a high-voltage pulse at a time when it is not intended, thus interfering with the implantation process.

Additional shielding of the control signal generator is provided by placing zinc braid over the coaxial wire used to monitor the sample holder voltage. This braid is grounded at the oscilloscope end of the coax and is not connected to anything at the probe end of the coax near the sample holder. This is necessary because the coax can act as an antenna, picking up radio frequency pulses generated by high-voltage pulses on the sample holder, and transmitting them down the coax to the control signal generator. It should be stated that any arcing or corona occuring around or near the sample holder insulating cylinder or high-voltage switching circuit can also cause radio frequency interference. Therefore, it is important to inspect all areas at high voltage, when the high-voltage is turned on, in a dark environment on a regular basis to detect the presence of any corona or arcing.

10. List and Identification of Components

Listed below in Table II.4 throughout the following pages is every electrical, mechanical, and optical component used in building the high-voltage switching circuit. The component number, the location in the high-voltage switching circuit, the manufacturer's part number, and the place of availability are included. Acronyms are used to indentify the location of each component. Components located in the high-voltage switching circuit box and not on a circuit board are identified by HVSCB in Table II.4. Those in the power distribution box are identified by PDB, in the fiber optic transmitter by FOT, in the fiber optic receiver by FOR, in the control grid power transistor circuit by CGPTC, in the control grid power supply by CGPS, in the screen grid power supply by SGPS, in the directly-heated cathode power transistor circuit by DHCPTC, and in the high-voltage switching circuit enclosure HVSCE. For the location of the components, Source 1 refers to Exide Battery Co. in Knoxville, Source 2 to Newark Electronics in Knoxville, Source 3 to Shield's Electronics in Knoxville, Source 4 to Hamilton-Avenet Electronics in Atlanta, Source 5 to the Electrical and Computer Engineering Department's Parts Store, and Source 6 to Gamma High-Voltage Research in Ormond Beach, Florida.

Table II.4

List of Components for High-Voltage Switching Circuit

Component	Location	Part No.	Source
B1, battery	HVSCB	D8DP	1
F1C, fuse	HVSCB	20F622	2
FB1-FB5, fuseblock	PDB	81F4195	2
F1A, fuse	PDB	N/A	2
F2, fuse	PDB	27F702	2
F3, fuse	PDB	27F845	2
F4, fuse	PDB	N/A	2
F5, fuse	PDB	N/A	2
F6, fuse	PDB	27F583	2
F7, fuse	PDB	27F583	2
F8, fuse	PDB	N/A	2
F9, fuse	PDB	27F836	2
F10, fuse	PDB	27F882	2
F1B, fuse	FOT	28F047	2
PS1, power supply	FOT	84-05-150	2
L1, neon lamp	FOT	NE151A	2
S1, SPST switch	FOT	SP1004	2
W1, grounded cord	FOT	PG-3	2
R1, 2K, 1/4W, resistor	FOT	N/A	2
R2, 1K, 1/4W, resistor	FOT	N/A	2
R3, 34.9 Ohms, 1W, resistor	FOT	N/A	2
R4, 10 Ohms, 1/4W, resistor	FOT	N/A	2
R5, 500 Ohms, 1/4W, resistor	FOT	N/A	2
DIP1, dip switch	FOT	ADF02	2
IC1, integrated circuit	FOT	NTE7400	2

Table II.4
Continued

List of Components for
High-Voltage Switching Circuit

Component	Location	Part No.	Source
D1, fiber optic transmitter	FOT	HFBR-1204	4
Q1, bipolar transistor	FOT	SK 3859	3
B/C1, coaxial connector	FOT	39F1321	2
C1, 0.1 uF capacitor	FOT	47F556	2
C2, 100 uF, tant. capacitor	FOT	47F426	2
PCB1, printed circuit board	FOT	RR-1	5
E1, plastic enclosure	FOT	87F287	3
W2, coaxial cable	FOT	46F8479WF	5
LG1, fiber optic light guide with SMA connectors	FOT	HFBR-3021	4
D2, fiber optic receiver with amplifier	FOR	HFBR-2204	4
MC1,MC2, fiber optic mounting hardware	FOT, FOR	HFBR-4202	4
V1, 5.5 V DC, varistor	FOR	V8ZA2	2
Z1, 6.2 V DC, Zener diode	FOR	1N525A	2
IC1, integrated circuit, negative 5-Volt regulator	FOR	UA7905	2
B1, 9 Volt battery	FOR	N/A	5
RLY1, microrelay	FOR,SGPS	45F330	2
C1, 22 uF electrolytic capacitor	FOR	46F1026	2
C2, 0.01 uF mylar capacitor	FOR	47F566	2
CNR1, 4-pin miniconnector	FOR	41-084	3
CNR2, 6-pin miniconnector	FOR	41-086	3
IC1, dual voltage comparator	CGPTC	LM 393N	2
R1, 100 K, 1/4 W resistor	CGPTC	N/A	5
R2, 10 K, 1/4 W resistor	CGPTC	N/A	5

Table II.4
Continued

List of Components for
High-Voltage Switching Circuit

Component	Location	Part No.	Source
R3, 1 K, 1/4 W resistor	CGPTC	N/A	5
R4, 1 K, 1/2 W resistor	CGPTC	N/A	5
R5, 300 Ohm, 1/2 W resistor	CGPTC	N/A	5
R6, 1.2 K, 1/2 W resistor	CGPTC	N/A	5
Q1, Q2, Q5, TMOS P-channel power transistor	CGPTC	MTP2P45	2
Q3, Q4, TMOS N-channel power transistor	CGPTC	MTP2N90	2
V1, 420 V DC, varistor	CGPTC	V321DA60	2
PCB2, printed circuit board	CGPTC	RR-2	3, 5
CNR1, CNR2, 6-pin high current connector	CGPTC	87F6754	2
HS1, HS2, HS3, HS4, HS5, low-power finned heat sink	CGPTC	291-36H	3
SKT1, 8-pin dip socket	CGPTC	67F1800	2
PS1, 500-Volt DC to DC converter	CGPS	UC40-0.4P12	6
IC1, high-power adjustable voltage regulator	CGPS	SK 9344	3
HS1, high-power finned heat sink	CGPS	295-40H	3
R1, 500 Ohm, potentiometer	CGPS	N/A	5
R2, 5K, potentiometer	CGPS	N/A	5
FN1, cooling fan	CGPS		2
IC1, integrated circuit, adjustable voltage regulator	DHCPTC	SK 9215	3

Table II.4
Continued

List of Components for
High-Voltage Switching Circuit

Component	Location	Part No.	Source
R1, 220 Ohm, potentiometer	DHCPTC	N/A	5
R2, 1.11 K, potentiometer	DHCPTC	N/A	5
R3, 10 K, 1/4 W resistor	DHCPTC	N/A	5
IC2, integrated circuit, operational amplifier	DHCPTC	SK 3692	3
Q1, Q2, Q3, Q4, Q5, Q6, TMOS N-channel power transistor	DHCPTC	MTP12N06	2
CNR1, CNR2, 6-pin high-current connector	DHCPTC	87F6754	2
PCB1, printed circuit board	DHCPTC	RR-3	5
SKT2, 8-pin dip socket	DHCPTC	67F1800	2
HS1, HS2, HS3, HS4, HS5, HS6, high power finned heat sinks	DHCPTC	296-14G	2
VT1, 1000 W vacuum tetrode power grid tube	HVSCB	4PR1000A-8189	5, 7
SKT2, air-system socket	HVSCB	SK-510	5, 7
CH1, air chimney	HVSCB	SK-506	5, 7
FN2, FN3, cooling fans, 120 cfm, 12 V DC	HVSCE	44F4036	2
FN4, cooling fan 120 cfm, 120 V AC	HVSCE	87F3621	2
S1, knife switch, DPST	HVSC	N/A	5
PS2, 1500 V DC to DC converter	SGPS	UC15-1.5P/12	6

CHAPTER 3

PLASMA ION IMPLANTATION IN A UNIFORM PENNING DISCHARGE

The initial testing of the high-voltage switching circuit designed and built for plasma ion implantation was conducted at the UTK Plasma Science Laboratory in an existing modified Penning discharge in a uniform magnetic field. F. M. Penning (Penning et al., 1937, 1949) developed this type of discharge as a vacuum gauge. The Penning discharge has been the vacuum system of choice for many plasma experiments due to its simplicity and ease of plasma generation at low pressures. This vacuum system was used because of its availability at the time our plasma ion implantation research was initiated. In this chapter, the results of the high-voltage switching circuit tests, the first plasma ion implantation, and the results of several additional tests will be presented. It is necessary to include the results of the high-voltage switching circuit tests here, because a proper evaluation of the circuit's performance can be conducted only in a plasma environment.

A. The Penning Discharge Vacuum System

The vacuum system used initially is illustrated in Figure III.1. It is constructed of 6" (15.2 cm) pyrex pipe joined by viton rubber gaskets. The central section of the vacuum system in which the

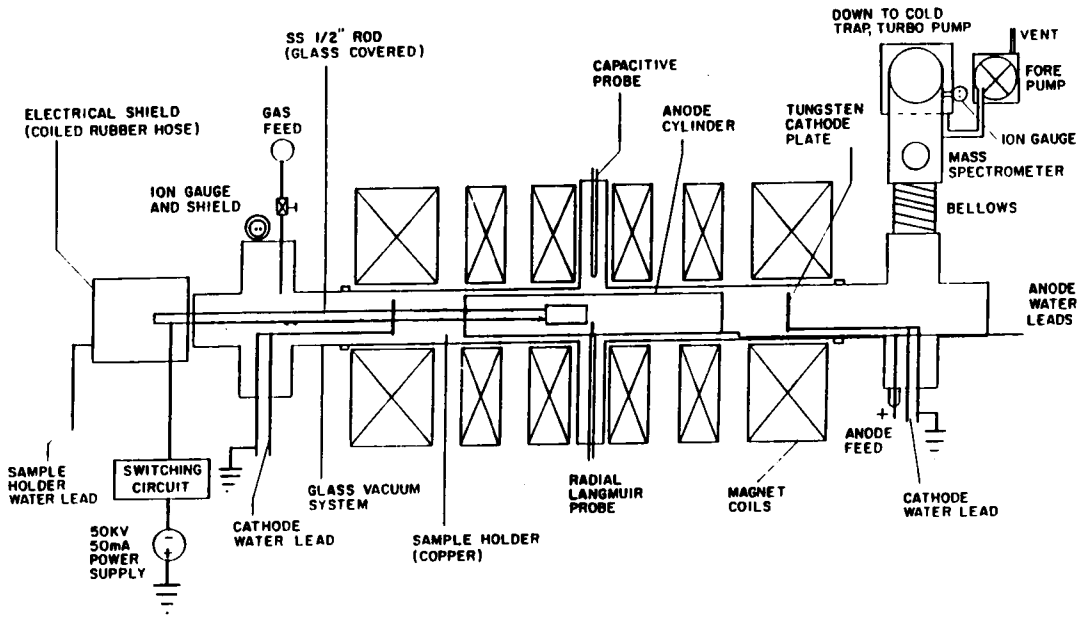


Figure III.1 The Penning discharge with the copper anode cylinder electrode arrangement used in the first plasma ion implantation experiment.

plasma is generated consists of a 47" (119 cm) long section of 6" (15.2 cm) diameter pyrex pipe with three 1.75" (4.4 cm) centimeter diameter extension arms located at the midplane. These arms can be used to insert such plasma diagnostic sensors as Langmuir and capacitive probes. On each end of this central section is a tee. On the South end, the tee is used to mount the A-lite fitting and cooling cylinder for the sample holder, and for cathode and anode electrical and water line connections. On the North end, the tee is used for the vacuum pumping exhaust and also cathode and anode electrical and water line connections.

Inside the central section, several geometrical arrangements of anodes and cathodes can be inserted to set up different boundary conditions on the plasma. In the initial testing and plasma ion implantation procedures, the anode was a 5" (12.7 cm) diameter, 32" (81.3 cm) long, water-cooled, copper cylinder with its midpoint positioned at the midplane, and axisymmetric with the vacuum system. The cathode on the North end of the vacuum system consisted of one 1/4" (0.64 cm) diameter spiral copper coil positioned at the maximum of the magnetic field. The side of this cathode facing the plasma was covered by a tungsten plate with a 1/2" (1.3 cm) diameter hole in its center. This hole was provided to allow an ion beam to pass out of the plasma and into a diagnostic instrument. This instrument could be a retarding potential energy analyzer to measure the ion energy distribution, or it could be a mass spectrometer to determine the neutral and ion masses in the plasma. The cathode on the South end of the vacuum system is also made of

1/4" (0.64 cm) diameter copper tubing wound like a coiled helical spring with a 5" (12.7 cm) hole on axis. This cathode arrangement is necessary to allow for the insertion and removal of the sample holder. The inside diameter of this coil is 5" (12.7 cm), which is sufficient for samples as large as 3" (7.6 cm) to 4" (10.2 cm) in diameter. These cathodes were used for all of the plasma ion implantation experiments conducted in the Penning discharge.

The operating pressure required by this Penning discharge is maintained by a three-stage pumping system. The vacuum pumping system consists of a Duo-Seal Model 3917 mechanical forepump in series with a Pfeiffer-Balzers Model TPH 170 turbomolecular pump. The turbomolecular pump is in series with a CVC, Inc. cold trap cooled by a Polycold Model PCT-200 cryogenic refrigerator, which can reach a temperature of -140 degrees Celsius. The cold trap can be isolated from the vacuum system by closing a gate valve above the cold trap. The forepump alone can reach pressures of about 30 millitorr. Pressures above this level are measured by a Ion Equipment Co. Model TGC-101 thermocouple gauge control connected to two thermocouple gauges. One of them, TG1, is located on the exit line of the turbomolecular pump, and the other, TG2, is located above the entrance to the gate valve. Gas pressures below 1 millitorr are measured by two Bayard-Alpert ionization gauge tubes located at each end of the vacuum system. One reads the pump head gauge pressure, located in a tee on the North end of the main vacuum system. The other is the inlet gauge pressure on the South end, located near the gas inlet valve. These gauge pressures are digitally

presented by two Varian Model 880 ionization gauge controls with fool-proof protection circuitry for the ionization gauge tubes. During operation of the plasma, neutral gas is continuously pumped out. The background gases as well as reaction products of plasma chemistry are monitored by a Veeco Model SPI-10 monopole residual gas analyzer (mass spectrometer) which was initially mounted at the pumping end of the vacuum system in a non-line-of-sight position to the plasma. In later experiments, the gas analyzer was moved to a position on the North end of the vacuum system to take measurements in a line-of-sight position on the plasma axis. For operating procedures for the vacuum system, refer to Appendix D.

B. The Magnetic Field Profile

The magnet coils, which enclose the 6" (15.2 cm) diameter pyrex pipe, were positioned to form a uniform magnetic field profile along most of the usable length of this pipe. The magnetic field is provided by 16 water-cooled coils. The normalized field profile (Spence, 1990) along the axis is shown in Figure III.2. At a maximum coil current of 900 A and in its uniform region, it has an intensity of about 0.184 Tesla. At its end, where the magnetic field maximum occurs, it has an intensity of about 0.14 Tesla. This maximum acts like a reflector for some of the ions traveling along

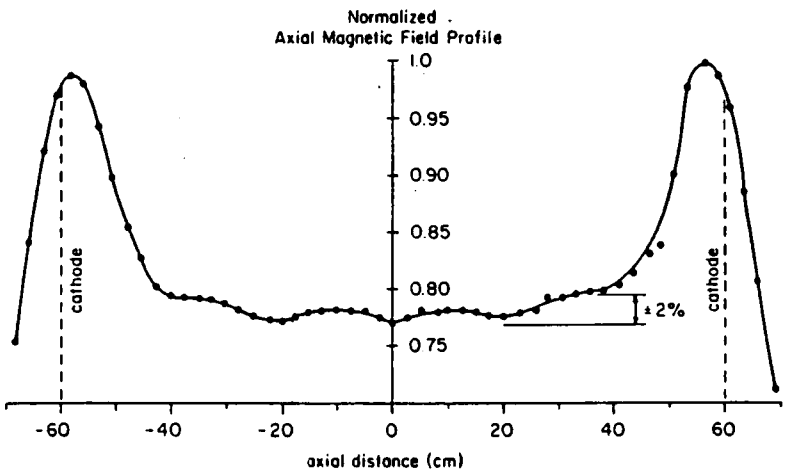


Figure III.2 The magnetic field profile for the modified Penning discharge used in all plasma ion implantation experiments (Spence, 1990).

the axis. In the uniform region, the parallel velocity of the ions behaves as if there were no magnetic field at all.

C. Powering the Penning Discharge

In the initial experiments, the power to the anodes and cathodes was supplied by a Del Electronic, Inc. Model 40-1000-1 40 kilovolt, 1 Ampere, oil-cooled DC power supply. The DC power was delivered by RG-638/U coaxial cable. This cable is connected to the anodes by an A-lite high-voltage insulator. On the inside of the vacuum interface, a No. 14 AWG wire with high dielectric strength insulation is connected between this A-lite insulator and the anode. This arrangement is used for each anode. The cathodes are connected to ground with No. 12 AWG wire. This connection is made outside the vacuum system for each cathode separately. In this system, both the anodes and cathodes must be water cooled. This is why they are usually made of 1/4" (0.64 cm) copper tubing, which can be easily fabricated into many electrode geometries. The high-voltage and the cooling water feedthroughs are located on two 6" (15.2 cm) diameter pyrex tees, one at each end of the vacuum system. The control of the power to the anodes and cathodes is discussed in Appendix C. The power for the magnet coils is supplied by a Teledyne-Pacific Model CV-1000 40 Volt, 1000 Ampere DC power supply that can supply up to 900 A. The maximum field

obtainable with this supply in this configuration is about 0.2 Tesla. For the operation of these coils, refer to Appendix C.

After shake-down tests with the high-voltage switching circuit, it was discovered that a voltage drop on the implantation voltage was due to the high internal resistance of the NJE, 50 kV, 50 mA, power supply. During these tests, at high implantation currents, the voltage drop was about one-half that of the implantation voltage from the NJE power supply. This problem was discovered by placing a high-voltage probe on the cathode of the vacuum tube to measure the negative high-voltage before it was switched, and then compare it with the voltage at the anode of the tube. Ideally, the voltage waveform for the cathode should have been a negative DC pulse. However, it was found that the negative high-voltage applied to the cathode became more positive during the implantation voltage pulse. The magnitude of this increase was about equal to the drop seen at the sample holder. At low current levels, the voltage drop was small. At high current levels, obtained when the pressure was increased, the voltage drops due to the high voltage power supply internal impedance were not negligible. The problem was corrected by exchanging the power supply feeding the Penning discharge and that feeding the high-voltage switching circuit.

With this change, the Penning discharge is now powered by the NJE, 50 kV, 50 mA power supply and is marked on its front panel accordingly. This is not a problem as long as high Penning discharge powers are not required. In this application, high plasma discharge powers are not required. The implantation power is furnished by

the Del Electronics, 40 kV, 1 A supply which has a low internal resistance. The voltage drop associated with this power supply was measured and found to be less than 500 V at negative potentials of 20 kV, an acceptable value.

D. Testing the High-Voltage Switching Circuit in the Penning Discharge

The high-voltage switching circuit was tested in the vacuum system pictured in Figure III.1. The sample holder used in these initial tests is pictured in Figure III.3. The sample holder consists of a 48" (121.9 cm) long, 1/2" (1.3 cm) diameter stainless steel tube with a concentrically positioned, 60.25" (153 cm) long, 1/8" (0.32 cm) diameter stainless steel tube. These two tubes deliver cooling water to a 3.94" (10 cm) long by 1" (2.54 cm) square copper block with a chamber in the center for the cooling water. The cooling water flows into the center tube and out through the supporting tube. The sample holder rod is inserted through an A-lite high-voltage insulator mounted to a 3/4" (1.9 cm) circular plexiglass plate, 11-1/2" (29.2 cm) in diameter. The plate is bolted to the cooling cylinder and has 8 aluminum bolts extending through it which are used to mount the plexiglass plate to the flange on the South end of the vacuum system. The sample holder contained no metal samples

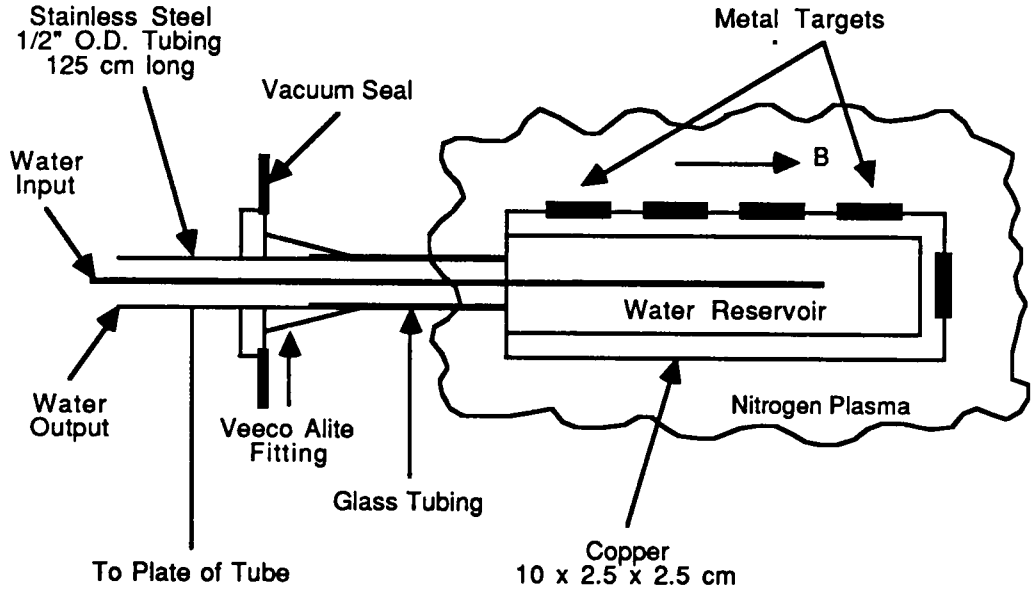


Figure III.3 The first sample holder system used in plasma ion implantation experiments.

during the high-voltage switching circuit tests and was inserted in the Penning discharge of Figure III.1.

Figure III.4 is a schematic diagram of the equipment used to test the high-voltage switching circuit. The implantation power source was connected to the cathode of the vacuum tube, and the sample holder was connected to the anode of the vacuum tube. The negative high-voltage pulse on the sample holder was the only waveform being measured here. To do this, two high-voltage probes were used. A Tektronix Model P 6015 high-voltage probe with a Tektronix Model 015-049 compensating box was connected to the Channel 1 input of a Tektronix Model 7600 oscilloscope. This probe is capable of measuring a 20,000-Volt DC or a 40,000-Volt AC signal at a maximum frequency of 110 kHz. The probe can measure up to 55 kV DC before breakdown. Thus, for implantation experiments below 50 kV, this probe will suffice. A Jennings Radio Corp. Model J-1003 capacitively-coupled high-voltage probe was connected to the Channel 2 input of the same oscilloscope. This probe is capable of measuring a 100,000-Volt AC signal at a maximum frequency of 20 MHz. After confirmation that both instruments read the same voltage and waveform shape, the input to Channel 1 was moved to Channel 2 and the pulse from the control signal generator was connected to Channel 1. This allowed us to compare the switching pulse of the control signal to the waveform of the high-voltage switching circuit voltage.

The control signal parameters, including the time that the negative biasing voltage was on, $t_{nb\ on}$, the time that the negative

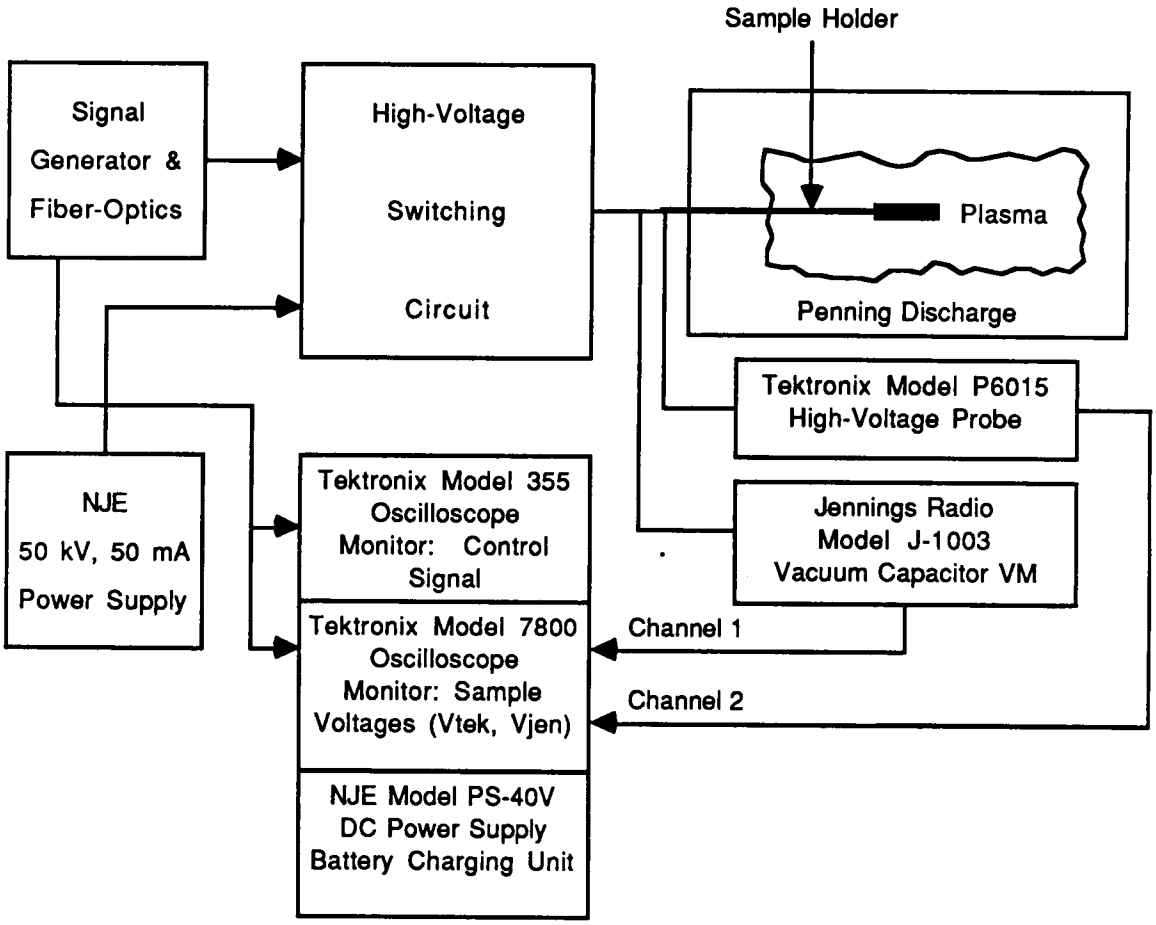


Figure III.4 The system used to test the high-voltage switching circuit and to conduct the first plasma ion implantation experiment.

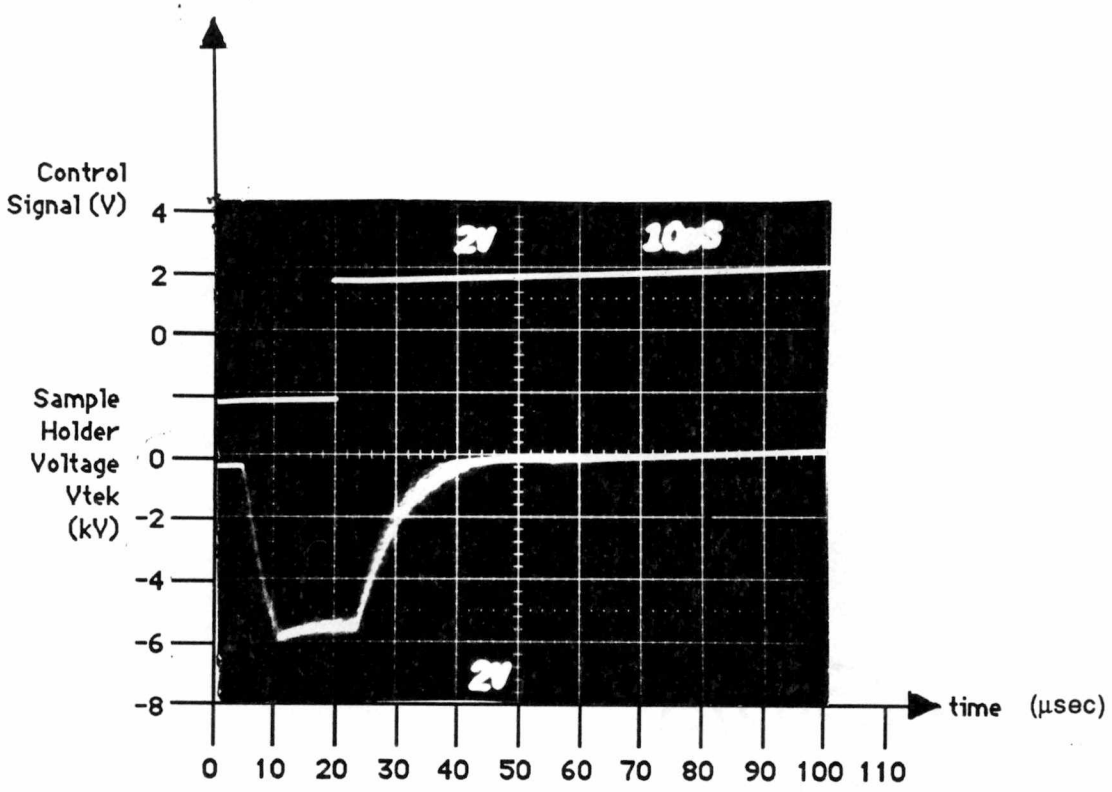


Figure III.5 (Run CCC-1) Oscillogram showing the control signal (upper trace with 2 V per vertical division) and the sample holder voltage (lower trace with -2 kV per vertical division) using the Tektronix probe for a negative bias-on time of 20 μsec, a negative bias-off time of 1 msec, a negative bias of - 5 kV, and a sample holder current of 2.6 mA. The Penning anode voltage was 1.7 kV, the anode current was 43 mA, the pressure was 70 μtorr, and the magnetic field was 0.148 Tesla. The amplitude of the probe voltage, including the plasma potential, is about 6 kV.

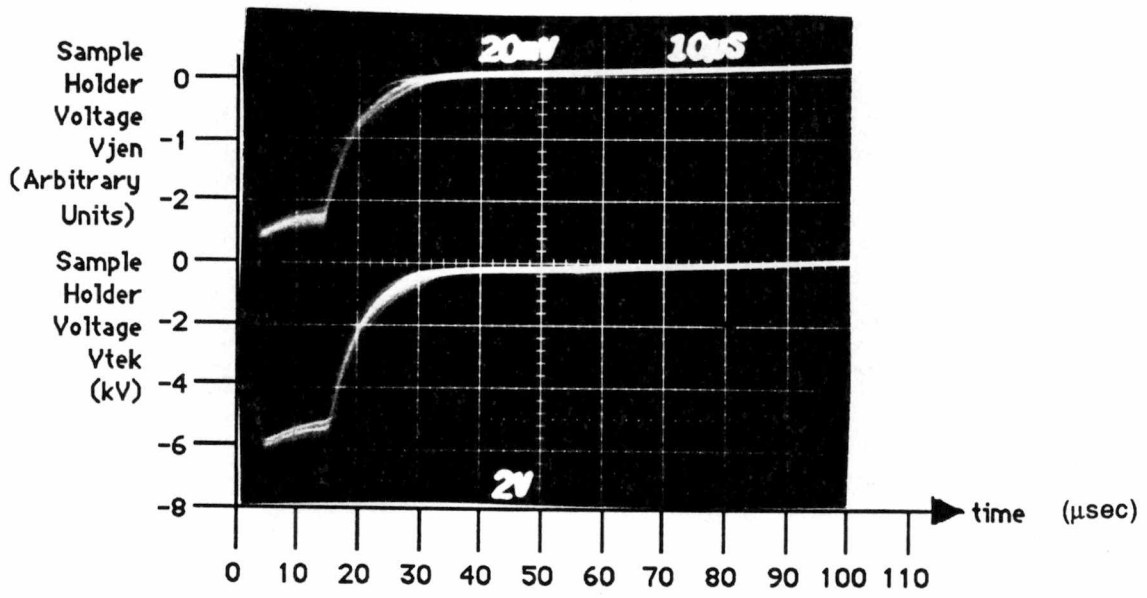


Figure III.6 (Run CCC-1) Oscillogram showing the sample holder voltage using the Jennings instrument (upper trace) and using the Tektronix probe (lower trace with -2 kV per vertical division) for the same HVSC and plasma conditions as in Figure III.5. The amplitude of the probe voltage, including the plasma potential, is about 6 kV.

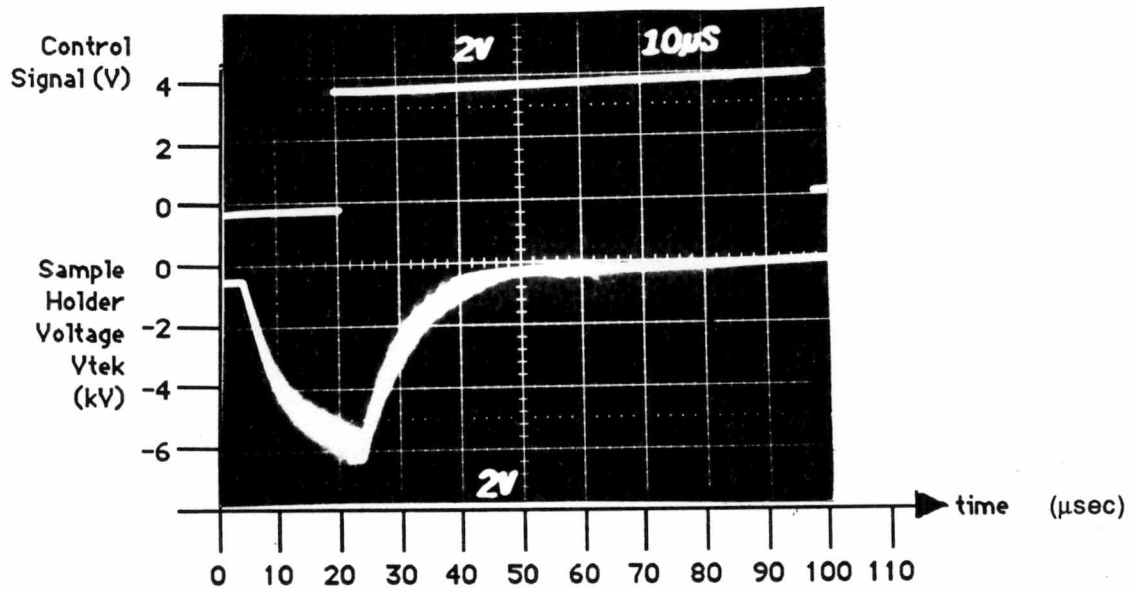


Figure III.7 (Run CCC-2) Oscillogram showing the control signal (upper trace with 2 V per vertical division) and the sample holder voltage (lower trace with -2 kV per vertical division) using the Tektronix probe for a negative bias-on time of 20 μsec, a negative bias-off time of 100 μsec, a negative bias of - 5 kV, and a sample holder current of 23 mA. The Penning anode voltage was 1.6 kV, the anode current was 62 mA, the pressure was 70 μtorr, and the magnetic field was 0.148 Tesla. The amplitude of the probe voltage, including the plasma potential, is about 6 kV.

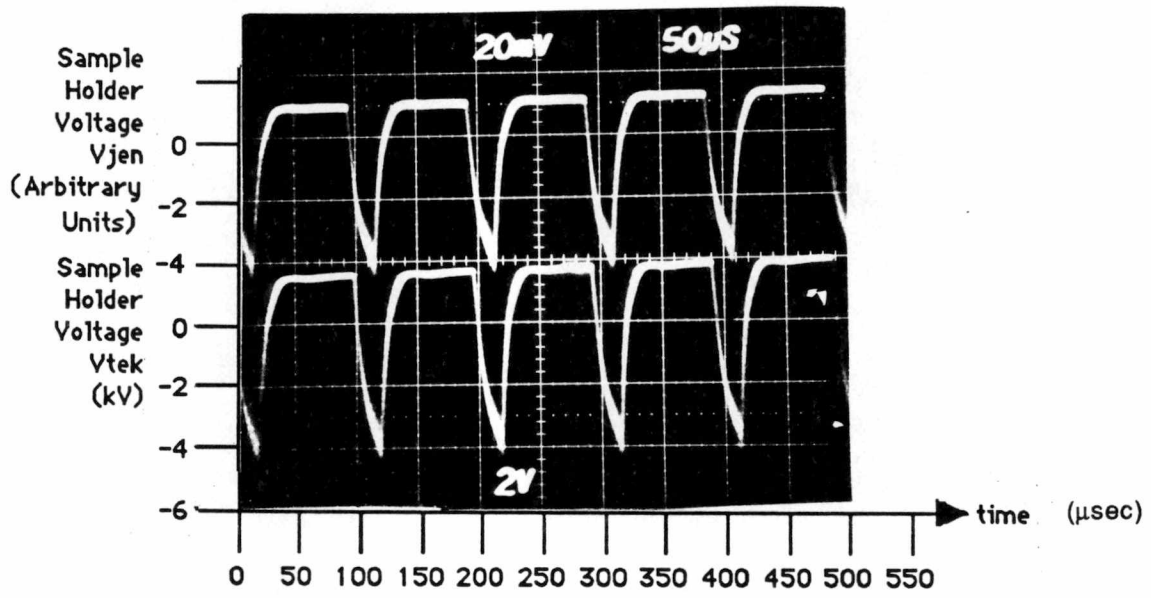


Figure III.8 (Run CCC-2) Oscillogram showing several sample holder voltage pulses using the Jennings instrument (upper trace) and the Tektronix probe (lower trace with -2 kV per vertical division). The HVSC and plasma conditions are the same as Figure III.7. The amplitude of the probe voltage for the lower trace, including the plasma potential, is about 6 kV.

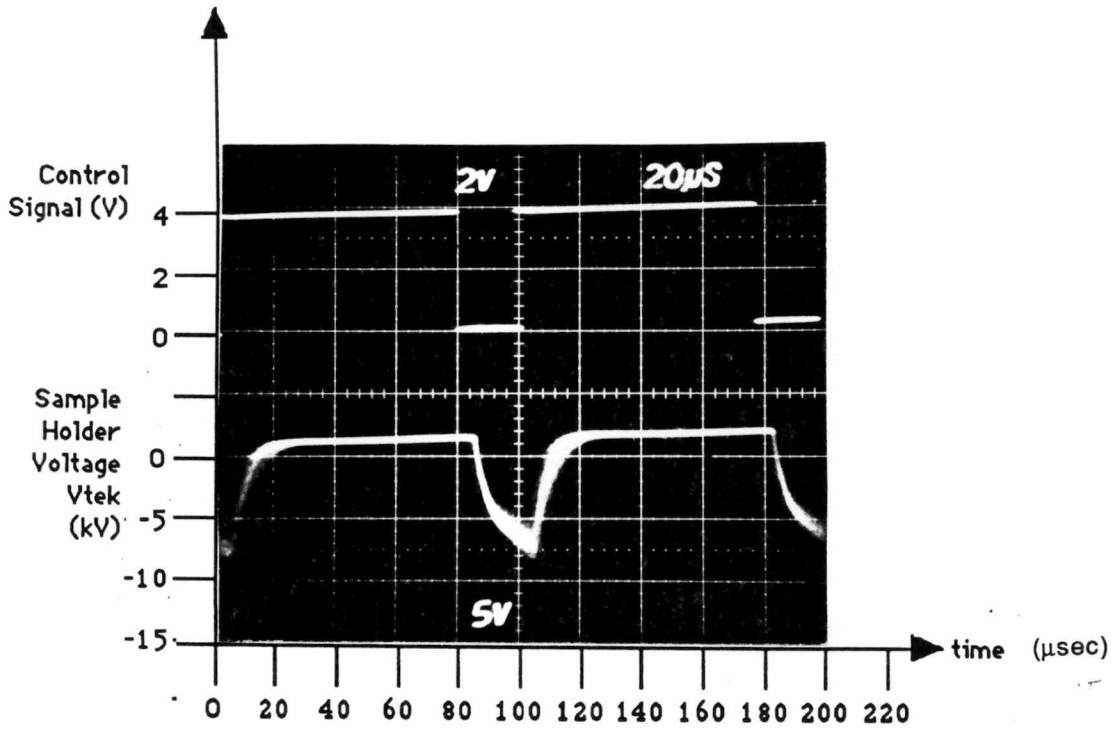


Figure III.9 (Run CCC-3) Oscillogram showing several control signal pulses (upper trace with 2 V per vertical division) and sample holder voltage pulses (lower trace with -5 kV per vertical division) using the Tektronix probe for a negative bias-on time of 20 μsec, a negative bias-off time of 80 μsec, a negative bias of - 10 kV, and a sample holder current of 50 mA. The Penning anode voltage was 1.35 kV, the anode current was 100 mA, the pressure was 73 μtorr, and the magnetic field was 0.148 Tesla. Notice the effects of the plasma potential above the zero mark. The amplitude of the probe voltage, including the plasma potential, is about 7.5 kV.

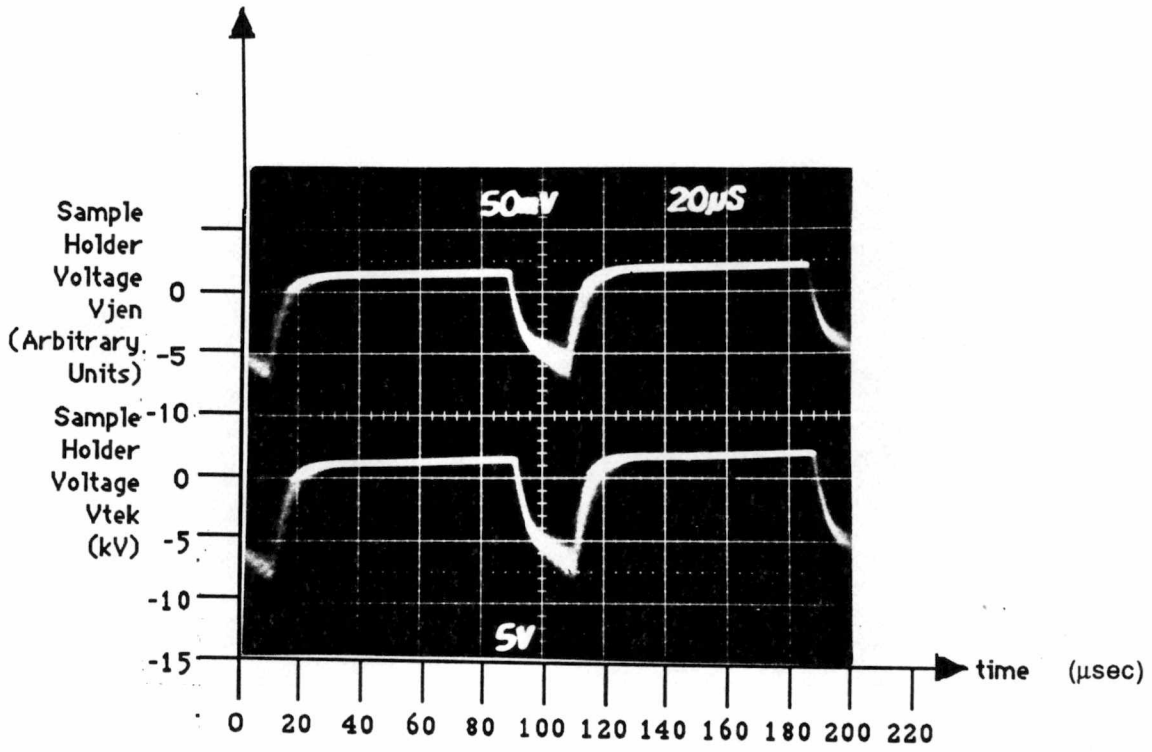


Figure III.10 (Run CCC-3) Oscillogram showing several sample holder voltage pulses using the Jennings instrument (upper trace) and the Tektronix probe (lower trace with -5 kV per vertical division). The HVSC and plasma conditions are the same as Figure III.9. The amplitude of the probe voltage for the lower trace, including the plasma potential, is about 7.5 kV.

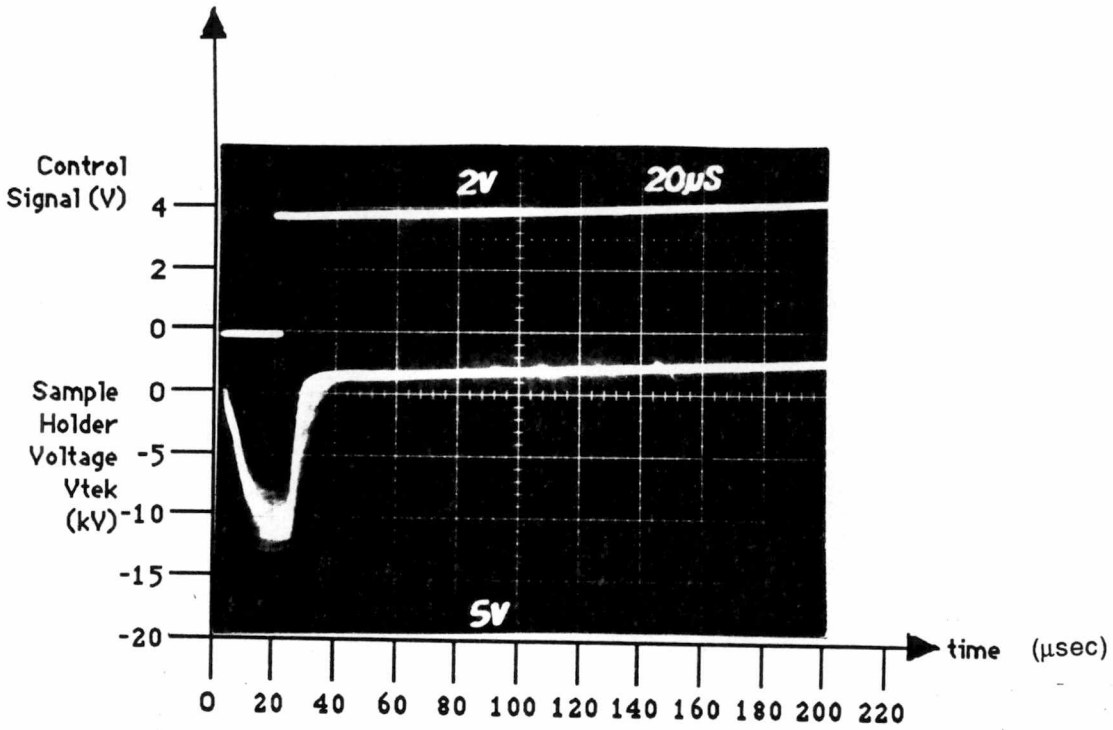


Figure III.11 (Run CCC-4) Oscillogram showing the control signal (upper trace with 2 V per vertical division) and the sample holder voltage (lower trace with -5 kV per vertical division) using the Tektronix probe for a negative bias-on time of 20 μsec, a negative bias-off time of 400 μsec, a negative bias of -15 kV, and a sample holder current of 16 mA. The Penning anode voltage was 1.5 kV, the anode current was 88 mA, the pressure was 66 μtorr, and the magnetic field was 0.148 Tesla. The amplitude of the probe voltage, including the plasma potential, is about 12.5 kV.

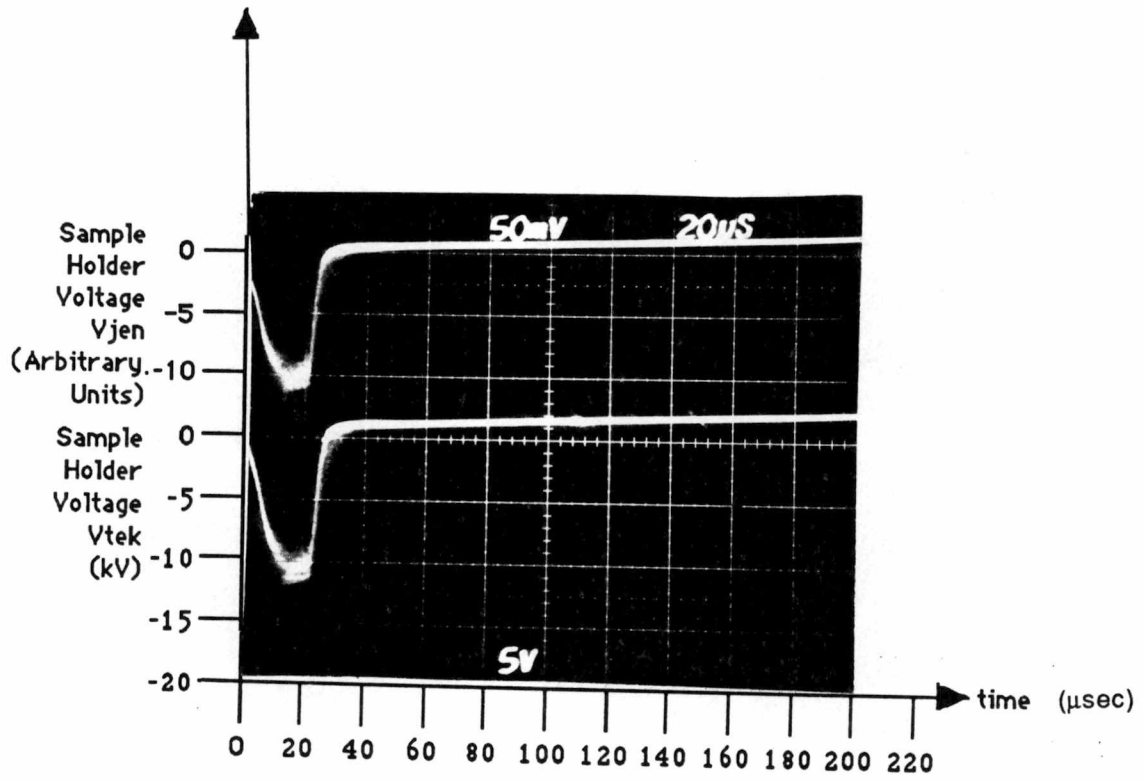


Figure III.12. (Run CCC-4) Oscillogram showing several sample holder voltage pulses using the Jennings instrument (upper trace) and the Tektronix probe (lower trace with -5 kV per vertical division). The HVSC and plasma conditions are the same as Figure III.11. The amplitude of the probe voltage for the lower trace, including the plasma potential, is about 12.5 kV.

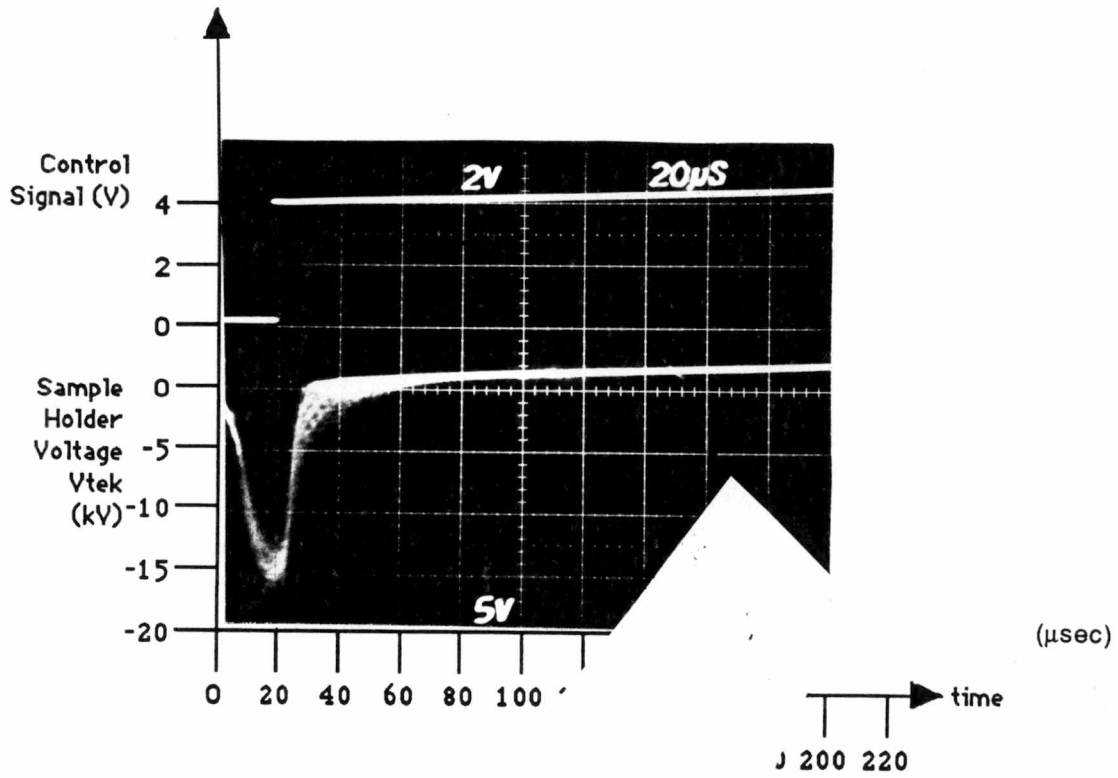


Figure III.13 (Run CCC-5) Oscillogram showing the control signal (upper trace with 2 V per vertical division) and the sample holder voltage (lower trace with -5 kV per vertical division) using the Tektronix probe for a negative bias-on time of 20 μsec, a negative bias-off time of 400 μsec, a negative bias of -20 kV, and a sample holder current of 33 mA. The Penning anode voltage was 1.3 kV, the anode current was 110 mA, the pressure was 16 μtorr, and the magnetic field was 0.148 Tesla. The amplitude of the probe voltage, including the plasma potential, is about 15 kV.

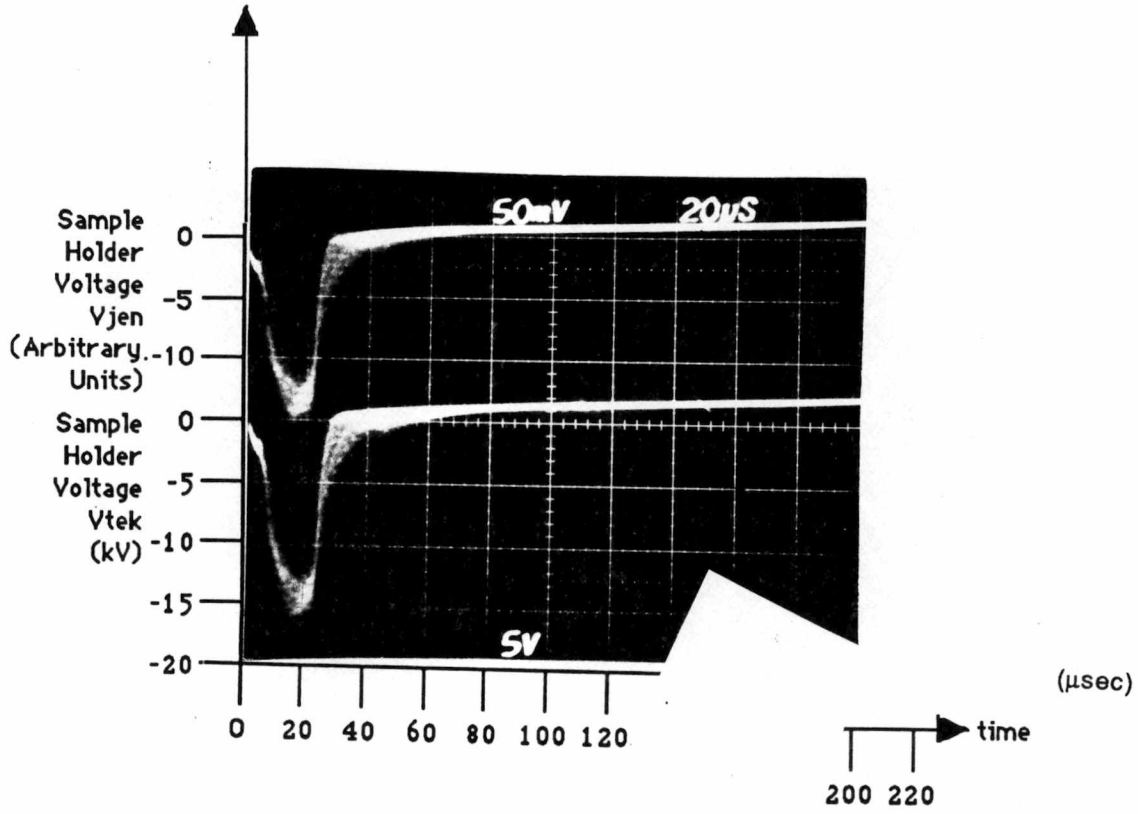


Figure III.14 (Run CCC-5) Oscillogram showing a sample holder voltage pulse using the Jennings instrument (upper trace) and the Tektronix probe (lower trace with -5 kV per vertical division). The HVSC and plasma conditions are the same as Figure III.13. The amplitude of the probe voltage for the lower trace, including the plasma potential, is about 15 kV.

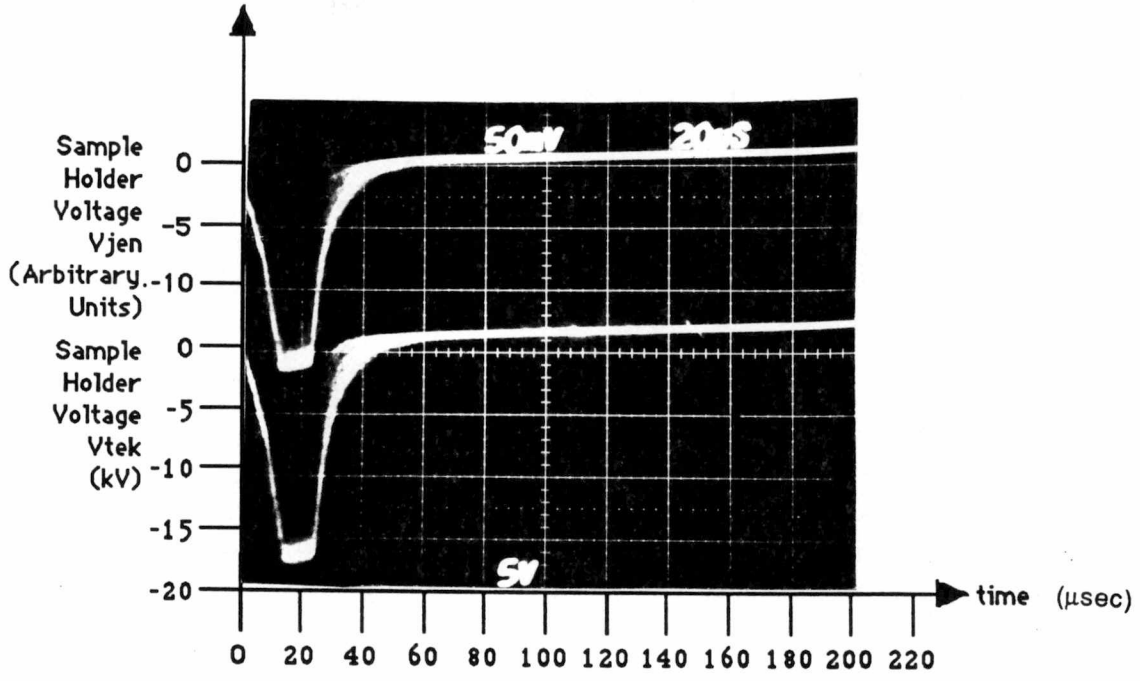


Figure III.15 (Run CCC-6) Oscillogram showing a sample holder voltage pulse using the Jennings instrument (upper trace) and the Tektronix probe (lower trace with -5 kV per vertical division) for a negative bias-on time of 20 μsec, a negative bias-off time of 1 msec, a negative bias of -20 kV, and a sample holder current of 9 mA. The Penning anode voltage was 1.6 kV, the anode current was 69 mA, the pressure was 65 μtorr, and the magnetic field was 0.148 Tesla. The amplitude of the probe voltage for the lower trace, including the plasma potential, is about 17 kV.

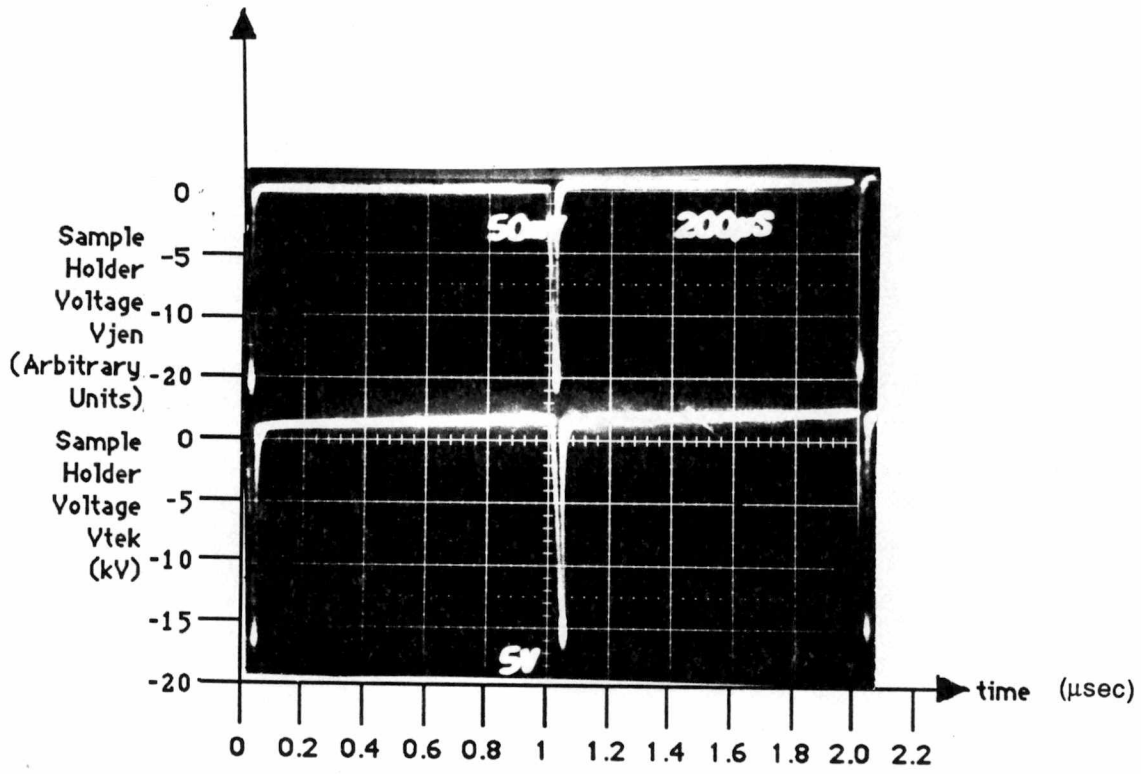


Figure III.16 (Run CCC-6) Oscillogram showing several sample holder voltage pulses using the Jennings instrument (upper trace) and the Tektronix probe (lower trace with -5 kV per vertical division). The HVSC and plasma conditions are the same as Figure III.15. The amplitude of the probe voltage for the lower trace, including the plasma potential, is about 17 kV.

biasing voltage was off, $t_{nb\ off}$, and the negative biasing voltage, V_{bias}, were being varied during these tests, to examine the effects of varying the switching times on the plasma. The high-voltage switching circuit and plasma parameters are listed in the figure caption for each run. Figures III.5 through III.16 represent the switching voltage signals of Runs CCC-1 through CCC-6, respectively. In these six runs, only the negative biasing voltage and the negative bias-off time were varied. The negative bias-on time was held constant at 20 microseconds. Figures III.17 through III.22 represent the switching voltage signals of Run CCC-7, in which only the negative bias-on time was varied. The purpose of this run was to observe the effects on the plasma of varying the negative bias-on time. Figures III. 23 through III.30 represent the switching voltage waveforms of Run CCC-8, where only the negative biasing voltage was varied, from -1 kV to -17.5 kV in 2.5 kV increments. The purpose of this run was to observe the amplitude and waveform of the negative pulse, measured by the two probes. The negative bias-on time and the negative bias-off time were held constant at 20 μsec and 1 msec, respectively.

Figures III.5 through III.8 represent the switching voltage signals of Runs CCC-1 and CCC-2, respectively, for a constant negative bias of -5,000 Volts DC on the implantation power source, and a constant negative bias-on time of 20 microseconds. In Figure III.5, note the approximately 5-μsec delay between the control signal and the switching voltage signal. This is due to time delays associated with the control grid circuitry and the operation of the tube. Also,

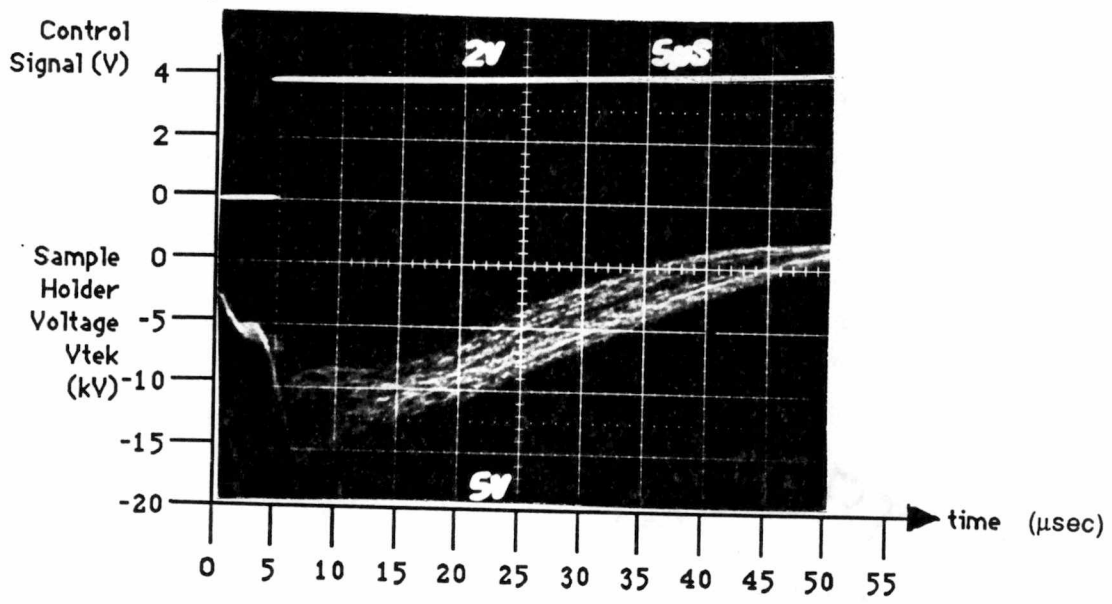


Figure III.17 (Run CCC-7) Oscillogram showing the control signal (upper trace with 2 V per vertical division) and the sample holder voltage (lower trace with -5 kV per vertical division) using the Tektronix probe for a negative bias-on time of 5 μsec, a negative bias-off time of 1 msec, and a negative bias of -20 kV. The amplitude of the sample holder voltage is 16.5 kV.

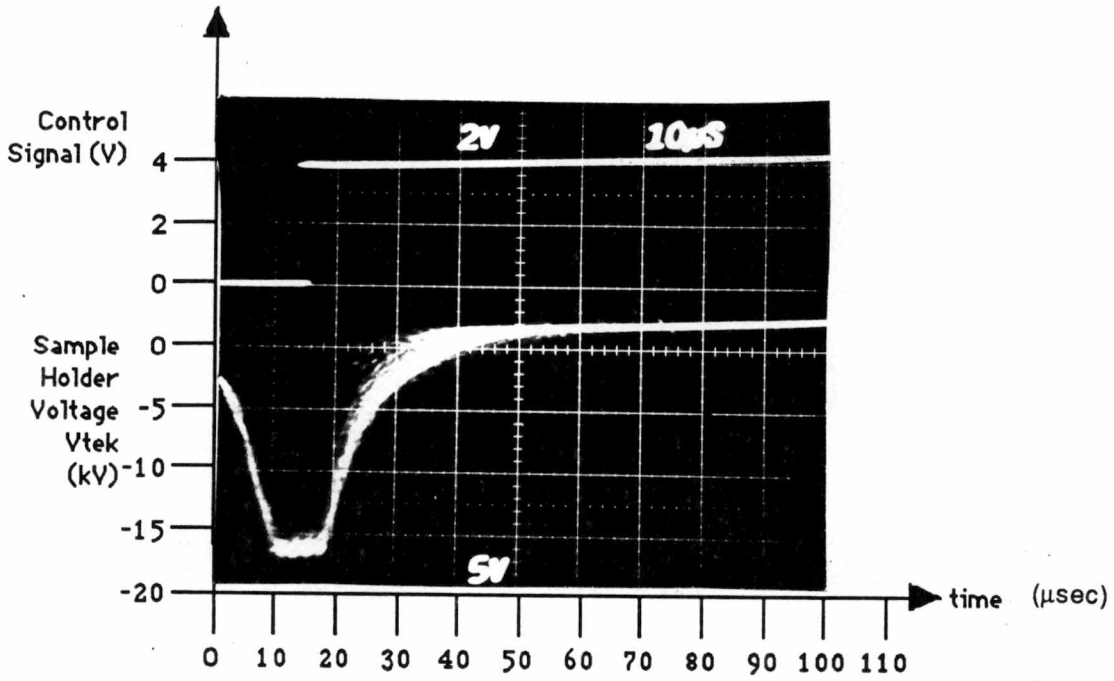


Figure III.18 (Run CCC-7) Oscillogram showing the control signal (upper trace with 2 V per vertical division) and the sample holder voltage (lower trace with -5 kV per vertical division) using the Tektronix probe for a negative bias-on time of 15 μsec, a negative bias-off time of 1 msec, and a negative bias of -20 kV. The amplitude of the sample holder voltage is 17.5 kV.

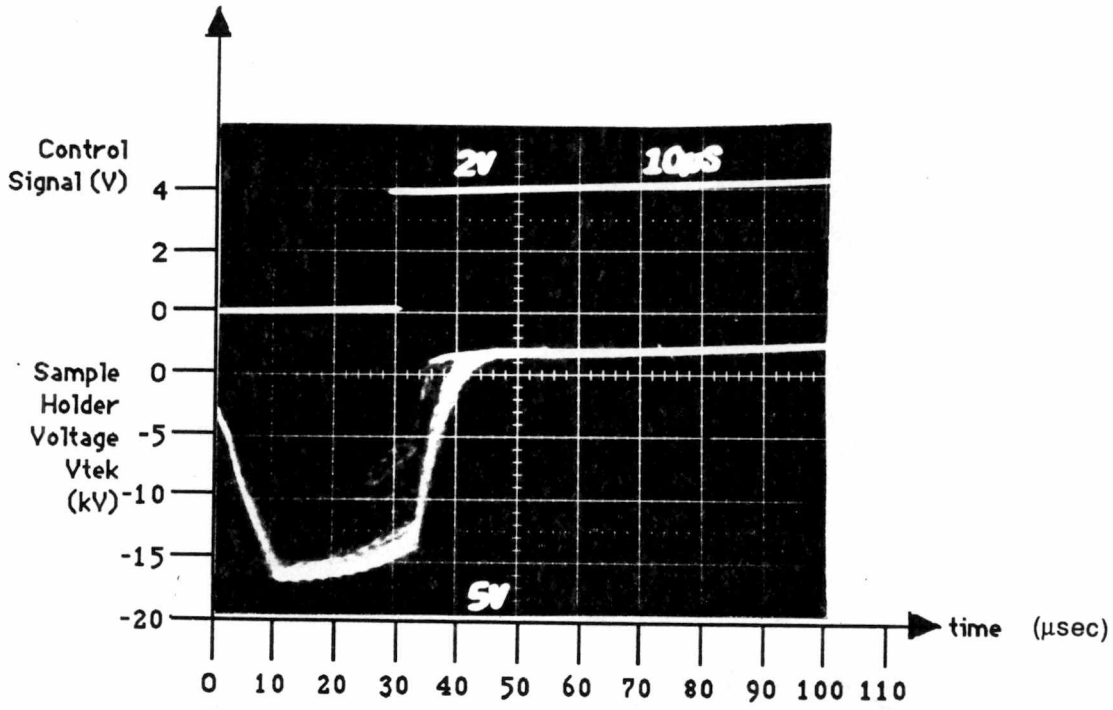


Figure III.19 (Run CCC-7) Oscillogram showing the control signal (upper trace with 2 V per vertical division) and the sample holder voltage (lower trace with -5 kV per vertical division) using the Tektronix probe for a negative bias-on time of 30 μsec, a negative bias-off time of 1 msec, and a negative bias of -20 kV. The amplitude of the sample holder voltage is 17.5 kV.

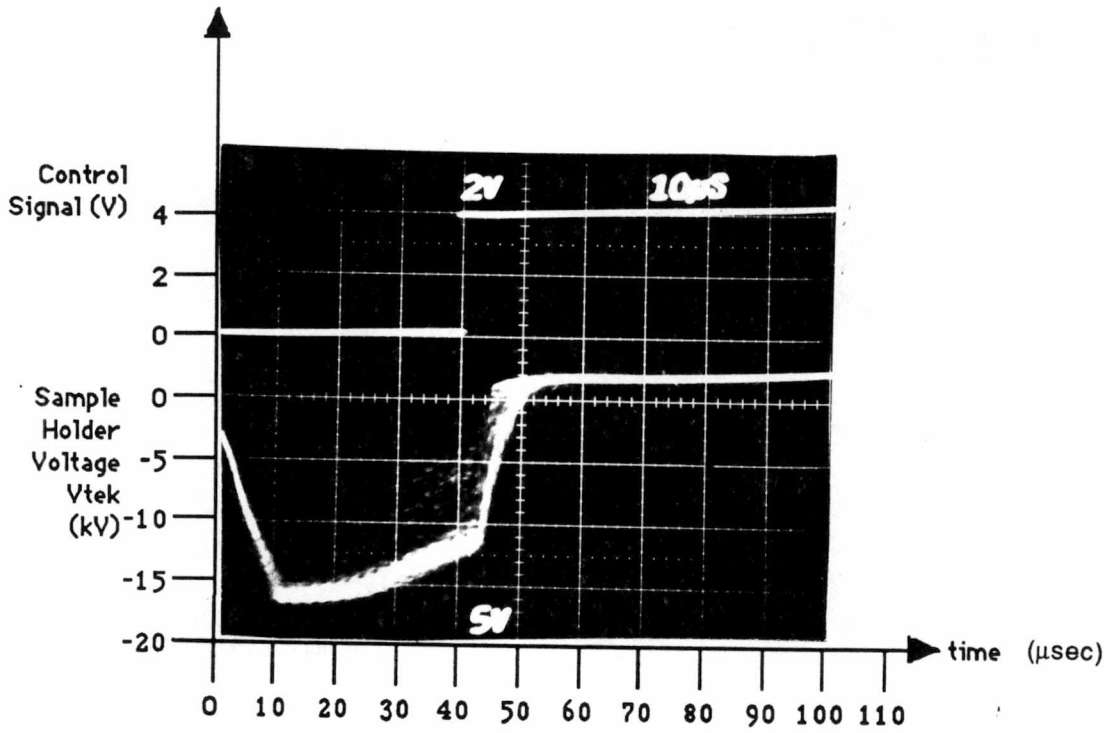


Figure III.20 (Run CCC-7) Oscillogram showing the control signal (upper trace with 2 V per vertical division) and the sample holder voltage (lower trace with -5 kV per vertical division) using the Tektronix probe for a negative bias-on time of 40 μsec, a negative bias-off time of 1 msec, and a negative bias of -20 kV. The amplitude of the sample holder voltage is 17.5 kV.

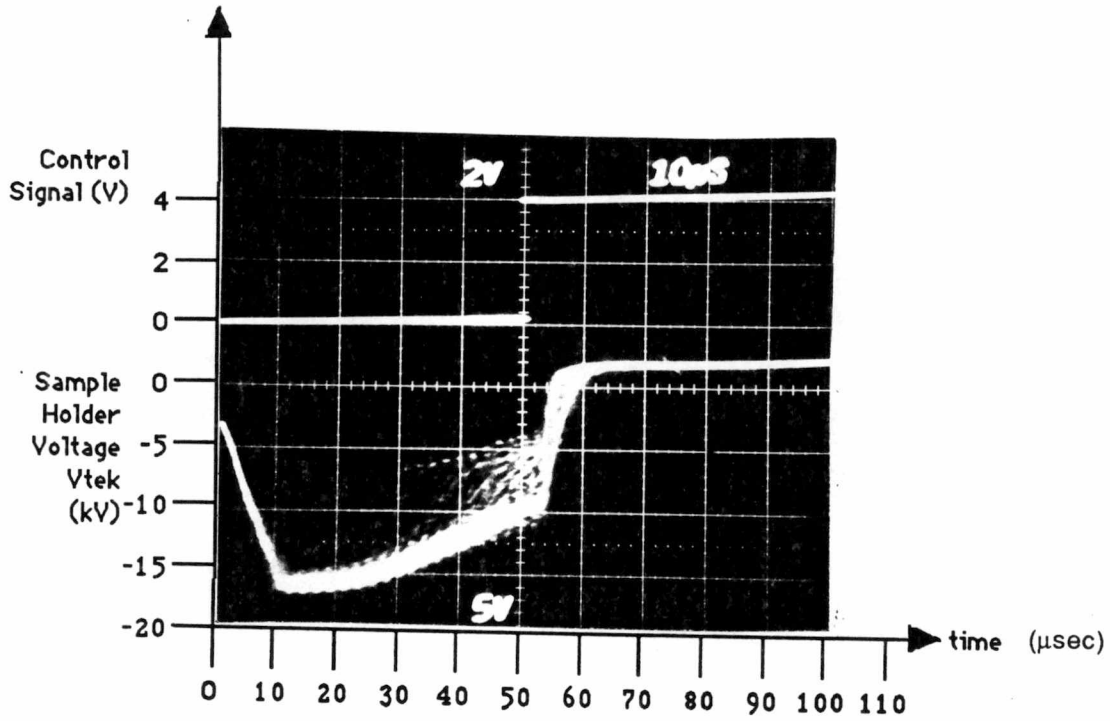


Figure III.21 (Run CCC-7) Oscillogram showing the control signal (upper trace with 2 V per vertical division) and the sample holder voltage (lower trace with -5 kV per vertical division) using the Tektronix probe for a negative bias-on time of 50 μsec, a negative bias-off time of 1 msec, and a negative bias of -20 kV. The amplitude of the sample holder voltage is 17.5 kV.

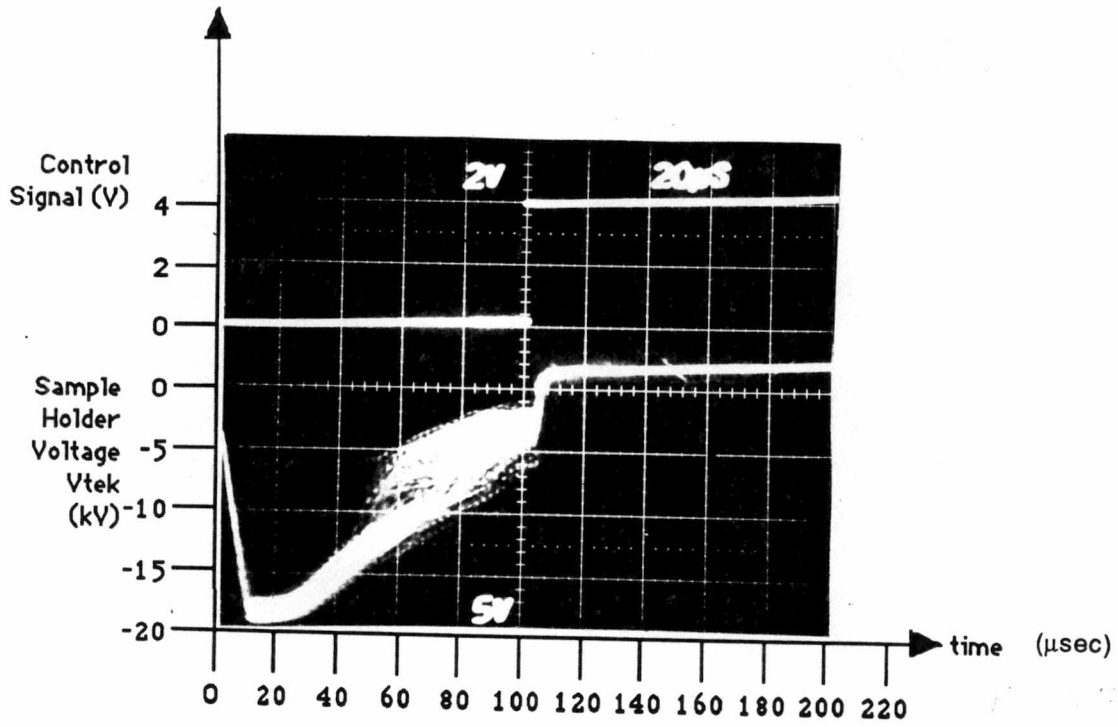


Figure III.22 (Run CCC-7) Oscillogram showing the control signal (upper trace with 2 V per vertical division) and the sample holder voltage (lower trace with -5 kV per vertical division) using the Tektronix probe for a negative bias-on time of 100 μsec, a negative bias-off time of 1 msec, and a negative bias of -20 kV. The amplitude of the sample holder voltage is 19 kV.

notice in Figure III.5 there is about a 6-μsec rise time and 22-μsec fall time. The rise time is determined by the charging-up-time of the stray capacitance between the sample holder and ground, and the distributed capacitance of the RG-8/U coaxial center conductor. The fall time, which is long, is determined by the time it takes for the negatively-charged sample holder to discharge.

When the vacuum tube is turned off, the current flow through the tube is almost instantaneously interrupted, and the sample holder is very negatively charged. Just after current interruption, the remaining charge cannot continue flowing through the tube and must somehow be removed. The plasma, biased to the plasma potential, removes this charge. As the charge is removed, the voltage on the sample holder begins to decrease. The amplitude of the signal measured with the Tektronix probe in Figure III.5 is about -5.6 kV. This trace is not aligned with the horizontal axis, because of the effects of the stray magnetic field on the cathode ray tube of the oscilloscope. In this trace, the zero on the vertical axis was the trace between the negative pulses. However, setting the zero in this way does not account for the plasma potential. If the zero had been set with no signal input to the oscilloscope, the trace between the negative pulses would have risen above zero to the plasma potential. In measuring the sample holder voltage, one will also find a decrease in the amplitude of the signal due to the constant screen grid biasing voltage of about 1.5 kV in the vacuum tube. In later figures, one will see the effects of the plasma potential in the oscillograms.

The negative bias-off time was decreased from 1 msec (Figures III.5 and III.6) to 100 μsec (Figure III.7), resulting in an increased duty cycle and instrumentally averaged sample holder current from 2.6 to 23 mA. In Figure III.7, the reduction of the negative bias-off time by a factor of about 10 resulted in a non-uniform voltage during the bias-on time. Figure III.8 shows several sample holder voltage pulses using the Jennings instrument (upper trace) and the Tektronix probe (lower trace). This comparison shows that the sample holder voltage pulse, measured with the Tektronix probe, is not frequency-attenuated due to the short rise time of the negative pulse, since the Jennings instrument is a high-frequency voltage-measuring device. The two signals are alike in their waveform shape. However, the amplitude of the voltage, measured with the Jennings instrument, is less than that measured with the Tektronix probe by a factor of about 1.2, because the Jennings instrument was out of calibration. This instrument was used only for comparing the frequency dependence of the two probes, and not for a comparison between their amplitudes, since the Tektronix probe was calibrated before measurements were taken.

Figures III.9 and III.10 represent the switching voltage signals of Run No. CCC-3 for a constant, negative biasing voltage of - 10 kV set on the implantation power supply, a negative bias-on time of 20 μsec, and a negative bias-off time of 80 μsec. A reduction of 20 μsec in the negative bias-off time resulted in negligible change in the voltage waveform shape, as it still appears to non-uniform during the bias-on time. In both Figures III.9 and III.10, the oscilloscope

was re-zeroed such that the effects of the plasma potential could be seen. In this case, the Penning anode voltage was set at 1.35 kV and the oscillogram revealed a plasma potential of about 1.5 kV. Also, notice that the amplitude of the negative pulse is only about 7.4 kV, with about 1.5 kV being dropped in the vacuum tube due to the screen grid supply, and the remainder in the plasma potential.

Figures III.11 and III.12 represent the switching voltage signals of Run CCC-4 for a constant, negative biasing-voltage of - 15 kV set on the implantation power source, a negative bias-on time of 20 μsec, and a negative bias-off time of 400 μsec. In Figure III.11, the amplitude of the switching voltage signal, measured with the Tektronix probe, is about 12 kV. The Penning anode voltage was set at about 1.5 kV, leaving about 1.5 kV again being dropped inside the vacuum tube. This signal appears to be uniform in voltage during the negative bias-on time for about 10 μsec. Figure III.12 is another pair of switching voltage waveforms using the two probes. Their waveform shape appears to be quite similar, resulting in a waveform, measured by the Tektronix probe, that is not frequency attenuated.

Figures III.13 and III.14 represent the switching voltage signals of Run CCC-5, where the negative biasing voltage was increased to - 20 kV. The negative bias-on time was 20 μsec and the negative bias-off time was 400 μsec. In both Figures III.13 and III.14, the amplitude of the negative switching voltage, measured by the Tektronix probe, was about 15 kV. With a screen grid voltage of 1.5 kV and a plasma potential of 1.3 kV, 2.2 kV is still unaccounted

for. The plasma in this run appears to be operating in the high-pressure mode, where the ion number density in the plasma is greater and more sample holder current can flow. With more current flow through the vacuum tube, it will act like a resistor if a resistive effect, such as a charge buildup around the screen grid or a limited current flow from the directly-heated cathode filament, is present within the tube. Thus, some additional voltage drop could be occurring within the tube.

Figures III.15 and III.16 of Run CCC-6 represent the switching voltage signals of Run CCC-6, for which the negative biasing-voltage was held at -20 kV and the negative bias-on time was held at 20 μsec, but the negative bias-off time was increased to 1 msec. In Figure III.15, each of the traces are again those measured by the two probes. That measured by the Tektronix probe (lower trace) resulted in an amplitude of about 18.6 kV, including the plasma potential, and leaving about 1.4 kV dropped in the vacuum tube due to the screen grid supply. This case appears to be better in voltage than that of Figures III. 13 and III.14. The plasma in this run (CCC-6) is operating in the low-pressure mode, in which the electron number density is less than in the high-pressure mode. In the low-pressure mode, the voltage amplitude of the negative pulses approaches the value set by the implantation power source and the voltage will be uniform in the negative bias-on time interval as indicated in both traces of Figure III.15. Figure III.16 represents a trace with several negative pulses, measured by the two probes,

which still indicate that the Tektronix probe is measuring the sample holder voltage with no change in the waveform shape.

Since one knows from Appendix A that if the bias-on time is not less than the plasma particle containment time and the time it takes for all of the ions to be withdrawn from the plasma, the plasma will be quenched, it is interesting to observe the switching voltage signals as the bias-on time is increased. In Figures III.17 through III.22 the bias-on time is increased from 5 μsec to 1 msec. The negative biasing voltage was set at -20 kV and the negative bias-off time was set at 1 msec. Figure III.17 shows the control signal set for a negative bias-on time of 5 μsec. The sample holder voltage amplitude, measured with the Tektronix probe, is about 16.5 kV. From this signal, it appears that the waveform does not remain at 16.5 kV for any significant amount of time. Some of this voltage drop may be due to the high voltage power supply being used during these tests. This is due to the short duration for the negative bias-on time. Since the high-voltage switching circuit takes about 4 μsec to build up the voltage on the sample holder, there is not sufficient time left for the sample holder to charge to the set voltage of -20 kV. The very long fall time of about 45 μsec is due to the plasma slowly draining the charge off of the sample holder. The scatter in this trace is due to the conductivity of the plasma changing very rapidly with time.

Figure III.18 represents a control signal (upper trace) with a negative bias-on time three times that of Figure III.17, 15 μsec. In this case, the negative switching signal (lower trace), measured with

the Tektronix probe, is quite uniform for about 4 μsec and it appears that the high-voltage switching circuit and the sample holder are functioning as expected. The amplitude of this signal is about 17.5 kV and the plasma potential is about 2 kV. In this case, it is taking about 15 μsec to remove the charge from the sample holder.

Figure III.19 illustrates a control signal (upper trace) with a negative bias-on time twice that of Figure III.18, 30 μsec. Notice that the negative switching signal during the bias-on time is less uniform than that of Figure III.18. Also, notice several scatter traces in the lower right corner of the negative switching signal. These represent the plasma slowly becoming depleted of its ion population. At this point, the bias-on time is probably slightly larger than the plasma particle containment time. The amplitude of this signal is still about 17.5 kV.

Increasing the bias-on time 10 additional microseconds to 40 μsec results in a more serious depletion of ions in the plasma as indicated by Figure III.20. An interesting observation is that as the bias-on time is increased, there are more scatter traces above the region of non-uniformity during the bias-on time of the negative pulse. Also, observe that the scatter traces are beginning to occur earlier during the bias-on time than that of Figure III.19. The amplitude of this signal is reduced to about 17 kV.

Figure III.21 is an oscillogram where the control signal negative bias-on time was increased to 50 μsec. The scatter traces are occurring more often and more of the negative pulse has become non-uniform, again resulting in a serious depletion of plasma ions.

Figure III.22, the last case, represents a negative switching signal that has a bias-on time of about 10 times its limit. The plasma is being very seriously depleted of its ions as indicated by the intense early part of the waveform where there are not enough ions available to carry charge away from the sample holder. The amplitude of the negative switching signal has increased to about 19 kV. It is obvious from Figures III.19 through III.22 that early in the negative pulse (the first 5 to 15 μsec), there are plenty of ions available in the plasma for the sample holder to draw on, but after the first 15 μsec, the plasma begins to experience its first loss of ions. At this point, the plasma already has an insufficient number of ions to keep it going and there is still a demand for more ions to the sample holder. More ions are withdrawn per unit time and the ion depletion grows even larger. This growing-loss-and-continued-demand cycle grows with time until the plasma has lost all of its ion population or the current through the sample holder has been interrupted (the high-voltage switching circuit turns off). From further examination of Figures III.18 through III.22, it can be seen that there are no scatter traces during the first 10 to 15 μsec of each negative pulse, indicating that the plasma particle containment is approximately 10 to 15 μsec.

In Figures III.23 through III.30, the upper trace represents the sample holder switching voltage signal measured with the Jennings instrument and the lower trace represents the same measured with the Tektronix probe. In each of the figure captions, the measured voltage for the two probes and the implantation power source

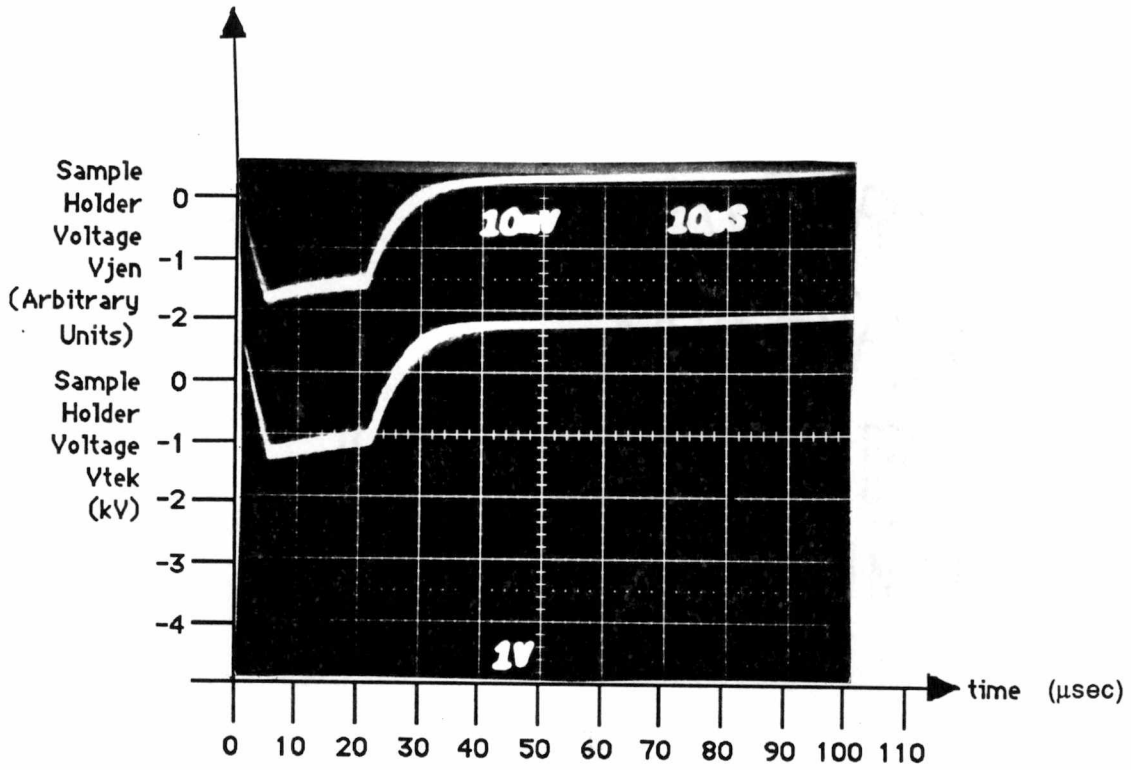


Figure III.23 (Run CCC-8) Oscillogram showing a sample holder voltage pulse using the Jennings instrument (upper trace) and the Tektronix probe (lower trace with -1 kV per vertical division) for a negative bias-on time of 20 μsec, a negative bias-off time of 1 msec, and a negative bias of -1 kV. The amplitude of the upper trace, in arbitrary units, was 1.9 kV and of the lower trace in calibrated units was -1.4 kV.

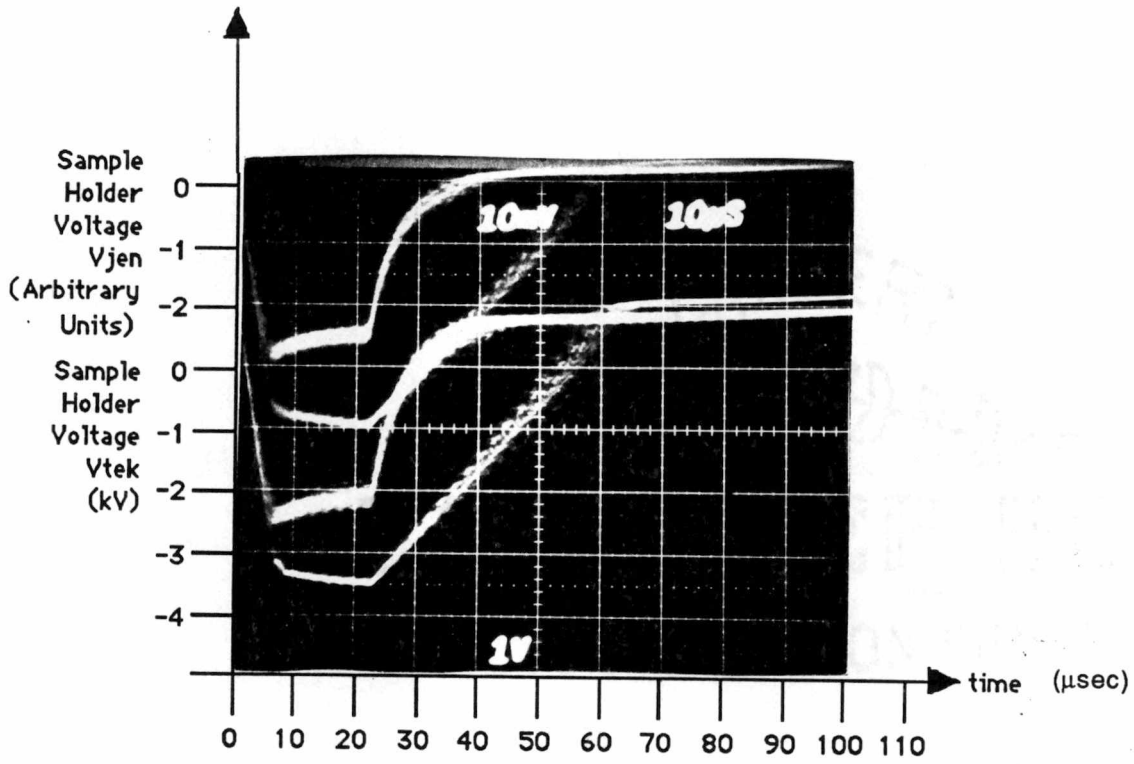


Figure III.24. (Run CCC-8) Oscillogram showing a sample holder voltage pulse using the Jennings instrument (upper trace) and the Tektronix probe (lower trace with -1 kV per vertical division) for a negative bias-on time of 20 μsec, a negative bias-off time of 1 msec, and a negative bias of -2.5 kV. The amplitude of the upper trace, in arbitrary units, was -2.9 kV and of the lower trace in calibrated units was -2.6 kV.

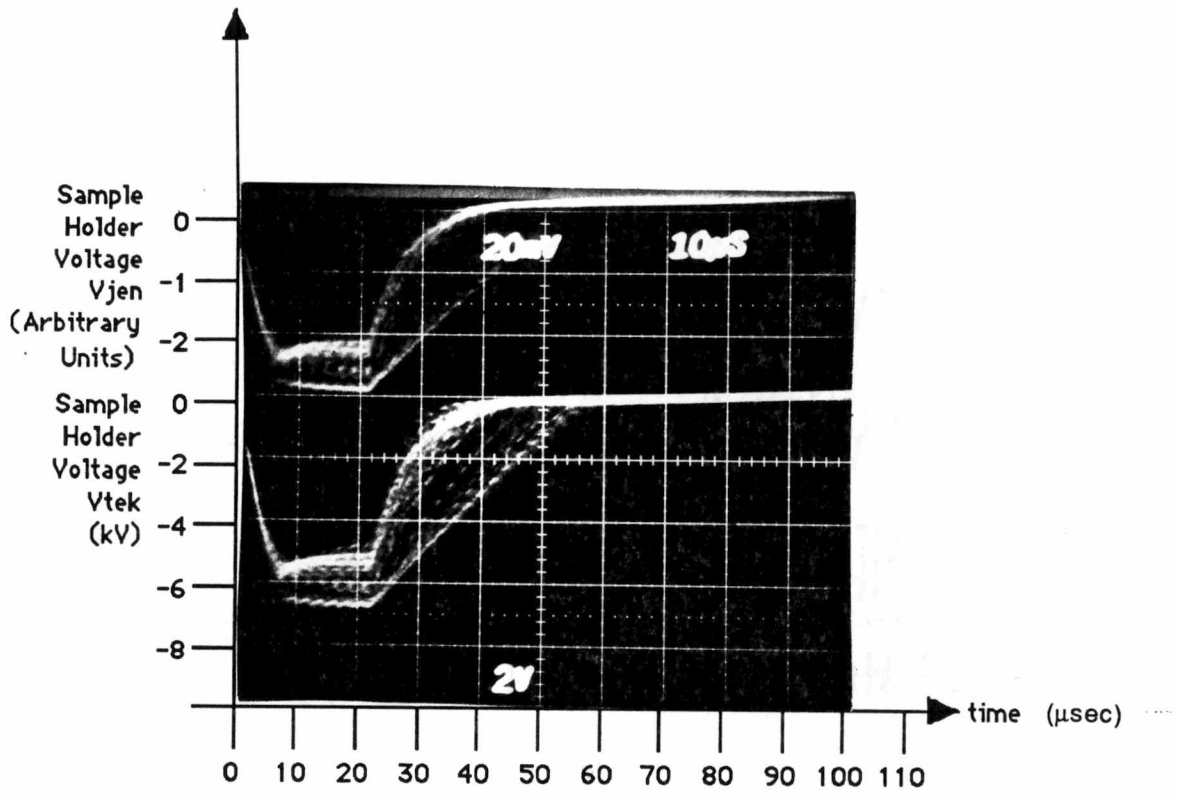


Figure III.25 (Run CCC-8) Oscillogram showing a sample holder voltage pulse using the Jennings instrument (upper trace) and the Tektronix probe (lower trace with -2 kV per vertical division) for a negative bias-on time of 20 μsec, a negative bias-off time of 1 msec, and a negative bias of -5 kV. The amplitude of the upper trace, in arbitrary units, was -5 kV and of the lower trace in calibrated units was -5 kV.

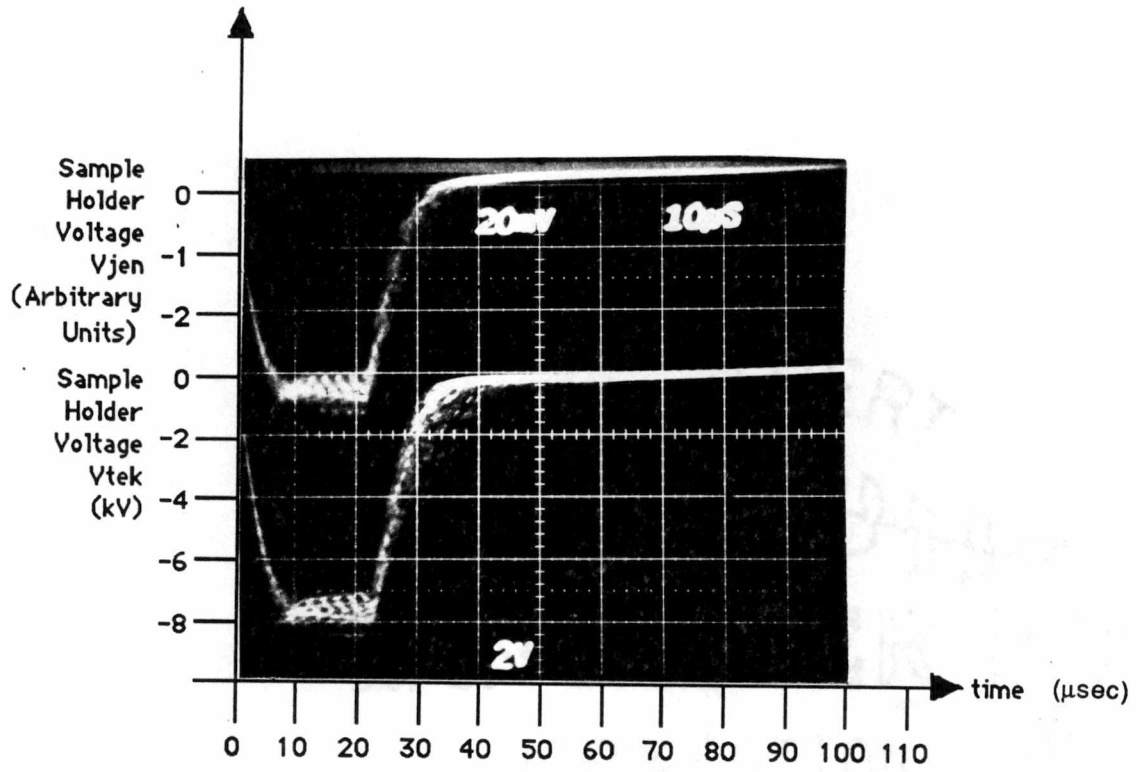


Figure III.26 (Run CCC-8) Oscillogram showing a sample holder voltage pulse using the Jennings instrument (upper trace) and the Tektronix probe (lower trace with -2 kV per vertical division) for a negative bias-on time of 20 μsec, a negative bias-off time of 1 msec, and a negative bias of -7.5 kV. The amplitude of the upper trace, in arbitrary units, was -6.8 kV and of the lower trace in calibrated units was -6.5 kV.

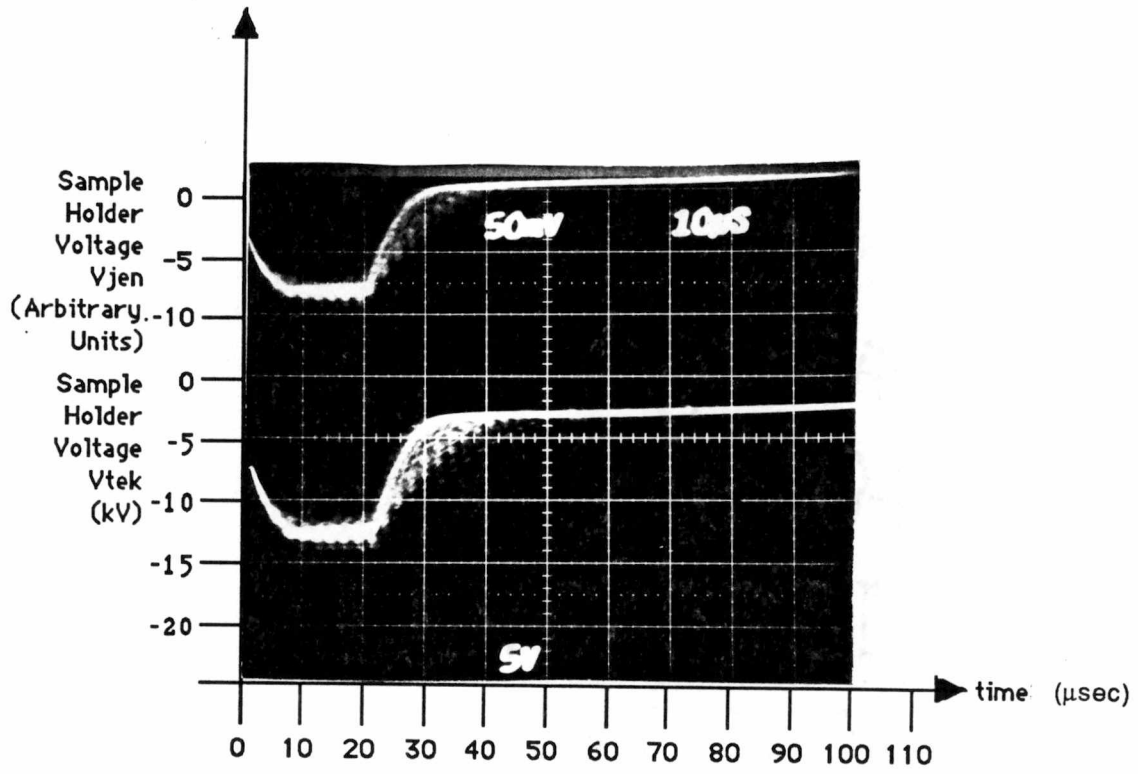


Figure III.27 (Run CCC-8) Oscillogram showing a sample holder voltage pulse using the Jennings instrument (upper trace) and the Tektronix probe (lower trace with -5 kV per vertical division) for a negative bias-on time of 20 µsec, a negative bias-off time of 1 msec, and a negative bias of -10 kV. The amplitude of the upper trace, in arbitrary units, was -8.5 kV and of the lower trace in calibrated units was -8.7 kV.

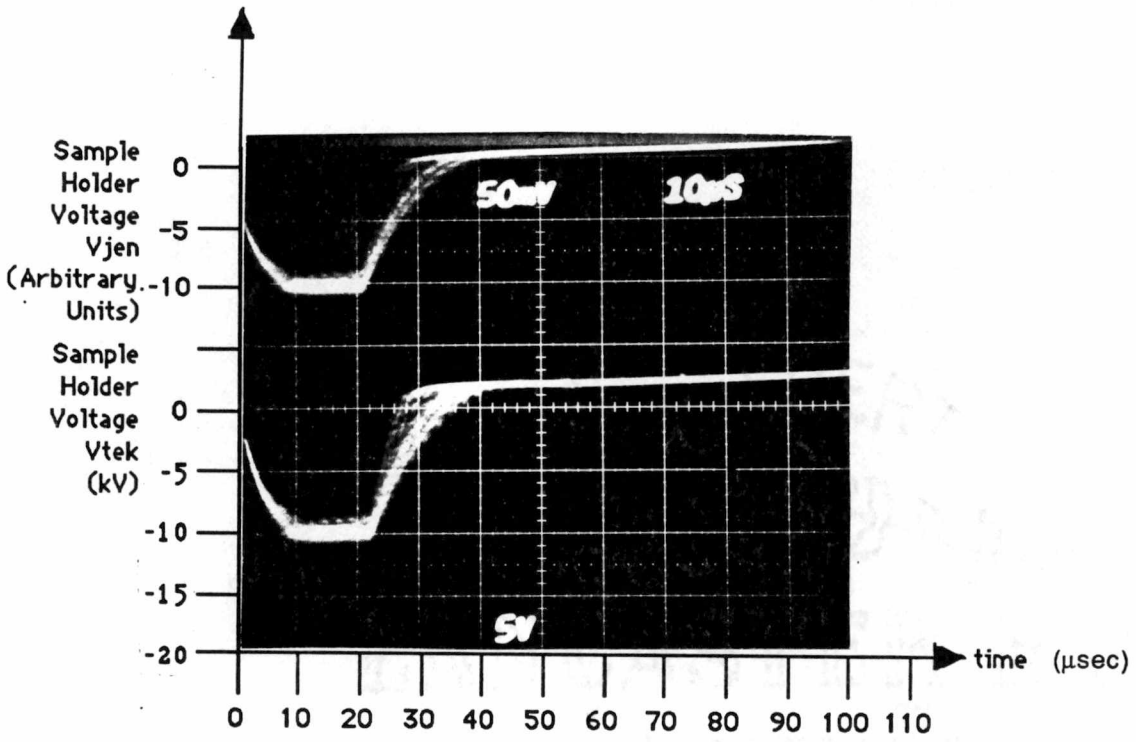


Figure III.28 (Run CCC-8) Oscillogram showing a sample holder voltage pulse using the Jennings instrument (upper trace) and the Tektronix probe (lower trace with -5 kV per vertical division) for a negative bias-on time of 20 μsec, a negative bias-off time of 1 msec, and a negative bias of -12.5 kV. The amplitude of the upper trace, in arbitrary units, was -11 kV and of the lower trace in calibrated units was -11 kV.

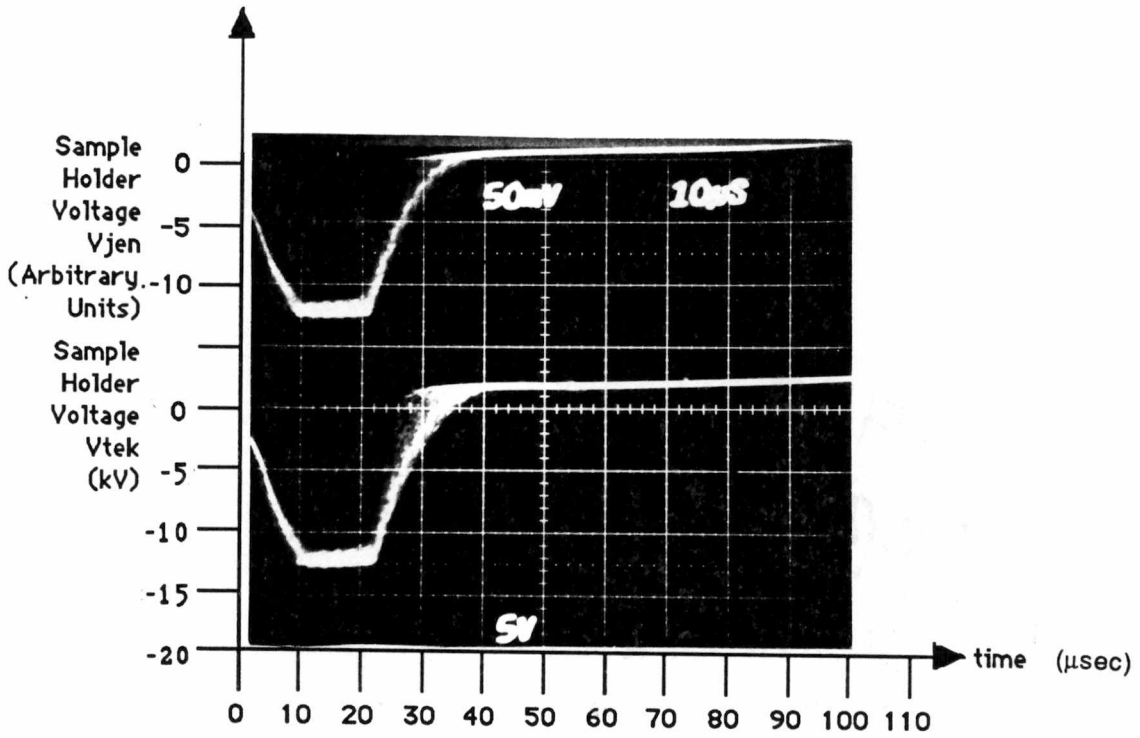


Figure III.29 (Run CCC-8) Oscillogram showing a sample holder voltage pulse using the Jennings instrument (upper trace) and the Tektronix probe (lower trace with -5 kV per vertical division) for a negative bias-on time of 20 μsec, a negative bias-off time of 1 msec, and a negative bias of -15 kV. The amplitude of the upper trace, in arbitrary units, was -12.5 kV and of the lower trace in calibrated units was -13 kV.

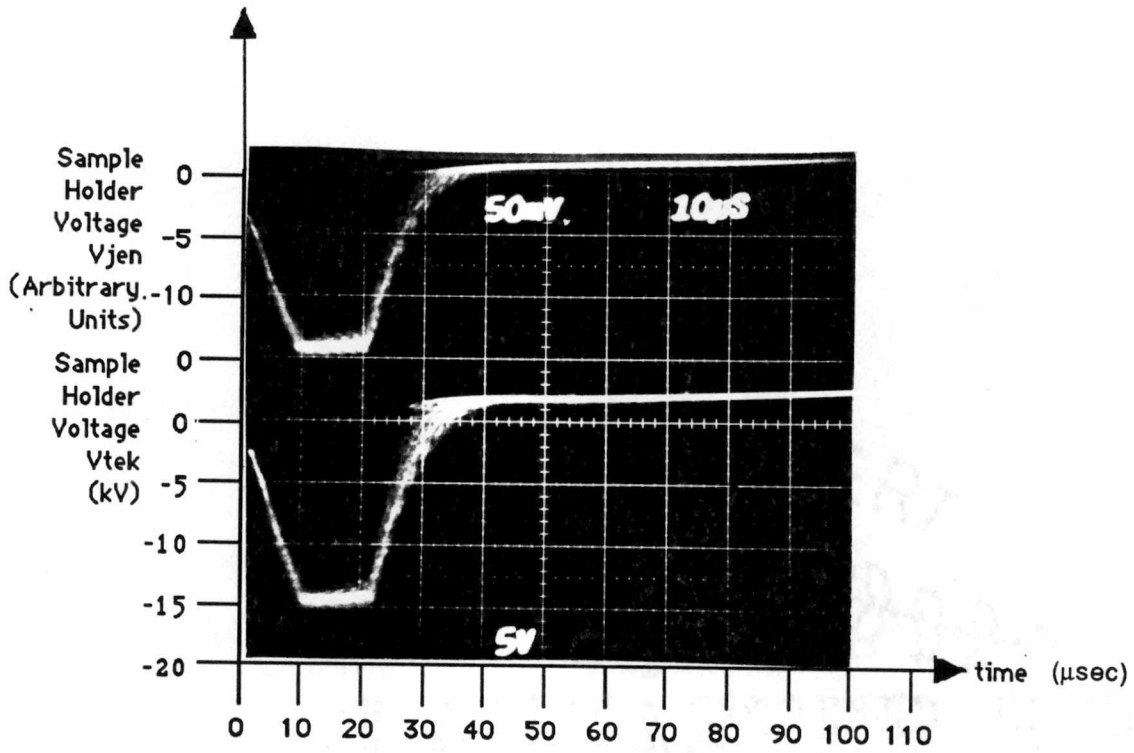


Figure III.30 (Run CCC-8) Oscillogram showing a sample holder voltage pulse using the Jennings instrument (upper trace) and the Tektronix probe (lower trace with -5 kV per vertical division) for a negative bias-on time of 20 μsec, a negative bias-off time of 1 msec, and a negative bias of -17.5 kV. The amplitude of the upper trace, in arbitrary units, was -14.5 kV and of the lower trace in calibrated units was -15 kV.

voltage on the NJE high-voltage power supply is presented. Of special interest are Figures III.24 through III.26, where the plasma spends part of its time in the low-pressure mode (trace with most negative voltage and longest fall time) and the remaining part of its time in the high-pressure mode (trace with least negative, most non-uniform voltage and shortest fall time). In these cases, the plasma conditions were such that the plasma was "on the edge" of the low- to high-pressure mode transition. Figures III.27 through III.30 are indicative of mode transitions, also. However, since their vertical scales are compressed as compared to Figures III.24 through III.26, the transition from a low- to high-pressure mode is not as noticeable as in the expanded, vertical-scale cases. The end result of these observations was that the Tektronix probe was suitable, based on frequency response and amplitude calibration, to measure the ion energies for a plasma ion implantation experiment. If ion energies above 40 keV (the pulsed maximum voltage of the Tektronix probe) are to be measured, the Jennings instrument, if used, must be calibrated.

For biasing voltage greater than -20 kV, Figure III.31 shows a high-voltage switching signal of -40 kV with a bias on time of 22 microseconds and a bias off time of 3 milliseconds. During this test, only the biasing potential was of interest and no plasma conditions were recorded. However, the switching circuit was stable at this high negative potential. It could be operated at even higher potentials in a plasma where high frequency turbulence is not present. Such a plasma, a microwave generated plasma, is the topic of this thesis.

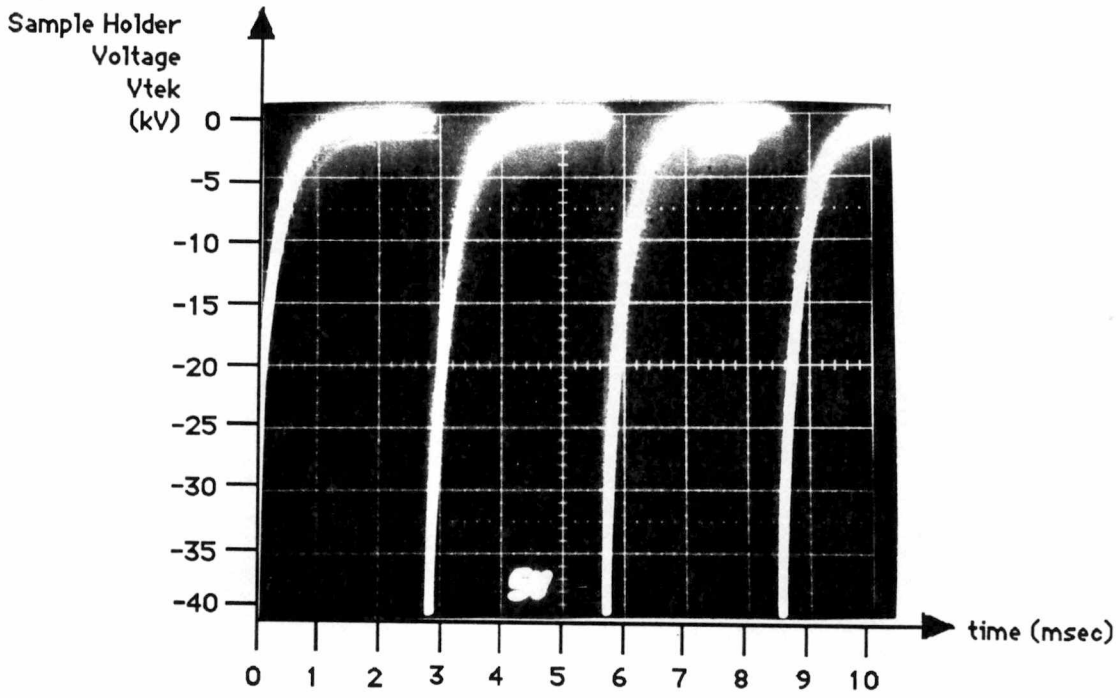


Figure III.31 Oscillogram showing a sample holder voltage pulse using the Tektronix instrument (-5 kV per vertical division) for a negative bias-on time of 22 μsec, a negative bias-off time of 3 msec, and a negative bias of - 45 kV with no plasma.

E. The First Plasma Ion Implantation

Upon completion and testing of the high-voltage switching circuit, four Type 304L stainless steel samples, measuring about 1" (2.54 cm) square, were mounted on the sample holder of Figure III.3. The sample holder was inserted into the Penning discharge containing the anode cylinder. This system is represented by Figure III.1. The bias-on time was set for 20 μsec by adjusting the delay time on the Wavetek signal generator and the bias-off time was set for 1 msec by setting its frequency to 1 kHz. The desired implantation parameters were 20 kV for the ion energy (circuit tested up to this potential at this time), 6.09 x 10^{17} ions/cm^3 for the ion fluence, 40 % mole fraction of nitrogen ions at a depth of 0.1 μm, and an exposure time of 20 minutes. The voltage and current waveforms were not recorded due to the lack of proper equipment during these early experiments.

The sample holder was removed from the system and the samples were taken over to the Materials Science and Engineering Department for In-Seop Lee, a doctoral candidate at that time, to analyze using an instrument called a potentiostat. A potentiostat is used to measure corrosion-related electrochemical properties such as pitting potential, etc. The pitting potential, one of the most significant properties, describes the potential at which the electrochemical current to the sample rapidly increases. It is often identified by a "knee" in the potentiostat curve which graphs current density on the abscissa and voltage on the ordinate. The rate of

voltage increase during this test was 1.2 V/hr and the sample was immersed in a 1 % NaCl salt water bath.

Figure III.32 is the potentiostat curve for the implanted sample nearest the midplane and for the unimplanted control sample. For the unimplanted sample, the pitting potential was about 500 mV. For the implanted sample, the pitting potential increased dramatically to a value of 1.2 V, an increase of over 200 %. This is an extremely beneficial effect as far as corrosion resistance is concerned.

F. Removing Samples from the Penning Discharge

The procedure for removing samples from the Penning discharge requires a very detailed step by step procedure, which is Appendix F.

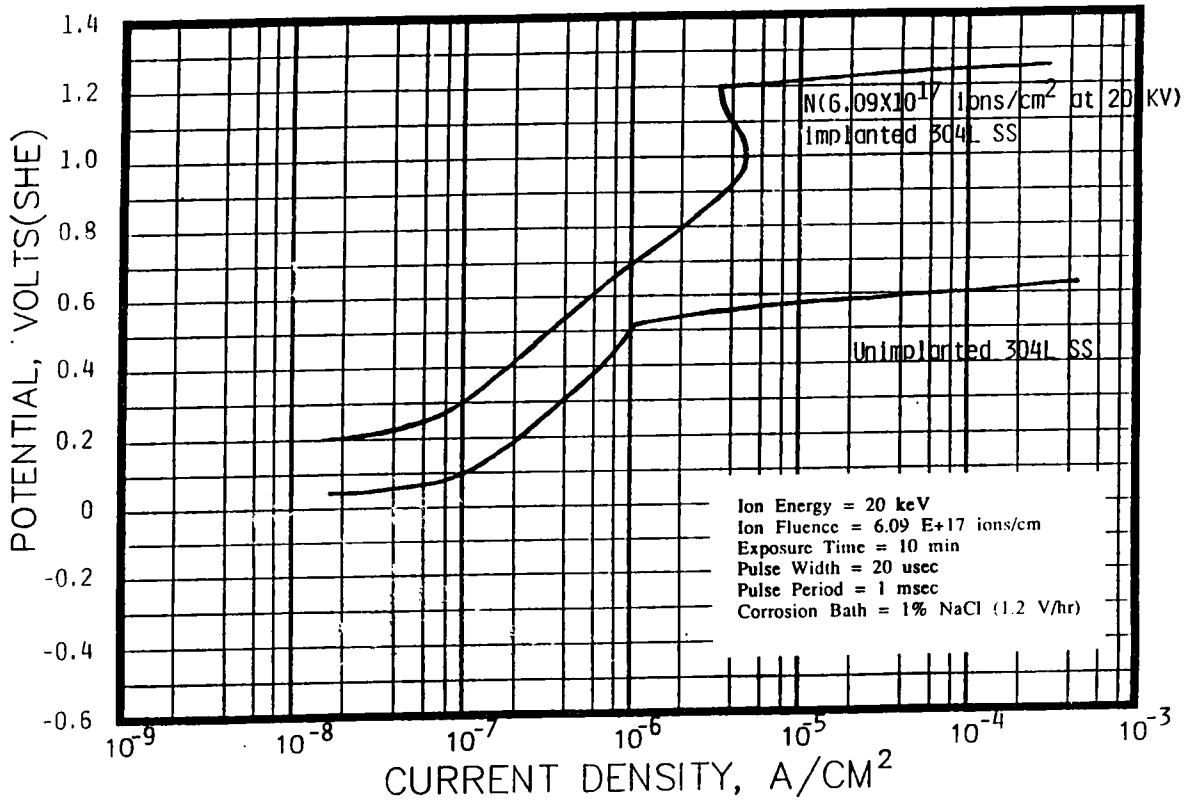


Figure III.32 Potentiostat curve graphing the current density on the abscissa and the applied potential between the sample and an electrode on the ordinate for the first plasma ion implantation experiment. The sample was Type 304L stainless steel immersed in a nitrogen plasma with a Penning anode voltage of 1.65 kV, a Penning anode current of 34 mA, a magnet coil current of 600 A, and pressures of 5.2 x 10^{-5} and 6.3 x 10^{-5} torr on the pumping end (North end) and gas inlet end (South end) of the vacuum system, respectively. The ion energy was about 20 keV for the nitrogen ions, the ion fluence was 6.09 x 10^{17} ions/cm^2, and the magnitude of the ion current was about 20 mA for a pulse width of 20 μsec, a pulse period of 1 msec, and a total exposure time of 10 minutes. The pitting potential of the unimplanted sample was 500 mV and that of the implanted sample was 1.2 V, an increase of more than 200 %.

CHAPTER 4

A NON-MAGNETIZED PLASMA FOR PLASMA ION IMPLANTATION

A. Advantages Over a Magnetized, DC Gaseous Discharge Plasma

As stated earlier in Chapter 3, ion trajectories are affected by the presence of changing magnetic fields resulting in a directionality of their incidence on a sample. The region in the Penning discharge where plasma ion implantation takes place has an approximately uniform magnetic field intensity. If this region were perfectly uniform with no variations in the magnetic field, then the ion trajectories along the field lines would be unaffected by the presence of the magnetic field. The presence of a magnetic field results in a considerable anisotropy in a direction perpendicular to the magnetic induction. In an industrial plasma application like plasma ion implantation, it is desirable that the ions be able to move isotropically as they are accelerated across the sheath, in a direction perpendicular to the sample surface. In addition to this, the power that is required to produce such magnetic fields (up to 0.2 Tesla) for the Penning discharge dominates the total power required to carry out the process. Thus, a strong motivation for using a non-magnetized plasma already exists even before discussing the "electrode" issue.

The uniform Penning discharge, a DC discharge, contains two electrodes: a cathode and an anode. The presence of electrodes, which are in contact with the plasma, can introduce impurities into the plasma. These impurities are undesirable since they can promote plasma-chemical reactions to produce unwanted byproducts (Baddour, 1967). The byproducts can be neutral compounds or they can be positively or negatively charged. Obviously, if they are positively charged, then in plasma ion implantation, they could be implanted into the sample, resulting in contamination of the sample at the surface. In addition, these unwanted byproducts, if neutral, may become ionized in the plasma. This ionization requires energy from the plasma that could otherwise be used to ionize the atoms of interest for plasma ion implantation.

The presence of DC electric fields in a Penning discharge along with magnetic fields, results in E x B drift forces which also give the ion motion directionality. Since the electric field is required to initiate and maintain breakdown of the gas, the only method of eliminating the drift forces is to remove the magnetic field. Thus, it is again desirable to use a non-magnetized plasma. Turning back to the subject of electric fields in the discharge region, it has been shown (Baddour, 1967) that AC electromagnetic waves in the radio and microwave frequency ranges, which are 2×10^5 to 10^9 and 10^9 to 10^{12} Hz, respectively, are capable of transferring a significant amount of their energy to free electrons in the electromagnetic wave. The upper frequency limit for the effective transfer of electromagnetic energy from the electric field to accelerate the

electrons is about 10 GHz. Experiments conducted at the Massachusetts Institute of Technology revealed that low microwave powers of about 100 Watts at a frequency of 2.45 GHz were capable of heating free electrons to kinetic temperatures above about 1 eV at a background pressure of about 10 Torr (Baddour, 1967).

Another of the advantages of creating a discharge using high-frequency electromagnetic radiation is the commercial availability of AC sources at these frequencies. In the microwave frequency range are widely used magnetron sources at 2.45 GHz, the "microwave-oven" frequency. These sources can provide up to several tens of kilowatts of continuous power. This power can be directed through a hollow metallic waveguide and delivered to a plasma in a specially-designed vacuum containment system, which serves as a microwave cavity and energy storage mechanism. The design of these cavities, which range from small rectangular metallic boxes to large right circular metal cylinders, is also a well-understood technology. In most microwave discharges, it is desired to have the electromagnetic energy uniformly distributed across the discharge volume. Unlike microwave cavities that store radiation in a specific mode, and which are used as resonators or filters, these cavities must store radiation at several modes to produce as uniform an electromagnetic field as possible. The objective is shared with ordinary microwave ovens, for example, where strong modal patterns result in local overheating of the food. Cavities of this type are referred to as multimode cavities. This is also a well-developed technology, as evidenced by the microwave-oven industry. Hence, it is not only desriable, but also

feasible from a technological point of view, to create a discharge, using high-frequency multimode electromagnetic radiation, to provide uniformity of the plasma over large volumes.

B. The Microwave Power Source

Most investigations of plasmas, which are powered by electromagnetic radiation, require continuous wave (CW) or very fast pulsed sources. These sources, from lowest to highest frequency ranges, are the tunnel diode oscillators (up to 1 GHz), the harmonic generators (up to 150 GHz), the magnetrons (0.5 GHz to 100 GHz), the klystrons (2 to 120 GHz), and the traveling-wave oscillators (0.5 to 220 GHz). The electromagnetic radiation source used in this work is the magnetron, operating at a frequency of 2.45 GHz. Magnetrons are used in many high-power applications not only because of their high powers, but also because of their high efficiencies (40 to 70%) (Soohoo, 1971). In plasma research, they are used in the heating of plasmas and the scattering or transmission of microwaves over long distances when studying atmospheric or space plasmas. Magnetrons require high-voltages, ranging from 5 to 60 kV, for their operation. Continuous wave magnetron sources are available in powers up to a few tens of kilowatts (Heald, et al., 1978).

Two microwave power sources were available for use in this experiment. One of them is a Varian-Eimac Model PPS-2.5 microwave power pack. The other, a later model, is a Varian-Eimac

Model PPS-2.5AS microwave power pack. The circuits of these two units are different, but the principles used in these units to generate microwave power using a magnetron tube are the same. The microwave power source selected for this system is the Model PPS-2.5AS Varian Power Pack. This unit has more diagnostics, which allow the user to more easily monitor the unit while it is operating. This power pack employs a self-contained, water-cooled magnetron which can deliver up to 3 kW CW at a frequency of 2.45 GHz plus or minus 25 MHz (0.025 GHz). A side and front view of the power pack is shown in Figure IV.1. The power pack is powered by 30 Amperes of 110/208-240 Volts AC power at a frequency of 60 Hz. The power pack is connected to the 208 delta voltage source located in the UTK Plasma Science Laboratory. Only one phase of the delta (phase leg to phase leg) was used to supply power to the three-pole step-up transformer which delivers high-voltage to the magnetron. The control circuitry for the power pack is powered by 120 Volts AC taken from one of the above phase legs to the grounded neutral. Figure IV.2 shows these power connections. The water-cooling of the magnetron is provided by pumped distilled water contained in a reservoir located inside the power pack unit.

Characterization of the microwave power sources was carried out by the system of Figure IV.3. The output waveguide port on the side of the power pack was connected to the "Transmitter" side of a Varian Model EW3-DPM3S detector assembly which measures forward microwave power (FWD) and reflected microwave power (REF). This detector assembly has two BNC connectors attached to it.

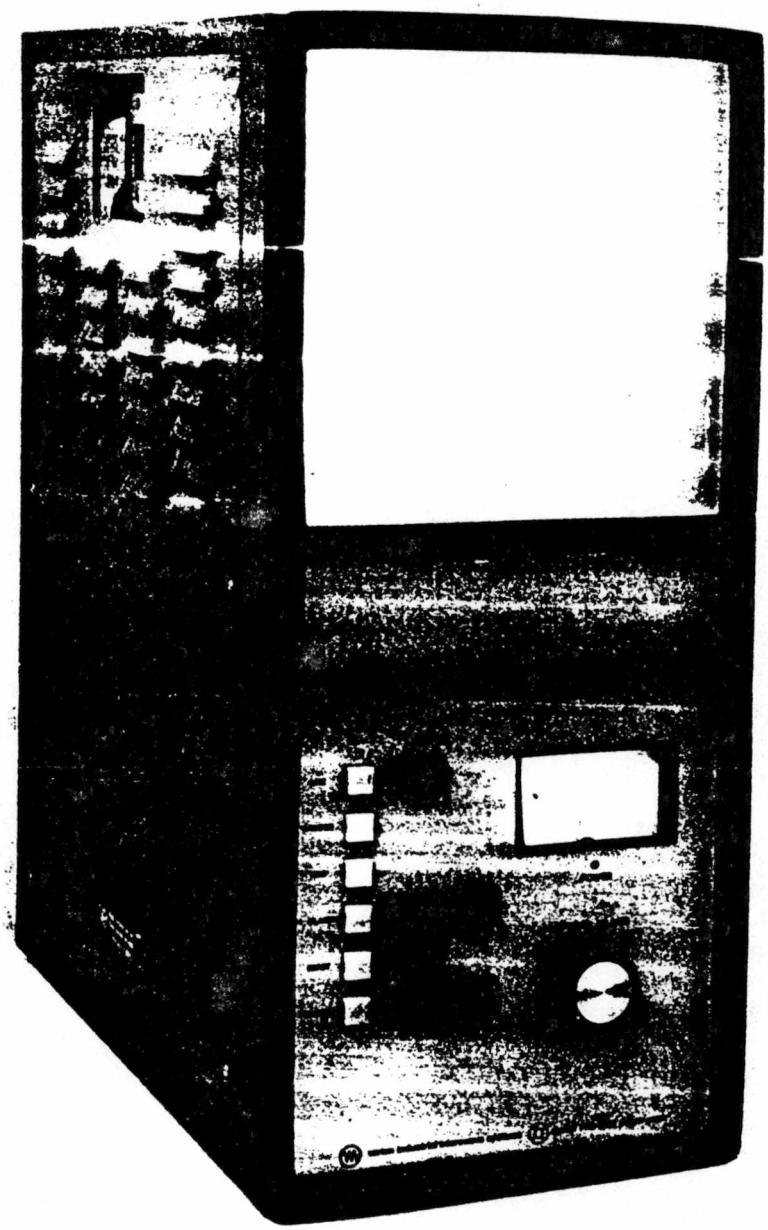


Figure IV.1 Side and front view of Varian-Eimac Model PPS-2.5AS Power Pack. Side view shows microwave port using WR-340 waveguide with rectangular flanges. Front view shows six diagnostic indicators (left), six momentary on/off pushbuttons for controlling power pack (middle and right), a power adjust knob (bottom far right) connected to a variac which controls the magnetron power level, and a magnetron output power meter (top far right).

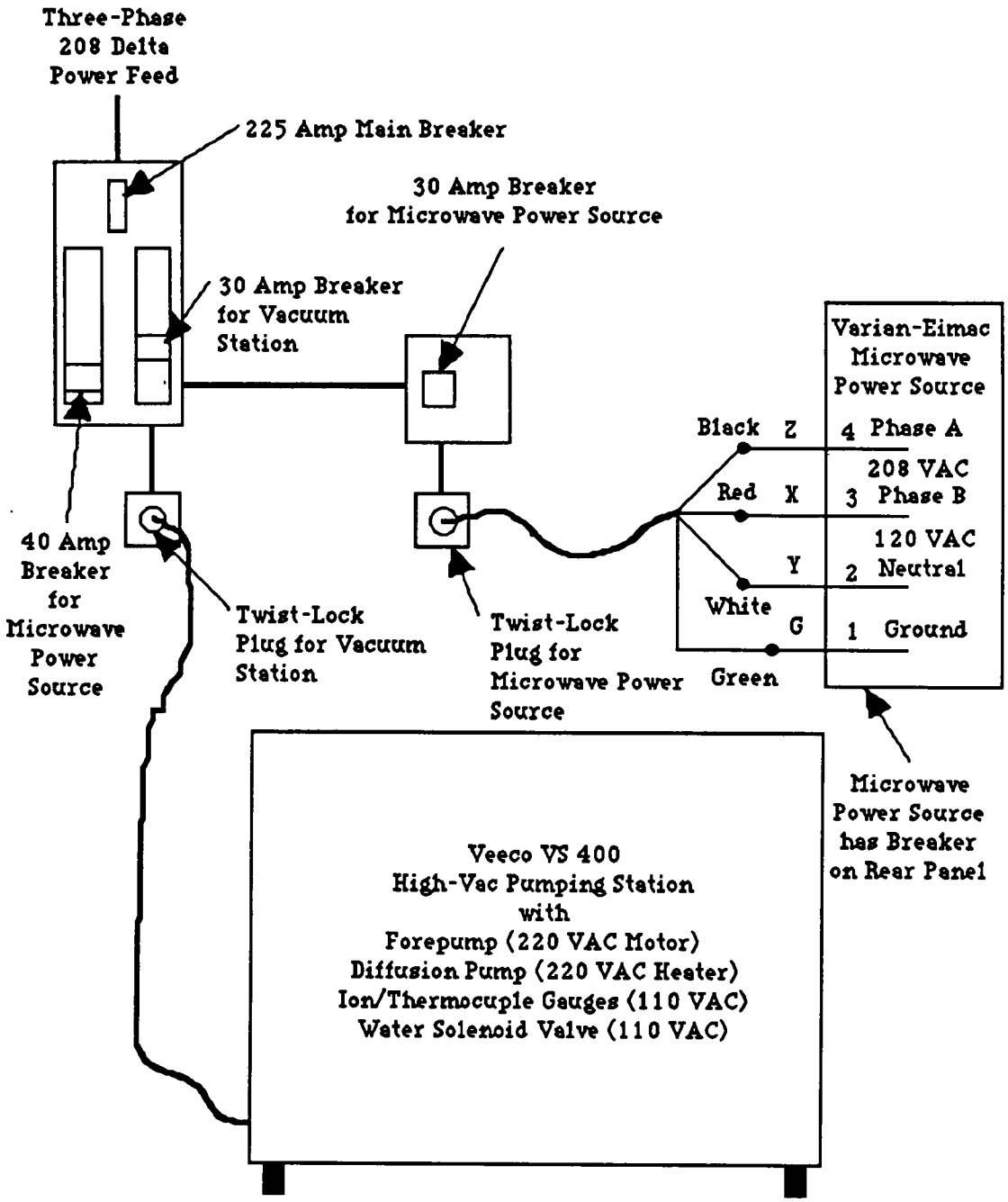


Figure IV.2 Power feed connections for microwave generated plasma. The entire experiment is fed from the 225 Amp panel. The voltage between phases A and B from the main breaker panel are used to power the magnetron in the microwave power source and the forepump and diffusion pump in the vacuum station. The voltage between phase B and the neutral is used to power the control circuits in the microwave power source and the ion and thermocouple gauges and water solenoid in the vacuum station.

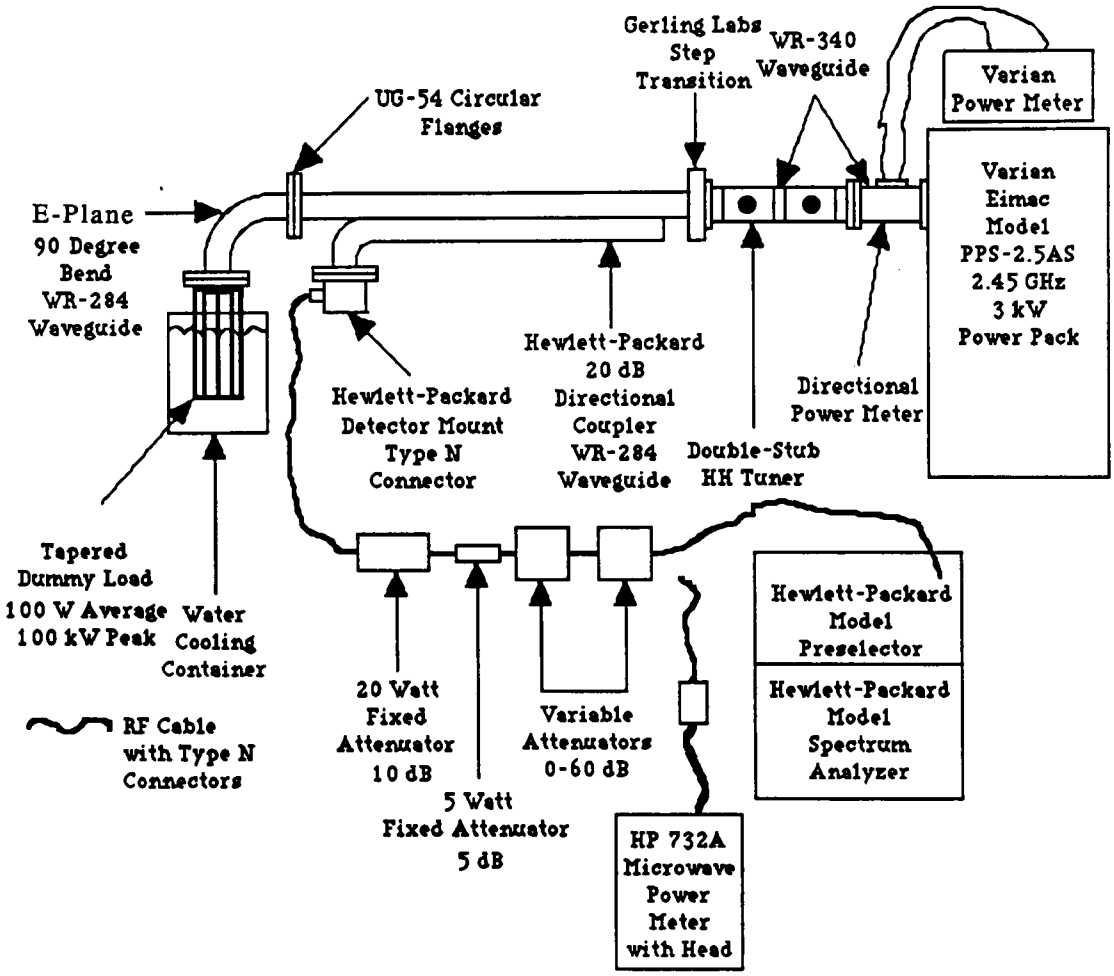


Figure IV.3 Apparatus for measuring the power spectrum for each of the two microwave sources. This was also necessary to determine if the microwave sources would operate at the desired power levels of 2.5 to 3 kW.

The signal from this assembly is delivered to a Varian Model EQ3-DPM3S meter box through two triax cables. The triax cables have an extra shield which is used to help shield against stray high-frequency signals from the center conductor. The "Load" side of this detector assembly is connected to a Varian Model EW3-HH double-stub tuner (power matching device). This microwave device is used to tune out any reflections from the Gerling Labs Model GL 315 step-transition mounted to the output side of the HH tuner since the latter it is not a tappered section. The Gerling Labs transistion "steps" from one waveguide size (WR-340) to another (WR-284) and is designed to provide a minimum reflectance due, to the particular length of the transistion. The waveguides are connected to the step transistion with 1/4-20 x 3/4" stainless steel bolts. Each waveguide connection also has one grounding strap made from zinc braiding, to insure a good electrical connection between the flanges. Only one strap is to be used per flange connection.

The output side of the step transition is connected to the input of a Hewlett-Packard Model S 752D 20 dB directional coupler. This directional coupler was used to couple a small amount of the 2.45 GHz-microwave power in order to analyze the power spectrum. The power input to the directional coupler is reduced by a factor of 100 (20 dB attenuation) by the time it appears at the coupled output port. The remaining part of the microwave power is directed through an E-plane, 90 degree bend into a dummy load. The dummy load, a Royal Microwave Devices Model S707 microwave device, is rated at 100 W average power and 100 kW peak power. Power

levels exceeding the average level of 100 W were dumped onto this load. However, since the load is normally air-cooled by fins acting as heat sinks, and since it was partially immersed in cool water for these tests, it was able to withstand average power levels as high as 3 kW for short durations. It is not recommended that such large power levels be delivered to this dummy load for more than a few minutes. If the dummy load fails while at high power levels, serious damage to the taper inside the load and to the magnetron due to high reflected power levels will result. It is important that the microwave power source not be operated without a load (open-ended) as the magnetron could be damaged or human RF protection criteria could be exceeded.

A PRD Electronics Model 365-A diode detector is mounted at the 20 dB-attenuated output port of the directional coupler. This detector can only withstand small amounts of power before failure. At 3 kW, 30 W of microwave power is delivered to this detector. Before the microwave power from the directional coupler can be input to the spectrum analyzer, it must be further attenuated, since it has only been attenuated by 20 dB at this point. To do this, several fixed and variable attenuators were used. At the output of the diode detector, a DC to 4 GHz Narda Model 766-3 20-W, heatsinked, fixed attenuator (3 dB) is used. This fixed attenuator is used at this position in the line because it is desired that most of the power be absorbed before it reaches the variable attenuators. The variable attenuators cannot absorb power levels of 30 W. Another fixed attenuator, a Microlab Model AD-06N, of 6 dB and 5 W is then

connected to the output of the 20-W device. It is also heatsinked and helps to absorb even more of the microwave power before it reaches the variable attenuators. Two variable attenuators, ranging from 0 to 60 dB each, are then connected, leaving an open output on the last variable attenuator. Each of these attenuators operates in the 2.45 GHz frequency range. Figure IV.4 is a plot of the attenuation versus frequency for all of the attenuating devices from the end of the directional coupler to the last variable attenuator. The attenuation of these devices at 2.45 GHz is 40 dB and of the directional coupler is 20 dB, making the total attenuation 60 dB. Therefore, the forward power could be measured with the spectrum analyzer or with a microwave power meter.

Before the power spectrum was measured, the power levels were checked with a microwave power meter. The coax from the last variable attenuator was connected to a Hewlett-Packard Model 478A thermistor mount microwave power detector head. The head was connected to a Hewlett-Packard Model 732A microwave power meter. The measurements made with the Varian Model EW3-DPM3S directional power meter and meter box can be compared with the microwave power meter on the front panel of the microwave power source. Figure IV.5 is representative of these measurements with the apparatus of Figure IV.3. They do not agree because the Varian power meter on the front of the microwave power source measures the average power input to the magnetron. The HP732A microwave power meter measures the average power output emitted from the magnetron. The HP meter had a Hewlett-Packard Model 478A

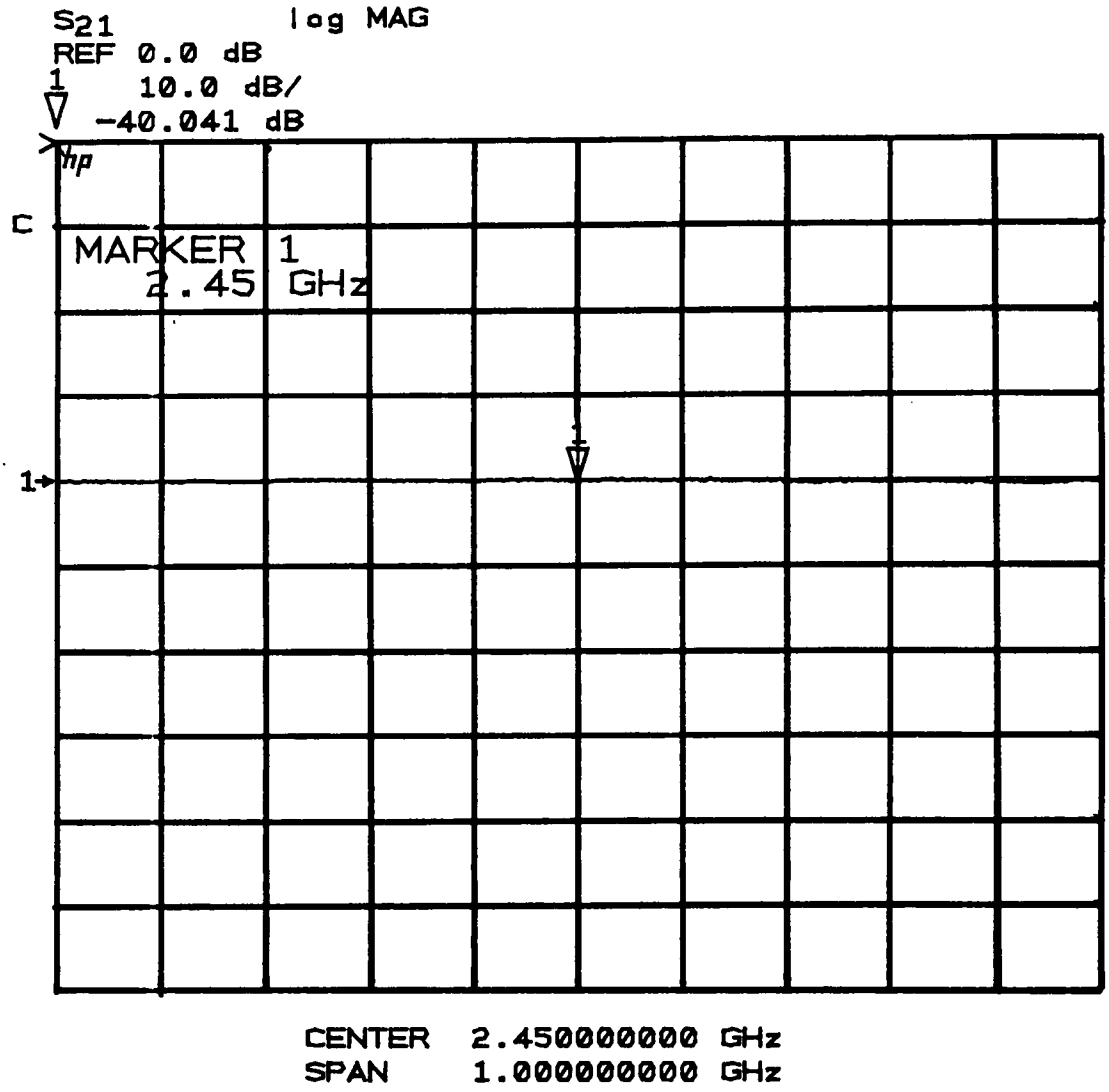


Figure IV.4 Graph of transmission coefficient, S_{21}, generated with the Hewlett-Packard 8510 Network Analyzer for the two fixed attenuators and the two variable attenuators used in measuring the power spectrum of the microwave power sources.

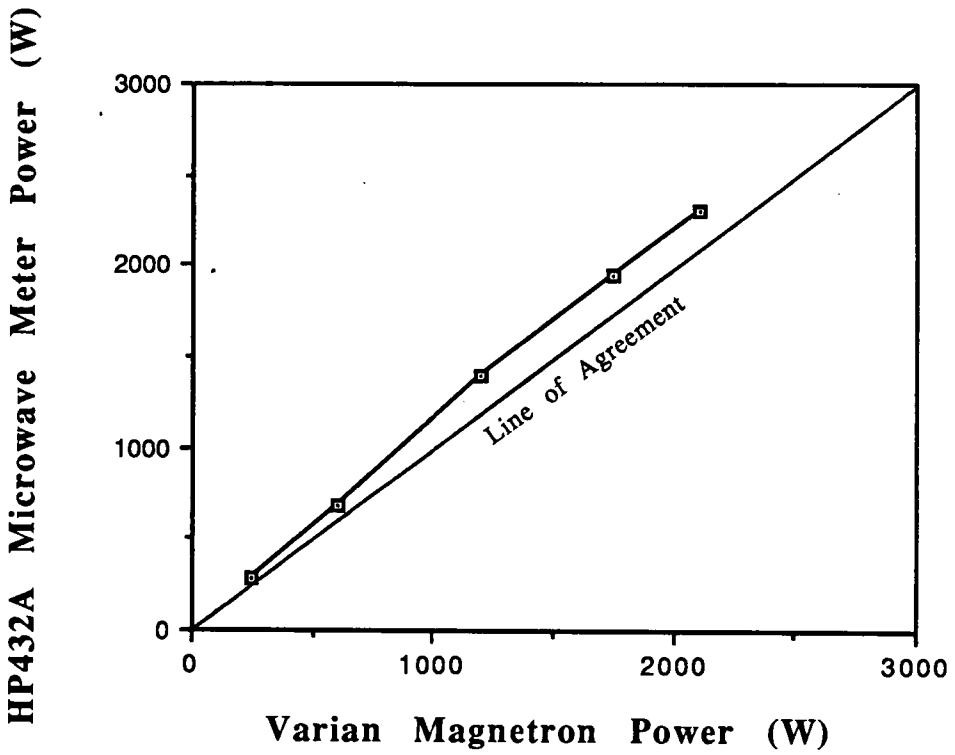


Figure IV.5 Graph of the Varian magnetron power on the microwave source control panel versus the forward power as measured by the HP732A microwave power meter.

thermistor mount power detector head connected to it which operates at the 2.45 GHz frequency. The measurements made with the Hewlett-Packard meter are more accurate measurements since the directional power meter is only intended to give a rough estimate of the forward and reflected power and the microwave power meter on the front panel of the microwave power source measures the product of the input current and voltage to the magnetron tube. The magnetron input power can also be compared with the forward power measured with the Varian power meter box. Figure IV.6 is representative of these measurements made with the same apparatus. Hence, the microwave power measurements made, when characterizing the microwave plasma, should be made with the Hewlett-Packard microwave power meter via a directional coupler just before the microwaves enter the cavity.

To capture the spectrum of the microwave power source, the coax was removed from the microwave power detector head and connected to the input of the Hewlett-Packard Model 8445B automatic preselector for the spectrum analyzer. The preselector output was connected to the input of the Hewlet-Packard Model 8555A spectrum analyzer. The spectrum analyzer sweeps across a preselected frequency band centered at a preselected center frequency and measures the power of the source at each discrete frequency. In all of these power spectrum measurements, the center frequency was set at 2.45 GHz. A power spectrum analysis was conducted for each of the two microwave sources.

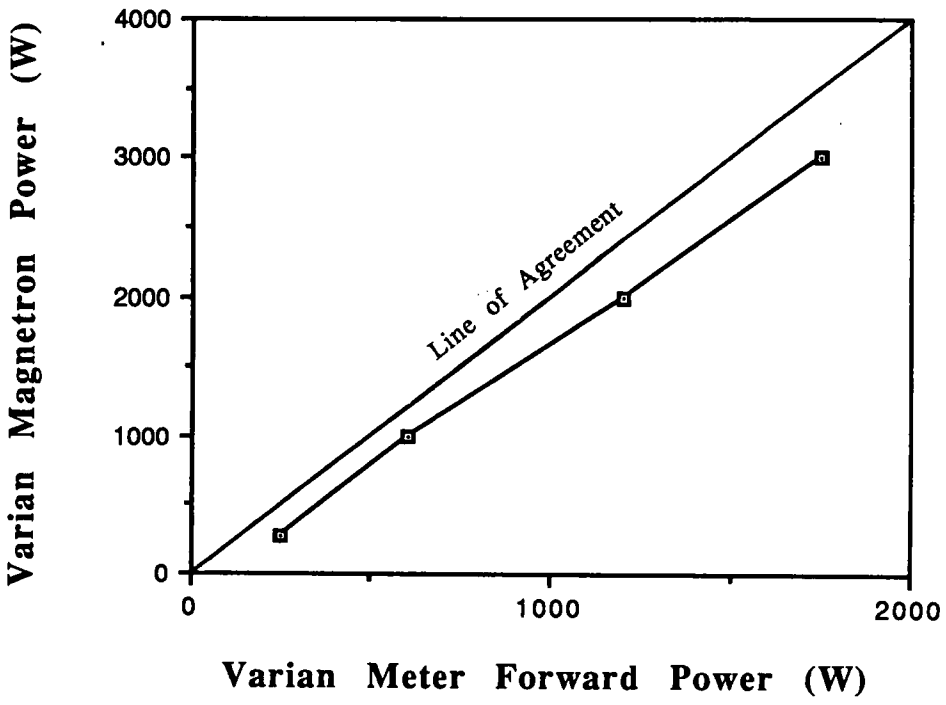


Figure IV.6 Graph of the Varian magnetron power on the microwave source control panel versus the forward power as indicated by the power meter of the Varian power meter box.

Once the microwave power source was turned on and the magnetron filament was allowed to warm up, the magnetron power was slowly increased while it was monitored on the Varian meter box and on the screen of the spectrum analyzer. As the power was increased, the reflected power due to the step transistion was tuned out using the HH tuner at each power level. Spectra were taken for several forward power levels. The power levels examined for the Model PPS-2.5AS power pack were 500, 1000, 1500, and 2500 W as indicated by the Varian meter box. These spectra are presented in Figures IV.7 through IV.10, respectively. The bandwidth here was set at 3 kHz and the scanwidth was set at 2 MHz. The logarithmic reference level was set at 10 dB and the input attenuation was set to give 10 mW at the reference level.

Beginning with Figure IV.7, at a power level of 500 W measured with the Varian power meter, the line with a power level of 159 kW (-8 dBm), the largest line in this spectrum, is at a frequency slightly above 2.45 GHz, 2.45032 GHz. The logarithmic reference level was set at 10 dBm. The signal at this frequency carries the majority of the power. The slight deviation in frequency from 2.45 GHz of this line is expected. This is not a problem in our application, and does not have a detrimental effect on the operation of the microwave cavity. This line may shift in frequency and/or power with time as the magnetron warms up. There are several other lines at lower frequencies with significant power. In this application, a microwave source with a strong line at 2.45 GHz and several other medium-power lines at frequencies above and below

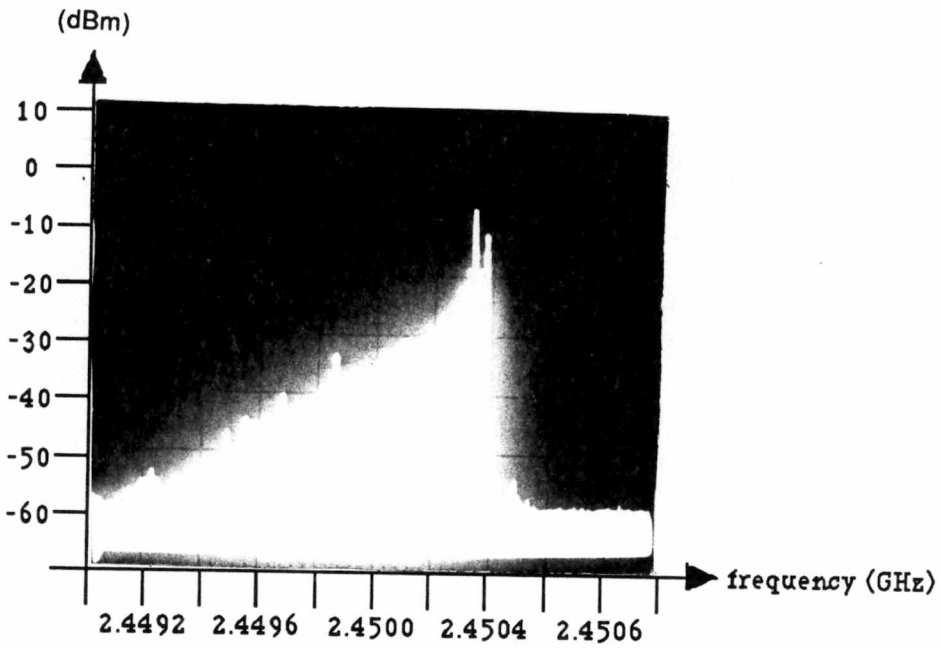


Figure IV.7 Power spectrum from HP 8555A spectrum analyzer for Varian Model PPS-2.5AS microwave power source. The largest peak is at 2.45032 GHz with a power of 159 W. The power measurements were 500 W forward power and 10 W reflected power on the Varian power meter, 300 W on the power source power meter, and 340 W on the HP732A microwave power meter. The spectrum indicates a non-uniform spread with a concentration of power below 2.45032 GHz.

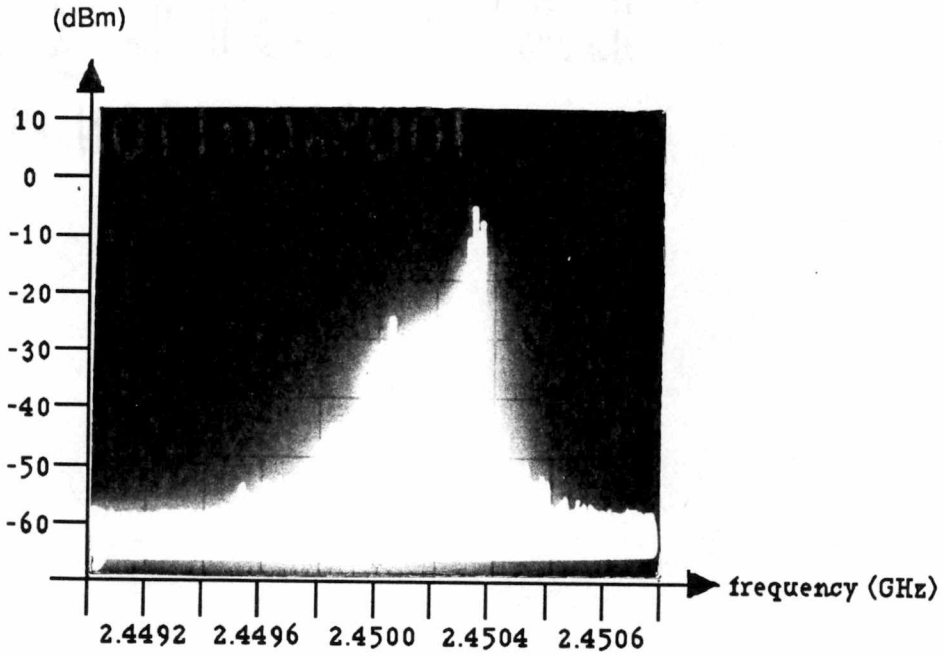


Figure IV.8 Power spectrum from HP 8555A spectrum analyzer for Varian Model PPS-2.5AS microwave power source. · The largest peak is at 2.45032 GHz with a power of 251.2 W. The power measurements were 1 kW forward power and 20 W reflected power on the Varian power meter, 750 W on the power source power meter, and 980 W on the HP732A microwave power meter. The spectrum indicates a non-uniform spread with a concentration of power below 2.45032 GHz.

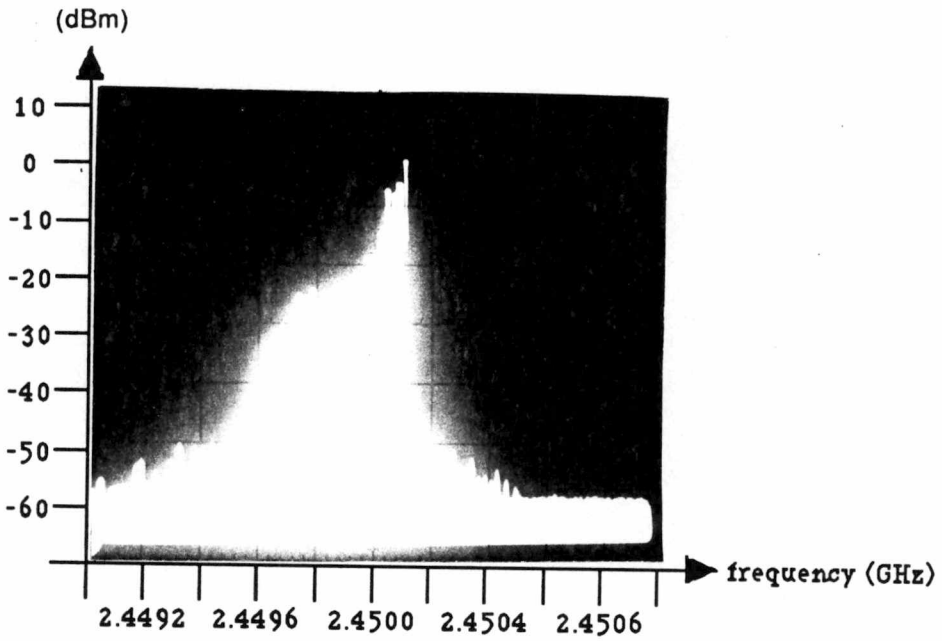


Figure IV.9 Power spectrum from HP 8555A spectrum analyzer for Varian Model PPS-2.5AS microwave power source. The largest peak is at 2.4501 GHz with a power of 630.4 W. The power measurements were 1.5 kW forward power and 30 W reflected power on the Varian power meter, 1.35 kW on the power source power meter, and 1.65 kW on the HP732A microwave power meter. The spectrum indicates a non-uniform spread with a concentration of power below 2.4501 GHz.

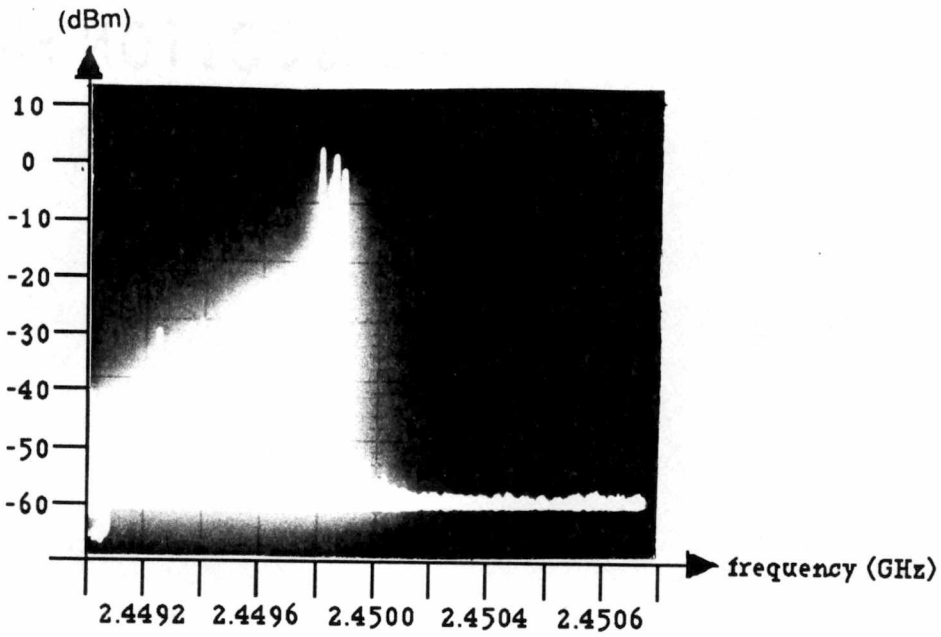


Figure IV.10 Power spectrum from HP 8555A spectrum analyzer for Varian Model PPS-2.5AS microwave power source. The largest peak is at 2.4498 GHz with a power of 794.3 W. The power measurements were 2.5 kW forward power and 75 W reflected power on the Varian power meter, 2.6 kW on the power source power meter, and 3.2 kW on the HP732A microwave power meter. The spectrum indicates a non-uniform spread with a concentration of power below 2.4498 GHz.

the frequency of 2.45 GHz, tapering off in exponential form, would be a more desired spectrum, because more microwave power would be spread over other frequencies, making the probability of excitation of other modes greater. However, in these magnetrons, it is often found (Dyer, 1990) that their spectra are non-symmetrical about their center frequency (2.45 GHz in this case).

Figure IV.8 shows of a spectrum with 1 kW of forward power as measured with the Varian power meter. The most intense line is at a frequency of 2.45032 GHz, and was found not to move in frequency above or below the largest line in Figure IV.7 which had a level of 251.2 (-6 dBm). The shape of this spectrum was found to differ from that of Figure IV.7, in that microwave power at lower frequency has been shifted toward 2.45 GHz. The power spectrum seems to be compressing as the power increases. Also, several small peaks appear above 2.45 GHz.

In Figure IV.9, where the forward power on the Varian power meter was 1.5 kW, the largest peak at a frequency of 2.4501 GHz has moved closer to 2.45 GHz with a power of 630.4 kW (-2 dBm) as indicated by the spectrum analyzer. The spectra of Figures IV.8 and IV.9 are quite similar, except that there are more peaks appearing on both sides of the region of concentrated power in Figure IV.9.

Figure IV.10 represents a spectrum with several large peaks. The largest one with a power of 794.3 W (-1 dBm) on the spectrum analyzer is at a frequency of 2.4498 GHz. There are several large peaks at frequencies above 2.4498 GHz. The Varian power meter indicated a forward power of 2.5 kW and the Hewlett-Packard Model

732A microwave power meter indicated a power of 3.2 kW. The power level adjustment on the microwave power source was at its full clockwise rotation. From the spectrum, it is obvious that the microwave power is again spread out at frequencies below 2.45 GHz with insignificant powers at frequencies above 2.45 GHz. For this experiment, the Varian power meter will be used as a diagnostic only to indicate the presence of microwave power at the exit of the generator, especially since this device was intended to be used with the microwave power source. In the data taking, the Hewlett-Packard Model 732A microwave power meter will be used to measure the power just before entry into the cavity. This selection was made since it is a better instrument and it has been calibrated.

In Figures IV.11 through IV.14, the same type of measurements were conducted using the second microwave power source, the Varian Model PPS-2.5 microwave power pack. The only setting on the spectrum analyzer that was changed was the scanwidth. It was compressed to 5 MHz so that the spectrum would appear on the screen with a center frequency of 2.45 GHz. From these figures, it is obvious that the spectrum is shifted further down in frequency in this microwave source than the previous one. Figures IV.11 through IV.14 are representative of 680 W, 1.4, 1.95, and 2.3 kW, respectively on the Hewlett-Packard 732A microwave power meter. The shape of the spectrum at this scanwidth does not change significantly with increasing power. The power level of the largest peaks from the power spectra in Figures IV.11 through IV.14 are 316 W (-5 dBm), 631 W (-2 dBm), 1.58 kW (2 dBm), and 2.51 kW

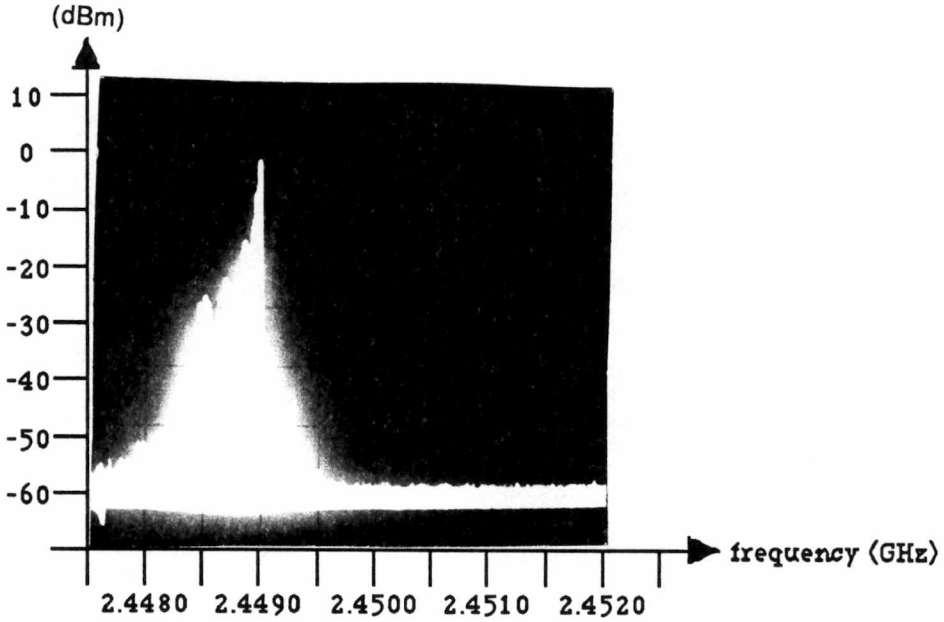


Figure IV.11 Power spectrum from HP 8555A spectrum analyzer for Varian Model PPS-2.5 microwave power source. The largest peak is at 2.449 GHz with a power of 316.2 W. The power measurements were 1 kW forward power and 20 W reflected power on the Varian power meter, 600 W on the power source power meter, and 680 W on the HP732A microwave power meter. The spectrum indicates a non-uniform spread with a concentration of power below 2.449 GHz.

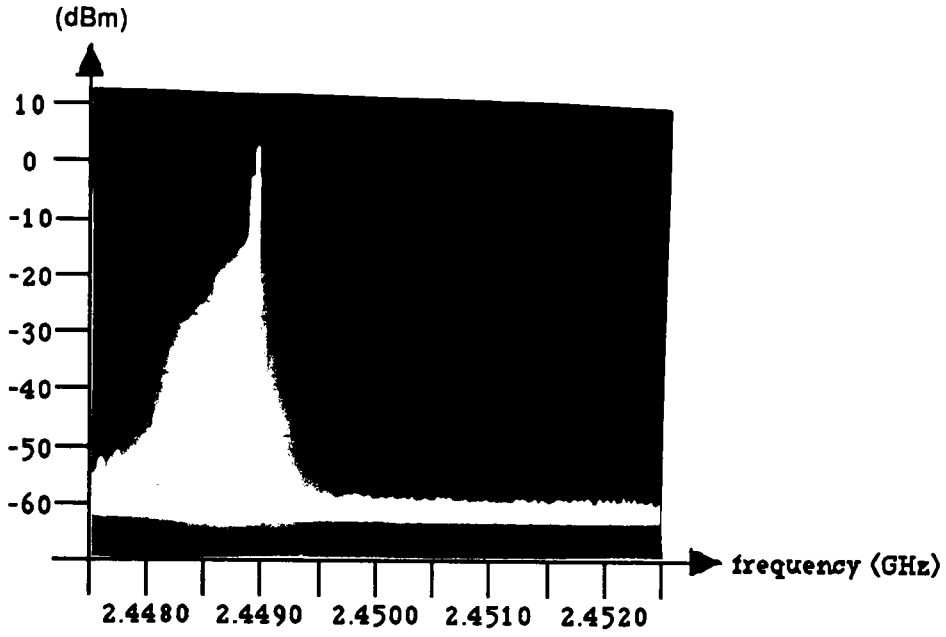


Figure IV.12 Power spectrum from HP 8555A spectrum analyzer for Varian Model PPS-2.5 microwave power source. The largest peak is at 2.4488 GHz with a power of 630.9 W. The power measurements were 2 kW forward power and 40 W reflected power on the Varian power meter, 1200 W on the power source power meter, and 1400 W on the HP732A microwave power meter. The spectrum indicates a non-uniform spread with a concentration of power below 2.4488 GHz.

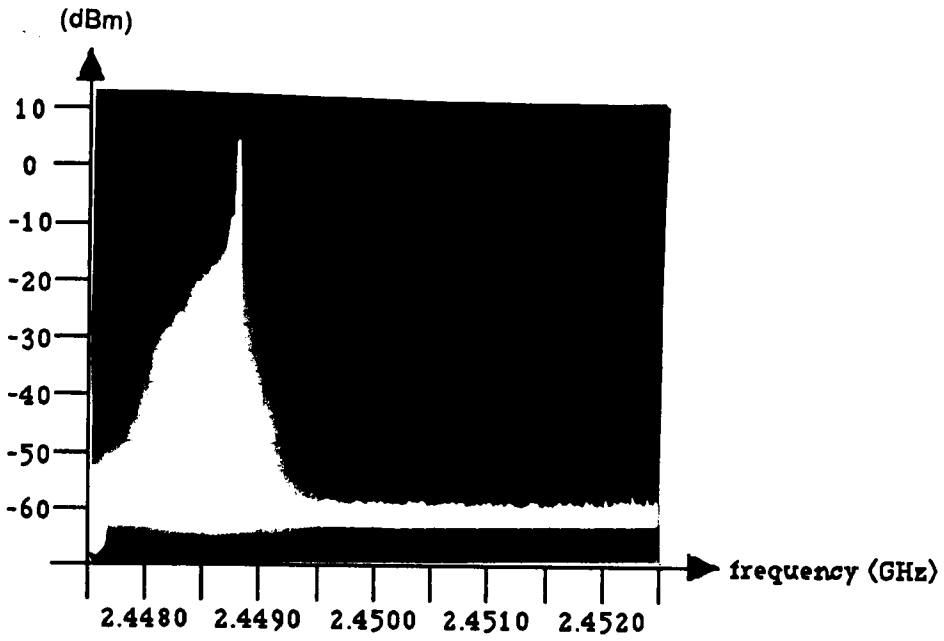


Figure IV.13 Power spectrum from HP 8555A spectrum analyzer for Varian Model PPS-2.5 microwave power source. The largest peak is at 2.44875 GHz with a power of 1.58 kW. The power measurements were 3 kW forward power and 50 W reflected power on the Varian power meter, 1750 W on the power source power meter, and 1950 W on the HP732A microwave power meter. The spectrum indicates a non-uniform spread with a concentration of power below 2.44875 GHz.

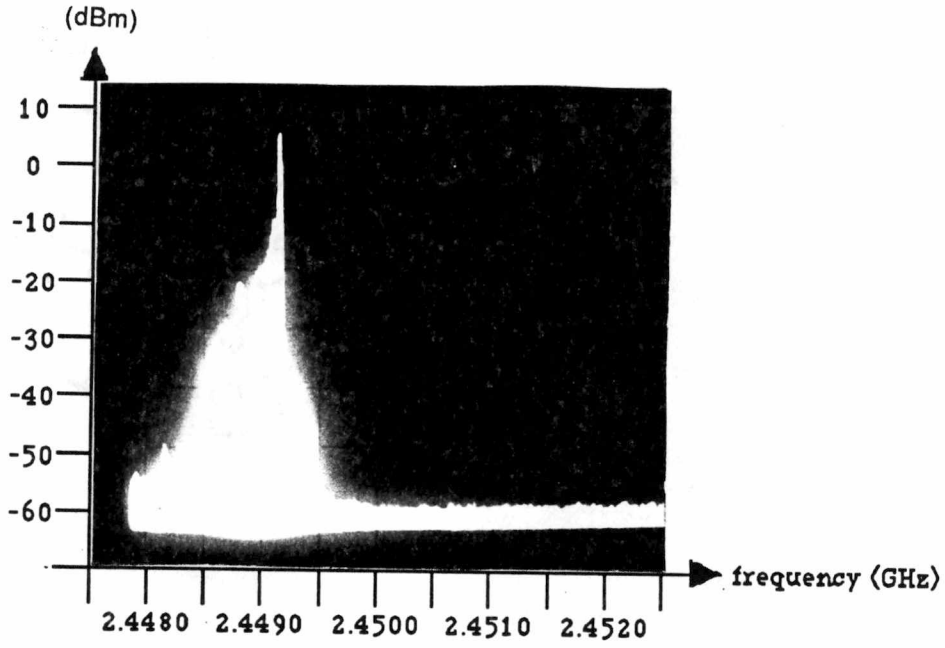


Figure IV.14 Power spectrum from HP 8555A spectrum analyzer for Varian Model PPS-2.5 microwave power source. The largest peak is at 2.44865 GHz with a power of 2.51 kW. The power measurements were greater than 3 kW forward power (meter pegged) and 60 W reflected power on the Varian power meter, 2100 W on the power source power meter, and 2300 W on the HP732A microwave power meter. The spectrum indicates a non-uniform spread with a concentration of power below 2.44865 GHz.

(4 dBm), respectively, where the logarithmic reference level was 10 dBm. The spectra are again non-symmetrical with most of their power content below a frequency of 2.4490 GHz. From a comparison of the spectra of both sources, it appears that the spectrum of the Varian Model PPS-2.5AS source is the desired source, since it has a wider power spectrum. A source with a wider power spectrum may excite more higher order modes than a source with a narrow one.

At this time, it is desirable to define a quantity called the Q of a microwave cavity. This quantity is important in choosing the driving frequency and is also important in characterizing the performance of the microwave cavity. The Q in all resonant systems is defined as the product of the radian driving frequency and the quotient of the time-averaged energy stored in the system and the energy loss per second in the system. A general mathematical expression for Q is given by

$$Q = \frac{\omega\,(\text{time-averaged energy stored in the system})}{(\text{energy loss per sec in the system})} \qquad \text{(IV.1)}$$

A broad power spectrum of the microwave power source will lead to a cavity in which many modes can be excited. This is desirable in this application since a microwave plasma with uniform radial number density across most of the radius is desired.

C. The Multimode Microwave Cavity

1. Choosing a Geometry

In selecting a geometry for the microwave cavity, several issues are involved which range from mathematical, to practical in the mechanical sense. Microwave cavities can be constructed from many types of materials, the choice of which often influences the design one wishes to use. Cavities which have irregular boundaries, or dimensions not a modal multiple of the wavelength, will tend to help excite more modes than cavities with simple geometries or modal patterns. For these reasons, and for simplicity of fabrication, one may favor a spherical or a cylindrical cavity.

In terms of the mathematical theory of a microwave cavity, the selection of a rectangular geometry involves only sine and cosine functions which are easy to manipulate. If a cylindrical or spherical cavity is selected, the equations describing the electromagnetic field distributions involve Bessel functions or other less familiar mathematical functions. In applications where more than one excited mode is present, the information of most interest is an approximate calculation of the Q of the cavity, for its dominant modes. For a cavity exciting only one mode, the Q will be very sharp. For a cavity exciting many modes, as in this application, the Q will large and broad. Each mode will store a fractional part of the electromagnetic energy contained within the power spectrum of the source. Actually, a spherical cavity, which is symmetrical in all three

dimensions, is not as good as a cylindrical cavity for a multimode application since the latter is symmetrical in only two directions. Hence, if one can deal with Bessel functions, the choice of a cylindrical cavity is a good one for a multimode cavity. A cylindrical cavity can have flat or irregularly-shaped end caps, such as hemispherical end caps. A cylindrical cavity with hemispherical end caps will tend to break up more modes resulting in a better multimode cavity (Collin, 1966).

For comparison, there are several other methods of promoting multimode operation. For example, a rectangular cavity may be used if it has mode mixing apparatus. In microwave ovens, many more modes are created by passing radiation from the magnetron through a rotating metal fan which scatters it across the cavity. In addition to this, irregularly-shaped obstructions placed in any type of closed cavity can serve as mode mixers to help create more modes.

While in the process of designing a vacuum system for a plasma generation system, regardless of the method of excitation, it is desirable to refine the configuration to reduce the number of joints or seals that need to be made. Before selecting the basic configuration, one must determine the level of vacuum to be achieved. This not only depends upon the vacuum pumps, but also on the type of vacuum seals used. Regardless whether a glass or metal vacuum system is chosen, it is necessary to select proper seals and flanges to insure a good vacuum. Once a range for the operating vacuum pressure is chosen, the base pressure (pressure before any gas is fed into the system) should be 100 to 1000 times lower. The

base pressure, which ranges from 0.01 to 10 μtorr, will determine the type of containment system and seals to use.

In this application, a glass, quartz, or a metal vacuum system could be used. A microwave generated plasma has been created in a glass vacuum system using Pyrex tubing (Boswell, et al., 1989). The problems with a glass vacuum system are the power flux incident upon the inner walls, the degassing of stored water vapor in the glass when it heats up, and the fact that it can be easily broken or damaged. In this application, a glass vacuum system was deemed undesirable due to the water vapor problem, since one of the objectives of this work is to create a moderately clean plasma for plasma ion implantation. In addition, if a glass vacuum system were used, some type of metal surface to define the cavity boundaries would have to be placed on the inside or outside of the vacuum system, since a glass or quartz container is transparent to microwave radiation. The metal could be a perforated cage with the dimensions of the holes much smaller than the wavelength of the radiation. This was not chosen because the Q of this type of cavity would be very low. A wall which can serve as a vacuum container and a microwave energy reflector should be chosen.

Having established that a metallic vacuum system is desired for a multimode microwave cavity in this application, another aspect must be considered before choosing the geometry even though a cylindrical cavity is preferred. Since the cavity will be made of a metal, it is desired that the number of vacuum weldments be kept to a minimum. If the cavity were rectangular, a vacuum weldment

would have to be made at every joint where two planes intersect. For the cavity alone, with no ports, twelve vacuum welds would have to be made. If a cylindrical cavity is chosen, only the top and bottom flanges would have to be welded. For large cylinders, these welds are the majority of the welds. This cylinder can be a seamless, or one with one welded seam, if the cylinder was rolled from a flat plate. Carefully controlled welding systems and quality controlled factory pressure tests insure that a cylinder with a welded seam would be just as good as a seamless cylinder. There are special ASM codes which must be followed when performing a vacuum weld. Most organizations are not as fortunate as the University of Tennessee's Materials Science and Engineering Mechanical Systems Shop to have experienced vacuum welders and welding equipment, not to mention a state-of-the-art welding research laboratory that is world renowned.

The choice of a metallic cylindrical cavity with hemispherical or ellipsoidal ends would be ideal for this application. However, the mechanical difficulties and increased costs in manufacturing hemispherical ends is significant, and beyond our means here at UTK. For this reason, a metallic cavity in the shape of a cylinder with flat end caps was chosen.

2. Choosing a Metallic Material

The choice of a metallic material for a multimode microwave cavity is significant due to the high Q's desired in a system in which the storage of microwave energy is important. Later in this chapter, an expression for the Q of a cylindrical cavity with flat end caps will be presented. The Q of a cylindrical cavity for a particular mode increases as the skin depth (depth of penetration of the microwave energy into the inner cavity wall) decreases (Collin, 1966 p. 327). The skin depth is dependent upon the resistivity of the material and inversely dependent upon the driving frequency of the microwave energy and the permeability of the metallic material. The driving frequency is fixed at 2.45 GHz, and the permeability would be fixed if a non-magnetic material were chosen. A smaller skin depth is achieved if a material with a low resistivity is chosen.

One of the commonly used materials for the construction of vacuum systems is Type 316 stainless steel. This material is well-suited for this application since the research involves implantation of stainless steels, specifically Type 304. Type 316 stainless steel has a small resistivity (74 nanohm-meters) versus one of the most widely used stainless steels, such as Type 304L, which has a high resistivity (600 nanohm-meters) and is also non-magnetic. Type 316 stainless steel is also well-suited for corrosive environments should a chemically reactive ion species be used for some of our plasma ion implantation tests. Another advantage of choosing Type 316 stainless steel is its weldability for vacuum-tight applications.

However, the machining of this material is difficult. Of course, achieving a low base pressure (0.1 to 1 μtorr) is of more concern than the machinability. The inside and outside of this cylinder will remain unfinished. This is not a problem in this application, as long as the crevices and pores on the inside surface are properly cleaned before pumpdown. Therefore, the multimode microwave cavity was determined to be cylindrical with flat end caps and constructed of Type 316 stainless steel.

3. Choosing the Dimensions

The radius and length of a right circular cylindrical cavity with flat end caps are the dimensions that govern how much microwave energy is stored in each mode at its operating frequency. Figure IV.15 (Heald, et al., 1978) is a graph of a quantity called the form factor as a function of the dimensions of the cavity. The form factor, given by Eq. (IV.2), is the product of the Q of the cavity and the skin depth, divided by the wavelength of a particular mode. The reason for defining such a quantitative expression is that the cavity variables making up the form factor are dependent only upon the geometry and material of the cylinder. The other independent variables determining the form factor are fixed. These are the mode numbers (defined below) which are integer values, and the values of the Bessel function for which its derivative goes to zero. The form factor is given by

$$Q\frac{\delta_s}{\lambda_0}, \qquad \text{(IV.2)}$$

where **Q** is the Q of the cavity, δ_s is the skin depth, and λ_0 is the wavelength of a particular mode. This is a dimensionless quantity and is graphed on the ordinate. The abscissa describes the dimensions of the cavity and is given by

$$\frac{2a}{d}, \qquad \text{(IV.3)}$$

where **a** is radius of the inner wall and **d** is the length of the right circular cylinder.

In the presentation of Figure IV.15, it is necessary to define a "mode." In a right circular cylinder and in many other three-dimensional microwave cavities, the maxima along an electromagnetic wave are described by three numbers called mode numbers. In this analysis, the first number will be donoted by an "n", the second by an "m", and the third by an "l" (L, not a one). In other words, the subscripts nml pertain to the number of variations in the standing-wave pattern inside the cylindrical cavity. Since the microwave energy transmitted by the magnetron in the Varian microwave power supply is transmitted in the TE_{01} (transverse electric) mode, the modes of interest here will be TE modes. They are denoted by TE_{nml}. A TE_{011} mode in a cylindrical cavity is analogous to a TE_{01} traveling in a circular wave guide which is one

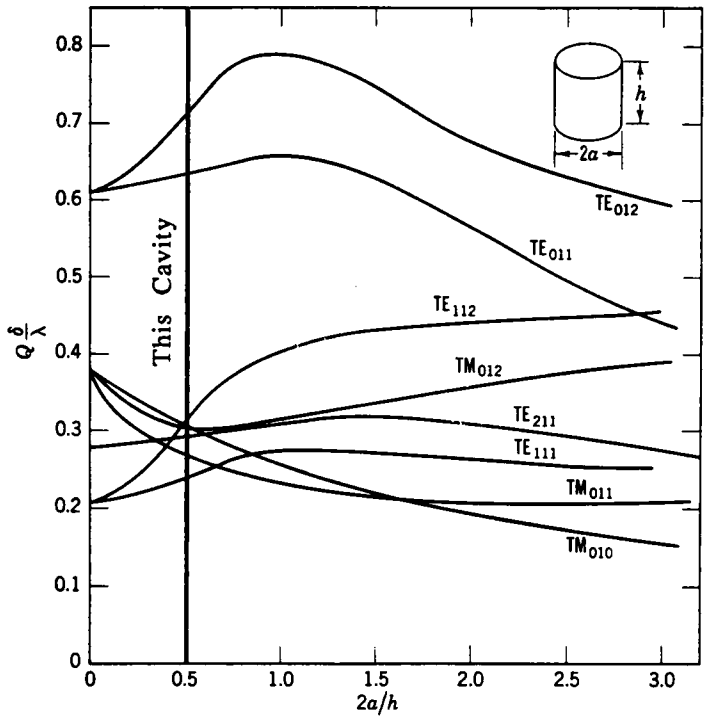


Figure IV.15 Graph of the geometry factor, 2a/d, versus the form factor for several TE and TM modes in a right circular cylinder. Only the TE modes are of interest since those are the ones being launched (Heald, et al., 1978).

unit long in length. TE_{nm0} modes do not exist as no electromagnetic wave can travel in a waveguide which has zero length.

The value of Eq. (IV.2) above determines the value of the form factor. For values of Eq. (IV.2) which approach unity, the form factor is maximum for several modes (cf. Figure IV.15). Thus, cylindrical cavities, the length of which is twice their diameter, can store maximum microwave energy. In this research, a cylindrical cavity having an outside diameter of 20" (50.8 cm) and a length of 40" (101.6 cm) was selected. For this cavity (cf Figure IV.15), a vertical line at a geometry factor of about 0.5 can be drawn. These dimensions were selected to allow us to implant large objects such as gears, which have diameters of several inches, and other large objects of interest to either corrosion resistance, hardness, or wear resistance.

Once the diameter and length of the cavity were selected, the wall thickness of the cylinder must be determined. To avoid collapse under vacuum and mechanical impact, a wall thickness of 0.25" (0.635 cm) or greater will suffice. A value of 0.375" (0.953 cm) for the wall thickness was selected because of its availability. For a 20" (50.8 cm) cylinder with a wall thickness of 0.375" (0.953 cm), the inside diameter is 19.25" (48.9 cm). This inside diameter is sufficient. The cylinder length was specified as 40" (101.6 cm). Extra length was specified in case the factory cuts were not acceptable to the machinsts. The actual length of the cylinder, when received, was 40.1875" (102.1 cm) and the factory cuts were satisfactory. With these values for the diameter and length, the

value of Eq. (IV.3) is 0.479. According to Figure IV.15, this corresponds to form factors to the left of, but near, several maxima which are acceptable for the storage of microwave energy. Calculations of these form factors and for the Q of several low and high order modes will be presented later in this chapter.

4. The Cavity Q's

As stated earlier, the Q of any cavity is the product of the radian driving frequency and the quotient of the time-average energy stored in the cavity and the energy lost per second in the cavity. Before the Q of the cavity can be determined, the field distributions of the forward and backward propagating TE_{nml} electromagnetic waves must be known. For a right circular cylinder, these are well known and describe the field distribution in circular waveguides. The coordinate system used in describing these waves is the cylindrical coordinate system, which depends upon the radius, r, the length along the axis of the cavity, z, and the angle, ϕ. The magnetic field distributions are denoted by an H and the electric field distributions are denoted by an E. These fields are for the TE modes of operation only, since the microwave being launched is a TE mode.

The magnetic field distribution (Collin, 1966) along the axis of the cylinder in the z direction for a circular waveguide is given by

$$H_z = J_n\left(\frac{p'_{nm} r}{a}\right)\cos\phi\left(A^+ e^{-j\beta_{nm} z} + A^- e^{j\beta_{nm} z}\right) \quad \text{(IV.4)}$$

where $J_n(p'_{nm}\, r / a)$ is the value of the Bessel function of the nth kind at a radius r for a fixed inside radius a. p'_{nm} are the roots of

$$\frac{dJ_n(k_c r)}{dr} = 0 \qquad \text{(IV.5)}$$

at r = a. $A+$ and A^- are constants for the positive and negative electromagnetic waves and j is the square root of -1. β_{nm} is the propagation constant for each mode and is given by

$$\beta_{nm} = \left[k_0^{\,2} - \left(\frac{p'_{nm}}{a}\right)^2\right]^{1/2} \qquad \text{(IV.6)}$$

where k_0 is the wave number for each resonant mode given by

$$k_0 = \frac{2\pi f_{nml}}{c} \qquad \text{(IV.7)}$$

f_{nml} is the resonant frequency for each mode and c is the speed of light.

The radial distribution of the magnetic field is given by

$$H_r = -\left(\frac{j\beta_{nm} p'_{nm}}{a k^2_{c,nm}}\right) J'_n\left(\frac{p'_{nm} r}{a}\right)\cos\phi\left(A^+ e^{-j\beta_{nm} z} - A^- e^{j\beta_{nm} z}\right) \quad \text{(IV.8)}$$

where $k_{c,nm}$ are the eigenvalues for Equation (IV.9) and are given by

$$k_{c,nm} = \frac{p'_{nm}}{a} . \qquad \text{(IV.9)}$$

The azimuthal magnetic field distribution is given by

$$H_\phi = -\left(\frac{jn\beta_{nm}}{rk^2_{c,nm}}\right) J_n\left(\frac{p'_{nm}r}{a}\right) \sin\phi \left(A^+ e^{-j\beta_{nm}z} - A^- e^{j\beta_{nm}z}\right) \qquad \text{(IV.10)}$$

For a right circular cylinder excited by TE modes, there is no electric field along the z-axis. Thus,

$$E_z = 0 . \qquad \text{(IV.11)}$$

The radial electric field distribution is the product of the wave impedance for each mode and the angular magnetic field distribution, given by

$$E_r = Z_{h,nm} H_\phi . \qquad \text{(IV.12)}$$

The azimuthal electric field distribution is the negative of the product of the wave impedance for each mode and the radial magnetic field distribution,

$$E_\phi = - Z_{h,nm} H_r , \qquad \text{(IV.13)}$$

where $Z_{h,nm}$ is the wave impedance for each mode given by

$$Z_{h,nm} = \frac{k_0}{\beta_{nm}} Z_0 \qquad \text{(IV.14)}$$

Some of the electric and magnetic field patterns (Gandhi, 1981) for several TE modes are shown in Figure IV.16. The mode number l cannot equal 0 because of the transverse electric fields of the reflecting electromagnetic waves. As the mode numbers in Figure IV.16 increase, the field configurations become more coupled and complicated (Gandhi, 1981).

In order to find the Q for each mode, the time-average energy stored in the microwave cavity and the power loss deposited into the cavity walls must be calculated. The stored energy, **W**, is given by

$$W = \frac{\varepsilon_0}{2} \int_0^a \int_0^{2\pi} \int_0^d \left(|E_r|^2 + |E_\phi|^2 \right) r \, d\phi \, dr \, dz \qquad \text{(IV.15)}$$

and the power loss in the walls is given by

$$P_l = \frac{R_m}{2} \int_{walls} |\vec{H}_{tan}|^2 \, dS \qquad \text{(IV.16)}$$

where R_m is the surface resistivity. After much calculus, the form factor for a right circular cylinder with flat end caps is given by

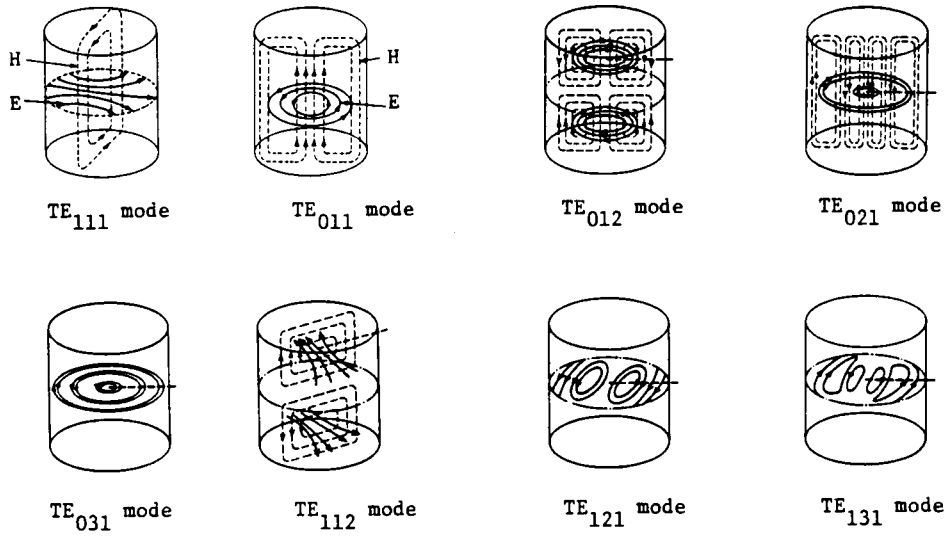


Figure IV.16 Electric and magnetic field configurations of some TE_{nml} modes in a right circular cylindrical multimode microwave cavity (Gandhi, 1981).

$$Q\frac{\delta_s}{\lambda_0} = \frac{\left[1-\left(\frac{n}{p'_{nm}}\right)^2\right]\left[(p'_{nm})^2+\left(\frac{l\pi a}{d}\right)^2\right]^{3/2}}{2\pi\left[(p'_{nm})^2+\frac{2a}{d}\left(\frac{l\pi a}{d}\right)^2+\left(1-\frac{2a}{d}\right)\left(\frac{nl\pi a}{p'_{nm}d}\right)^2\right]}, \quad \text{(IV.17)}$$

and is only dependent upon p'_{nm}, the zero of the derivative of the Bessel function, the cavity dimensions **a** and **d**, and the three mode numbers **n**, **m**, and **l**.

To find the Q of the cavity, it is only necessary to calculate the skin depth, given by

$$\delta_s = (\pi \sigma f \mu_0)^{-1/2}, \quad \text{(IV.18)}$$

where σ is the conductivity in siemens (1/ohm-meters) of the wall material and is the inverse of the wall resistivity, **f** is the driving frequency of the electromagnetic energy in Hz, and μ_0 is the permeability of the wall material. Since the wall material is Type 316 stainless steel, which is a non-magnetic material, the standard value of $4\pi \times 10^{-7}$ H/m for the permeability is used.

It is also necessary to determine the resonant wavelength for each mode. This is given by

$$\lambda_0 = \frac{4}{\sqrt{\left(\frac{2l}{d}\right)^2+\left(\frac{2p'_{nm}}{\pi a}\right)^2}}. \quad \text{(IV.19)}$$

To simplify the calculation of the Q for several modes, a simple computer program was written in the True Basic computer language. The computer program is given in Appendix G and the results for several low and high order modes are given in Table IV.1.

5. The Q with a Plasma

If the microwave cavity contains no plasma, then the Q of the system will simply be the vacuum Q of the cavity including the wall losses (Collin, 1967). In this application, the plasma serves as the load on the microwave energy and will fill most of the cavity volume. The plasma is a lossy dielectric. Just how lossy will be approximated in the next section.

If a medium is contained in the vacuum volume of the multimode microwave cavity, the quality factor due to a lossy dielectric denoted by, Q_d, is given by

$$Q_d = \frac{\varepsilon'}{\varepsilon''}, \qquad \text{(IV.20)}$$

where ε' is the real part of the complex dielectric constant and ε'' is the imaginary part of the complex dielectric constant. The complex dielectric constant is given by

$$\varepsilon = \varepsilon' - j\varepsilon'', \qquad \text{(IV.21)}$$

Table IV.1

Unloaded Quality Factor (Q) of Several Low and High Order Modes in the Multimode Microwave Cavity

TE Mode Number nml	Quality Factor
011	91,920
012	96,962
013	104,247
014	112,622
021	90,656
022	92,262
023	94,820
024	98,172
111	67,102
112	74,541
113	81,431
114	86,450
121	87,817
122	90,348
123	94,244
124	99,110
131	89,232
132	90,297
133	90,017
134	94,317
211	52,372
212	54,684

Table IV.1
Continued

Unloaded Quality Factor (Q) of Several Low and High Order Modes in the Multimode Microwave Cavity

TE Mode Number nml	Quality Factor
213	57,545
214	60,318
221	82,590
222	84,041
223	86,333
224	89,299
311	44,516
312	45,499
313	46,869
314	48,376
321	77,798
322	78,711
323	80,173
324	82,103
411	39,307
412	39,809
413	40,551
414	41,428

where j is the imaginary unit (Collin, 1967).

These dielectric quantities can be approximated by several methods. Electron motions within a plasma are damped due to collisions. In this application, it is assumed that the electrons are ionizing diatomic nitrogen to produce a diatomic nitrogen ion with one electron missing. This damping term is a viscous damping term and is proportional to velocity. This viscous damping term is directly proportional to the electron momentum collision frequency for momentum transfer between an electron and a neutral atom. The solution to the equation of motion for these electrons yields a complex conductivity (Heald, et al., 1978). This is known as the Lorentz conductivity and is given by

$$\sigma = \sigma_r + j\sigma_i = \frac{n_e e^2}{m_e(\nu_c + j\omega)}, \qquad \text{(IV.22)}$$

where σ is the complex conductivity, σ_r is the real part, σ_i is the imaginary part, n_e is the electron number density, m_e is the electron mass, ν_c is the collision frequency for collisions between electrons and neutral atoms or molecules, and ω is the radian frequency of the electromagnetic radiation injected into the cavity.

The complex Lorentz dielectric constant corresponding to the above complex conductivity is given by

$$\varepsilon = \left(1 - \frac{\omega_{pe}^{\,2}}{\omega^2 + \nu_c^{\,2}}\right) - j\left(\frac{\omega_{pe}^{\,2}\nu_c}{\omega(\omega^2 + \nu_c^{\,2})}\right), \qquad \text{(IV.23)}$$

where ω_{pe} is the electron plasma frequency and is given by (Heald, et al., 1978)

$$\omega_{pe} = \sqrt{\frac{n_e e^2}{\varepsilon_0 m_e}}. \qquad \text{(IV.24)}$$

Since the complex dielectric constant for the plasma depends on the collision frequency, it is necessary to know its value. Several experimentalists have investigated the dependence of electron collision frequency on electron kinetic temperature and background pressure for various gases. In our application, the plasma is generated from nitrogen gas at relatively high pressures. Upon investigation of the plasma in the uniform Penning discharge, it was determined that a pressure above about 1 x 10^{-4} Torr is sufficient. At this pressure, the data of Geller and Hosea (Geller, et al., 1968) indicate that the electron collision frequency for an electron kinetic temperature of 3 eV, a reasonable assumption for our plasma, is about 600 kHz.

This microwave plasma has a maximum electron number density which depends upon the driving frequency of the electromagnetic radiation, 2.45 GHz. If the electron plasma frequency takes on this value, then the maximum number density would be 7.45 x 10^{16} electrons/m^3.

If the plasma stabilizes at this electron number density or any value below the critical number density, the microwave radiation will pass through the plasma diameter. It is not desirable for this to happen, but for the radiation to be absorbed by the plasma in creating and maintaining it. In order to maintain the plasma, the plasma must store the radiation, determined by the plasma quality factor. A computer program, written in True Basic that calculates the quality factor of the plasma is given in Appendix H. The results of these calculations for the plasma quality factor for electron plasma frequencies ranging from 3.5×10^9 to 5.7×10^9 radians/sec, corresponding to electron number densities ranging from 3.85×10^{15} to 1.02×10^{16} electrons/m^3, are 74,906 and 25,699, respectively. The values of the plasma quality factor in between these limits are listed in Table IV.2 and the graph for electron number density versus plasma quality factor is presented in Figure IV.17. From Figure IV.17, it is obvious that electron number densities greater than 1×10^{10} electrons/cm^3 (1×10^{16} electrons/m^3) result in plasma quality factors less than 30,000.

The loaded quality factor, Q', including the lossy dielectric of the plasma is given by

$$Q' = \left(\frac{1}{Q_d} + \frac{1}{Q} \right)^{-1} \qquad \text{(IV.25)}$$

Referring to Table IV.1, most of the quality factors for the modes are very high, on the order of 80,000 or 90,000. With these quality

Table IV.2

Plasma Quality Factor

Electron Number Density (x 10^9 cm^{-3})	Plasma Quality Factor
3.85	74,906
4.07	70,579
4.30	66,598
4.54	62,927
4.78	59,534
5.03	56,393
5.28	53,479
5.54	50,771
5.81	48,249
6.08	45,897
6.36	43,701
6.65	41,646
6.94	39,720
7.24	37,914
7.55	36,218
7.86	34,622
8.17	33,119
8.50	31,702
8.83	30,364
9.16	29,100
9.51	27,904
9.86	26,772
10.2	25,699

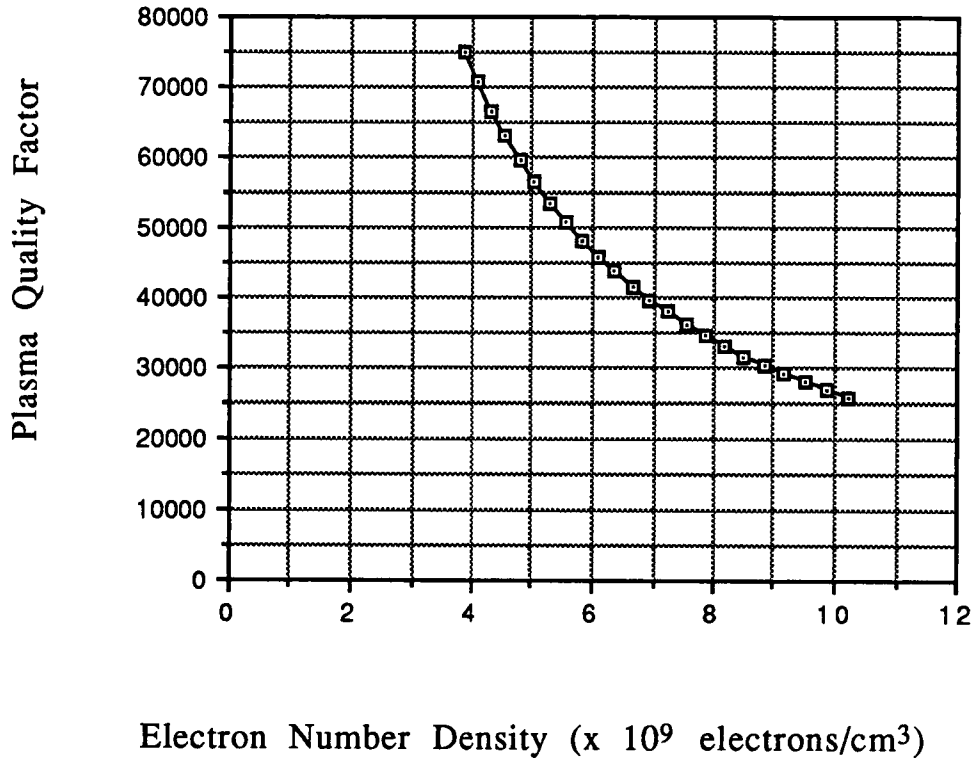


Figure IV.17 Graph of electron number density versus plasma quality factor for the plasma in the multimode microwave cavity with an electron collision frequency of 600 kHz and a microwave driving frequency of 2.45 GHz.

factors and a plasma quality factor of about 30,000, the loaded quality factor may be expected to be on the order of 20,000. It is not possible to determine which modes will be dominant in the plasma-filled cavity, because it is not known what fraction of the energy contained in the TE_{10} mode, delivered from the microwave generator, will be stored in which nml modes. A further difficulty is that the plasma is a continuously changing load, since the electron collision frequency is also continuously changing.

6. Microwave Discharge Mechanism

For a microwave discharge, the maximum electric field built up in the discharge and the corresponding power density are of interest. The highest possible average power density can be calculated by taking the ratio of the maximum microwave power to the volume of the vacuum cavity. The volume of a cylindrical cavity with flat ends is given by

$$V = \pi a^2 d , \qquad \text{(IV.26)}$$

and has a value of 0.192 m^3 for our cavity. For a microwave power level of 2.5 kW, the maximum rated power level of our source, the power density has a maximum value of about 13 kW/m^3 available to heat the plasma.

In a microwave discharge with a maximum AC electric field strength, E_{max}, the average power transferred to a gas per unit volume is given by (Baddour, 1967)

$$P = \frac{e^2 n_e E_{max}^2}{2 m_e} \frac{\nu_c}{\nu_c^2 + \omega^2} \qquad \text{(IV.27)}$$

For an electron collision frequency of 600 kHz, an electromagnetic radiation frequency of 2.45 GHz, an assumed maximum electron number density of 1.02×10^{16} electrons/m^3, and a power density of 13 kW/m^3, the maximum electric field within the microwave cavity is 755 V/cm. This is within the expected electric fields, ranging from 500 to 20,000 V/cm, for microwave discharges. The average energy density stored by this maximum electric field is given by

$$U_{max} = \frac{1}{4} \varepsilon_0 E_{max}^2 , \qquad \text{(IV.28)}$$

and has a value of 1.26×10^{-2} J/m^3.

Not only is the value of the electron number density on axis important, but so also is its radial distribution, since it is desired to have the capability to implant objects in a plasma where the ion number density is approximately uniform. The characteristic diffusion length, denoted by Λ, is helpful in describing the

uniformity of the number density. For a right circular cylinder, it is (Hirsh, et al., 1978)

$$\frac{1}{\Lambda^2} = \left(\frac{\pi}{d}\right)^2 + \left(\frac{2.405}{a}\right)^2 \qquad \text{(IV.29)}$$

It is desirable to have this characteristic diffusion length as large as possible. In our cavity, the value of Λ has the value 9.70 cm. This is about 40 % of the radius of the vacuum vessel. At radii greater than this value, the electron number density will decrease rapidly to a minimum value at the radius of the cavity.

The values of the electron number density, electron kinetic temperature, and characteristic diffusion length in the vacuum vessel are not restricted to the values in this example. The application of an array of small permanent magnets on the outside of the vacuum vessel should improve the plasma uniformity and density.

7. Vacuum System Design

The geometry, radius, length, and material of the vacuum vessel have already been specified. The remaining specifications of the vacuum system involve the size and location of any service and diagnostic ports. The vacuum vessel is quite large by laboratory standards, with more than enough surface area for several sizeable ports. The arrangement of ports in the initial design of a vacuum

vessel is important, since modifications are difficult after fabrication of the vessel.

Before our final design was arrived at, many alternatives were examined. One of the most important design decisions was the position of the central axis. In most applications where cylindrical plasmas are used, the central axis would be horizontal. Due to the weight of the vacuum vessel, this orientation would allow its weight to be supported by the vacuum pumping station. However, this application involves high voltages, on the order of a few tens of kilovolts. In the future, the bias potential for ion implantation could be as high as -100 kV. The presence of such high voltages is dangerous if protective features are not designed into the system. To help prevent electrocution, the central axis of the vacuum vessel was made vertical, to position the high-voltage feed-through up out of easy reach. This was also chosen because the sample holder for plasma ion implantation must be inserted or extracted along a significant distance, which would interfere with laboratory operations. Therefore, it was decided to place the sample holder on the axis of the top flange of the vacuum vessel, and extend down into the plasma. The vacuum vessel radius provides isolation from the sample holder inside the vessel. Outside the vacuum vessel, the height of the vacuum vessel provides adequate electrical isolation. Since most laboratory ceilings are around 15 to 20 feet high, the height of 8 feet for the complete system is not a problem, even when the extraction of a sample holder system required an additional 5 feet.

The vacuum vessel with its central axis vertical, must rest on a support structure. Since the vacuum pumping station has a base plate on its upper surface, it was decided to locate the vacuum pumping port on the bottom flange plate of the vacuum tank. The base plate contains an O-ring groove using a #249 Viton O-ring. The vacuum pumping port axis is concentric with the vacuum vessel axis. The inside diameter of the base plate port on the vacuum pumping station is 3.75" (9.5 cm). Hence, for maximum pumping speed, it was decided that the diameter of the vacuum pumping port would also be 3.75" (9.5 cm), constructed of Type 316 stainless steel, 3.5" (8.9 cm) inside diameter pipe. The pipe length was chosen to be 8" (20.3 cm). This length allows the installation of gas feeds, vacuum gauges, or any needed diagnostic instruments on the bottom flange plate. Also, this allows room for installing the bolts that connect this port to the vacuum pumping station base plate, since these are relatively large bolts.

The flange on the vacuum pumping port was constructed of a Type 316 stainless steel, 3/4" (1.9 cm) thick plate. The construction of this port will support more than the weight of the entire vacuum vessel with all components connected to it. However, the vacuum pumping station is limited to a nominal weight of not more than 200 lbs. Thus, some additional support structure is desirable to support the vacuum tank. The vacuum pumping flange port is pictured in Figure IV.18. A color photograph of this port installed on a milling machine is pictured in Figure IV.19.

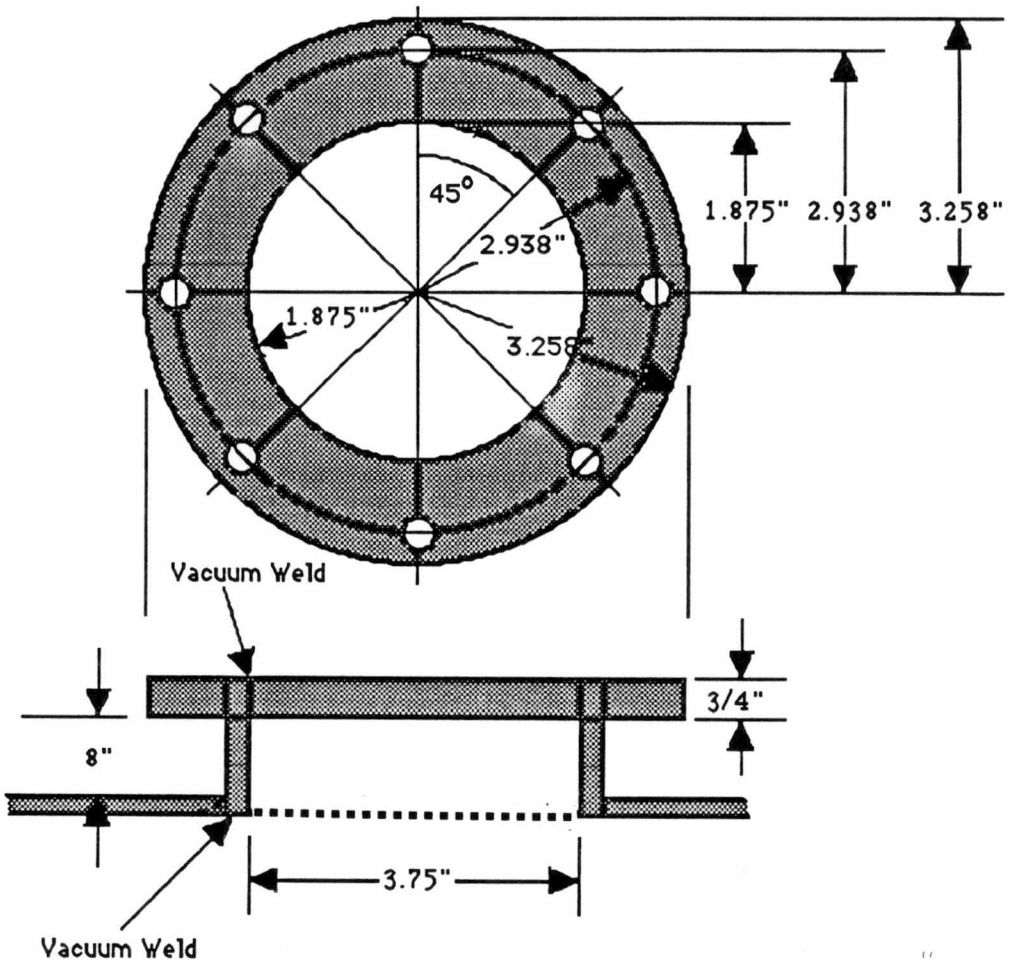


Figure IV.18 Vacuum pumping flange port used in multimode microwave cavity showing the maximum pumping cross-section of 3.75". The thickness of the flange is 3/4". The dotted line indicates the microwave shielding necessary to keep microwaves from getting inside the vacuum pumping system.

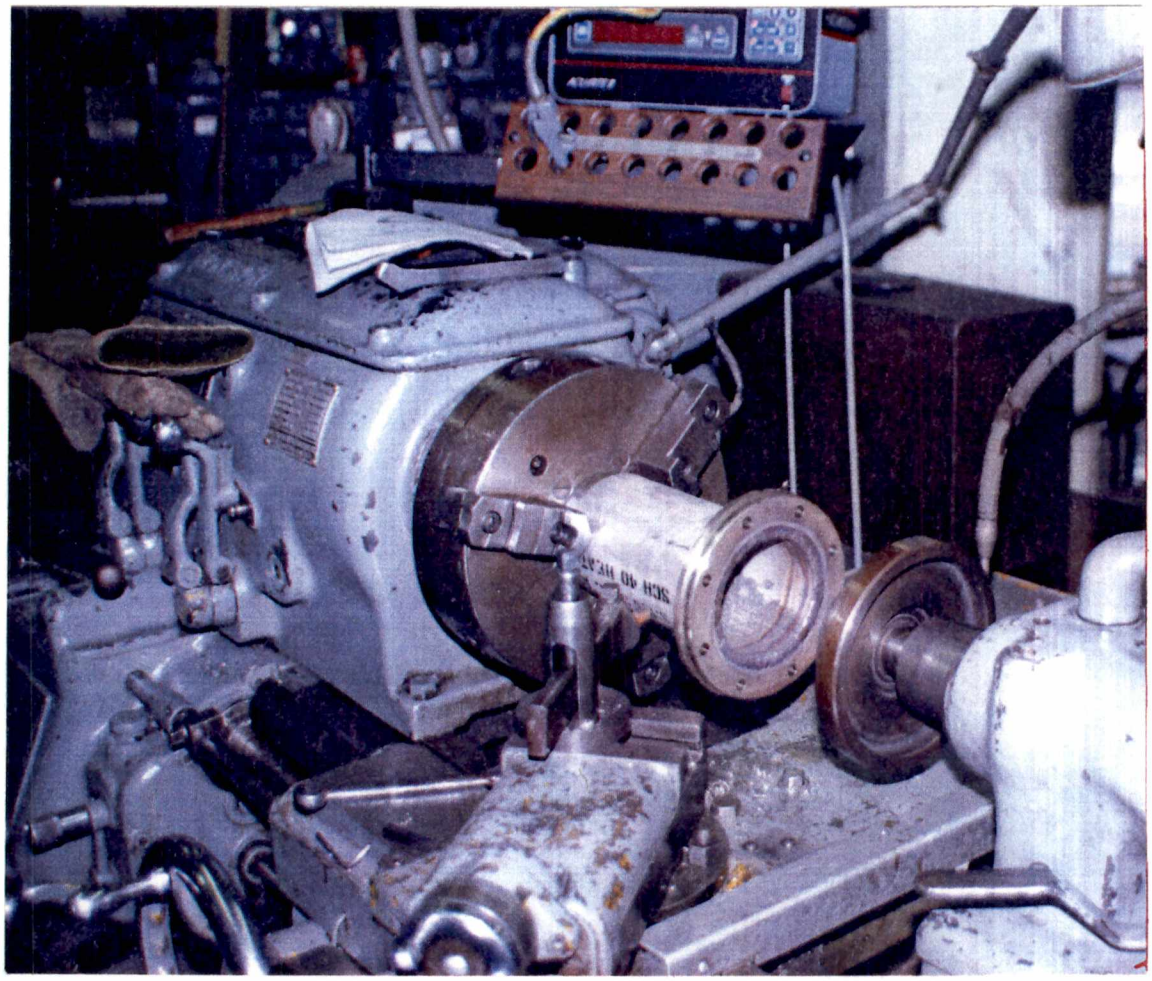


Figure IV.19 A color photograph of the vacuum pumping port installed on a milling machine for the finishing of the flange surface. Notice the vacuum weld on its end. This port will be welded on the bottom flange plate of the cavity.

The top and bottom flange plates are important components in this vacuum system. Since the background pressure is expected to range between 0.1 to 1 μtorr, the thickness of these plates is crucial to the mechanical stability of the vacuum vessel to implosion when the system is under vacuum. The thickness of these plates was chosen to be 3/4" (1.9 cm). This thickness is sufficient, since only a thin layer (less than 0.050" (0.13 cm) thick) is expected to be machined off due to imperfections in the raw material, which is not finished to a vacuum grade texture. In order to have flexibility in the placement of gas feeds, vacuum gauges, and diagnostic instruments, it was decided that each flange plate (top and bottom) have four standard 4" (10.2 cm) flange ports machined at 0, 90, 180, and 270 degree positions. The selection of the size of these ports was chosen because a standard 4" (10.2 cm) flange with four bolt holes is common to many instruments accompanying flanges such as mass spectrometers and A-lite insulators. For the vacuum seals on the top and bottom flange plates, it was decided that Viton O-rings would be used. It is good practice not to machine the O-ring groove in a flange plate or ring permanently fixed to a large vacuum vessel, should they become damaged and need re-working. However, it was decided that the O-ring groove be machined in the complementary ring flange mating with the top and bottom flange plates. For the vacuum seals on the 4" (10.2 cm) flange ports, the standard 4" (10.2 cm) flange plates include the O-ring groove. There are nine standard 4" (10.2 cm) flange ports, including the axial port for the sample holder A-lite fitting, in the top and bottom flange plates. One of

these ports on the bottom flange plate will be used for the gas feed, and on the top flange plate, one to mount a Bayard-Alpert ionization gauge tube to measure pressures below 1 mTorr. Two lifting hooks, which thread only into the top flange plate, can be used to remove the top flange plate, when the sample holder must be removed or when access to the inside of the vacuum tank is needed. Four hooks, which extend through the top flange plate and top ring flange, can be used to pick up the entire vacuum vessel. A lifting device, which can be connected to these four hooks, was made to connect the vacuum vessel to the overhead chain hoist, positioned over the axis of the tank. The top flange plate is pictured in Figure IV.20 and the bottom flange plate is pictured in Figure IV.21.

Not only are the top and bottom flange plates important to the design of the vacuum vessel, but the detailed design of the top and bottom ring flanges are also important since very low base pressures are required. The thickness of these ring flanges was chosen to be 3/4" (1.9 cm). Both ring flanges are symmetrical and identical in design. A critical part of the design was to select an O-ring that would not interfere with the chamfer needed for the vacuum welds. The chamfer is a 37.5 degree angle machined into the inside of both ring flanges and could extend into the ring flange as much as 1/4" (0.64 cm). The outside diameter of the ring flanges was about 26" (66 cm). An overlap of 3" (7.6 cm) from the outside diameter was selected to allow clearance for the O-ring groove and the sixteen bolt holes. This is sufficient to insure a firm connection to the flange plates since, under vacuum, there will be a large inward-bowing

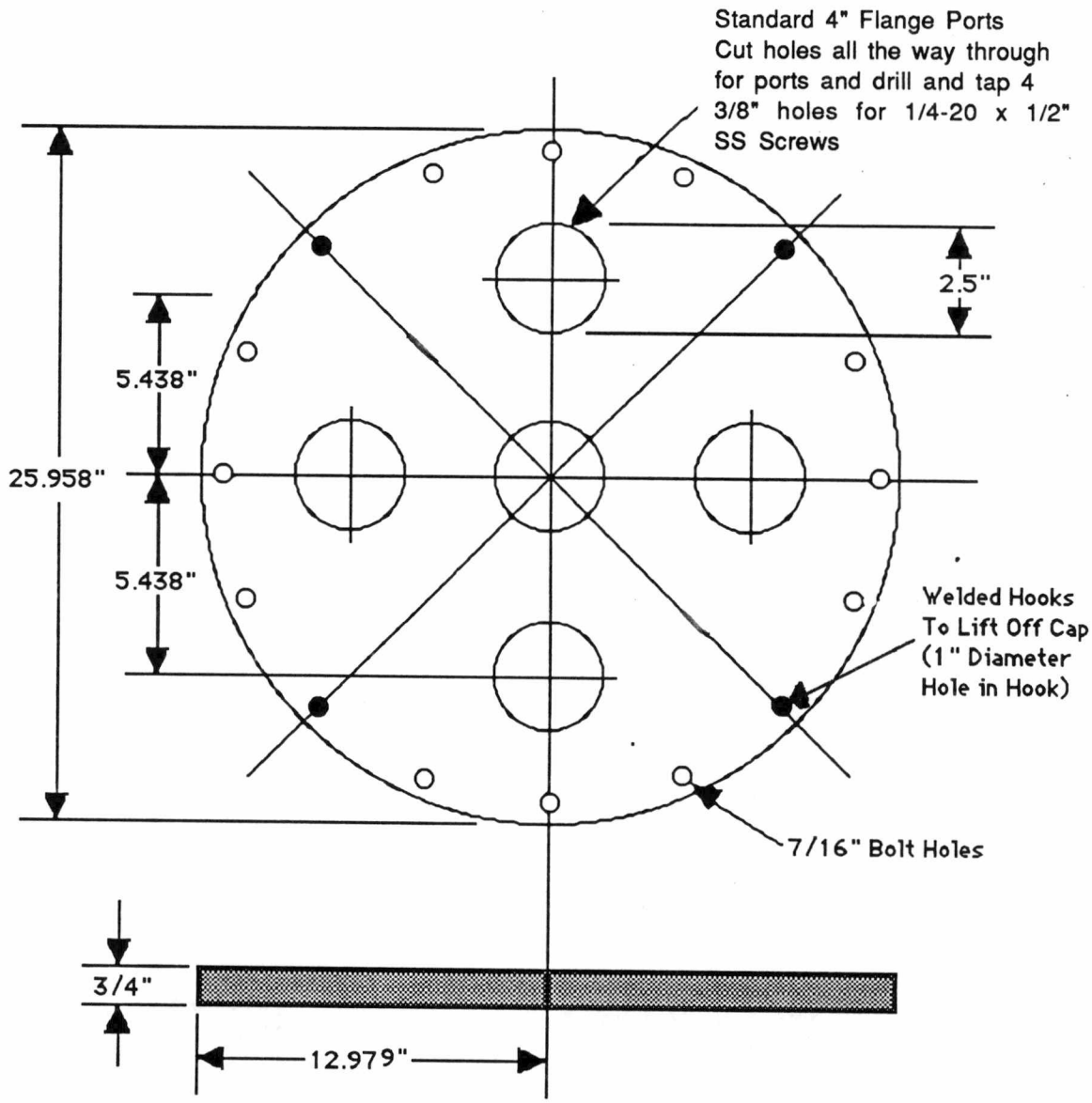


Figure IV.20 Top flange plate used in the multimode microwave cavity including five standard 4" flange ports, sixteen bolt holes, and four threaded eye hooks for lifting. The center standard 4" flange port is for the sample holder A-lite insulator. The thickness of the flange is 3/4".

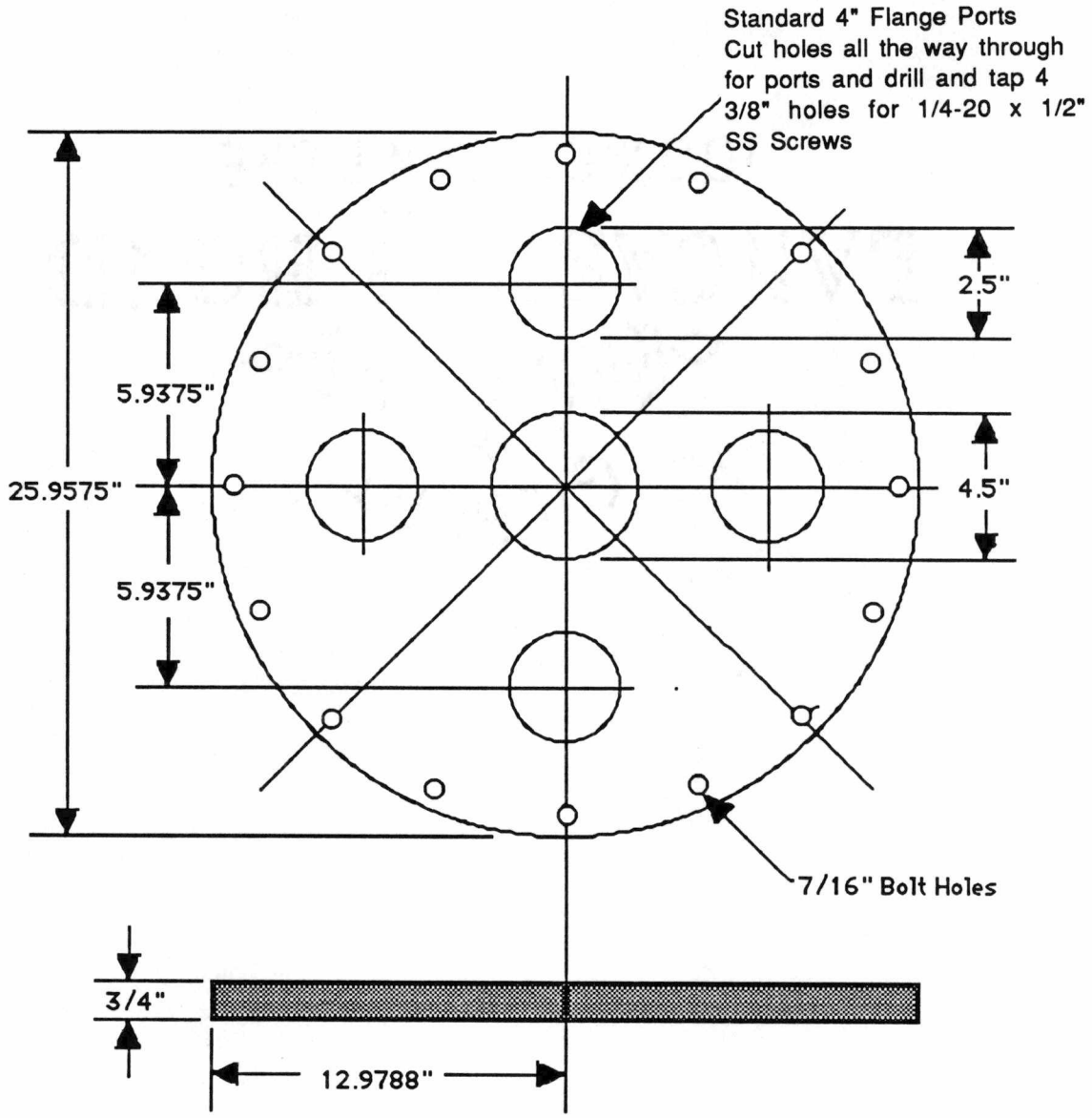


Figure IV.21 Bottom flange plate used in the multimode microwave cavity including four standard 4" flange ports, one vacuum pumping port, and sixteen bolt holes. The thickness of the flange is 3/4".

force on the outside of the flange plates. The bolt holes were not threaded and stainless steel bolts 3" (7.6 cm) long were selected. The seal chosen for this application was a #471 Viton O-ring which measures 22" (55.9 cm) x 22-1/2" (57.2 cm) and has a 1/4" (0.64 cm) diameter cross-section. This O-ring is seamless and was molded. Three O-rings were purchased in order to have one backup. The flange used for both the top and bottom is shown in Figure IV.22. Figure IV.23 is a color photograph of Ray Bellamy vacuum welding a layer of Type 316 stainless steel to the chamfered grooves between the outer edge of the cylinder and the inner edge of one of the ring flanges. The welder is a T.I.G. (Tungsten Inert Gas) welder using argon gas.

To provide for diagnostic instruments used to characterize the plasma across its diameter, three standard 4" (10.2 cm) flange ports were located at a distance of 1/4 of the cavity length, 10" (25.4 cm) from the bottom flange plate. The thickness of these flanges was 3/4" (1.9 cm) with an inside diameter of 2.5" (6.4 cm) to achieve maximum cross-section within the geometric constraint of the standard 4" (10.2 cm) flange plates. These ports are located at 0, 90, and 270 degree locations, with 0° at the front of the vacuum vessel. The 0° degree location is such that the microwave port (to be described later) is on the right-hand side of the vacuum vessel. One diagnostic instrument for which these ports were designed is the polarization diplexing microwave interferometer. This diagnostic may be used to analyze the integrated electron number density across the plasma diameter. Thus, the 90° and 270° diagnostic

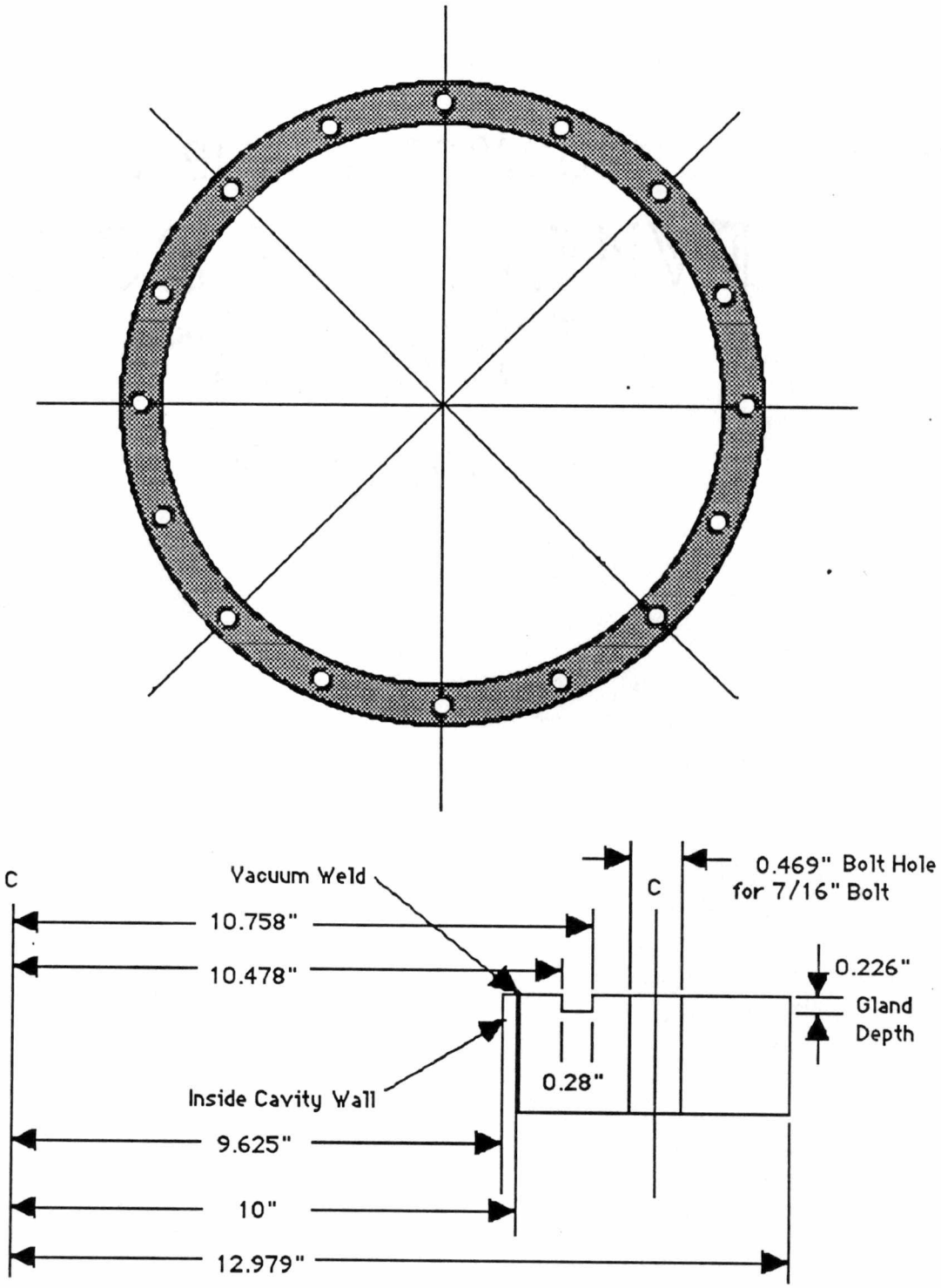


Figure IV.22 Ring flanges for top and bottom flange plates used in the multimode microwave cavity, showing a cross-section with the cavity side wall, O-ring groove, and bolt holes. Vacuum weld does not show chamfer. The thickness of the flange is 3/4".

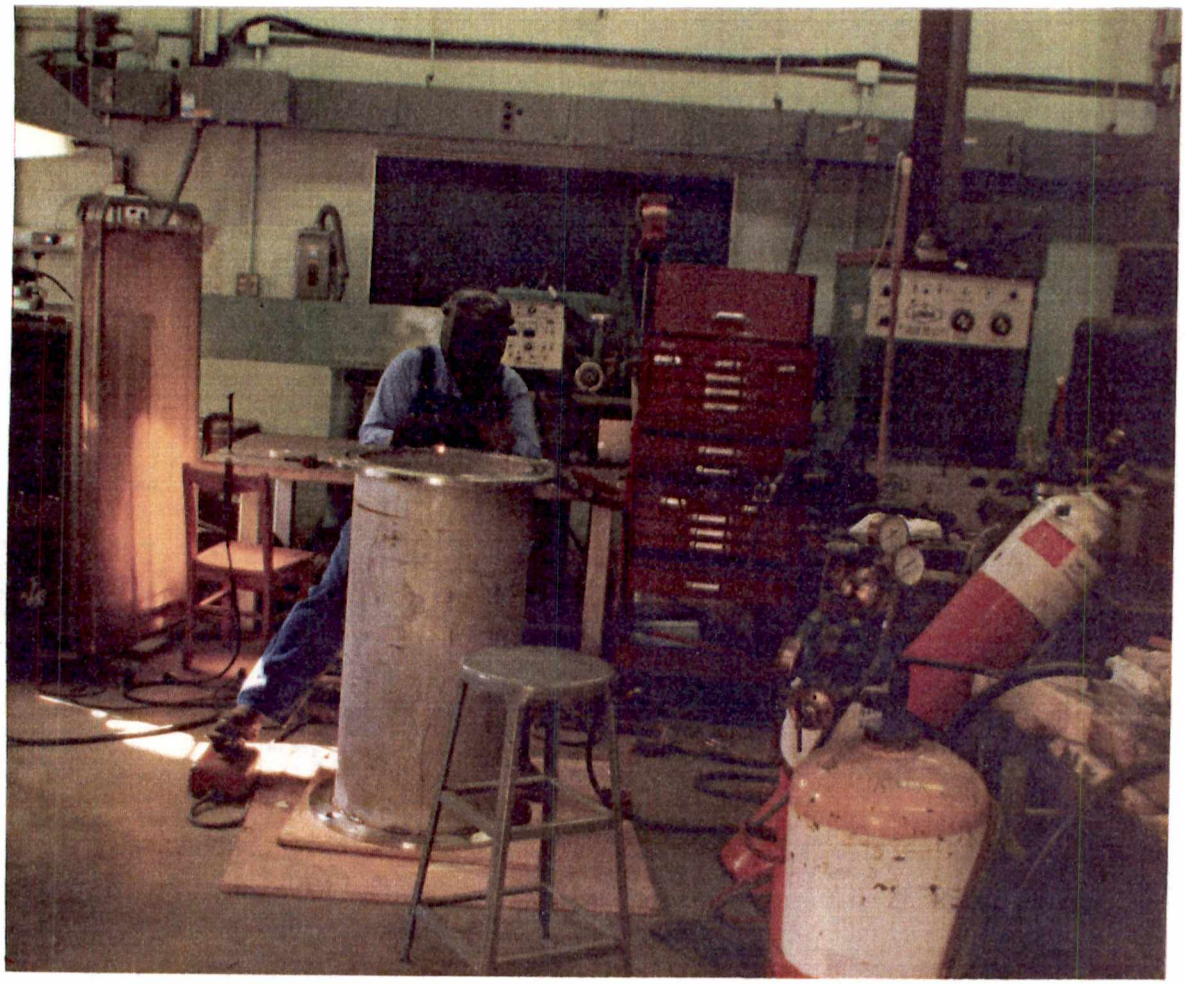


Figure IV.23 A color photograph of Ray Bellamy vacuum welding a layer of Type 316 stainless steel to the chamfered grooves between the outer edge of the cylinder and the inner edge of one of the ring flanges. The welder is a T.I.G. (Tungsten Inert Gas) welder using argon gas.

ports are available for this diagnostic. A known microwave signal can be injected at the 90° diagnostic port and the resulting, phase shifted, attenuated microwave signal will exit the 270° diagnostic port. The 0° diagnostic port can be used to measure scattered microwave radiation or other diagnostic measurements. However, since the midplane location is where plasma ion implantation will be carried out, a Langmuir probe will be inserted through a standard 4" (10.2 cm) flange plate on this port. The probe will be moveable radially through a Veeco fitting, to characterize the plasma electron number density profile along the radius. Figure IV.24 is a drawing of one of these diagnostic ports.

The 180° diagnostic port at the cavity midplane was reserved for the mass spectrometer sensor head. The flange plate required by this device is not a standard 4" (10.2 cm) flange. It contains an O-ring groove, because the flange which was supplied by the manufacturer does not. Two #335 Viton O-rings which measure 2-3/4" x 3-1/8" with a 3/16" diameters were purchased, one for a backup. The mass spectrometer sensor head is irregularly shaped, and contains a permanent magnet mounted on a bent support arm. On the end of this support arm is mounted an electronic amplifier contained in a small canister. This sensor head should not suffer any shock or vibration. Thus, it was mounted on the rear of the vacuum vessel, away from areas tafficked by laboratory personnel. In the initial testing of this new system, laboratory space was limited. Thus, the vacuum station and vessel was rotated 180° and the microwaves were piped over the microwave power supply into the

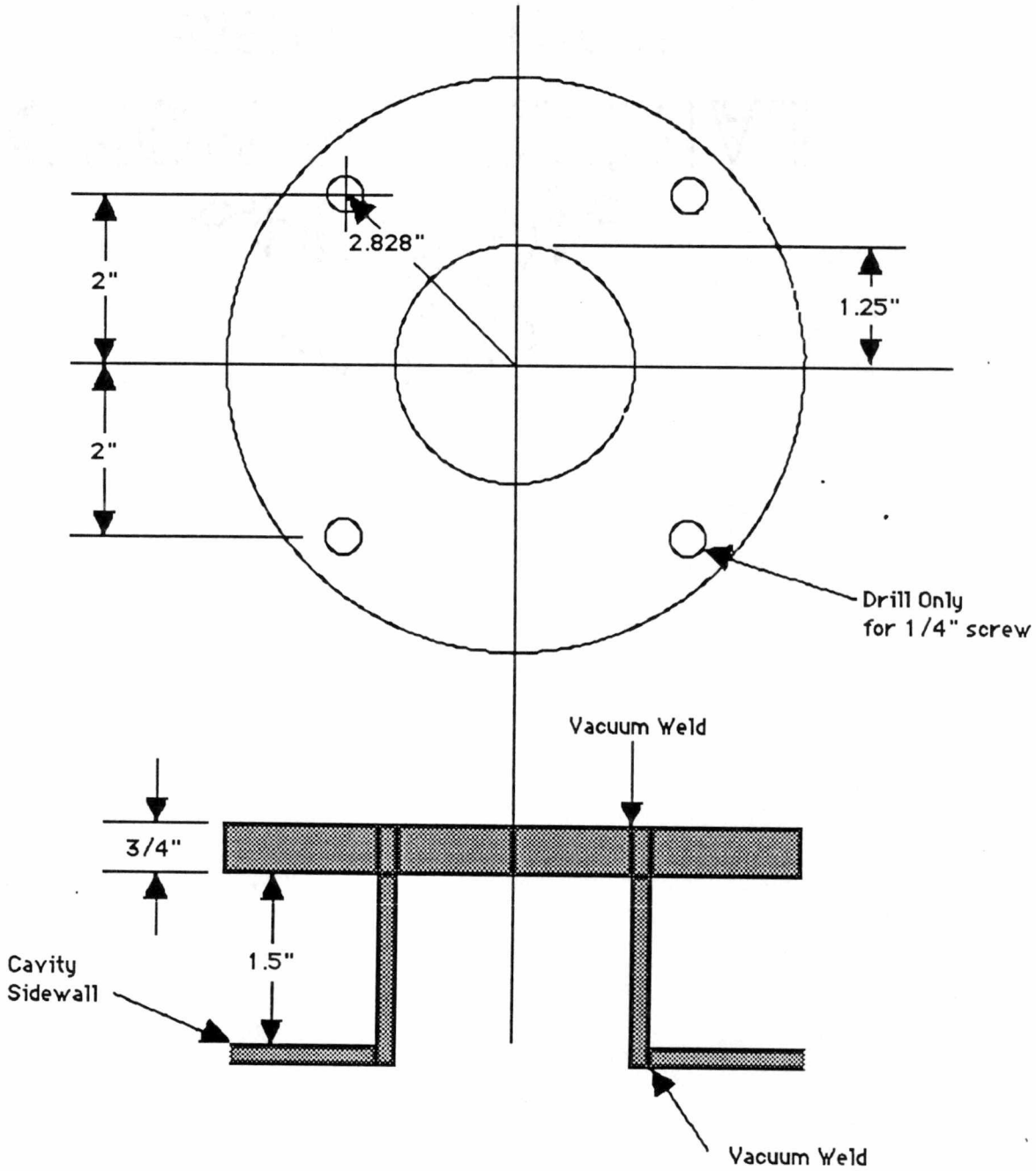


Figure IV.24: Diagnostic port flange used in the multimode microwave cavity at a distance of 10" (25.4 cm) from the bottom flange plate. Three are used at azimuthal locations of 0°, 90°, and 270°. The thickness of the flange is 3/4" (1.91 cm).

cavity. In a laboratory where space is not a problem, the vacuum station and vessel would be facing the inside of the laboratory, placing the mass spectrometer sensor head against the wall. In the future, one can design a metal can to protect the sensor head, but at this time, no such protection was included in the design. A drawing of the mass spectrometer flange port is shown in Figure IV.25.

In order to create and maintain the plasma, the microwave energy must enter the multimode microwave cavity with minimal reflected power. To accomplish this, it was decided to use a circular microwave waveguide port with a diameter of 3.36" (8.5 cm). This diameter is larger than the diagonal measure of a WR-284 waveguide which is 3-1/8" (7.9 cm). The use of a circular port allows flexibility in changing the size of the microwave waveguide, should a lower frequency be used to create the plasma. The microwave waveguide port in this application was designed to fit a circular UG-54 choke flange. Since the choke flange contains an O-ring groove, no O-ring in the microwave waveguide port is desired. This flange contains threaded bolt holes for 1/4-20 stainless steel bolts commonly used in the assembly of microwave hardware. The circular section was selected to be made of Type 316, 3-1/4" (8.3 cm) inside diameter stainless steel tubing with a wall thickness of 1/4" (0.64 cm).

Due to the 2-5/8" (6.7 cm) neck of this circular port, the microwaves may never enter the cavity. This length is almost one diameter and thus a standing wave could be set up along this length. In order to maintain the flexibility of modifying the waveguide size

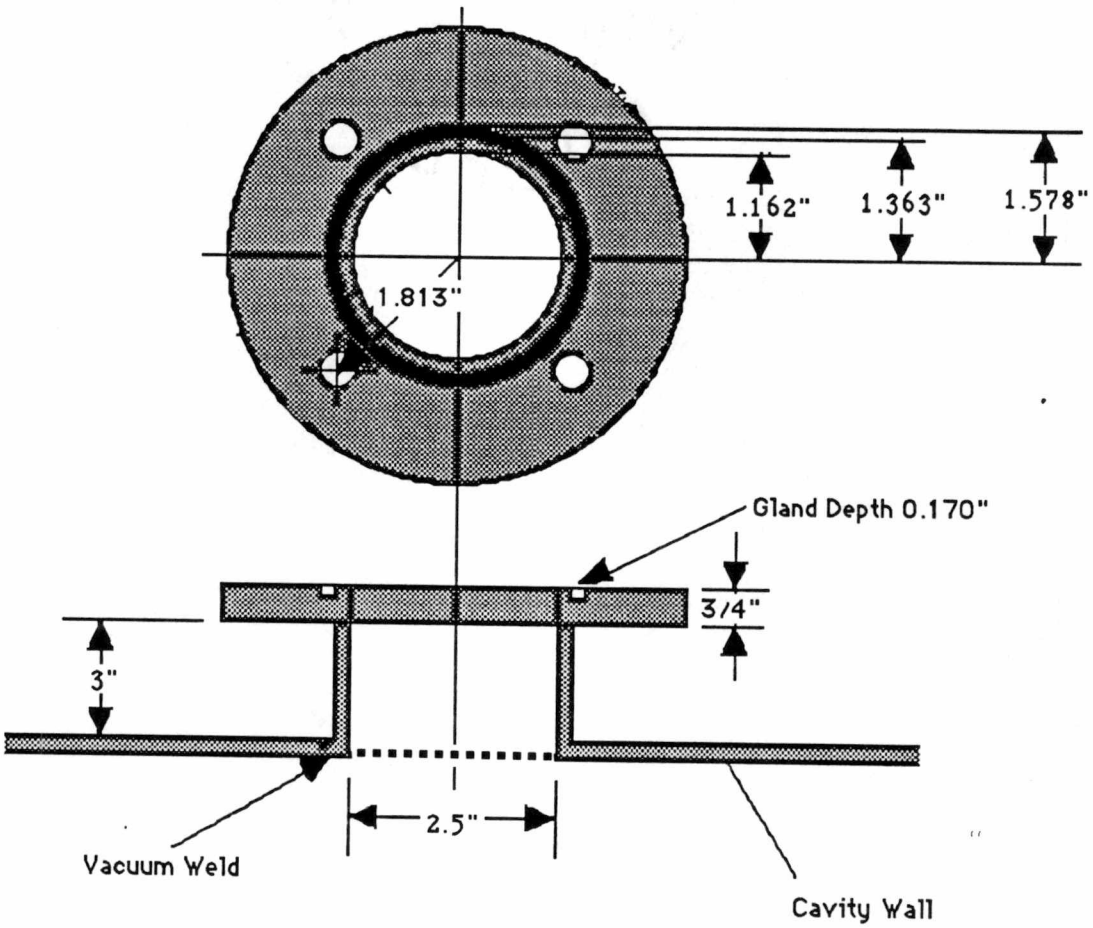


Figure IV.25 Mass spectrometer flange port used in the multimode microwave cavity showing the O-ring groove and the non-standard holt hole pattern. The thickness of the flange is 3/4" (1.9 cm). The dotted line indicates the microwave shielding necessary to keep microwaves from getting inside the mass spectrometer sensor head.

if desirable and in order to maintain reasonable impedance matching between the source and the cavity, a cylindrical brass insert was made to convert the circular port to a rectangular port. The size of the rectangular port was specified to fit WR-284 waveguide, since we are using this size waveguide after the step transition. This insert must establish good electrical contact to its adjacent waveguide flange, the microwave window. To do this, four 1/8" (0.32 cm) holes were drilled on the microwave window side of the insert near its outer circumferential edge. Four overlapping holes were drilled on the choke flange of the microwave window, also near its outer circumferential edge. These were tapped for small allen head screws. Once assembled, the insert and the microwave window may be inserted into the circular port and bolted on.

The location of this port along the length of the vacuum vessel was selected to be asymmetric with the center. The distance of 14" from the top of the cavity will also help to break the modes after they are injected into the cavity. Also, it is not advisable to position such a port in a location where the microwave energy has a direct line-of-sight across the diameter to an open port on the outside of the cavity.

The problem of a vacuum interface is not addressed by the selection of this port. However, our UG-54 choke flange must have a #345 Viton O-ring which measures 4" (10.2 cm) x 4-1/2" (11.4 cm) and has a 1/4" (0.64 cm) diameter cross section. This topic will be discussed further in the section in this chapter on microwave hardware. Figure IV.26 illustrates the microwave waveguide port.

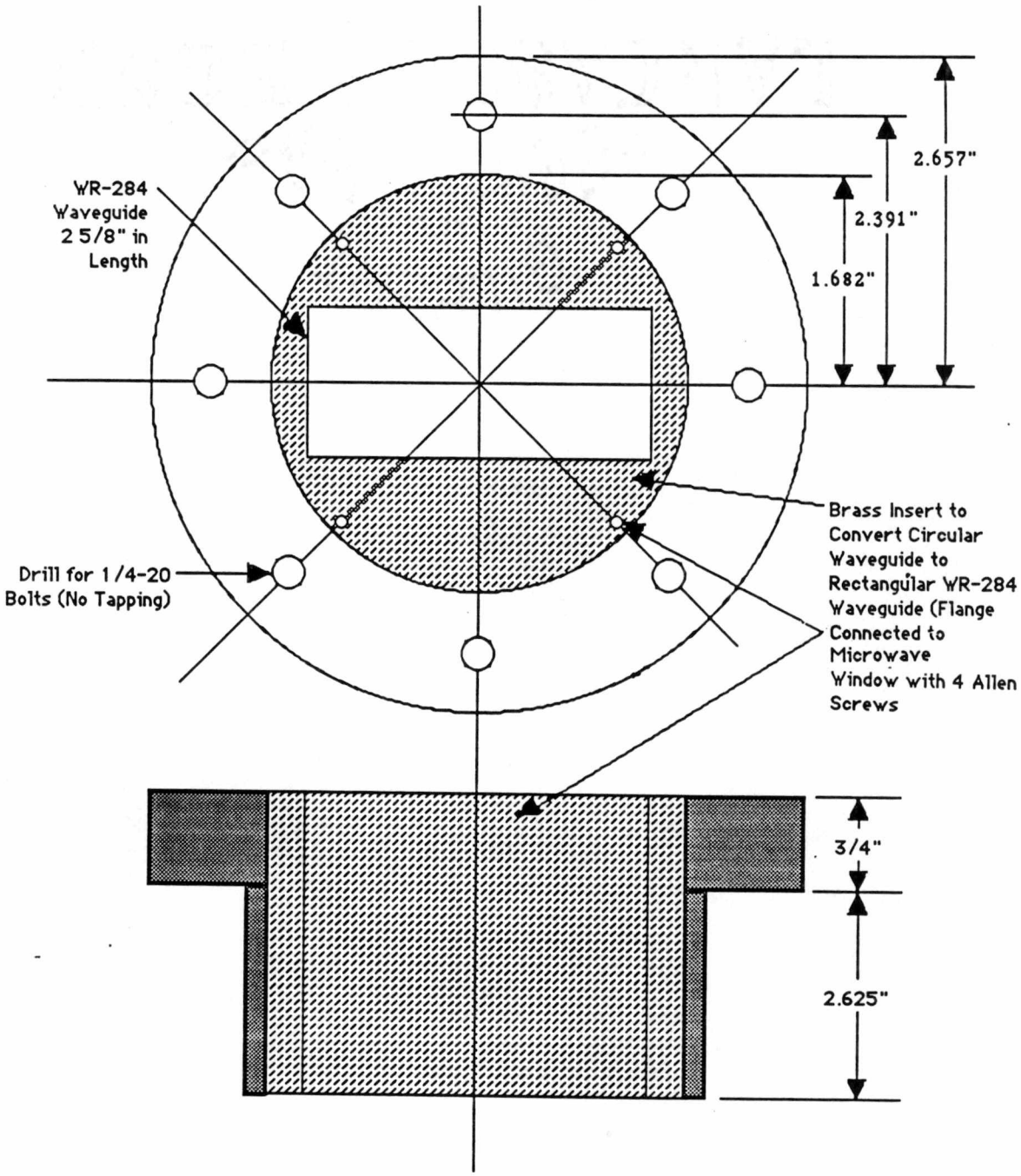


Figure IV.26 Microwave waveguide flange port used in the multimode microwave cavity showing the overlap of the WR-284 waveguide on the short circular waveguide section. The thickness of the flange is 3/4".

No plasma containment system is complete without a diagnostic viewport which allows the plasma to be seen with the human eye. The human eye can be a useful diagnostic, and should be taken advantage of when conducting plasma experiments. Two diagnostic viewports of 4" (10.2 cm) diameter are positioned at the 0° and 270° locations at the midplane. The axial location of these ports was at the midplane, so the end of the sample holder could be observed during a plasma ion implantation experiment. This flange contains an O-ring groove because the mating flange cover was selected to be a 3/4" circular plexiglass disc. The selection of this material is consistent with the low base pressures mentioned earlier and allows sufficient observation of the plasma. This flange contains eight non-threaded bolt holes for attachment of the flange cover to the port flange. It was also 3/4" (1.9 cm) thick, to use the material remaining from the machining of the large top and bottom ring flanges. The circular extension for this flange port was made of Type 316, 4" (10.2 cm) inside diameter stainless steel tubing with a wall thickness of 1/4" (0.64 cm). It extends a length of 1.5" (3.8 cm) from the outside vacuum vessel wall. Figure IV.27 is a diagram of the diagnostic viewport flanges used on this microwave cavity.

Figure IV.28 shows the complete multimode microwave cavity with all ports labeled except the mass spectrometer port, which is located on the rear of the tank. With the selection and specification of the vacuum vessel components complete, the design was delivered to the Mechanical Systems Machine Shop in the Materials Science and

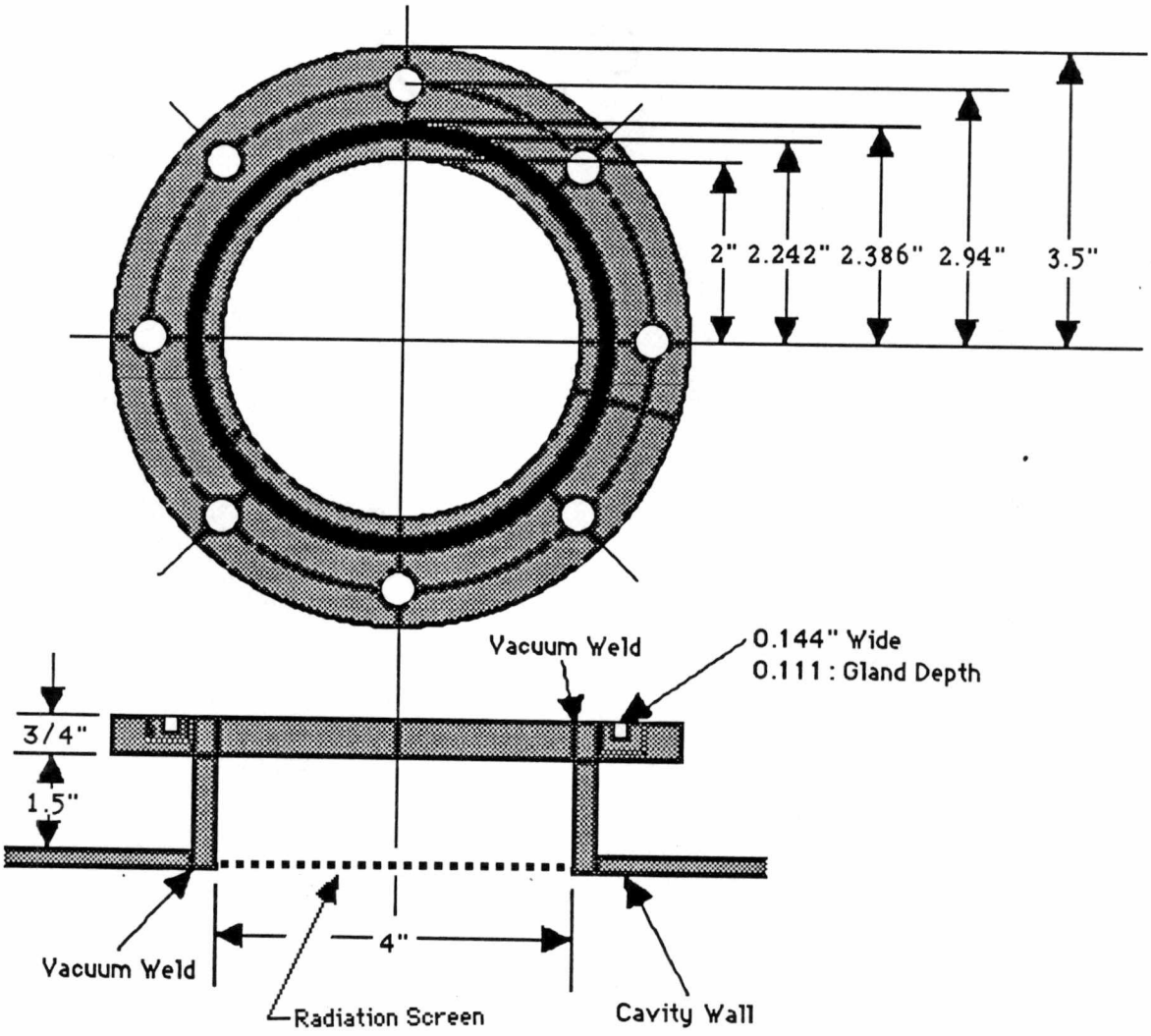


Figure IV.27 Diagnostic viewport flange used in the multimode microwave cavity. The viewing cross-section is 4" (10.2 cm) in diameter. The thickness of the flange is 3/4" (1.9 cm). The dotted line indicates the microwave shielding necessary to keep microwaves from leaving the cavity.

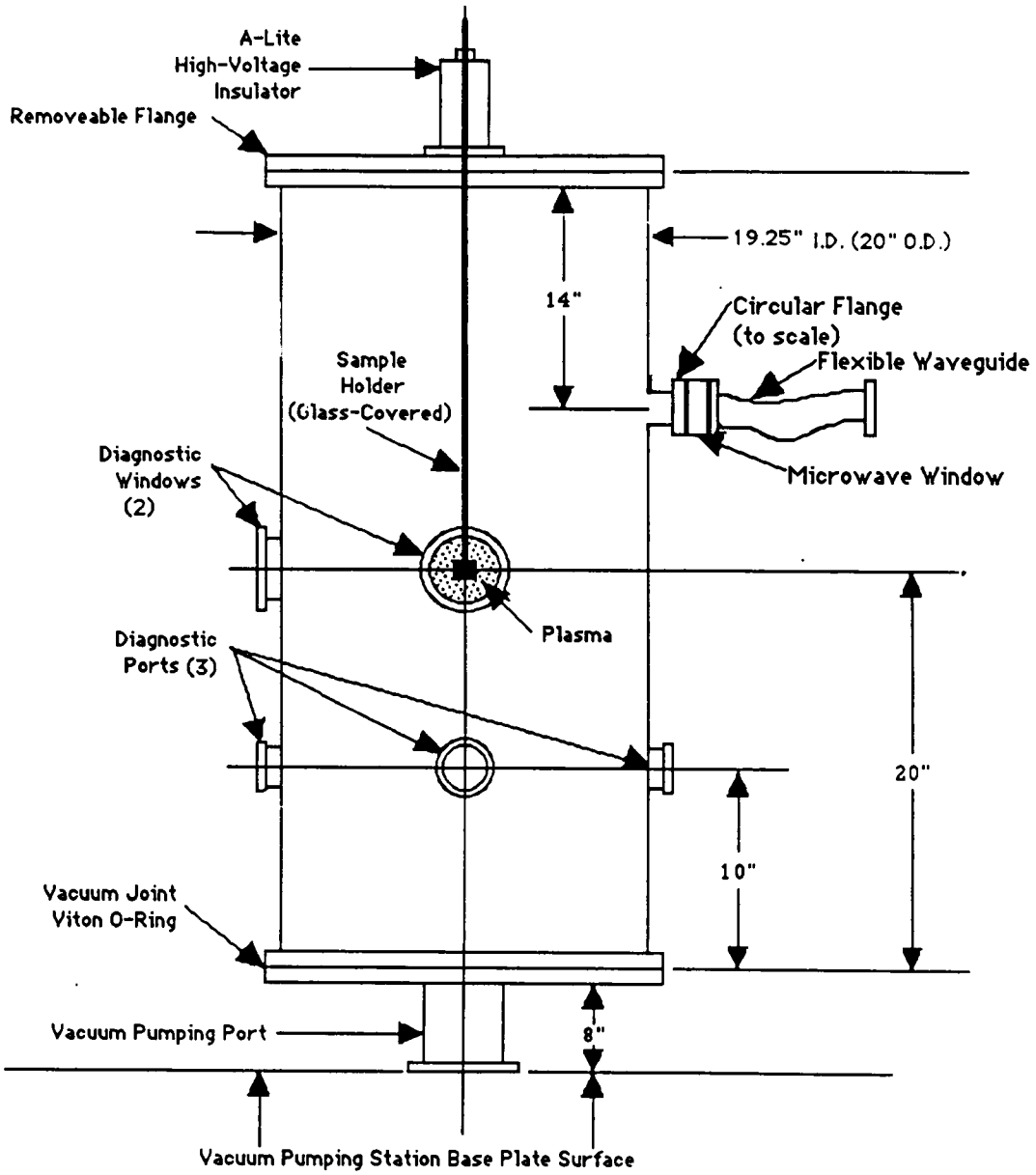


Figure IV.28 The complete multimode microwave cavity showing all ports except the mass spectrometer port on the rear of the tank. The vacuum vessel sits directly on top of the vacuum station, not pictured here.

Engineering Department for fabrication by a crew led by Mr. Douglas Fielden, Foreman.

8. The Waveguide-Vacuum Interface

A reliable interface between the incoming microwave radiation and the interior of the vacuum vessel is required to maintain a vacuum within the cavity. Many types of interface materials are available. These range from simple, inexpensive mica, mylar, or teflon sheets to complicated, expensive covar or quartz windows. High-vapor pressure materials must be avoided in order to achieve low vacuum pressures. The type of interface selected also depends upon the average microwave power to be injected through the interface. The interface material must have a low loss coefficient so that it will not overheat. If overheating occurs due to a microwave electric field breakdown, as can happen in underrated materials, the vacuum can be lost. It is also desired to have low loss interfaces in order to deliver maximum power to the microwave cavity (Heald, et al., 1978).

The microwave interface selected for this application is constructed of teflon-fiberglass material. It has a low loss coefficient and is a matched device. It can withstand an average CW power of 10 kW at the low end of the operating frequency for WR-284 waveguide and up to 27 kW at the high end. It can also withstand a

peak power of 15 MW. This is adequate for this application, since not more than 6 kW will be injected into the cavity.

The selection of such interfaces also involves the specification of the type of flanges to be included. Microwave interface assemblies can be obtained in choke/flat, choke/choke, flat/choke, or flat/flat flanges. In this application, the vacuum side of the interface was specified to be a choke and the microwave power side was specified to be a standard UG-54 circular flange. The choke is necessary to achieve a vacuum seal with a Viton O-ring between the microwave window and cavity flange connection.

9. Tuning and Matching

In Figure IV.29, two matching devices are included in the microwave system. One is located on the output side of the directional power meter that is connected to the microwave power source. This is a double-stub, or HH, tuner, because adjusting its stubs affects the H-plane microwave signal. This device is used to tune out reflections due to the step transition section mounted on the output side of the HH-tuner. It is possible to tune out virtually all of the reflections due to this transition. After the microwave energy passes through the E-plane bend, which is a WR-284 size waveguide, it then passes through a straight section of waveguide made to a length such that the microwave power source rests on the laboratory floor. The microwave energy then passes through a second E-plane

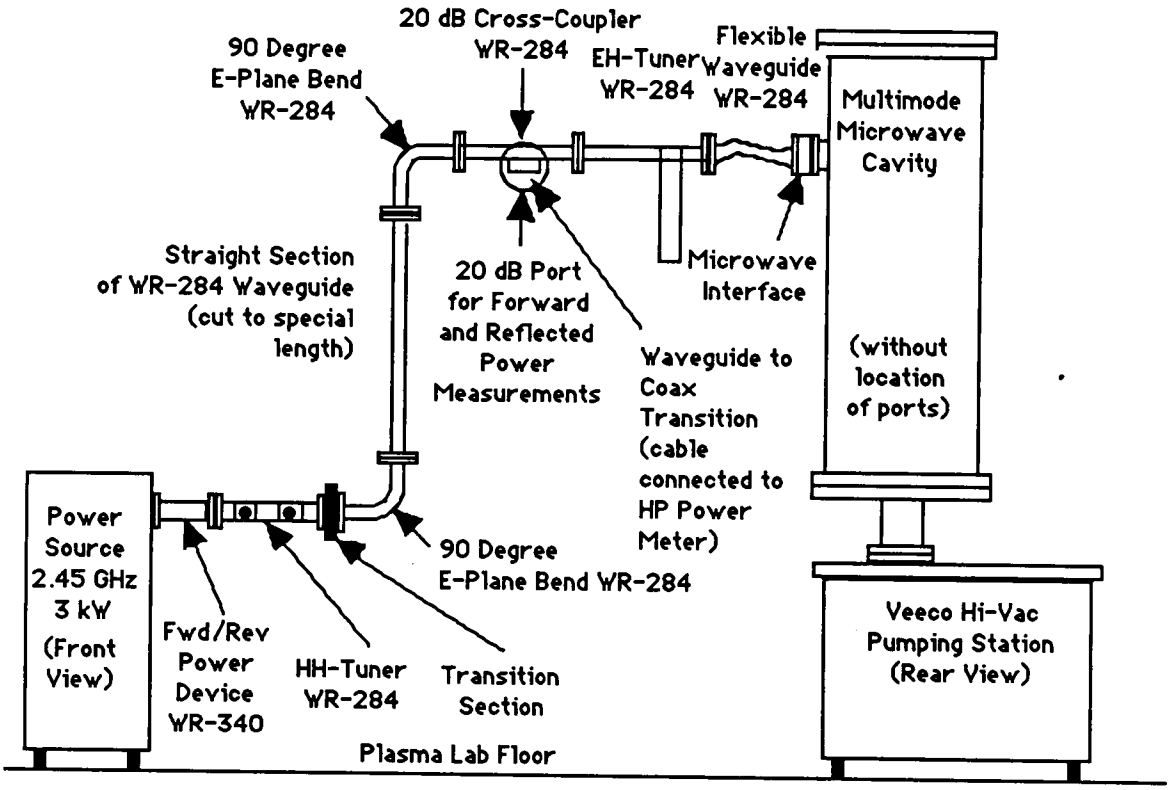


Figure IV.29 The complete experimental apparatus for the microwave generated plasma showing the microwave power source, the multimode microwave cavity, the high vacuum pumping station, and all necessary microwave hardware to create and maintain the plasma with microwave power.

bend. Then, it passes into a cross-power coupler where the forward and reflected powers are measured. After this, it passes into a second matching device, a DeMornay-Bonardi Model DBL-979-1 E-H tuner, a single-stub device. This is used to match out discontinuities in the waveguide system. This unit is preferred for high power applications and has a VSWR of less than 1.02 at the center frequency. This tuner is included in the design because reflections from the multimode microwave cavity should be tuned out. These reflections can be tuned out with no medium (plasma) in the microwave cavity when microwave power is applied. However, if an attempt is made to tune out reflections when the plasma is present, difficulties may result from a time-varying plasma conductivity (electron number density) and thus plasma impedance. Some optimal operating condition may be reached, but this condition may drift and reflections from the cavity may reappear. After the microwave power leaves the cross-power coupler, it is input to a WR-284 12" (30.5 cm) flexible waveguide. This removes any stress which may be incident upon the microwave interface. After this, the microwave power then passes through the microwave interface and into the cavity. Figure IV.30 is a color photograph of the microwave generator (green) with the microwave hardware installed. To the right of this generator is the high-vacuum pumping station with a chain hoist suspended from the ceiling over the vacuum pumping port of the pumping station. Figure IV.31 is a color photograph of the complete microwave generated plasma apparatus for plasma ion implantation studies.



Figure IV.30 A color photograph of the microwave generator (green) with the microwave hardware installed. To the right of this generator is the high-vacuum pumping station with a chain hoist suspended from the ceiling over the vacuum pumping port of the pumping station.

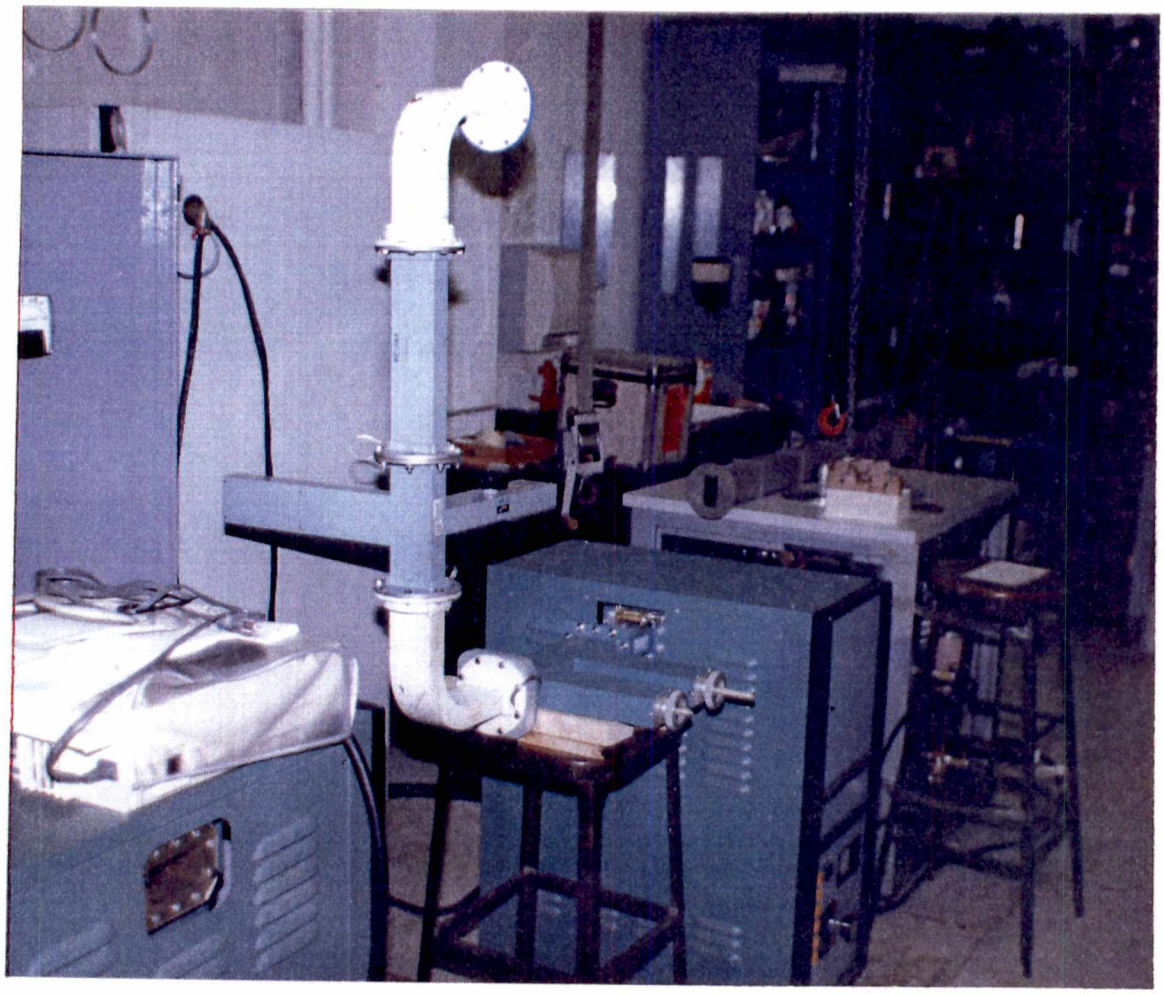


Figure IV.31 A color photograph of the complete microwave generated plasma apparatus for plasma ion implantation studies.

10. Enhancing the Electron Number Density

As presented earlier, the characteristic diffusion length is a measure of the extent to which the electron number density will be radially uniform in the plasma. The larger it is, the more uniform is the plasma electron number density profile. The microwave discharges of Pomathiod and Boswell included arrays of oriented ceramic permanent magnets mounted on the inside (Pomathiod, et al., 1984) and outside (Boswell, et al., 1989) of the plasma containment vessels, respectively. The work of Boswell reported that the electron number density without the multipole permanent magnets was not uniform in either the radial or axial directions. However, when twenty-four sets of multipole permanent magnets were arranged in a checkerboard array around the outside of a glass cylinder about 30 cm in diameter, the electron number density became uniform over about a 10 cm diameter. The magnetic field at the center of one of these magnets was about 600 G (0.06 Tesla). The characteristic diffusion length of this cylinder was about 7 cm, comparable to the size of the region of uniformity. These results were very encouraging in their implications for the plasma in this application.

The work of Pomathiod did not report whether or how much the uniformity of the electron number density was enhanced by the multipoles. For a checkerboard array of oriented ceramic magnets, the dimensions of which measured 1.6" (4 cm) x 0.79" (2 cm) x 0.39" (1 cm), with a magnet spacing of 1" (2.5 cm) in both the axial and

azimuthal directions, the electron number density was not enhanced above the critical density (7.45×10^{16} electrons/m^3) at a frequency of 2.45 GHz. However, it was reported that, with magnets in place, the electron number density did not increase significantly beyond the critical density with increasing microwave input power. It has also been demonstrated (Suzuki, et al., 1983) that saturation can occur for densities above the critical value (at 2.45 GHz). Above saturation (Sermet, 1975), the electron density still increases but much more weakly with microwave input power. The effect of the magnets with a 1" (2.5 cm) spacing was to reflect the plasma from the magnetic wall and inprove the average particle containment time.

Upon the examination of these two experiments, it was decided to use a checkerboard array of oriented ceramic permanent magnets mounted on the outside surface of the vacuum vessel. The vacuum vessel is non-magnetic. The magnets selected are 1.9" (4.7 cm) x 0.87" (2.2 cm) x 0.37" (0.95 cm) in dimension, and the magnetic field strength at the center on the face is 3900 G (0.39 Tesla). The non-magnetic wall thickness will reduce the field strength exposed to the plasma. The direction of magnetization of these magnets is such that they produce cusps extending into the vacuum vessel. These cusps reflect the plasma electrons adiabatically, thus improving their containment.

Figure IV.32 is a diagram of our checkerboard array of magnets. For a spacing of 1" (1.27 cm) between the magnets in both the axial and azimuthal directions, it takes seventeen rows and 34

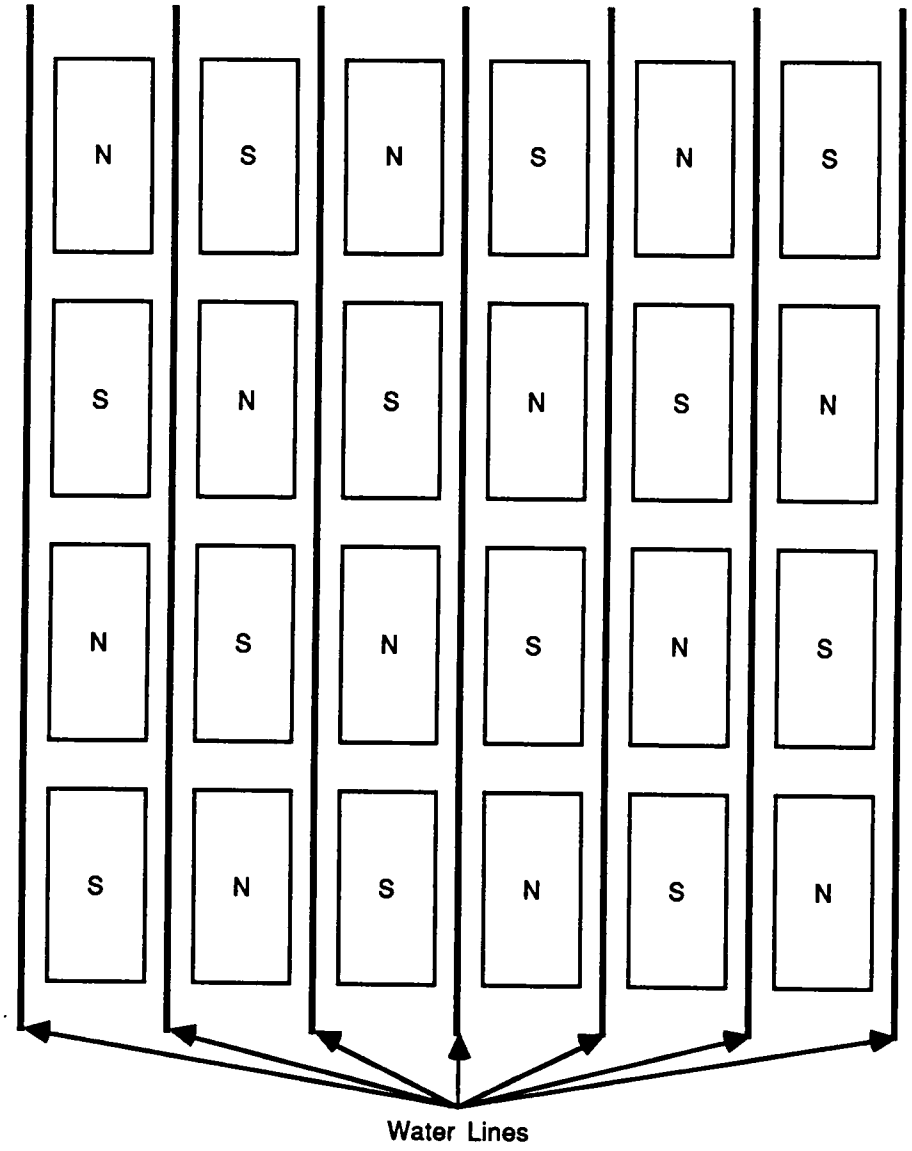


Figure IV.32 Checkerboard array of oriented ceramic permanent magnets that can be wrapped around a cylindrical containment vessel. The arrangement of water lines of opposing flows between each column of magnets provides for the cooling of the cavity wall.

columns of magnets to cover the surface area of the cylinder, excluding the end caps. This requires a total of 578 magnets. Figure IV.33 is a schematic of the magnetic field lines on the inside of the cavity wall in a cross-sectional view. Note that the magnets at the end of the cylinder are arranged in a checkerboard (North, South, North, South, ...) geometry.

For the end caps, on which a majority of the surface area is taken up by ports, a "flower" arrangement of the magnets was used. In a radial direction, from a location near the center of the top flange plate to a location just inside the cavity wall, seven of these magnets are required. In the azimuthal direction, beginning at a radius of about 8.9 cm (3.5") from the center and maintaining a separation of 1.27 cm, it takes eight magnets to complete the azimuthal array. The spacing of these magnets increases as the radius increases, if the magnets are aligned in a straight line. For the top flange plate, about 56 magnets arranged in a "flower" configuration are required. This arrangement is shown in Figure IV.34, and should magnetically shield the plasma from the inner surface of this flange plate.

The direction of magnetization of these magnets on the flange plates is important. If the tank magnet nearest the end of the cavity has its magnetization vector pointing towards the center of the cavity, then the magnet on the flange plate directly in line with the end wall magnet must have its vector pointing outward. This is to insure the transfer of the magnetic field line from the cavity side wall to the flange plate. The remaining magnets in this same line on the flange plate must have their vectors pointing in the same

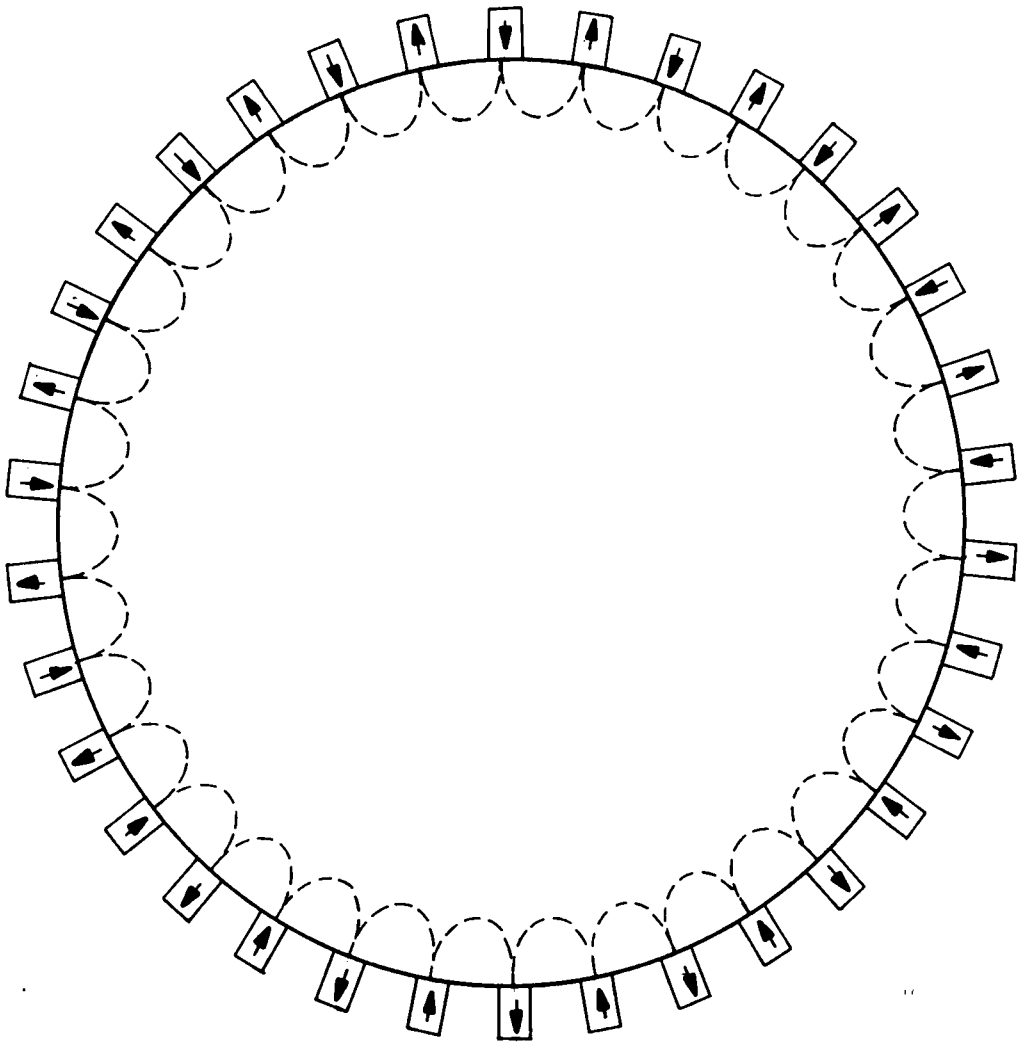


Figure IV.33 Cross-section of the multimode microwave cavity showing the 34 columns of permanent magnets equally spaced in the azimuthal direction. A vertical copper water line is placed between each column which cools the cavity walls. The magnets are arranged such that adjacent magnets in a row are in a North, South configuration so that cusps form at the face of the magnets.

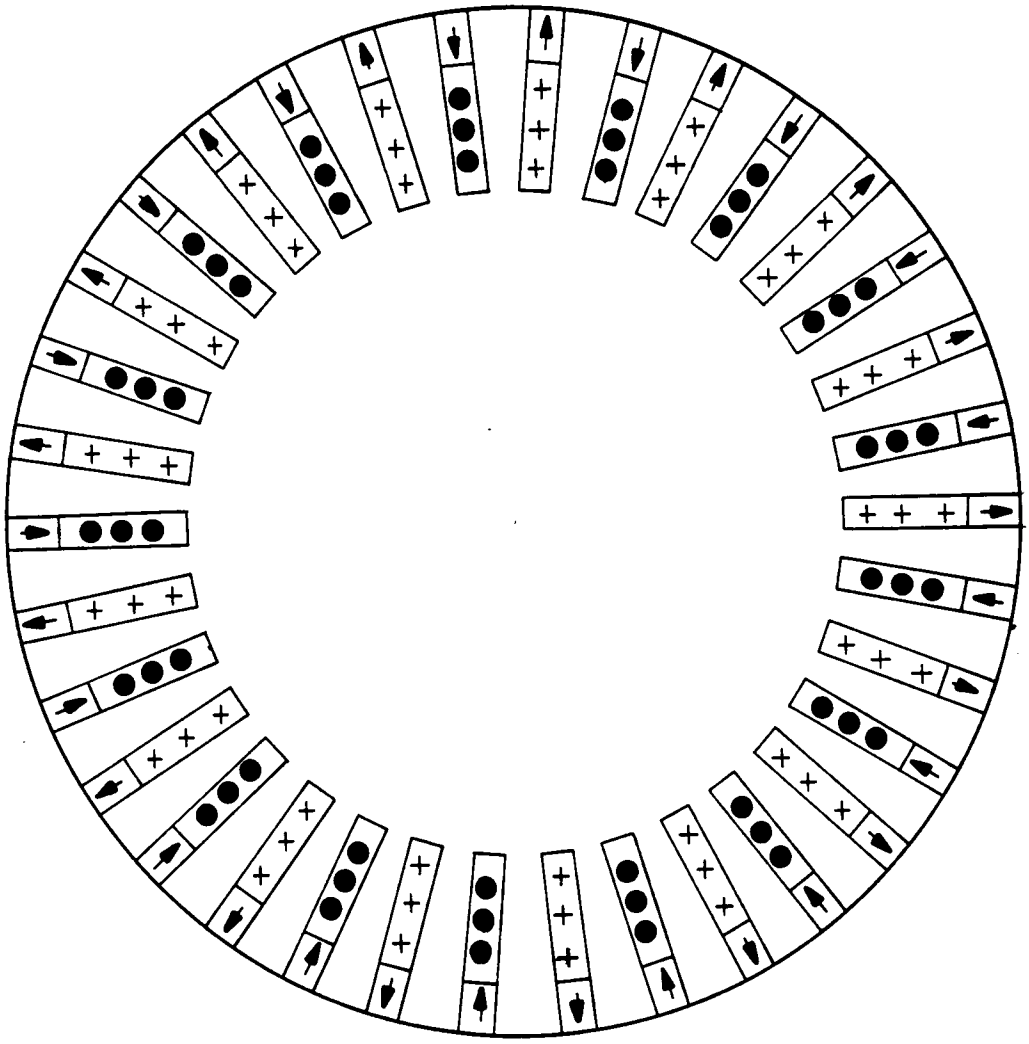


Figure IV.34 Geometrical configuration of permanent magnets on top and bottom flange plates. The magnets are arranged in a "flower" pattern with 34 "petals". The magnetization vectors of each magnet in a "petal" are all pointing in the same direction. The vectors of adjacent "petals" are opposing, giving a concentric cusp pattern of magnetic field lines on the inside surface of the flange plate. The vectors of a "petal" are arranged such that the corresponding vector of the magnet on the outer surface of the cavity wall nearest the flange plate opposes those of the "petal". This provides a magnetic field line from the inner surface of the cavity wall to the inner surface of the flange plate.

direction. The row of magnets on the flange plate adjacent to this row must have their vectors pointing in the opposite direction. About the same number of magnets will be used for the bottom flange plate. Therefore, a total of about 690 permanent magnets were needed. 950 permanent magnets were obtained and others can be readily obtained, if needed, from a nearby Radio Shack. The magnets were obtained from Job Master Corp., a manufacturer of magnets, who also supplies Radio Shack with permanent magnets.

The permanent magnets on the outside of the vacuum vessel were mounted in a way that provided easy adjustment of the magnet spacings as well as rotation of the magnetization vectors. The system chosen is called Mak-A-Clamp™ Model 4002. This is a simple compression mounting system which uses hose clamp connector rings. Each ring clamp that holds a row of magnets to the outside cavity wall is made up of two bands. These bands are easily connected together since they have mating ends. The remaining ends which come back together on theirself at the joint, are connected by a tightening mechanism which is adjustable with a screwdriver. The metal band is Type 300 stainless steel, is 1/2" (1.27 cm) wide, and up to 100" (254 cm) in length. The circumference of the outside cavity wall with the magnets in place is about 68" (172.7 cm).

Another modification to the permanent magnets may be made to increase the magnetic field strength along the inner surface of the vacuum vessel. This increase will further enhance the confinement of the electrons, resulting in a further enhancement of the electron

number density. It can be achieved by putting a magnetic flux concentrator strip on the outer face of the magnets. It is important to note that the application of a metal strip with too great a thickness will have a detrimental effect on the magnetic field. Thus, for these permanent magnets, the metal strip thickness was chosen to be 1/3 of the magnet thickness, or 1/8" (0.32 cm). Each column of permanent magnets can have a 1/8" (0.32 cm) thick, 7/8" (2.2 cm) wide strip of magnetic material placed on their outside surfaces. The material chosen for this was standard carbon steel with a 40" length. This is a total length of over 153 feet of steel stripping. The addition of this stripping actually helps to complete the magnetic circuit in the vertical direction. The completion of this circuit allows more magnetic field strength to appear on the front face and less on the rear face where it is not needed.

11. Cooling the Cavity Walls

The experiments of Pomathiod (Pomathiod, et al., 1989) and Boswell (Boswell, et al., 1984) operated microwave powers of up to 1.5 kW. Neither experiment employed water cooling of the cavity side walls, since they used glass walls and relatively low power levels. However, the microwave power levels injected into this microwave cavity can be as high as 3 kW, if one microwave power source is used, and can be as high as 6 kW, if two sources are paralleled together. The water lines were chosen to be Type 316,

1/4" (0.64 cm) diameter hard drawn copper tubing. For simplicity, the orientation of the water lines was chosen to be parallel to the columns of magnets. Since there are 34 columns of magnets, there must also be 34 vertical water lines with each having a length of 40". Thus, the total length of tubing required was about 113 feet (5.4 m).

The top and bottom flanges are 3/4" (10.2 cm) thick and are made of Type 316 stainless steel, resulting in a minimal amount of heat transfer from the inner surface, exposed to the plasma, to the outer surface. For the top flange, 22 % of the available surface area is taken up by standard 4" flanges and 48 % by permanent magnets, leaving only 30 % for water lines. For the bottom flange, 33 %. The presence of the permanent magnets will help shield the plasma from the magnetic walls, resulting in a slight decrease in the amount of microwave power deposited on the magnetic walls. With this, the top and bottom flanges were not water cooled. During an experiment, careful attention should be paid to the possible warming of these end plates, since no water cooling is included.

Other components of the experiment that are water cooled include the magnetron tube in the microwave power source and the diffusion pump and cold trap in the high vacuum pumping station.

12. The High Vacuum Pumping Station

In order to achieve base pressures as low as 0.1 μtorr and operating pressures ranging from 10 to 100 μtorr, a vacuum

pumping station with adequate pumping speed is needed. A Veeco Vacuum, Inc. Model VS-400 Hi-Vac Pumping Station was obtained from UTK storage facilities. This vacuum station was obtained for the UTK Plasma Science Laboratory by Prof. J. Reece Roth during an equipment scrounging expedition at NASA and DoD installations. This piece of vacuum equipment was brought to the UTK Plasma Science Laboratory for disassembly and renovation. The vacuum pumping station was dirty, having been stored for many years. Every component was removed from the vacuum pumping station and was examined for wear. It appeared that the vacuum pumping station had hardly been used. This was evidenced by the good condition of the forepump and diffusion pump. All of the vacuum seals in this pumping station were replaced with new Viton O-rings. There were a few teflon seals. These were also replaced. Blanked-off base pressures as low as 0.01 μtorr were achieved upon initial testing of the vacuum system with liquid nitrogen in the cold trap.

The vacuum pumping station consists of three pumping stages: a forepump, a diffusion pump, and a cold trap. The forepump is a Duo-Seal Model 3917 piston pump which can pump up to 17 cfm free air. The diffusion pump is a Veeco Vacuum, Inc., Model EP41W water-cooled (0.2 gallons per minute), 220 V AC, 500 W, 4" pump. It was in excellent condition and showed very little oxidation or breakdown product accumulation in its interior. The cold trap is a Veeco Vacuum, Inc., Model LH-4 liquid nitrogen trap containing a 1/2 L cooling finger. The cold trap and the diffusion pump are separated by a water-cooled baffle which helps to prevent diffusion

pump oil from entering the vacuum vessel. The system contains all the necessary valves, except the gas feed microleak, for operating the vacuum system in several modes.

Figure IV.35 represents the valving system for the high vacuum pumping station. There are five valves which are used to control the system. The vacuum base plate represents the flange interface with the multimode microwave cavity. The vacuum pumping port on the bottom of the cavity connects to the base plate.

Proper sequencing of these valves is crucial to the proper operation of the vacuum pumping station and to the vacuum measurement instruments. With the cavity at atmospheric pressure, the following steps should be followed in pumping it down. It is assumed that the microleak valve located on the bottom flange plate of the cavity is closed. It is also assumed that the only vacuum gauge operating is the thermocouple gauge (to be discussed later). With power to the vacuum pumping station on, indicated by illumination of the yellow neon light in the center of the control panel, both circuit breakers, one for the mechanical pump on the left, and one for the diffusion pump on the right, should be in the off position. Valve No. 1 is the gate valve. This valve has a large cross-sectional area and is a sliding gate actuated by turning a crank at the top of the control panel. Valve No. 2 is the foreline valve, separating the diffusion pump from the forepump. Valve No. 3 is the roughing valve, and is used when first pumping down the system from atmosphere. Valve No. 4 is a vent valve, and may be used to bleed

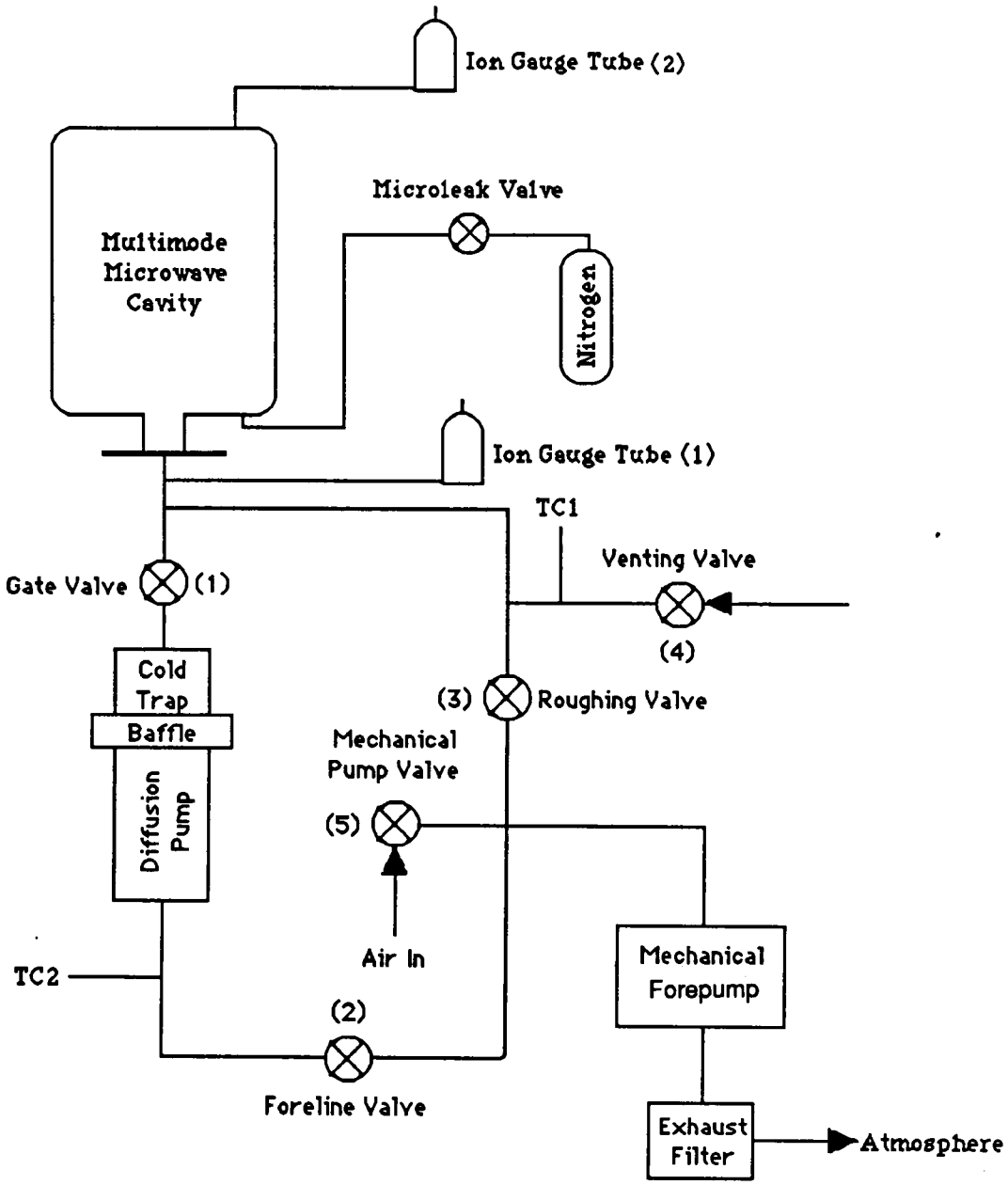


Figure IV.35 Valving system for high vacuum pumping station used in the microwave generated plasma ion implantation experiment. Arrows indicate the flow of atmospheric gases only.

the vacuum system up to atmosphere. Valve No. 5 is the vent to the forepump.

For vacuum pressure measurement above 1 mtorr, there are two thermocouple gauges, TC1 and TC2. TC1 is located in the roughing line between the vacuum pumping port and the forepump. TC2 is located in the foreline between the diffusion pump output and the mechanical forepump. For pressures below 1 mtorr, there are two Bayard-Alpert ionization gauge tubes, IG1 and IG2. IG1 is located on the vacuum pumping station and monitors the pressure at the pumping head. IG2 is located on the far end of the vacuum vessel to measure the operating pressure at that location.

The Lesker Model IG-5200 vacuum gauge system can automatically monitor the outputs of these gauges. It contains two channels for thermocouple gauges, and one channel for an ionization gauge. This instrument has been preprogrammed for these gauges. Upon powering up the unit, the value of TC1 will automatically be read. This is displayed on a digital slide scale ranging from atmosphere to 1 torr, and also defaulted to a digital readout on the front panel. The pressure of TC2 may be observed by pressing the button marked "TC2". It will read for 5 seconds and automatically revert back to TC1. When the pressure is below 1 mtorr, the unit will automatically turn on the ionization gauge and look for a reading below 1 mtorr. If there is no reading below this value, then the unit will revert back to TC1. This is repeated every 5 minutes after the first 1 mtorr reading is reached on TC1 until the vacuum system is below 1 mtorr. Since this unit contains only one channel for an

ionization gauge, the cable connecting the unit to the gauge will have to be removed from IG1 and connected to IG2 before the plasma is turned on.

The diffusion pump may be isolated from the microwave cavity and the forepump by closing Valve No.'s 1 and 2. This is important when bleeding the cavity up to atmosphere, since it is desired not to mix diffusion pump oil with forepump oil at any time. If this does occur, the diffusion pump and forepump oils must be drained and the pumps must be cleaned and refilled with new oil.

To pump the system down, the vacuum system can be operated in two ways. Pumping the initial vacuum can be achieved through the diffusion pump with its power turned off, or it can be achieved through Valve No. 3, bypassing the diffusion pump. The latter method is the most foolproof, but the former saves time. Pertaining to the latter method, Valve No.'s 1, 4, and 5 should be closed. Valve No.'s 2 and 3 should be open. After this, the forepump should be turned on. Examining the digital slide scale on the front panel of the Lesker digital vacuum gauge, one will find that the small digital indicators will begin to illuminate in a pattern traveling to the left. This indicates that the pressure is going down, beginning from atmosphere (760 torr) down to a minimum of 1 mtorr. The readout on this digital slide scale is connected to the digital readout for the first thermocouple gauge (TC1). This pumping condition needs to continue until the pressure in the cavity is less than 1 mtorr. When this condition is reached, the vacuum gauge will automatically turn

on the ion gauge tube to see if the pressure is below 1 mtorr. If not, it will revert back to the thermocouple gauge readout (TC1).

When the pressure in the vacuum vessel and the roughing line is below 1 mtorr, Valve No. 3 may be closed while the forepump continues to run. If the two pressure readings monitored by TC1 and TC2 are approximately equal, Valve No. 1 can be opened. The pressures of TC1 and TC2 must be close in order to have a negligible pressure gradient on each side of the diffusion pump. If these pressures are below 30 mtorr, power may be applied to the diffusion pump. When this is done by placing the switch marked "Diffusion Pump" on the right of the vacuum system control panel in the "On" position, the water to the diffusion pump is automatically turned on by engaging a solenoid on the rear of the pumping station. Cooling water begins to flow through the diffusion pump and the baffle and exits into the sewer system. When the pressure monitored by TC1 first reaches 1 mtorr, the power to the ionization gauge tube will be automatically applied. If its output reading is above 1 mtorr, it will be turned off. This will be repeated every 5 minutes until it can continuously remain on. At this time, the pumping down procedures are complete and the vacuum system may be allowed to run overnight, achieving a minimum pressure.

To achieve even lower pressures, the cold trap may be filled with liquid nitrogen. The liquid nitrogen must be poured through a funnel into the opening located on top of the vacuum pumping station. This is difficult because of the overhang of the bottom flange over the table. The capacity of the cooling finger inside the cold trap

allows for about 8 hours of operation. During this procedure, some of the liquid nitrogen will be boiled away at warm surfaces. After it achieves thermal equilibrium, the finger must be refilled with additional liquid nitrogen. Once refilled, it will last for about 8 hours, and base pressures as low as 2.0 μtorr can be achieved. These base pressures are acceptable for starting the plasma on background gases.

To bleed up the cavity to atmosphere, the vacuum pumping station does not have to be turned off, or bled up to atmosphere itself. If the microleak valve is closed, Valve No.'s 1 and 3 must be closed. This isolates the cavity from the vacuum pumps, allowing Valve No. 4 to be used to bring the cavity to atmospheric pressure.

Some of the changes to the microwave cavity might include removal of the sample holder, changing diagnostic instruments, or flange plates. Once this has been done, Valve No. 4 must be closed, with valve 1 and 3 still closed and the diffusion pump off. To pump the system down from this condition, Valve No.'s 1 and 2 must be opened. Opening Valve No. 3 will not affect the pressure in the diffusion pump. After the pressure in the roughing line reaches 30 mtorr or lower Valve No. 3 must be closed and the diffusion pump turned on. The system is now set for normal operation.

13. The Mass Spectrometer and Various Mass Spectra

For this kind of industrial application, it is important to monitor the relative amount of neutral gases or ions in the system, both without the plasma, and during plasma ion implantation. To do this, a microprocessor-based, personal computer controlled mass spectrometer was purchased from Vacuum Technology, Inc. (VTI) in Oak Ridge, Tennessee at a cost of less than $10,000.

This system has the capability of monitoring mass spectra over various mass ranges. The minimum mass that it can resolve is 2 Daltons and the maximum is 250 Daltons, using a Faraday cup arrangement. The unit can display a spectrum in several modes. It can display a raw spectrum including all noise within the system. It can also display individual peaks at integer masses when it is desired to eliminate the noise. The unit can also be set up to perform a fast analysis by quickly scanning the selected range and displaying the percentage concentration of the first five largest peaks. One particular advantage of this unit is that a spectrum of some type is always on the computer monitor. In other words, during a scan, part of the most recent spectrum is displayed at the same time new data are captured. This allows comparison between the spectra.

Another way of comparing the spectra is to take advantage of the library and storage capabilities of the unit. Over 100 known spectra of gases and compounds have been prestored in the library. These can be recalled at any time an active spectrum is displayed on the screen. The known spectrum will appear with a dotted line, so

the two can be compared. Also, many spectra can be stored to memory at any time without resetting the unit or stopping its operation. This is advantageous during an experimental run, so that one can obtain a detailed picture of exactly what gas species were present. This is especially valuable in such industrial applications as plasma ion implantation.

Some additional features of this mass spectrometer are the inclusion of two filaments in the sensor head; ability to change the spectrum axes to log or linear scales or a combination of both; ability to increase or decrease the scan time or number of data points averaged to compute the height of a peak; and self-contained, easy calibration procedures to calibrate the mass range and the relative intensity levels.

Several spectra are presented below. These spectra were captured with only the mass spectrometer sensor head connected to the vacuum pumping station, via a pyrex reducer pipe. This procedure was followed to analyze impurities which were present in a newly reconditioned vacuum station, and also to gain experience in operating the new mass spectrometer system.

Figure IV.36 shows a typical mass spectrum ranging from 2 to 250 Daltons, the full mass range of the unit. The base pressure during this scan was 0.7 μtorr, with no liquid nitrogen in the cold trap. Notice, especially at high masses, the presence of noise in the spectrum. At low masses, the largest peak is water vapor at mass 18. This peak will be present in all mass spectra since water vapor is pervasive in all vacuum vessels, regardless of pumping capabilities.

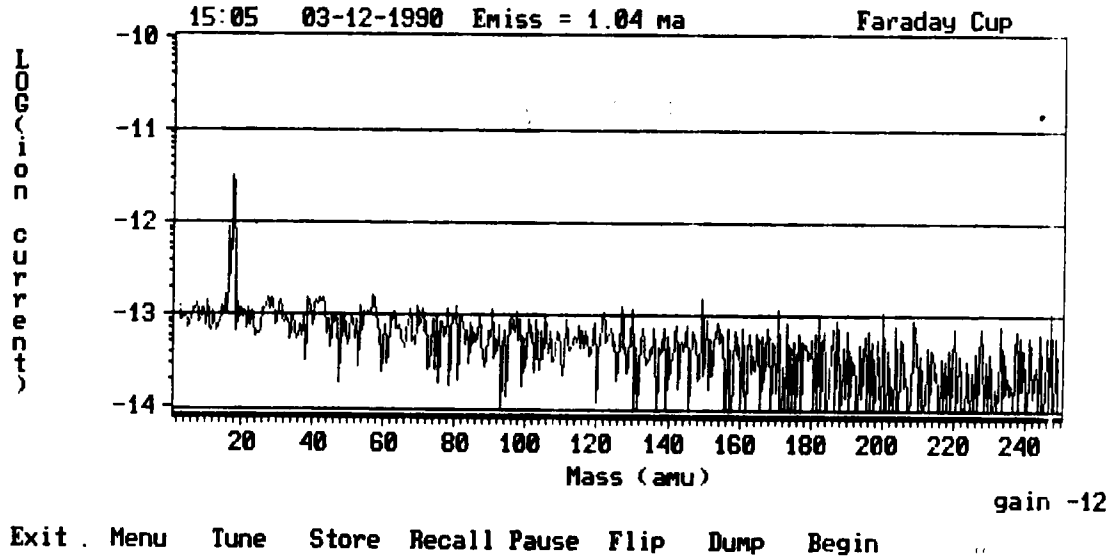


Figure IV.36 A mass spectrum taken with the microprocessor-based mass spectrometer set up in the analog mode for a mass range of 2 to 250 Daltons. Notice the large peak at a mass of about 18. This is the water vapor peak. The spectrum at higher masses represents mostly noise.

There are no other significant peaks in this spectrum. The mass range of interest for this application, the implantation of nitrogen, is from about 2 to 45 Daltons.

Figure IV.37 is a spectrum taken in the fast analysis mode for an expanded mass scale ranging from 2 to 45 Daltons. This spectrum is a histogram. A spectrum of this type is of interest in this application, since the noise is eliminated, and the relative height of the peaks can be monitored at all times. This spectrum was taken at a base pressure of 0.026 μtorr, with liquid nitrogen in the cold trap. The small information box in the upper right hand corner lists the five largest components in the spectrum with their name on the left and their percentage concentration on the right, corrected for gauge factor. This is very useful when comparing relative peak intensities. For this spectrum with no input gas feed, the water vapor component dominates at 51.7 percent. Without liquid nitrogen in the cold trap, this percentage could be as high as 70 %. The next most dominant component was hydrogen, with 37 %. This is also common in most spectra, since hydrogen is a light element and thus difficult to pump away. Water vapor tends to stick to the inner surfaces of vacuum vessels. This makes it difficult to pump away. Other components are methane, nitrogen, and helium with percentage concentrations of 5.2, 4.2, and 1.3, respectively. Figure IV.38 is the same spectrum for the conditions of Figure IV.37. Notice that there is a significant amount of noise between the peaks and at masses above 20.

Figure IV.39 and IV.40 are spectra for vacuum pressures of 0.77 and 0.03 μtorr, without and with liquid nitrogen, respectively,

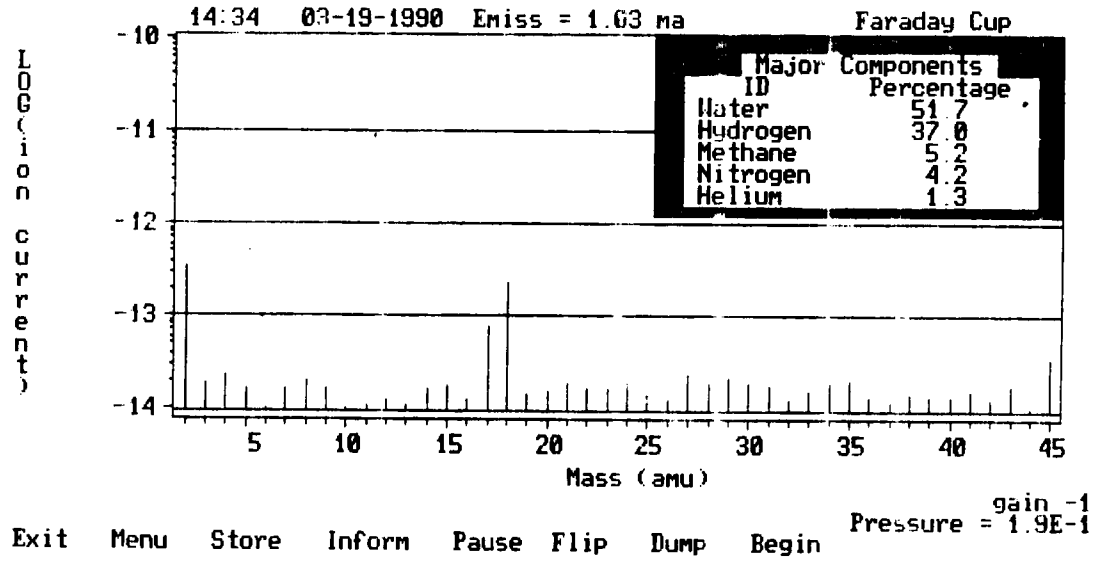


Figure IV.37 A mass spectrum taken with the microprocessor-based mass spectrometer set up in the histogram mode (fast analysis) for a mass range of 2 to 45 Daltons. Notice the large peak at a mass of about 18 and 2. This is the water vapor and hydrogen peak.

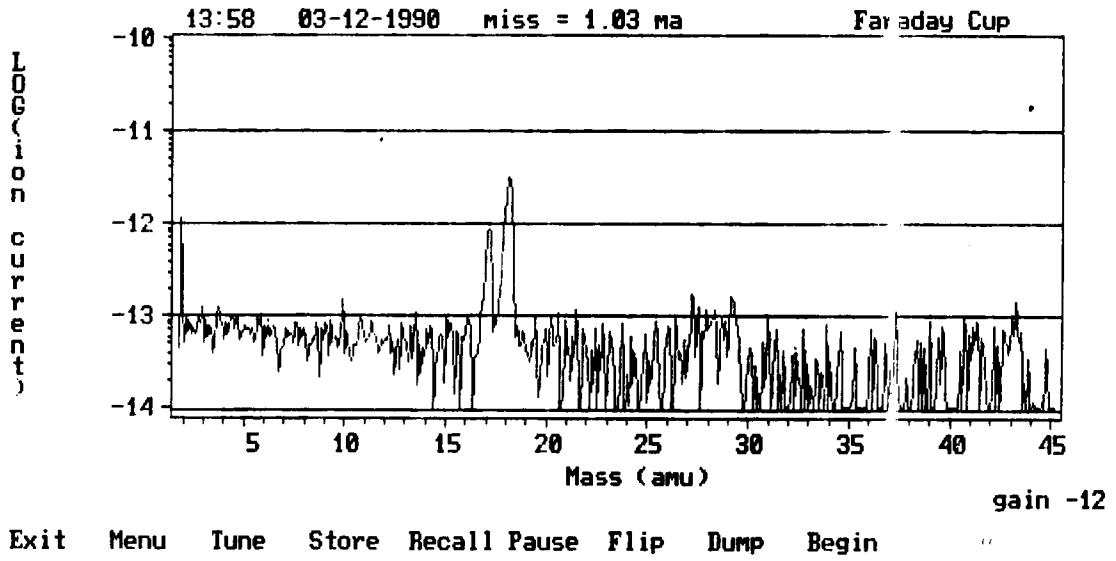


Figure IV.38 A mass spectrum taken with the microprocessor-based mass spectrometer set up in the analog mode for a mass range of 2 to 45 Daltons. Notice the large peak at a mass of about 18, 17, and 2. This is the water vapor and hydrogen peak. The noise between the peaks and at higher masses above 20 makes the spectrum difficult to interpret when using the instrument as a monitoring device during an experiment.

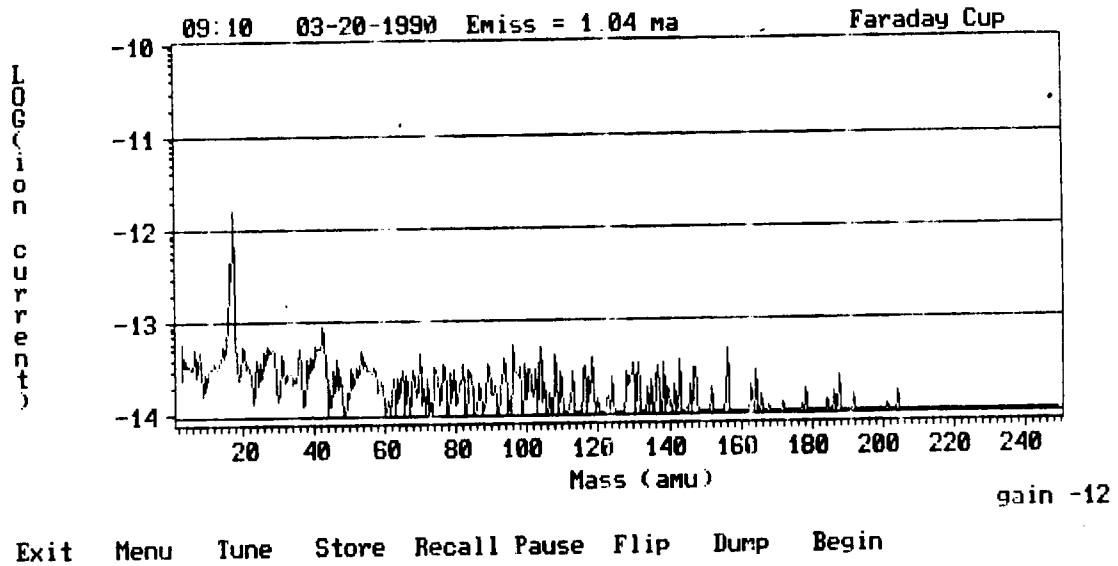


Figure IV.39 A mass spectrum taken with the microprocessor-based mass spectrometer set up in the analog mode for a mass range of 2 to 250 Daltons at a base pressure of 0.77 μtorr with no liquid nitrogen in the cold trap. Notice the large peaks at a mass of about 18 and 41. This is the water vapor and pumping oil peak.

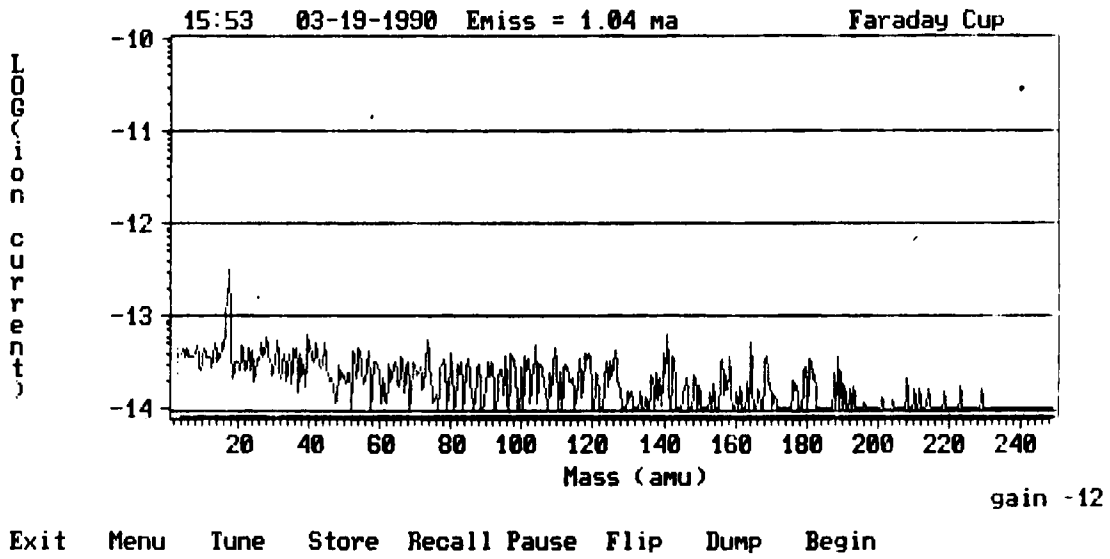


Figure IV.40 A mass spectrum taken with the microprocessor-based mass spectrometer set up in the analog mode for a mass range of 2 to 250 Daltons at a base pressure of 0.03 μ torr with liquid nitrogen in the cold trap. Notice the peaks at a mass of about 18 and 41 have been reduced significantly. This is the water vapor and pumping oil peak.

for a mass range from 2 to 250 Daltons. Figure IV.38 contains a water vapor peak at a intensity level of about 1.9 x 10^{-12} and another peak at 41 with a level of about 9 x 10^{-14}. Upon the addition of liquid nitrogen, these peaks were reduced to 3.5 x 10^{-13} and 5 x 10^{-14}, a reduction in impurity level of about 5 and 2, respectively. The water vapor peak was reduced significantly and would be reduced further if plasma discharge cleaning were used to clean the inside of the cavity. Figures IV.39 and IV.40 provide a paired comparison of spectra with and without the addition of liquid nitrogen to the cold trap to trap impurities on the surface of the cooling finger.

14. Starting the Plasma

The starting of a plasma is an important procedure, because some energy sources used to maintain the plasma, are not sufficient to cause initial breakdown. This is often the case in radio frequency and microwave generated plasmas. Such plasmas can be started in several ways. A carbon electrode can be inserted into the active volume. A high potential can be placed on the rod which will generate an electric field between the rod and the grounded wall of the containment system (if metal). Another method often used is to insert an electrode, such as a small copper ring or rod, insulated from the container's ground. A Tesla coil, which generates high RF voltages on its tip, can be placed in contact with the copper ring or

rod. The Tesla coil can even be touched to the containment device in a location where the strong electric fields around the Tesla coil tip can propagate through an insulating wall to cause plasma breakdown.

In this application, a 1/2" (1.27 cm) outside diameter, sealed copper tube, which is about 10" (25.4 cm) long and may be inserted into or withdrawn from the containment volume, is used along with a Tesla coil to start the plasma when needed. Once the plasma is started, the microwave power can be increased to the desired level. The Tesla coil can then be turned off and the copper tube can be withdrawn so it does not act as a radiator for the microwave energy. In addition to this, a cylindrical shield, made of sheet metal, can be placed over the rod to shield any microwave radiation from laboratory personnel.

15. Conclusions

The high-voltage switching circuit along with the MPF (Microwave Plasma Facility) was completed and ready to ignite the first plasma for characterization. The base pressure of the MPF is suitable for a plasma operating pressure as low as 2 microtorr. After starting the plasma and characterizing its plasma and floating potential, ion and electron kinetic temperatures, and ion and electron number densities, one could estimate the maximum expected diameter for which a uniform flux of ions could be expected to

impinge upon a target for plasma ion implantation. However, the object, as discussed earlier, does not have to be planar. The object could be complex and other plasma characteristics could be carried out to gather additional information for the locations of interest.

BIBLIOGRAPHY

BIBLIOGRAPHY

1. Baddour, Raymond F., The Application of Plasmas to Chemical Processing, M.I.T. Press, Cambridge, MA, 1967.

2. Bernius, Mark T. and Ara Chutkian (1989), "High-Voltage, Full-Floating 10-MHz Square-Wave Generator with Phase Control", Rev. Sci. Instrum., Vol. 60, No. 4, pp. 779-782.

3. Boswell, R. W., A. J. Perry, and M. Emami (1989), "Multipole Confined Diffusion Plasma Produced by 13.56 MHz Electrodeless Source", J. Vac. Sci. Technology, Vol. 7, No. 6, pp. 660-665.

4. Brown, Sanborn C., Introduction to Electrical Discharges in Gases, John Wiley & Sons, Inc., New York, NY, 1966.

5. Chang, Kai, Handbook of Microwave Engineering, Volume 1, Microwave Passive and Antenna Components, John Wiley & Sons, Inc., New York, NY, 1989.

6. Chirlan, Paul M. and Armen H. Zemanian, Electronics, McGraw-Hill Book Company, New York, NY, 1961.

7. Collin, Robert E., Foundations for Microwave Engineering, McGraw-Hill Book Company, New York, NY, 1966.

8. Conrad, J.R. (1987), "Sheath Thickness and Potential Profiles of Ion-Matrix Sheaths for Cylindrical and Spherical Electrodes", J. Appl. Phys., Vol. 62, No. 3, pp.777-779.

9. Cowburn, J. W., "Plasma Etching and Reactive Ion Etching", Course Notes, 1983.

10. Dearnaley, G., J. H. Freeman, R. S. Nelson, and J. Stephen, Defects in Crystalline Solids, "Ion Implantation", Volume 8, North-Holland Publishing Co., 1973, p. 729.

11. DeMornay & Bonardi Microwave Equipment Catalog and Reference Handbook No. C-6, Division of Datapulse, Inc., Pasadena, CA, (1967), p. A57.

12. Destler, William W. and Victor Granatstein, "Elements of Microwave Engineering", The University of Maryland, College Park, MD, (1990).

13. Dyer, Fred, Personal Communication, 1989.

14. Gandhi, Om P., Microwave Engineering and Applications, Pergamon Press, New York, NY, 1981.

15. Geller, R. and J. Hosea, "Electron Collision Frequencies", Euratom-C.E.A., Fontenay-aux-Roses, (Seine) France, Report No. EUR-CEA-FC-459, March 1968.

16. General Electric Corporation, GE-MOV® Metal Oxide Varistors: Transient Voltage Suppression, Fifth Edition, General Electric Corporation of U.S.A., Semiconductor Division, Liverpool, NY, (1986).

17. Heald, M. A. and C. B. Wharton, Plasma Diagnostics with Microwaves, Robert E. Krieger Publishing Company, Huntington, NY, 1978.

18. Hill, W, Ryland, Electronics in Engineering, McGraw-Hill Book Company, New York, NY, 1961.

19. Keebler, P.F., John E. Crowley, and J.R. Roth, "A High-Voltage Switching Circuit for Rapid Plasma Ion Implantation", Paper 5P29, Proceedings of the 1989 IEEE International Conference on Plasma Science, May 22-24, 1989, Buffalo, NY, IEEE Catalog No. 89CH2760-7 (1989) p. 149.

20. Keebler, P.F., John E. Crowley, and J.R. Roth, "A High-Voltage Switching Circuit for Rapid Plasma Ion Implantation", APS Bulletin (1989).

21. Keebler, P.F. and J.R. Roth, "A Microwave Generated Plasma for Ion Implantation Studies", Paper 3P3-13, Proceedings of the 1990 IEEE International Conference on Plasma Science, May 21-23, 1990, Oakland, CA, IEEE Catalog No. 90CH2857-1 (1990) p. 161.

22. Liao, Samuel Y., Microwave Circuit Analysis and Amplifier Design, Prentice-Hall, Inc., Englewood Cliffs, NJ, 1987.

23. Moreno, Theodore, Microwave Transmission Design Data, Dover Publishing Inc., New York, NY, 1948.

24. Penning, F.M. (1937), "Ein Neues Manometer Fur Niedrige Gasdrucke, Insbesondere Zwischen E-3 Und E-5 MM", Physica IV, No. 2, pp. 71-75.

25. Penning, F.M. and K. Nienhuis (1949), "Construction and Application of a New Design of the Philips Vacuum Gauge", Philips Tech. Rev., Vol. 11, No. 116, pp. 116-122.

26. Pomathiod, L., R. Debrie, Y. Arnal, and J. Pelletier (1984), "Microwave Excitation of Large Volumes of Plasma at Electron Cyclotron Resonance in Multipolar Confinement", Physics Letters, Vol. 106A, No. 7, pp. 301-304.

27. Roth, J.R., Introduction to Fusion Energy, Ibis Publishing, Charlottesville, VA, 1986.

28. Roth, J.R. (1987), "Theory of Plasma Ion Implantation for Hardening Metals", Paper 6Y6, Proceedings of the 1987 IEEE International Conference on Plasma Science, June 1-3, 1987, Arlington, VA, IEEE Catalog No. 87CH2451-3 (1987) pp. 123-124.

29. Roth, J.R. and Raymond A. Buchanan, "Corrosion Inhibition by Plasma Ion Implantation", Unsolicited Proposal, The University of Tennessee, College of Engineering, Knoxville, TN, (1989).

30. Roth, J.R. and Raymond A. Buchanan, "Corrosion Inhibition by Plasma Ion Implantation", Semiannual Report, The University of Tennessee, College of Engineering, Knoxville, TN, (1990).

31. Roth, J.R., Personal Communication, 1990.

32. Ryder, John D., Engineering Electronics with Industrial Applications and Control, McGraw-Hill Book Company, New York, NY, 1957.

33. Slater, John C., Microwave Electronics, D. Van Nostrand Company, New York, NY, 1950.

34. Soohoo, Ronald F., Microwave Electronics, Addison-Wesley Publishing Company, Reading, MA, 1971.

35. Varian-Eimac Corporation, Care and Feeding of Power Grid Tubes, Fourth Edition, Variam-Eimac Corporation, San Carlos, CA, 1982.

36. Wavetek Instruction Manual, Model 191, 20 MHz Pulse/Function Generator, Wavetek, Inc., San Diego, CA, 1983.

APPENDICES

APPENDIX A

MACROSCOPIC THEORY OF PLASMA ION IMPLANTATION

MACROSCOPIC THEORY OF PLASMA ION IMPLANTATION

Like many industrial applications, where improvement of a material requires an improvement in its processing, modification of the ion implantation process to include plasmas may further enhance the properties of the material and increase the efficiency of the process itself. In Chapter 1, ion beam implantation was discussed before plasma ion implantation because it historically preceded the latter. Figure I.1 is useful to compare the two processes in a way which illustrates their relative advantages and disadvantages. The plasma ion implantation theory given below illustrates why plasma ion implantation may be the preferred process. This improvement in the ion implantation process (Roth, 1987) manifests itself in three ways.

First, in order to economically implant charged particles into a material, high fluxes of the particles must be available. One of the most expensive methods of producing energetic charged particles is with high energy particle accelerators. Some of these accelerators might include cyclotrons, Van De Graaff accelerators, and even linear accelerators. Here, the ions gain their energy not by passing through accelerating grids but through processes that require expensive RF or ultra high voltage inherent to the accelerator technologies. Thus, large capital and operating costs limit such accelerators for application to ion implantation. Figure A.1 is a schematic of this scheme.

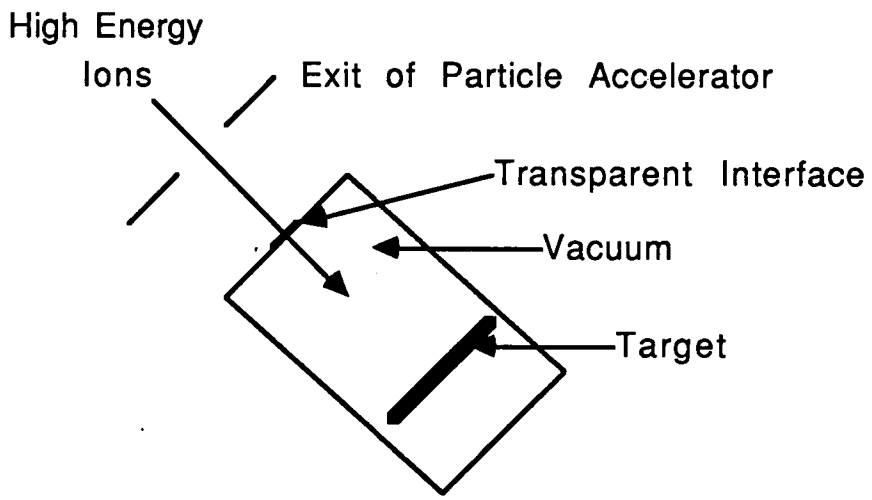


Figure A.1 An accelerator used as a device for accelerating ions to high energies for ion implantation. This method involves large capital equipment costs.

Early ion implantation experiments used ion beam implantation methods like that shown schematically in Figure I.1. In the source, ions are created within a plasma of small volume located outside the implantation region. Unlike ion production by high-energy accelerators, this method achieves the extraction and acceleration of the ions by the electric field between accelerating grids. Note that the containment vessel and the target are grounded so that the ions complete an electrical circuit. Since the source plasma is usually positive, the ions not only gain that energy (plasma potential), but they also gain much additional energy as they pass through the accelerating grid(s), roughly equal to the grid potential. The metal target to be implanted is inserted in a vacuum. The ions of energies from 20 keV to as much as 600 keV travel towards the target.

Secondly, in ion beam implantation, the beam is unidirectional. The angle which the ions travel with respect to the central axis is a direct function of the angle which the accelerating grids make with the central axis. Thus, in order to direct the ion beam over the surface of a *flat* metal target larger than the beam diameter, one must steer the beam. Beam steering is relatively difficult and obviously, one cannot steer an ion beam to shadowed areas, much less to the opposite side of a *complex* target. Quasi-uniform ion beam deposition on a complex surface can be achieved by rotating or manipulating the target, but if the target is large and has many convoluted or protruding surfaces, target rotation can become difficult, or even impossible due to the weight and irregular geometry of the target.

By placing the target inside the ion source plasma, ions are available to the entire surface of the target. Hence, no beam steering is necessary and the coverage of the target with ions may be isotropic. Note that just placing the target in the ion source plasma does not result in the ions gaining the high energies required to implant the target surface.

A third problem associated with using ion beams comes into play if the target has a large cross-sectional area as compared to the ion beam. To effectively implant a large target without beam steering, one would have to increase the beam cross-sectional area, if the ion source has already reached its space-charge limit. This would increase the size and cost of the ion source.

A fourth limitation of ion beam implantation is that the number of ions the source can emit per unit area is limited by space-charge limited ion current flow. For the type of ion extraction used in ion beam implantation, the equation describing the space-charge limited current flow is

$$J_{ibl} = \frac{4\varepsilon_o}{9}\sqrt{\frac{2e}{m_i}}\frac{V_o^{3/2}}{d^2} \quad A/m^2 \qquad (A.1)$$

where ε_o is the permittivity of free space, 8.854 x 10^{-12} Farads per meter, e is the electronic charge, 1.609 x 10^{-19} Coulombs, m_i is the ion mass in kilograms, V_o is the accelerating voltage between the grids, and d is the spacing between the grids.

The space-charge limited current density is directly proportional to the three-halves power of the accelerating voltage and is inversely proportional to the square of the spacing between the accelerating grids. The electric field between these two grids is

$$E_o = \frac{V_o}{d} \text{ V / m}, \qquad \text{(A.2)}$$

and the flux of ions of mass m_i is Φ_{ibi}, and is

$$\Phi_{ibi} = \frac{J_{ibi}}{e} \text{ ions / m}^2 - \text{sec} \qquad \text{(A.3)}$$

Substituting Eq. (A.2) into Eq. (A.1) and then Eq. (A.1) into Eq. (A.3) gives the ion flux as a function of electric field for space-charge limited current flow,

$$\Phi_{ibi} = \frac{4\varepsilon_o}{9}\sqrt{\frac{2}{em_i V_o}}\, E_o^2 \text{ ions / m}^2 - \text{sec} \qquad \text{(A.4)}$$

This space-charge limited current can, in principle, be overcome by placing the target to be implanted inside the ion source plasma.

With the target located inside the ion source where ions are available and uniform over the target surface, the method of delivering energy to these ions for implantation can be discussed. First, let the ion source be a plasma in which ions and electrons are available in large quantities. Second, since the ions are positively

charged, a surface with a high negative potential will attract the ions and repel electrons, like a Langmuir probe in ion saturation. The maximum rate at which ions can be delivered is given by the ion saturation current of a Langmuir probe. The rate is

$$\Phi_{pii} = \frac{1}{4} n_i v_i \text{ ions / } m^2 - \text{sec} \qquad \text{(A.5)}$$

where n_i is the ion number density in ions per cubic meter, and v_i is the mean thermal velocity of the ions to the target. The mean thermal velocity of the ions is

$$v_i = \sqrt{\frac{8k\,T_i}{\pi m_i}} \text{ m / sec} \qquad \text{(A.6)}$$

where k is Boltzman's constant, 1.383 x 10^{-23} Joules per °Kelvin, and T_i is the ion kinetic temperature in °Kelvin. Substituting Eq. (A.6) into Eq. (A.5) gives the ion flux on the surface of the target as a function of the ion number density and ion kinetic temperature as

$$\Phi_{pii} = \frac{1}{4} n_i \sqrt{\frac{8\,k\,T_i}{\pi m_i}} \text{ ions / } m^2 - \text{sec} \qquad \text{(A.7)}$$

Taking the ratio of the ion flux incident on a target in ion saturation to the ion flux incident on a target from space-charge limited ion current flow, one arrives at

$$\frac{\Phi_{pii}}{\Phi_{ibi}} = \frac{9 n_i e}{8 \varepsilon_o E_o^2} \sqrt{\frac{T_i V_o}{\pi}} \qquad \text{(A.8)}$$

which is a dimensionless quantity, is independent of the mass of the ions, and is a function of ion kinetic temperature, T_i, now measured in electron-volts.

Substituting numerical values for the constants given in Eq. (A.8) yields an expression dependent upon two additional parameters other than the ion number density and kinetic temperature-the potential applied on the target, V_o, and the electric field in the region between the grids of the space-charge limited ion source, E_o. At the NASA Lewis Research Center, it was found that for long term operation of mercury ion engines without electrical breakdown, the electric field, E_o, should be no more than one-million volts per meter (Roth, 1990). Also, assume that the implantation voltage is V_o = 50,000 volts, giving an energy for each singly-charged ion, of 50 keV. Applying these assumptions to Eq. (A.8) gives an expression for the ratio of the two ion fluxes as a function only of the ion number density and kinetic temperature. Converting the ion number density to cubic centimeters and the ion kinetic temperature to electron-volts, one obtains

$$\frac{\Phi_{pii}}{\Phi_{ibi}} = 2.57 \times 10^{-12} n_i \sqrt{T_i} \qquad \text{(A.8a)}$$

The ion kinetic temperature is plotted against the ion number density in Figure A.2 on a logarithmic-logarithmic graph. Lines of negative slope are shown where the ratio is constant and less than unity, unity, and greater than unity. The lines with a ratio less than unity describe the situation for which the flux due to ions from space-charge limited ion current flow is greater than the flux due to ions crossing the sheath in the isotropic case of plasma ion implantation. Notice that the operating regime of Penning discharges overlaps into this area and that the normal operating point of the Penning discharge in the UTK Plasma Science Laboratory is in this regime for an ion temperature of about 150 eV and an ion number density of about 3 $x10^9$ ions per cubic centimeter. Thus, since it is desirable to obtain the greatest ion flux in order to keep the implantation process time to a minimum, one may not wish to operate in this regime for industrial applications.

Above the line where the ratio is greater than unity, the ion flux due to ions crossing the sheath and impinging on a target surrounded by a plasma is greater than that due to space-charge limited ion current flow. In order to operate in this regime, one would have to trade ion kinetic temperature for an increased ion number density, if plasma ion implantation were to be used. Thus, a range of ion temperatures and number densities is possible in which plasma ion implantation is better than ion beam implantation as far as implantation processing time is concerned. Also, notice that the operating regime of discharges created by microwave radiation is shifted upward compared to the Penning discharge operating regime,

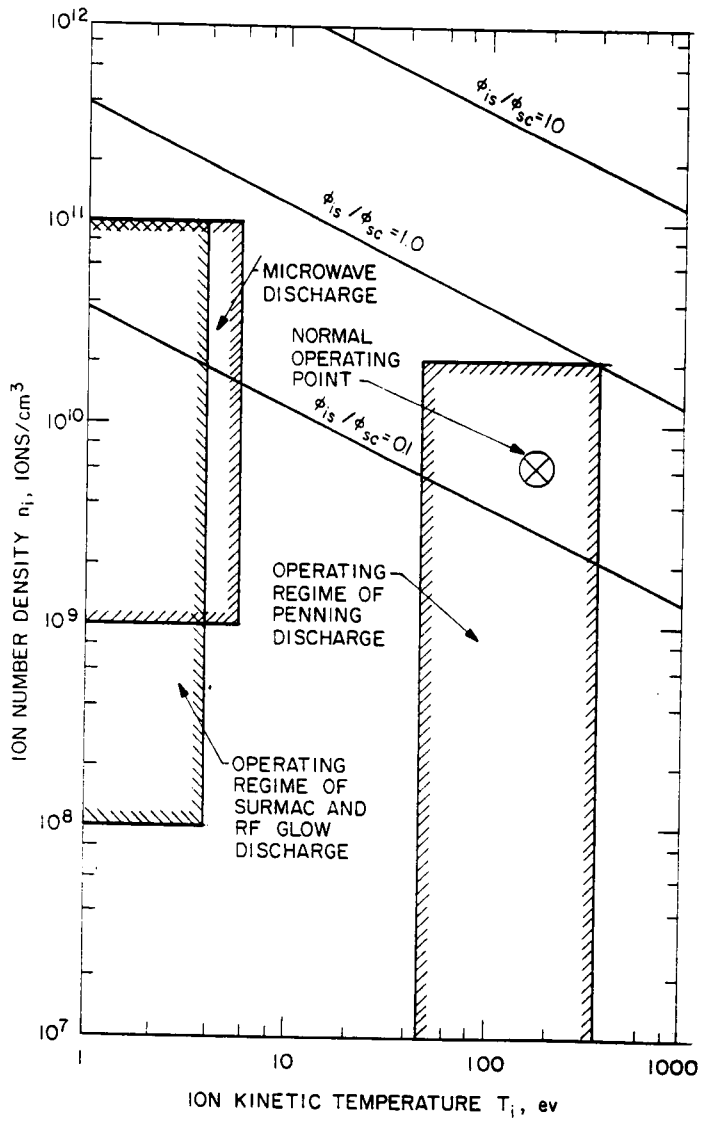


Figure A.2 Graph of ion kinetic temperature versus ion number density showing three regions for the ratio of plasma ion implantation to ion beam implantation fluxes. Also shown are operating regions for three different types of plasmas. Particular interest is given to the region of the microwave discharge. This region extends from 10^9 to 10^{11} ions/cm^3 in ion number density and from 1 to 6 eV in ion kinetic temperature. For this application where a microwave discharge was to be designed, the assumed ion number density was 10^{10} ions/cm^3 and 2 eV for the ion kinetic temperature. The cross hatch indicates this point.

but lies below the line where the ratio of ion fluxes is unity. One might construct an RF plasma discharge system operating above the line where the ratio is unity, for which the ion number density is on the order of 10^{12} ions per cubic centimeter and the ion kinetic temperatures below about 10 eV.

Third, it is known that an object, such as a probe placed inside a plasma will form a sheath, the approximate thickness of which is the Debye distance. This distance is a function of the electron kinetic temperature and the electron number density, and is

$$\lambda_D \doteq \sqrt{\frac{\varepsilon_o k T_e}{n_e e^2}} = \sqrt{\frac{\varepsilon_o T_e}{n_e e}} \text{ m} \qquad \text{(A.9)}$$

where ε_o is the permitivity of free space, T_e is the electron kinetic temperature in electron-volts, n_e is the electron number density in electrons per cubic meter, and e is the electronic charge. If the units of electron number density are in electrons per cubic centimeter, the Debye distance becomes

$$\lambda_D = 743.4 \sqrt{\frac{T_e}{n_e}} \text{ cm} \qquad \text{(A.10)}$$

Consider a plot of electron kinetic temperature versus number density for various Debye distances in a quasi-neutral plasma as illustrated in Figure A.3. For electron kinetic temperatures above about 20 eV and for ion number densities below about 4 x 10^9 ions

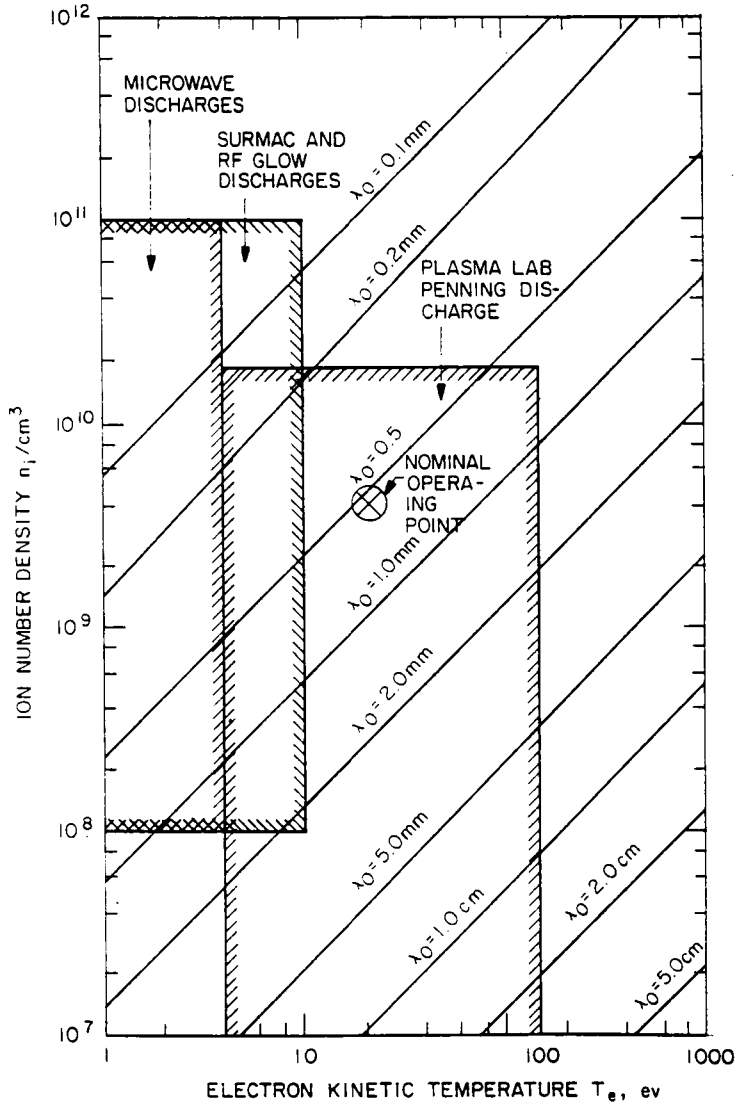


Figure A.3 Graph of electron kinetic temperature versus ion number density (quasi neutral plasma assumed) showing ten regions for the Debye distance ranging from more than 5 cm to less than 0.1 mm. Also shown are operating regions for three different types of plasmas. Particular interest is given to the region of the microwave discharge. This region extends from 10^8 to 10^{11} ions/cm^3 in ion number density and from 1 to 4 eV in ion kinetic temperature. Number densities larger than 10^{10} ions/cm^3 are achievable especially if the ion is singly charged resulting in a Debye distance on the order of 0.1 mm. For this application where a microwave discharge was to be designed, the assumed ion number density was 10^{10} ions/cm^3 and 2 eV for the ion kinetic temperature. The cross hatch indicates this point.

per cubic centimeter (the normal operating point for the Penning discharge), the Debye distance is greater than about 0.5 millimeter. This indicates that in this region an object which is finely detailed (detail dimensions less than 0.5 mm) could not be ion implanted uniformly over the whole surface. The UTK Plasma Science Laboratory Penning discharge operates in the regime of Debye distances from less than 1 centimeter to about one-half of a millimeter. However, its ion number density is limited to values less than about 2×10^{10} ions per cubic centimeter. For radio frequency glow discharges, the regime of Debye distances ranges from less than 1 millimeter to about a tenth of a millimeter. Thus, objects with very finely detailed surfaces could be more uniformly implanted using radio frequency glow discharges. It was the objective of this research to design, build, and operate such an RF microwave discharge that could implant small scale objects with small surface curvature.

Consider a target, which is to be plasma ion implanted, with a characteristic radius **R**. Three cases, shown in Figures A.4, A.5, and A.6, will be considered, in which the ratio of the Debye distance to **R** is either greater than unity, unity, or less than unity. When the Debye distance is greater than the radius of the target surface curvature, the ions are accelerated across the sheath, and the target surface is not uniformly implanted. Most of the implantation takes place at the "summits" and "valleys" of the surface curvature, and not along the inclines. Now consider Figure A.5 for which the Debye length is approximately equal to the radius of curvature of the

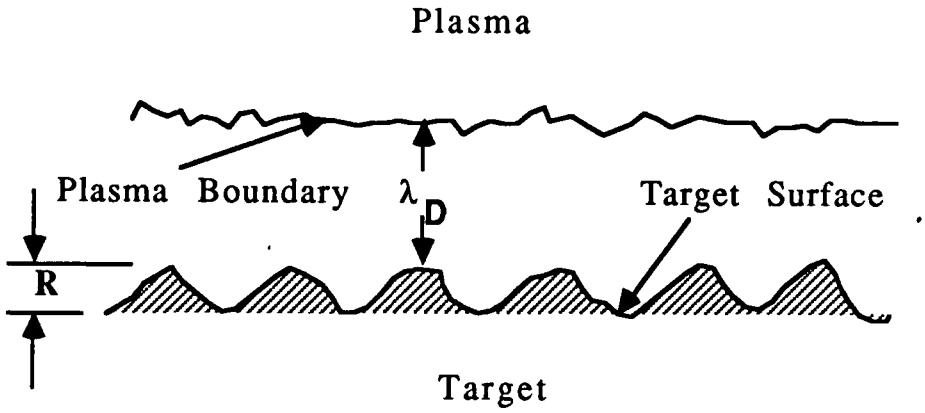


Figure A.4 The case where the Debye distance is much greater than the characteristic radius of the roughness of the surface. In this case, ions that cross the sheath and strike the surface in a "valley" or at the "crest" will implant deeper than those impinging on the "hills." Those that strike "hills" can cause sputtering of the surface and non-uniform implantation of the material surface will result.

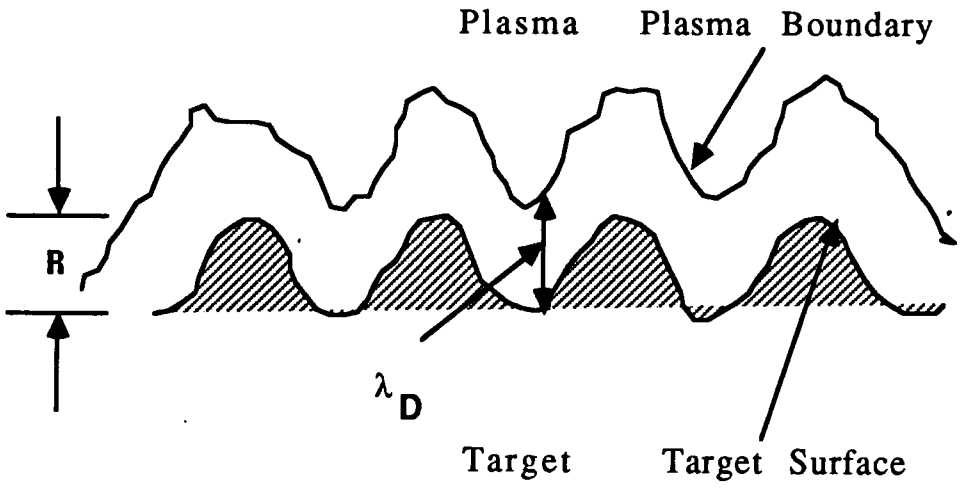


Figure A.5 The case where the Debye distance is approximately equal to the characteristic radius of the roughness of the surface. The ions that cross the sheath and strike the surface strike it with ion trajectories more perpendicular to the material's surface than in the previous case in Figure II.3. This results in a more uniform implantation of ions across the surface.

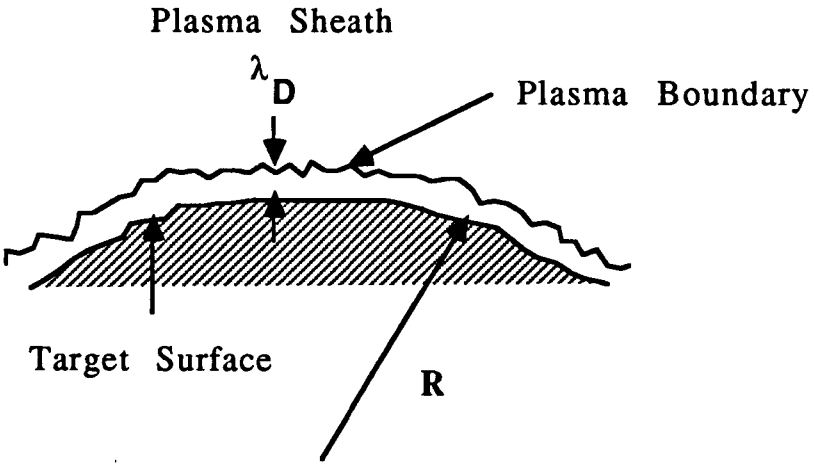


Figure A.6 The case where the Debye distance is much less than the characteristic radius of the roughness of the surface. In this case, the plasma tends to "hug" the object. The ideal plasma ion implantation case would be where the Debye distance has a value of zero. Then, the plasma would fill all surface imperfections and the ions would be implanted across the surface in a totally uniform manner. However, this is not possible; but, the Debye distance can be very small, resulting in a good condition for implanting complex objects with fine details.

surface. In this case, the surface is more uniformly implanted than previously, and the plasma is tending to "hug" the target more, but not enough to uniformly implant a gear with small teeth or a mechanical screw. Finally, consider Figure A.6 in which the Debye distance is much smaller than the radius of surface curvature. In this case, the plasma is hugging the target to the point where the target is being uniformly implanted all over its surface. Thus, the difficulty in implanting complex or small scale objects using ion beam implantation can be overcome by implanting in a plasma where the Debye distance is very small.

Now that some insight to the ratio of the Debye distance to the effective radius of the surface roughness has been gained, the phenomena within a Debye distance of the surface can be discussed. The electric field is very high in this region, since its thickness is on the order of a few millimeters and the plasma potential is usually several thousand volts. If a negative potential of several tens of kilovolts is placed on a metallic target in the plasma, ions will be attracted to the sheath and accelerated to the target in this region of high electric field. Upon crossing, they gain energy which, in eV, is about equal to the potential applied to the target. However, the plasma potential will push the target potential up, hence the effective gain in energy as the ions cross the sheath is the difference in the applied target potential (ion implantation voltage), V_b, and the plasma potential, V_p, and is

$$V_i = |V_b| - |V_p| \ V \qquad \text{(A.11)}$$

Finally, from the above discussion, the implantation process is now called plasma ion implantation since the implantation is by ions from within a plasma. An analysis of what will happen if the ion implantation voltage, V_b , is held at a negative, constant value, follows.

In order to achieve a desired implantation effect, a minimum dose, or number of ions per unit area must be imbedded in the surface of the target material. Also, for the process to be industrially acceptable, the time that it takes for this to happen must not be excessive. The time it takes to achieve a desired dose will be determined.

If ions of atomic mass number, M_1, in kilograms per kilogram-atom are implanted into a metal surface made up of atoms with atomic mass number, M_2, in kilograms per kilogram-atom and whose density is ρ in kilograms per cubic meter, the number density of implanted ions, N, in ions per cubic meter with a mole fraction of implanted species, X, is given as

$$N = \frac{X A_o \rho}{X M_1 + (1 - X) M_2} \text{ ions / m}^3 \qquad \text{(A.12)}$$

where A_o is Avogadro's number and has the value 6.023 E+26 atoms per kilogram atom. If the surface of the metal sample is implanted to a depth l, the total dose, D, in ions per unit area, or ion fluence, is

$$D \equiv \Phi_{ions}\, t_o = \Phi_{pii} t_o = NI = \frac{XA_o \rho I}{XM_1 + (1-X)M_2} \quad \text{atoms / m}^2 \qquad (A.13)$$

where t_o is the total exposure time.

A Langmuir probe, when sufficiently negatively biased, has only ions incident upon its surface. Using the ion flux given by Eq. (A.7), for the flux of ions incident upon a metal sample surface when negatively biased, and substituting this into Eq. (A.13) for the ion fluence, one obtains an expression for the total exposure time,

$$t_o = \frac{NI}{\Phi_{pii}} = \frac{4XA_o \rho I}{n_i [XM_1 + (1-X)M_2]} \sqrt{\frac{\pi m_i}{8e\, T_i}} \quad \text{seconds} \qquad (A.14)$$

in which all of the variables were defined earlier. When the ion number density increases, the ions available for implantation in the plasma increase. This, of course, allows more ions per unit area per unit time to be withdrawn from the plasma and implanted into the metal sample; hence, the total exposure time to achieve a desired percentage mole fraction over an implantation depth in a metal sample decreases.

When withdrawing a significant number of ions from a plasma, it is necessary to consider how many ions are extracted per unit time, because each plasma ion has a finite lifetime in the plasma. If the exposure time, or the ion removal time, exceeds the average lifetime of the plasma ions, the plasma will be seriously depleted of its ion population and the plasma could be extinguished. To

determine the duration within which ions can be removed from the plasma, the plasma particle containment time, denoted by t_c, must be determined. This is determined from the current to the anode, I_{Anode}, in the plasma, which may be written

$$I_{Anode} = \frac{Q}{t_c} \text{ Amperes}, \qquad \text{(A.15)}$$

where Q is the total charge in Coulombs in a plasma with volume V_{plasma}. The volume of a cylindrical plasma is

$$V_{plasma} = \pi a^2 L \text{ m}^3, \qquad \text{(A.16)}$$

where a is the plasma radius and L is the length of the plasma column. The total charge in the plasma is given in Coulombs as

$$Q = en_e V_{plasma} \text{ Coulombs} \qquad \text{(A.17)}$$

Substitution of Eq. (A.17) into Eq. (A.15) results in the particle containment time,

$$t_c = \frac{en_e V_{plasma}}{I_{Anode}} \text{ sec onds} \qquad \text{(A.18)}$$

Also of relevance in this application is the plasma energy containment time. This is the time it takes, on the average, for the

particles in the plasma to lose their total energy. The total energy of a quasi-neutral plasma containing both ions and electrons is

$$E = \frac{3}{2} n_e e (T_i' + T_e') V_{plasma} \quad \text{Joules} \qquad \text{(A.19)}$$

The input power of the plasma, denoted by P_{in}, may be determined by taking the ratio of the energy contained in the plasma to the plasma energy containment time denoted by t_e. Thus, the input power of the plasma in terms of plasma parameters is given in Watts as

$$P_{input} = \frac{E}{t_e} \quad \text{Watts} \qquad \text{(A.20)}$$

where E is taken from Eq. (A.19). Using this equation, the plasma energy containment time is

$$t_e = \frac{E}{P_{input}} \quad \text{sec onds} \qquad \text{(A.21)}$$

These characteristic plasma times, calculated for the uniform Penning discharge, will be presented in Chapter 3.

Another time quantity of interest in plasma ion implantation is how long it would take for <u>all</u> of the plasma ions to impinge upon the metal sample. This is denoted by t_{max} and is

$$t_{max} = \frac{n_i V_{plasma}}{\Phi_{pii} A_{sh}} \text{ seconds} \qquad \text{(A.22)}$$

where Φ_{pii} is the ion flux incident upon the metal surface during plasma ion implantation and A_{sh} is the surface area of the metal exposed to the plasma. Thus, if the ion number density or the plasma volume increases, it will take longer for all of the plasma ions to be lost on the sample surface area. If either the ion flux or the sample surface area are increased, the time required for all of the plasma ions to be lost on the sample will decrease.

The time interval for which the negative biasing voltage can be applied to the metal sample without extinguishing the plasma must therefore be the least of the three times discussed above. This is

$$t_{nb\ on} = \min \{t_c, t_e, t_{max}\} \quad \text{sec} \qquad \text{(A.23)}$$

As long as the total required sample exposure time, t_o, is longer than the minimum discussed above, a switch, which can periodically apply the negative bias for a minimum time and then remove it, will be needed, since the sample cannot be completely implanted in a single shot. As will be seen in Chapter 4, the values of **X** and **I** for which beneficial effects of nitrogen ion implantation are obtainable result in total exposure times many orders of magnitude greater than most characteristic plasma times, especially for the steady-state plasmas obtainable by conventional methods.

After the maximum allowable biasing time for the metal sample has been determined, the total number of exposures, denoted by **N.E.**, for a desired implantation effect must be calculated. This is given as

$$\mathbf{N.E.} = \frac{t_o}{t_{nb\ on}} \qquad \text{(A.24)}$$

This quantity can have values of many hundreds of thousands. Obviously, a high-speed switching device, which can apply negative pulses very rapidly, is required.

Since a high-speed switch is desirable, it is now convenient to define a duty cycle, denoted by **F**, which is the ratio of the time the sample is negatively biased to the switching signal period, **T**. The pulse period, **T**, is given in seconds as

$$T = t_{nb\ on} + t_{nb\ off} \quad \text{sec}, \qquad \text{(A.25)}$$

and the duty cycle is given as

$$F = \frac{t_{nb\ on}}{t_{nb\ on} + t_{nb\ off}} \times 100 \qquad \text{(A.26)}$$

The time that it takes to complete the plasma ion implantation process, or the 'elapsed process time' denoted by t_{ept}, is simply the product of the total number of exposures, **N.E.**, and the pulse period,

T, or the quotient of the total exposure time, t_o, and the duty cycle, F. This is given in seconds as

$$t_{ept} = N.E.(t_{nb\ on} + t_{nb\ off}) = \frac{t_o}{F} \quad sec \qquad (A.27)$$

The total number of ions implanted, N_{ii}, into the surface area, A_{sh}, of a metal sample is

$$N_{ii} = F_i A_{sh} \quad ions \qquad (A.28)$$

where D is the ion dose in ions per square meter. If each ion has a charge of e, 1.602 E-19 Coulombs, and the ions are assumed to be singly ionized, then the number of ions implanted into the metal surface per second is given as

$$\frac{\bar{I}_{sh}}{e} \ (ions), \qquad (A.29)$$

where $\bar{I}_{sh}$ is the average ion current flowing into the metal sample during one complete plasma ion implantation process. The total number of ions delivered to the sample surface is then

$$N_{ii} = \frac{\bar{I}_{sh}\, t_{ept}}{e} \quad ions \qquad (A.30)$$

Hence, the elapsed time for the plasma ion implantation process is

$$t_{ept} = \frac{e F_i A_{sh}}{\Gamma_{sh}} \quad \text{sec} \qquad (A.31)$$

When conducting plasma ion implantation, the dose, or ion fluence, **D**, is the implantation characteristic that is calculated as a function of duty cycle, average current, and elapsed process time for a fixed sample area exposed to the plasma. This is illustrated graphically on logarithmic-logarithmic paper in Figure A.7. This graph was drawn for a fixed sample area of 112.5 square centimeters. For a desired dose, the total exposure time may be chosen based on the average ion current.

Other approximations to plasma ion implantation theory have been presented. It was mentioned earlier that the degree of isotropy depends on the sheath thickness between the plasma boundary and the object to be implanted. Analytical expressions presented by the University of Wisconsin (Conrad, 1987) suggest that as the sheath begins to expand around a negatively biased object in a plasma, the initial period, called the ion-matrix phase, plays an important role in determining the ion fluence that reaches the object. The propagation velocity of the sheath is assumed to be roughly the ion acoustic velocity and depends on the ion energy distribution in the plasma and the ion fluence reaching the target during one implantation pulse. It was found that the geometry of the object governs the sheath thickness parameters. For planar objects, it depends only on the applied negative potential and the number density of the plasma. For cylindrical and spherical objects, the sheath thickness also

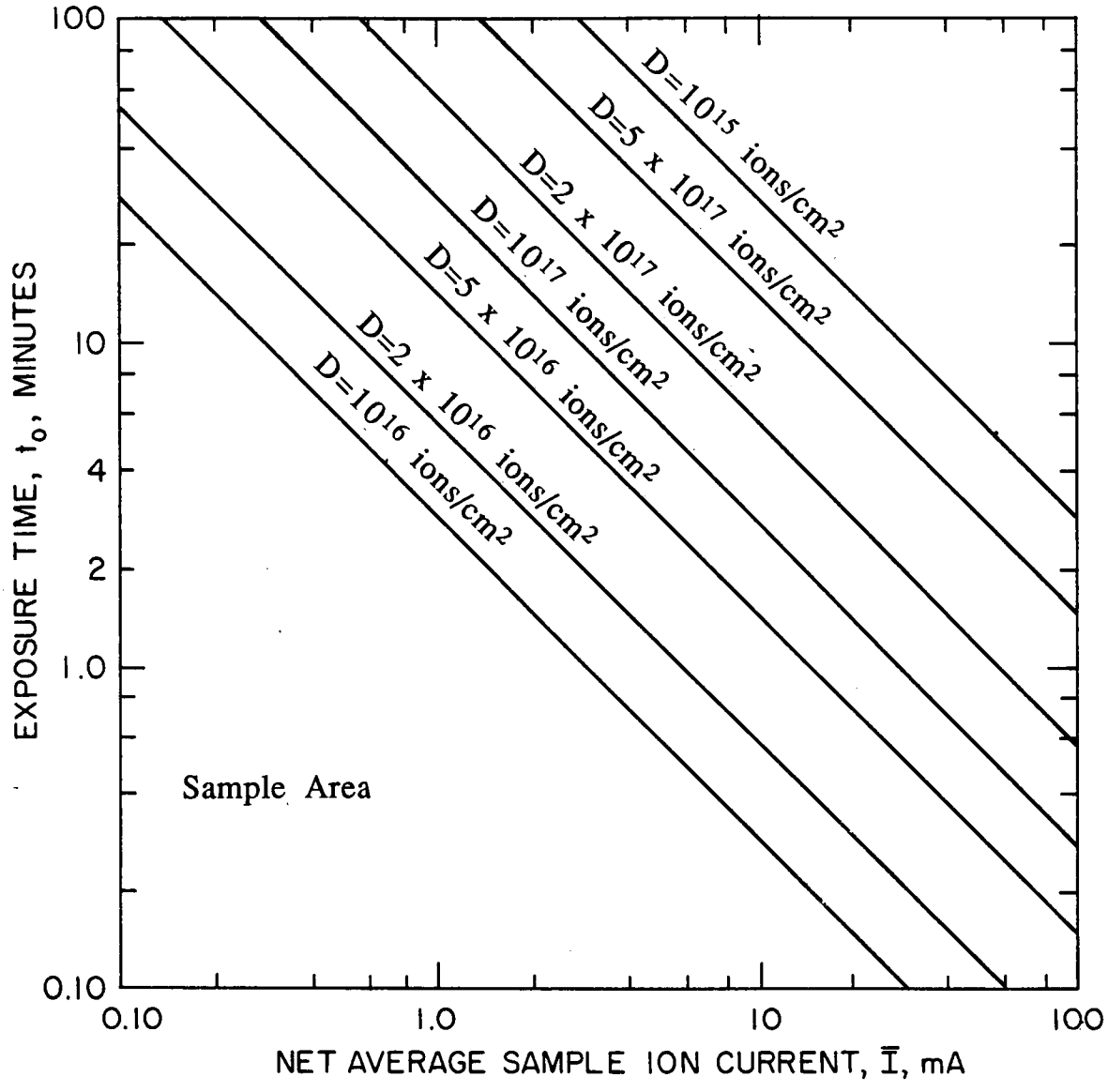


Figure A.7 A graph of the total exposure time on the ordinate versus the average ion current to the sample on the abscissa for a fixed sample area of 112.5 square centimeters.

depends on the radius of the object, with a weaker dependence on applied negative potential and plasma number density (Conrad, 1987).

APPENDIX B

CHARGING THE BATTERY IN THE HIGH-VOLTAGE SWITCHING CIRCUIT

CHARGING THE BATTERY IN THE HIGH-VOLTAGE SWITCHING CIRCUIT

The following procedures are required to recharge the storage battery inside the high-voltage switching circuit. The battery should be recharged just after one has inserted a new sample into the vacuum system, while the vacuum system is pumping down. The battery water level must be maintained with distilled water. In order to check this level, the high-voltage switching circuit lid must be removed. Care must be used to remove the six caps from the battery. The water level should be up to the bottom of the funnel pipe inside the battery. This can be determined visually. If a proper water level is not maintained, the battery could be permanently damaged, resulting in battery replacement. The implantation high voltage power supply must be turned off, as well as the high-voltage switching circuit power (knife switch up) before charging the battery. If not, a short circuit will result and damage the equipment.

A variable voltage, variable current, high-power DC power supply has been provided to recharge the battery. Attached to this supply are two No. 10 AWG stranded wire leads, one red and one black. At the end of these leads is a long brass rod with a banana plug connected to each. In the lid of the HVSC are two holes drilled directly over the top of the battery terminal posts. In the posts are two holes drilled to fit the banana plugs. Make sure that the cooling fans are on before charging the battery. If not, hydrogen vapors could build up in the HVSC enclosure and could result in an explosion

if the circuit is operated with a buildup of hydrogen vapor inside the box.

Before the leads can be attached to the battery through the holes in the lid, the voltage on the charging supply must be set. To do this, follow the procedures below.

- Turn on the equipment rack by pushing up on the left-most switch on the bottom panel.
- Turn on the charging power supply and allow it to warm up.
- Obtain a digital voltmeter and set it to measure DC voltage.
- Clip the voltmeter leads onto the end of the charging leads and turn on the power supply.
- Set the voltage using the "Output Voltage" control knob to 12.7 Volts DC. The voltage is now set and should not have to be adjusted again. If the voltage seems hard to set, the current control may be set to zero. The power supply will not operate freely unless the current control is slightly turned on. One may have to turn the current control slightly up (to about 1) to set the voltage.
- Turn off the charging supply and set the current control back to zero if it was moved.
- Insert the red lead into the hole marked "Positive" and the black lead into the hole marked "Negative".
- Turn on the charging supply and note the current.
- Set the charging current by adjusting the knob marked "Output Current Adjust" to the point where the current meter reads about 3 Amperes.

Allow the battery to charge at this current level overnight. If one wishes to charge the battery more slowly, the current level may be set to about 1 ampere. This is called a trickle charge and does just as good a job as a fast charge. The manufacturer recommends a slow charge for extended life of the battery. After the charge is complete, turn off the power supply and carefully remove the charging leads.

APPENDIX C

THE PLASMA ION IMPLANTATION PROCESS USING THE PENNING DISCHARGE

THE PLASMA ION IMPLANTATION PROCESS USING THE PENNING DISCHARGE

After the plasma in the Penning discharge has been stabilized, plasma ion implantation may be carried out. Before this is done, record the plasma conditions: the magnet coil current, the Penning anode voltage and current, the pump head and gas inlet pressures, and significant peaks on the mass spectrometer. Since the Del Electronics power supply is being used as the power supply for the HVSC, its polarity connections must be reversed. This is done by following three short steps. First, in the back of the Del Electronics Power Supply Control Panel is a polarity reversing switch. Move this gang switch to the position marked "-". It may be difficult to find underneath all the wiring. Second, go over to the oil tank (left most large gray cabinet) and remove one of the plexiglass covers protecting the high-voltage knobs. Coming out of the top of the tank are two coaxial cables with large knurled knobs on their opposite ends. Unscrew each knurled knob and gently pull up on the coax. On the end of each coax is a banana plug. For negative polarity connections, these cables must be parallel to each other. They must not be crossed as is in the positive connection for running positive potential plasmas. Third, make sure the correct coaxial cable is connected to the high-voltage knob inside the plexiglass door. For this experiment, it will be marked "Ion Implantation Experiment". The assumptions made here before the negative high-voltage is applied are the following:

- The sample holder, with a sample mounted on the end, must be inserted in the South end of the vacuum system.

- The cooling water lines to the sample holder must be connected (order of connection does not matter).

- Before turning on the cooling water to the sample holder, both of the small needle valves at the end of the copper coils on the South end must be open. It is good practice to open the outlet first and then the inlet. After this, the cooling water may be turned on.

- The A-lite fitting (high-voltage insulator) must be grounded through the small black wire equipped with a quick disconnect terminal connection.

- The flange holding the sample holder and cooling hoses in place must also be grounded to the frame of the Penning discharge (yellow wire). The wire is simply placed on one of the flange bolts (nut side) holding the cooling cylinder in place.

- The black grounding wire extending from the side of the high-voltage measuring probe must be connected to the copper ground braiding connected to the frame of the Penning discharge.

- The RG-8/U 50,000-Volt coaxial wire coming from the high-voltage switching circuit must be inserted through the hole provided in the side of the cooling cylinder. This wire must be connected to the sample holder rod by means of a small hose clamp with no sharp edges. The sample holder must be cleaned with acetone before and after this wire is connected to keep body grease from building up on high-voltage components. This wire must also be inserted through the current transformer before connection it to the sample holder if a current measurement is to be made.

- The Tektronix high-voltage measuring probe must be

attached to the top of the cooling cylinder. Masking tape application will suffice.

- The red wire leading from the tip of this probe must be connected to the sample holder rod by means of its alligator clip. Make sure this connection is tight and will not slip off during the implantation. The other end has a compensating box connected to it. This box converts the voltage signal so that it can be input to the oscilloscope. The compensating box has a female coaxial connector which is connected to Channel 2 of the Implantation Monitoring Oscilloscope. Caution: Do not try to reconnect this red wire when the plasma is on unless the sample holder is grounded first. If it is not grounded, it will float at the plasma potential.

- The triax cable, a clear looking coaxial cable intended to shield against radio frequency interference, must be connected to the high-frequency, high-current transformer. The other end must be connected to Channel 1 of the Implantation Monitoring Oscilloscope.

- The ends of the rubber cooling hoses inside the cooling cylinder must be connected to the water connections at the end of the sample holder. Note that center cooling tube in the sample holder is free to move and must NOT be jammed against the end of the copper block at the end of the sample holder. If this occurs, no cooling water will flow to the reservoir inside the copper block and the sample will not be cooled properly.

- If the sample holder is inserted far enough into the vacuum system so that its end does not extend beyond the end of the cooling cylinder, then the circular plexiglass plate must be installed on the end of the cooling cylinder to protect one from high-voltage breakdowns should they occur. If not, then it is advised that caution be taken when conducting the implantation.

- The two doors on the radio frequency Faraday cage surrounding the high-voltage switching circuit and one-half of the Penning discharge must be closed.

- The grounding wand, connected to the side frame of the Penning discharge, must be near the inside of these doors hanging on the hook that is provided.

- The cooling fans for the high-voltage switching circuit must be turned on. They are powered by a 12-Volt DC power supply resting on the left frame of the Penning discharge. These fans are usually left running at all times to keep the hydrogen vapors from the battery from building up inside the high-voltage switching circuit. The cooling fan directly on the South end of the system, mounted on the outside of the high-voltage switching circuit, must be connected to a standard 110-Volt AC outlet.

- The cooling fans inside the high-voltage switching circuit must be powered up. This is done by clipping a small alligator clip to the knife switch after opening the lid of the box.

- The main power switch on the front panel of the Plasma Ion Implantation Control System must be turned on. This is the left most switch on the very bottom panel. This also turns on the cooling fans inside this equipment rack.

- The oscilloscope for monitoring the control signal must be turned on and allowed to warm up for a few minutes. Also, the oscilloscope for monitoring the implantation voltage and current must be turned on. The zero marker for the scope monitoring the implantation voltage and current must be set in order to get a proper reading. Set the time base for this scope to 10 microseconds per division to get a good trace of the voltage waveform during the implantation.

- Make sure the fiber optic cable is connected to the fiber optic transmitter and to the inside of the high-voltage switching circuit. It is not advisible to disconnect this cable unless the switching circuit is to be moved or unless the Plasma Ion Implantation Control System equipment rack is to be moved. Moving or disconnecting the fiber optic cable unecessarily could result in permanent damage to the cable. The fiber

optic cable is enclosed is a 1/2" section of tygon tubing for protection. This is to keep the cable from becoming damaged or bent.

Now that all connections have been made from the high-voltage switching circuit to the Penning discharge system, the implantation process can be started. The following procedures must be followed when implanting a sample using the Penning discharge.

- Turn on the control signal generator by pressing the small black button under the frequency knob.

- Look at the trace on the oscilloscope above it and make sure the signal pulse width is set properly (about 10 to 35 microseconds). To increase this time, turn the "Pulse Width" knob clockwise and watch the pulse widen. The range is from 20 nanoseconds to 100 milliseconds in seven ranges. Change the time base on this scope to examine the time between pulses and make sure it is set to the proper time (about 1 millisecond or longer). To change this time, decrease the frequency on the signal generator by turning the frequency knob counterclockwise. The amplitude of this signal should be about 4 Volts. Set the time base to 10 microseconds per division so that it can be compared to the voltage waveform on the scope below.

- Turn on the fiber optic transmitter by flipping up the switch on its front panel. This transmitter is located to the left of the control signal generator. The green light on the front of the transmitter should come on.

- Turn on the implantation power supply, the Del Electronics power supply, typically used to generate plasmas in the laboratory. This power supply is used for the high-voltage switching circuit because of its low internal impedance. A high internal impedance results in a large (1/2) voltage drop within the supply. Before the supply can be operated, the main switch must be turned on. This is a large disconnect

switch located on the front of the Del Electronics gray power supply enclosure on the South end of the laboratory.

- Go over to the Del Electronics Power Supply Control Panel and switch on the main control system switch. This is a simple off/on toggle switch. This is only to be done if the plasma is stable. If it is not, then wait until it stabilizes before implanting.

- Set the high-voltage meter range switch to the lowest scale (0.1) and the current range switch to the lowest scale (0.1). The overvoltage and overcurrent control knobs should be set to around 100 %.

- Press the green button marked "Start" to apply high-voltage to the high-voltage switching circuit. A loud switching action will be heard.

- If the plasma is still stable at this time, turn on the high-voltage switching circuit by depressing the small wooden dowel rod extending out of the top of the box. It is all right to open one of the Faraday cage doors to do this. Notice if the filament is glowing a bright orange. If not, the battery needs recharging and refer to the section on "Charging the Battery in the High-Voltage Switching Circuit".

- Once the circuit is on, the negative high-voltage may be applied to the sample. Press and hold the green button marked "Raise" to increase the high-voltage to the cathode of the tube. No sound will be heard; however, the voltage meter on the left will start to rise. The current meter on the right will not rise at first. If the overcurrent or overvoltage protection circuit become activated, a red indicator will illuminate on the panel telling the user which one it is. Press the red button marked "Reset" to reset either the overvoltage or overcurrent. The overcurrent is tripped more often than the overvoltage. Once the is corrected, the "Start" button may be pressed again.

- Check the Implantation Monitoring Oscilloscope. One should see a small pulse. If so, the circuit is switching the

high-voltage. Careful examination should reveal the plasma potential. This is why the signal will appear to be off zero when it was actually zeroed before.

- The implantation voltage may be increased by pressing the button marked "Raise" on the front of the implantation power source. Holding this button in increases the voltage. Notice the volt meter on the left indicating the voltage on the HVSC. It should be set to the highest scale (0 to 50,000 Volts). Increase the voltage and watch the Implantation Monitoring Oscilloscope, the pressure on the ion gauges, and the volt meter on the implantation power source. As the voltage is increased, the pressure may also increase. If the voltage waveform does not remain flat during the pulse width, increase the pressure until it reaches at least 100 microtorr on the gas inlet end of the system. The Penning anode current should be set to about 10 or 20 milliamperes. This adjustment made be made easily by lowering the Penning anode voltage by turning the large variac knob counterclockwise. Once the voltage waveform is flat again, increase the implantation voltage again. Iterate between increasing the implantation voltage and decreasing the pressure until one can reach the desired negative high-voltage. A slight increase in the gas pressure will result in a more square waveform. However, there is a tradeoff between constant voltage during the pulse and a square waveform.

- Once the desired implantation voltage is reached, start timing the process and continue until the desired exposure time is reached. At the end of the exposure time, lower the voltage on the HVSC by pressing the button on the implantation power source marked "Stop". This button will turn off the HVSC. After the "Stop" button has been pressed, raise the dowel rod on the HVSC, turning the HVSC off.

- During the implantation, take several pictures of the voltage and current waveforms and record their times on the back of the picture.

- Press the red "Stop" button on the NJE power supply control

panel. The plasma will extinguish. It is not necessary to set the Variac to zero to turn the plasma off, but it is good practice.

- Close the gas inlet valve.
- Lower the magnet coil current by pressing down on the momentary switch to the "Lower" position and lower the current to zero.
- Turn off the magnet coil current supply by pushing the toggle switch to the "Off" position.
- Pull down on the disconnect switch behind the magnet coil power supply. The large fan will stop.
- Set the Variac on the Penning discharge power source to zero so that it will not be forgotten for the next experiment.
- Turn off the main breaker on the front of the control panel on the NJE power supply.
- Pull down on the disconnect switch located on the front of the Del Electronics HVSC power supply.
- Refer to the section on "Removing the Sample Holder" for the procedures on changing the sample.

APPENDIX D

OPERATING THE PENNING DISCHARGE PLASMA FOR PLASMA ION IMPLANTATION

OPERATING THE PENNING DISCHARGE PLASMA FOR PLASMA ION IMPLANTATION

It is assumed that the background pressures are below 5 microtorr and that the sample holder is in the vacuum system. It is also assumed that all power supplies connected to the Penning discharge and the plasma ion implantation system (except those related to the vacuum system) are turned off. The Penning discharge is powered by the NJE power supply, since the Del Electronics power supply is needed for the switching circuit because of its low internal impedance. Also, the gas inlet should be closed along with the K-bottle valve and the regulator handle should be free to move (gas off). The following procedures are recommended for carrying out a plasma ion implantation.

- If the pressure is below 5 microtorr, check to make sure that the cooling water valves to the sample holder are both open. If not, open the outlet first and then the inlet.

- Check to make sure that valve No. 7 is open. This valve should always remain open unless repair to the cathodes or anodes is needed. This valve is located under the wooden support structure supporting the turbo pump and cold trap.

- Apply cooling water to the magnet coils, anodes, cathodes, and sample holder by opening valve No. 6. Feel the sides of the coils to see if they feel cool. If not, do not apply power.

- Turn on the magnet coil power supply source by pushing up on the large disconnect switch handle behind the Magnet Coil Power Supply. A loud sound of air blowing will be heard.

- Turn the power switch, located on the front of the Magnet Coil Power Supply, to the on position.

- Press up on the momentary switch ("Raise" position) to increase the magnet coil current to the desired value (usually 800 Amperes). A loud noise will be heard. This is the large Variac rotating. Do not be alarmed.

- Turn on the Penning anode power supply source (NJE power supply) by pushing up on the main breaker located on the left of the control panel.

- Set the current scale on the left to the highest range setting (0 to 50 mA). The Penning anode current should not be operated above 50 mA. Set the voltage scale to the lowest range setting (0 to 12.5 kV). It will not take much potential to cause breakdown in the discharge. About 750 V should suffice. However, at the point of breakdown, the current will suddenly increase and a plasma will appear in the vacuum system region when the magnetic field is uniform. If the current meter 'pegs' out, lower the high-voltage a small amount by rotating the large variac counterclockwise until the current no longer pegs the meter. The plasma current may oscillate between low and high current levels (10 to 50 milliamperes). This is the plasma switching back and forth between low and high pressure modes. This mode flipping may disappear as the plasma stabilizes or as the negative high-voltage is applied to the sample holder. This plasma is burning from background gas and will not last very long. If the overcurrent control trips out, the power to the anodes will be cut off and a red light will come on indicating an overcurrent situation. The control circuit has a reset button which will reset the condition. After this, restart the high-voltage by pressing the red "Start" button.

- Set the anode current to about 40 milliamperes by adjusting the variac.

- Quickly go over to the K-bottle and open up the K-bottle valve. Also, twist the regulator handle clockwise until the output line pressure needle reads about 10 psig.

- Slowly open the gas inlet valve and watch the ion gauges. At pressures around 200 microtorr and above, a plasma will appear and burn very brightly. The anode current may increase to levels around 50 milliamperes. Adjust the gas inlet valve until the plasma continues burning at pressures around 100 microtorr. Not much plasma is needed to carry out the implantation. This is the pressure at which the plasma is best stabilized for the implantation process.

- Once the plasma has stabilized (no mode flipping or arcing inside the vacuum system), the actual implantation process may begin.

APPENDIX E

OPERATING THE VACUUM SYSTEM IN THE PENNING DISCHARGE

OPERATING THE VACUUM SYSTEM IN THE PENNING DISCHARGE

This describes the procedure for pumping down the vacuum system in the uniform Penning discharge when used for plasma ion implantation. Here it is assumed that the system is at atmosphere and the sample holder is inserted into the vacuum system. It is also assumed that none of the vacuum pumps are powered up and that the cold trap refrigerator is at room temperature. It is necessary to begin at this stage in order to become familiar with the startup procedures of the vacuum system.

It is also necessary to learn how to control the vacuum pumps and other parts of the vacuum system. The forepump is the pump furtherest away, in pumping action, from the actual vacuum system. It rests on the floor on the North end of the system and is controlled by a toggle switch located on the front of the Penning Discharge Vacuum System Control Panel. On the input line of the forepump are two valves. One, valve No. 5, is used as a vent to the forepump input line and is usually not used. The other valve, No. 3, is used to pump on the vacuum system volume, bypassing the turbomolecular pump and the cold trap, when gate valve, (No. 1), is closed. Above this valve is valve No. 4 and an ion gauge. This valve is used to bleed up the vacuum system when valve No.'s 1 and 3 are closed and the turbomolecular pump is off. More about these operations will follow.

The next vacuum pump, which decreases the vacuum pressure to levels not obtainable by the forepump, is the turbomolecular

pump. The turbomolecular pump is vented to the forepump input through valve No. 2. It can be operated when the background pressure is below about 30 millitorr. This pump is water-cooled and must always be treated with care. It is a very expensive pump and expensive repairs can be avoided if proper operating procedures are followed. The cooling water is turned on by opening valve No.'s 8 and 10, behind the Magnet Coil Power Supply, against the wall. Note that the outlet line is located here and flows into a larger outlet line which has a valve on it, valve No. 9. This valve should always remain open unless the water lines need repair, as opening the water input valve with the water outlet valve closed will result in major damage to the turbo pump and refrigerator. The turbopump is controlled by its own control system, also located on the front of the Penning Discharge Vacuum System Control Panel. To activate this pump, depress the button marked "Pumping Unit" and the pump should begin to spin up, sounding like a jet engine as it reaches its maximum speed. Above this button is a needle which indicates when the pump has reached its maximum rotation speed. It will take a few minutes for the pump to reach its maximum speed. Refer to the operating manual for lubrication of this pump as this is crucial to its operation and life.

The next part of the vacuum system is called a cryogenic pump or a cold trap. Inside the cold trap are coils which are cooled by a refrigerator located near the vacuum system. The refrigerator is also water-cooled and if proper water flow is not delivered to it, it will

overheat and shut itself off and damage to the compressor could result. The cooling water is turned on by opening valve No.'s 8 and 11, behind the Magnet Coil Power Supply, against the wall. Note that the outlet water line is located here also and is always open as it has no valve. The output of the cold trap is vented to the input of the turbo pump. Hence, the input of the cold trap is the first vacuum pumping element that the gas in the vacuum system sees. The refrigerator is controlled by a toggle switch located on its front panel which is located against the wall under the window of the laboratory. Once the turbo pump is switched on, the refrigerator may also be switched on. Located on top of the refrigerator is a temperature indicator which reads the temperature of the cooling reservoir inside the refrigerator. After the refrigerator is switched on, the needle will begin to fall until it reaches about -130 degrees Celsius. This is the maximum cooling temperature it will reach. The cold trap and the turbo pump are separated by a large gate valve, valve No. 1, which will be used when pumping down and bleeding up the vacuum system. Now that the controls have been described, one can use the following steps to operate the vacuum system.

The pressure is read by two ion gauges located in the Penning Discharge Vacuum System Control Panel. One gauge is located at the pump head (North end) and will read the lowest pressure. The other is located at the gas inlet (South end) and will read higher pressures. The gas inlet valve is also located at the South end. Gas is fed from the K-bottle through a regulator and into a microvalve located on one

of the plexiglass flange plates on the South end of the vacuum system.

The state of the vacuum system controls is the following:

- The forepump, turbo pump, and refrigerator are off.
- All parts of the vacuum system are sealed and ready for pumping.
- Valves 1, 3, 4, and 5 are closed.
- Valve 2 is open.
- The ion gauges and mass spectrometer are off.
- The cooling water to the turbo pump and refrigerator is off (valves 8 and 9 open, 10 and 11 closed). It is not necessary to close valves 8 and 9 unless repair to these water line is necessary.
- The gas inlet valve is off.

The following steps should be followed when pumping down the vacuum system:

- Turn on the cooling water to the turbo pump and refrigerator by opening valves 10 and 11.
- Open valve 3 to allow air from inside the vacuum system to slowly flow into the forepump when it is turned on.
- Turn on the forepump.
- Open valve 1 to fully open position and then close it one-half a turn.

- Close valve 3.
- Wait until the pressure on the thermocouple gauge (switched on TG2) gets to about 30 millitorr or less.
- After the pressure on the thermocouple gauge is about 30 millitorr, turn on the turbo pump.
- Watch the rotation needle.
- Turn on the refrigerator.
- Wait for about 12 to 24 hours and then turn on both ion gauges by turning on the power switch and then pushing up on the filament switch. The pressure on the pump head (North end) should be about 2 microtorr and on the gas inlet (South end) should be about 3 or 4 microtorr.
- The mass spectrometer can now be turned on by switching the power switch on its front panel to the "Filament On" position.

The system is now ready for experimental use. Refer to the section on "Operating the Penning Discharge Plasma for Plasma Ion Implantation" for procedures to start up the plasma.

APPENDIX F

CHANGING THE SAMPLE AFTER A PLASMA ION IMPLANTATION EXPERIMENT

CHANGING THE SAMPLE AFTER A PLASMA ION IMPLANTATION EXPERIMENT

Once the sample has been implanted, it must be removed from the vacuum system and another sample must be inserted back into the vacuum system for another implantation. At the present time, the vacuum system contains no airlock for sample holder removal. Due to this limitation, careful procedures must be followed when removing the sample holder.

It is assumed that the Penning anode power supply (NJE power supply) and the magnet coil power supply have been shut down. It is also assumed that the gas inlet has been turned off. Relating to the implantation system, it is assumed that the high-voltage switching circuit and the implantation power source both have been turned off. Once these systems have been shut down, the vacuum system may be left unattended with the sample still in the vacuum system if one chooses to remove the sample holder at a later time.

Before the sample holder can be removed, part of the vacuum system must be shut down. It is not necessary to shut the entire vacuum system down because this will lengthen the time between implantations. It is the objective of this work to implant many samples and several can be implanted in one week if the proper vacuum system procedures are followed.

The following steps must be carried out.

- Turn off both ion gauge filaments by pressing down on the button marked "Filament" and then release it. The power to the ion gauge control may be turned off if necessary. It may be left on if it is to be used later on that day.

- Make sure that the mass spectrometer is switched completely off. If not, the filament will be burned out if the vacuum system is taken up to atmosphere and the mass spectrometer will have to be repaired. The repair will take about 2 hours and requires that the vacuum system be brought up to atmosphere. To achieve base pressures as low as that before the mass spectrometer burned out will take as long as 10 hours. Thus, avoid burning out the mass spectrometer by never operating it unless the pressure is below 10^{-3} torr. Also, never leave the mass spectrometer turned on when it is not needed.

- Turn off the turbomolecular pump by pressing the button marked "Pumping Unit" and then release it. The turbo pump will begin to spin down.

- Wait approximately 5 minutes for the turbo pump to come to a stop. Just because the rotation needle falls quickly in the red zone (to the left) does not mean that the turbo pump has come to a complete stop.

- Close valve No. 1, the gate valve, completely. Tighten it one-half a turn.

- Open valve No. 4 to bleed the vacuum system up to atmosphere. Watch the thermocouple gauge (it should be switched on TG2) as the valve is opened.

- After reaching atmospheric pressure, close valve No. 4.

- Go to the South end of the vacuum system.

- Remove the circular plexiglass plate from the end of the cooling cylinder by removing the four screws. Do not lose the screws.

- Use the grounding wand and touch it to the sample holder several times to make sure there is no charge left on it.

- Remove the zinc braid-shielded coax from the end of the Tektronix high-voltage probe by unscrewing the handle from the probe housing. Unplug the coax (standard B & C connection) from the probe sensor. Do not lose the handle.

- Unplug the black grounding wire coming out of the cooling cylinder. This grounds the base of the A-lite insulator. This is simply done by holding both ends of the connector (red) and pulling it apart.

- Unclip the alligator clip connecting the black lead of the Tektronix high-voltage probe to the Penning discharge frame. Do not remove the Tektronix probe from the cooling cylinder as this is not necessary.

- Using a 1/4" socket and a 1/4" rachet wrench, loosen the hose clamp that connects the high-voltage coaxial wire to the sample holder.

- Slip the high-voltage wire out of the hole in the side (gas inlet side) of the cooling cylinder. Do not take the wire out of the current transformer unless one intends to remove the lid from the circuit. Unecessary twisting of this wire could result in damage to the wire or damage to the head connector on the power grid tube inside the switching circuit.

- Make sure that the water flowing to the sample holder is turned off. If not, the magnet coil cooling water may need to be turned off. If the magnet coil cooling water is turned off (valve No. 6 for the inlet), both of the valves for the sample holder cooling water still must be turned off. Turn off the inlet valve first (laboratory side of the system). Then, turn off the outlet valve (window side of the system).

- Obtain a water bucket and a 1/4" nut driver and disconnect each rubber water line from their copper lines. Collect any water leaking out of the rubber hoses in the bucket.

- Turn on the air compressor (switch above the laboratory work bench) and let the air pressure build up for about two minutes.

- Using the air spray nozzle and while holding the water bucket under one of the rubber hoses from the cooling cylinder, inject a small amount of compressed air into the other rubber hose. The remaining cooling water in the sample holder will be forced out into the water bucket. This is to prevent the water from leaking into the high-voltage switching circuit and to make the sample holder system lighter when trying to remove it from the vacuum system. Take care not to let any water run down into the high-voltage switching circuit.

- Remove the flange nuts which join the sample holder cooling cylinder to the glass pipe of the vacuum system. Do not lose these nuts. Also, remove the yellow grounding wire from the flange only. Do not remove it from the Penning discharge frame.

- Slide the aluminum flange plate away from the bolts of the cooling cylinder and toward the North end of the vacuum system. The sample holder system is not free to be removed from the vacuum system.

- Standing on the laboratory side of the vacuum system and facing the side of the cooling cylinder, place both hands under the cooling cylinder and rotate the cylinder counter clockwise until both of the rubber hoses on the bottom are facing you (3:00 position). This is to keep them from getting tangled up in the supporting framework so that the cylinder does not have to be tilted at anytime when removing the sample holder. Pull slowly as there may be a small vacuum left in the system.

- With extreme care, gently continue pulling the cooling cylinder while slightly lifting up on it. Watch the inside of the vacuum system around the area where the sample holder rod is supported by the ceramic standoff bolted to the cathode support plate. The objective here is to keep from breaking the small glass dish around the copper sample holder block. Do not tilt or lift too much on the cooling cylinder as the glass dish may strike the anode ring and break. One must clear the anode ring first and then clear the cathode ring and the ceramic support. There is plenty of distance between the cathode ring and the end of the ceramic support to extract the sample holder block through. The sample holder is quite long and one must walk back away from the vacuum system while holding the cooling cylinder. Care must be taken not to slam the small glass dish against the end of the glass pipe on the vacuum system.

- Find a table with no clutter on its surface and lay the sample holder cooling cylinder down on it. Take care not to bump the end of the sample holder against anything as this contains the metal sample and it must not be scratched or touched in any way. Make sure that the cooling cylinder will not roll off the table. Place some type of pad under it for protection. This is needed to prevent the cylinder from rolling of the table and breaking upon impact with the floor.

- Obtain a plexiglass end cap which is provided. Install it on the end of the vacuum system where the sample holder was removed.

- The vacuum system needs to be kept as clean as possible while changing the sample. Go to the North end of the vacuum system.

- Open valve No. 3 and allow the forepump to pump on the vacuum system to help keep water vapor molecules out of the system. The gate valve, No. 1, is to remain closed, isolating the cold trap from the vacuum system. The refrigerator is also to remain on as it takes several hours for it to warm back up and this time can be saved.

- Obtain a small screwdriver, a cloth, a heat gun, and a petri dish. Remove the screws holding the metal sample on the copper block. Do not lose these screws as they are special screws. Take care not to drop or scratch the sample. Place the sample in the petri dish with its implanted face pointing up. Place the cover on the petri dish and tape it closed. Mark the tape according to the run number and date it for future record.

- Obtain a new sample with the holes drilled in the proper place. The sample should be in a clean petri dish obtained as a unit from the Department of Materials Science and Engineering. Make sure the new sample has no sharp edges. If it does, return it to the MSE department and have them round off the sharp edges.

- Obtain the same tools as above, a bottle of acetone and ethanol, a pair of thin rubber gloves, a small plastic brush, and several Q-tips.

- Clean the screws with ethanol and the plastic brush.

- Clean the surface of the copper block with ethanol and the cloth.

- Clean the back side of the metal sample with ethanol and the cloth.

- Carefully mount the metal sample to the copper block with the clean screws taking care not to scratch the surface of the sample with the screwdriver. Tighten the screws. The screws must be tight to insure good thermal and electrical contact between the sample and the copper block.

- Clean the surface of the sample by spraying acetone on it. Then, apply hot air from the heat gun to the surface to dry the acetone. Then, spray ethanol on the surface and dry it off with the heat gun. Once this is done, do not touch the sample surface for any reason.

- Examine the rubber gasket on the cooling cylinder. If the vacuum grease appears to be caked up or like jelly, carefully remove the gasket without tearing it. Clean both sides of the gasket and the plexiglass face with ethanol. If one cleans the gasket and plexiglass, be sure to reapply a thin coat to both side of the gasket and to the face of the plexiglass.

- Spray acetone along the glass sleeve covering the stainless steel sample holder. Wipe it off with a clean cloth and do not touch any of the glass afterwards. Examine the glass sleeve for sputtered copper. If present, clean it off with a fine grade sandpaper and a small amount of rubbing compound being careful not to break the glass.

- Now one is ready to reinsert the sample holder system back into the vacuum system. Go to the North end of the vacuum system.

- Close valve No. 3, isolating the forepump from the vacuum system.

- Open valve No. 4, allowing air to enter the vacuum system. Watch the thermocouple gauge (switched on TG2) as the system is bled up.

- After the pressure reaches atmosphere, close valve No. 4.

- Go to the South end of the vacuum system and remove the blank plexiglass flange plate.

- Examine the vacuum grease on the end of the glass pipe. If it appears to be caked up or like jelly, clean the end of the glass pipe with acetone. Wipe out this end of the vacuum system with acetone to an arm's length. If one cleans the end of the glass pipe, be sure to reapply a thin coat of vacuum grease to the clean end.

- Inspect the position of the anode ring as it could have been moved when the sample holder was removed if one accidentially bumped the sample holder against it. If it is not in place, reach into the vacuum system and move until it is in its place. It is desired that the cathodes, anodes, and sample holder be axisymmetric.

- Pick up the cooling cylinder with both hands placed underneath the cylinder and carefully insert the sample holder into the vacuum system taking care not to bump the sample on the glass pipe, ceramic support, cathode ring, or anode ring.

- Slide the cooling cylinder up to the end of the glass pipe until about a one-inch gap is between them. Align the flange plate bolt holes with the bolts extending from the plexiglass. Slide the flange plate over the bolts and gently slide the cooling cylinder into the vacuum system the rest of the way until its face fully seats against the glass pipe end.

- Replace the nuts on the flange bolts and tighten them with the hand only. Do not use a wrench or any tools to tighten these nuts as the glass vacuum system could be permanently damaged.

- Go to the North end of the vacuum system.

- Open valve No. 3, allowing the forepump to begin pumping on the vacuum system.

- Open valve No. 1, the gate valve, until its fully open. Close it one half a turn.

- Close valve No. 3.

- Allow the vacuum pressure to decrease for about 15 minutes.

- Go back to the South end of the vacuum system.

- Reconnect the sample holder water lines, the Tektronix high-voltage probe, the high-voltage coaxial wire, the black grounding lead for the A-lite insulator, the yellow grounding lead for the flange plate, and the red alligator clip to measure the implantation voltage. Make sure that the sample holder rod inside the cooling cylinder is also cleaned with acetone to help prevent corona discharges. If the triax cable was disconnected from the current transformer, reconnect it now.

- Open the outlet water valve on the sample holder cooling line.

- Open the inlet water valve on the sample holder cooling line.

- If the sample holder rod does not extend past the end of the cooling cylinder, replace the circular plexiglass cover on the end of the cooling cylinder with the four screws.

- Go back to the North end of the vacuum system.

- Examine the pressure on the thermocouple gauge (switched to TG2). It should now be around 30 or 40 millitorr. If not, wait until it is. If so, press the button marked "Pumping Unit" on the turbo pump control panel located on the front of the Penning Discharge Vacuum System Control Panel. One should hear the turbo pump spinning up and the rotation needle should begin to approach the green zone on the right.

Note that neither the refrigerator nor the forepump was ever switched off. The objective here is to change the sample in a time of about one hour. Allow the vacuum system to pump for 12 to 24 hours and then switch on the ion gauge tubes and examine the pressure. The ion gauge tubes should be degassed for about 30 minutes before pressure reading are taken. Once the pressure reaches about 2 microtorr, the vacuum system is set to conduct an ion implantation experiment.

APPENDIX G

A TRUE-BASIC™ PROGRAM FOR CALCULATING THE Q OF A MEDIUM-FREE RIGHT CIRCULAR CYLINDRICAL MULTIMODE MICROWAVE CAVITY RESONATOR

A TRUE-BASIC™ PROGRAM FOR CALCULATING THE Q OF A MEDIUM-FREE RIGHT CIRCULAR CYLINDRICAL MULTIMODE MICROWAVE CAVITY RESONATOR

The True-Basic™ program listed below was written to compute the quality factor (Q) of a medium-free right circular cylindrical multimode microwave cavity. The radius (r) and length (z) of the cavity have been set in the program to match the actual dimensions of the cylinder. The user is prompted for the first mode number (n), second mode number (m), third mode number (l), and the value of the extrema of the Bessel function (p'), to determine the value of the form factor (FF). The resonant wavelength for each mode is also computed based on p', r, and z. The resistivity of Type 316 stainless steel and the electromagnetic radiation driving freqency (2.45 GHz) is fixed in the program. The Q is then computed by taking the quotient of the product of the form factor (FF) and the resonant wavelength and the skin depth (SD). The program is listed below.

```
! Cylindrical Cavity Design Program
! This program calculates the form factor, resonant
! wavelength, and the Q for a cylindrical cavity resonator.
! Units of length are in meters.
! Units of frequency are in Hertz
!
! r = cavity radius
! cavity outside diameter is 20"
! wall thickness is 3/16"
! cavity inside diameter is 19.625" (49.8475 cm diameter)
let r = 0.249238
! z = cavity length
! cavity length is 40 3/16" (102.076 cm)
```

```
let z = 1.02076
! n = first mode number
input n
! m = second mode number
input m
! l = third mode number
input l
! p = extremma of Bessel function
input p
let A = (1-((n/p)^2))
let B = (p^2+((l*Pi*r)/z)^2)^1.5
let C = p^2
let D = ((2*r)/z)*((l*Pi*r)/z)^2
let E = (1-((2*r)/z))*((n*l*Pi*r)/(p*z))^2
let FF = (A*B)/((2*Pi)*(C+D+E))
! print A*B
! print C+D+E
print FF
!
! Calculate the resonant wavelength for each mode
! W = resonant wavelength for mode nml
let W = (2*Pi)/((p/r)^2 + ((l*Pi)/z)^2)^0.5
print W
!
! Form factor is Q x (skin depth/resonant frequency)
! Resistivity of 316 Stainless Steel is 74 nanoohm-meters
! Skin depth, SD, at f = 2.45 GHz is 2.766 E-6 m
let SD = 2.766e-6
! Calculate the Q of the nml mode
let Q = (FF*W)/SD
print Q
end
```

APPENDIX H

A TRUE-BASIC™ PROGRAM FOR CALCULATING THE Q OF A PLASMA BASED ON THE LORENTZ CONDUCTIVITY MODEL FOR ELECTRON COLLISIONS

A TRUE-BASIC™ PROGRAM FOR CALCULATING THE Q OF A PLASMA BASED ON THE LORENTZ CONDUCTIVITY MODEL FOR ELECTRON COLLISIONS

The True-Basic™ program listed below was written to compute the quality factor (Q) of a plasma based on the Lorentz conductivity model for electron collisions. For values of the electron plasma frequency below and near cutoff, for an electron collision frequency of 600 kHz, and for an electromagnetic radiation driving frequency of 2.45 GHz, the value of the complex dielectric constant was computed with e1 being the real part and e2 the imaginary part. The ratio of the real to the imaginary part (e1/e2) is the quality factor due to the plasma only (Qd). Values of electron number density versus plasma quality factor are graphed in Figure IV.17.

```
!let w =1.539379975111111e10
! input w
!open #1: PRINTER
for w = 3.5e9 to 7e9 step 8e7
let F = 41.2013e45*(1/w^4 - 4.21996e
let A = SQR(F)
let n = w^2*8.8542e-12*9.1091e-31/1.6(
let nu = 2*Pi*600e3
let w2 = 2*Pi*2.45e9
let e1 = 1-((w^2)/(w2^2+nu^2))
let e2 = (w^2*nu/w2)/(w2^2+nu^2)
let Qd = e1/e2
print w, n, Qd
next w
end
```

APPENDIX I

COMMENTS ON THE PRODUCTION OF THIS THESIS

COMMENTS ON THE PRODUCTION OF THIS THESIS

This thesis was written and prepared exclusively by Philip F. Keebler using his own Apple Macintosh SE/20 computer. The text was written using Microsoft Word 4.0 word processor. The figures were prepared using MacDraft and Superpaint 2.01 graphics packages. The manuscript was printed on a LaserWriter Plus laser printer.

VITA

The author was born in Knoxville, Tennessee, on December 21, 1963. Before attending high school, he worked weekends as an electrician's assistant. He attended Central High School in Knoxville, Tennessee and had a special interest in electricity, electronics, science, and mathematics. While attending Central, the author took a part-time job in April 1980 with Gentry-Griffey Funeral Chapel, Inc. under Jerry J. Griffey.

In January 1983, the author was admitted by the College of Engineering at The University of Tennessee, Knoxville with a major in Electrical Engineering. In August 1983, the author decided to leave the funeral home and become an employee of the East Tennessee Regional Juvenile Service Center under Richard L. Bean, Superintendent. His initial responsibilities were Control Room Operator on the "graveyard" shift, from which he was promoted to the evening shift where he worked directly with the youth at the Center. He continued in this post until December 1985.

At this time, the author decided to enroll in the Cooperative Engineering Program at The University of Tennessee, Knoxville. After looking at several companies, the author received an offer for co-op employment at Emerson Electric Company. This was the Chromalox Instruments and Controls Division under E. L. Wiegand. This post was located in a small town called LaVergne, Tennessee, two miles southeast of Nashville. He was one the highest paid beginning co-op students at the university at this time. He was

assigned to the Marketing Engineering Department where interaction with potential customers was required. He worked for two three-month periods with this company.

The author then returned to the funeral home in October 1986 and continued as a student at UTK until he graduated in August 1988 with a Bachelor of Science Degree in Electrical and Computer Engineering with Honors. He was on the Dean's list for 5 quarters.

The author was hired by Professor J. Reece Roth of the ECE Department as a Graduate Research Assistant, and reported to the UTK Plasma Science Laboratory on August 22, 1988. He was given the assignment of assisting with the design and fabrication of a high-voltage switching circuit to be used in a plasma ion implantation research program. He built and tested each individual system for the circuit and put it on line in early February 1989. The switch was used to implant the first stainless steel sample, which produced good results. Professor Roth then applied for a three-year grant for continued research in this field. Upon its award, the author was given the assignment of designing, building, testing, and characterizing a large volume microwave generated plasma.

Some graduate courses which the author has taken include the Electrical Engineering Mathematics Series, the Plasma Diagnostics Series, a course in designing VLSI (Very Large Scale Integrated) integrated circuits, the Industrial Plasma Engineering Series, the Plasma Science Seminar Series every semester, and two courses in advanced differential equations. In the VLSI course, the author developed the original idea. The chip was designed from scratch,

input to a special computer (SUN) with many state-of-the-art programs designed by the University of California, Berkeley, and tested after it was manufactured.

The author also made contributions to other research projects such as plasma heating by collisional magnetic pumping in a modified Penning discharge and plasma cloaking of military radar targets.

The author received his Master of Science degree in Electrical Engineering with a grade point average of 3.67 on a 4.0 scale on August 10, 1990.